



**Politecnico  
di Torino**

Politecnico di Torino

Environmental and Land Engineering  
A. Y. 2021/2022  
March 2022

# **Drone, aerial and satellite photogrammetry for 4D glacier survey and monitoring**

Supervisors:  
Prof. Alberto Cina  
Prof. Fabio Giulio Tonolo

Candidate:  
Myrta Maria Macelloni



*Ai miei genitori*

# **Ringraziamenti**

Un ringraziamento al CC-Glacier Lab e in particolare al professor A. Cina per avere accettato di guidami in questo percorso finale coinvolgendomi e insegnandomi l'applicazione di diverse tecniche geomatiche del rilievo sul campo all'elaborazione dei dati in ambiente glaciale, permettendomi di unire la mia grande passione per la montagna al lavoro di tesi.

Al professor F. Giulio Tonolo per il continuo e pronto supporto durante il tutto il periodo di elaborazione sempre con grande gentilezza e disponibilità.

Al Politecnico di Torino, in particolare ai docenti dell'indirizzo 'Climate change' per l'entusiasmo, il coinvolgimento, la disponibilità e la voglia di condividere le proprie conoscenze con gli studenti, che mi hanno fatto ritrovare la passione per lo studio.

Un ringraziamento all'Arpa Valle D'Aosta per il supporto in questo lavoro sul campo nelle missioni e per la gentile concessione delle immagini satellitari Pleiades.

Ai miei genitori, che mi hanno sostenuto in questa nuova scommessa, supportandomi quotidianamente tra i tanti alti e bassi, credendo sempre in me e condividendo gioie e dolori.

A Giorgia, il mio opposto, ma sostegno delle mie giornate, sempre presente per un consiglio, uno sfogo o una semplice chiacchierata, ormai una parte fondamentale della mia vita.

A Fra, alla casualità con cui è nata la nostra amicizia che mi fa sempre sorridere, a tutte le cose che abbiamo vissuto insieme, ai traguardi raggiunti e a tutto ciò che ci aspetta. So che non ci sarà distanza o luogo dove non ci ritroveremo.

A Dynis, per il coraggio di inseguire la propria via non senza difficoltà, per la condivisione e per la certezza che certi rapporti cambiano nella forma ma non nella sostanza.

A Giulia e Giulia, perché nonostante la lontananza, la mia assenza e le poche occasioni di stare insieme ci sono sempre.

Ad Antonello, per avermi insegnato tramite lo sci la disciplina, il sacrificio e la dedizione per il raggiungimento dei risultati, se oggi arrivo a questo traguardo è anche merito suo.

A tutti quelli che mi sono stati accanto in questo impegnativo percorso, vicini e lontani, che mi hanno sostenuto e incoraggiato in questi due intensi anni, capito la mia assenza e condiviso il poco tempo libero.



# Abstract

Mountainous and glacial environments are among the most sensitive to the impact of climate change. The current trend of constantly rising GreenHouse Gas (GHG) emission and the consequent temperatures growth have caused an increase in the equilibrium line (i.e. the line that separates the accumulation and ablation areas of a glacier) altitude and significant and constant reduction of glacial masses. The projection of the Intergovernmental Panel on Climate Change (IPCC) highlights how the largest snow mass loss is taking place in the regions with small glaciers like the Alps, with significant social and economic impacts.

Acting as indicators of climate change, glaciers are environments with delicate balances that should be monitored over time. The need for monitoring the glacier areas and the masses of melting snow has required the implementation of in-situ measurement campaigns and the application of different techniques for a systematic and continuous monitoring of these complex environments. Monitoring of these environments mainly takes place annually, to assess the extent of the glacier retreat at the end of the summer ablation period.

In the present research different Geomatics monitoring techniques were applied to the Rutor and Indren glaciers, both located in Valle d'Aosta (North-Western Italy). The two glaciers are characterised by different size, accessibility and characteristics. Different digital photogrammetry techniques were applied using aerial imagery, acquired both with a drone and a camera mounted on board of a light aircraft, as well as satellite imagery.

In situ measurement campaigns were carried out during summer 2021 to collect information, measure 3D coordinates of reference points (both natural and artificial marker) and put in place the necessary ground support and orientation of the photogrammetric flight scheduled for the end of September. Glacier 3D models were generated from both the image dataset acquired by the drone and the aerial photogrammetric flight, by comparing and analysing the results.

Subsequently, thanks to this 2021 model, it was possible to co-register a previous model built from aerial images acquired in 2020 in the same period, but without any ground control points (GCP). By comparing the two models it was possible to assess the glacier extent and volume retreat over one year.

The difficulties related to the equipment transportation and the limited accessibility of the areas to be monitored, together with the cost and risk of the measurement campaigns, are parameters of fundamental importance in the choice of the monitoring techniques to be adopted. GNSS data from the photogrammetric flight was therefore processed to obtain the camera positions and to build a 3D model by means of a direct photogrammetry approach (i.e. without using GPCs) for cross-comparison and validation of the results

obtained. The overall goal was to assess the positional accuracy of a 3D model based on direct photogrammetry to limit (or possibly skip) the field surveying phase.

Lastly, satellite photogrammetry based on a very high resolution (VHR) stereopair acquired by the Pleiades constellation was evaluated, analysing areas considered invariant over time, to understand its feasibility as a monitoring tool in wide glacial environments and the related 3D positional accuracy.

# Index

<b>ABSTRACT.....</b>	<b>6</b>
<b>FIGURE INDEX .....</b>	<b>10</b>
<b>TABLE INDEX.....</b>	<b>14</b>
<b>THE CRYOSPHERE AND ITS SENSITIVITY TO CLIMATE CHANGE.....</b>	<b>17</b>
<b>1.1 THE CRYOSPHERE AND ITS COMPONENTS .....</b>	<b>17</b>
<b>1.2 CRYOSPHERE AND CLIMATE CHANGE .....</b>	<b>21</b>
<b>CHAPTER 2.....</b>	<b>28</b>
<b>VALLE D'AOSTA GLACIERS: RUTOR AND INDREN GLACIERS.....</b>	<b>28</b>
<b>2.1 VALLE D'AOSTA GLACIERS .....</b>	<b>28</b>
<b>2.2 RUTOR GLACIER .....</b>	<b>30</b>
<b>2.2.1 Studies on the Rutor glacier .....</b>	<b>36</b>
<b>2.3 INDREN GLACIER .....</b>	<b>37</b>
<b>CHAPTER 3.....</b>	<b>41</b>
<b>GLACIER MONITORING TECHNIQUES.....</b>	<b>41</b>
<b>3.1 PHOTOGRAMMETRY, HINTS OF THEORY .....</b>	<b>41</b>
<b>3.2 RUTOR MONITORING CAMPAIGNS AND GROUND CONTROL POINTS .....</b>	<b>44</b>
<b>3.3 UAV (UNMANNED AERIAL VEHICLES):.....</b>	<b>58</b>
<b>3.3.1 DRONE PHOTOGRAMMETRY .....</b>	<b>58</b>
<b>3.3.2 DRONE MODEL .....</b>	<b>60</b>
<b>3.3.3 DISCUSSION .....</b>	<b>63</b>
<b>CHAPTER 4.....</b>	<b>64</b>
<b>PHOTOGRAMMETRIC FLIGHT OF RUTOR GLACIER.....</b>	<b>64</b>
<b>4.1 AIRCRAFT, IMU, CAMERA CHARACTERISTICS .....</b>	<b>64</b>
<b>4.2 PHOTOGRAMMETRIC FLIGHT DATA .....</b>	<b>65</b>
<b>4.3 2020 AND 2021 MODELS OF RUTOR GLACIER .....</b>	<b>66</b>
<b>4.4 DRONES CARTOGRAPHIC PRODUCTS .....</b>	<b>83</b>
<b>CHAPTER 5.....</b>	<b>87</b>
<b>GNSS DATA POST PROCESSING .....</b>	<b>87</b>
<b>5.1 FLIGHTPATH RECONSTRUCTION .....</b>	<b>87</b>
<b>5.2 IMU DATA .....</b>	<b>97</b>
<b>5.3 ANTENNA POSITION AT THE TIME OF THE SHOOTING .....</b>	<b>99</b>

5.4 COMPARISON BETWEEN GPS AND TA CAMERA CENTRES .....	105
5.5 DISCUSSION .....	120
<b>CHAPTER 6.....</b>	<b>121</b>
<b>PHOTOGRAMMETRIC PROCESSING OF STEREOSCOPIC SATELLITE IMAGES .....</b>	<b>121</b>
6.1 SATELLITE IMAGERY .....	121
6.2 PLEIADES CONSTELLATION .....	122
6.3 DATA PROCESSING .....	123
6.4 REFERENCE DATA .....	124
6.5 MODEL USED AND STEPS .....	125
6.6 CARTOGRAPHIC PRODUCTS.....	128
6.7 2021 AERIAL DSM AND 2017 SATELLITE DSM COMPARISON.....	134
<b>CHAPTER 7.....</b>	<b>146</b>
<b>INDREN GLACIER MONITORING .....</b>	<b>146</b>
7.1 INDREN CAMPAIGN.....	146
7.2 DRONE MODELS: DSM AND ORTHOPHOTO .....	150
7.3 GCP EXPERIMENTS.....	154
7.4 LIDAR MONITORING TECHNIQUE .....	155
7.5 DISCUSSION .....	156
<b>CHAPTER 8.....</b>	<b>157</b>
<b>CONCLUSIONS .....</b>	<b>157</b>
<b>ANNEX CHAPTER 4.....</b>	<b>162</b>
<b>RUTOR MONOGRAPHS .....</b>	<b>162</b>
MONOGRAFIE LAGO SERACCHI .....	162
RUTOR ALTO .....	184
<b>ANNEX CHAPTER 5.....</b>	<b>198</b>
<b>ANTENNA POSITION AT THE SHOOTING TIME.....</b>	<b>198</b>
COORDINATES COMPARISON TO OFFSET ESTIMATION OF 60 SELECTED SHOTS .....	198
COORDINATES AFTER 4 ITERATIONS.....	201
<b>BIBLIOGRAPHY .....</b>	<b>244</b>

# Figure Index

Figure 1 Glacier formation dynamics (Christopherson, 2010).....	20
Figure 2 IPCC AR5, Schematic of three types of glaciers located at different elevations, and their response to an upward shift of the equilibrium line altitude (ELA).....	23
Figure 3 Projected glacier mass evolution between 2015 and 2100 relative to each region's glacier mass in 2015 (100%) based on three Representative concentration pathways. (IPCC).....	24
Figure 4 World Glacier Monitoring Service (WGMS), Annual mass balance of reference glaciers with more than 30 years of ongoing glaciological measurements .....	25
Figure 5 Google Earth, Rutor geographical overview .....	30
Figure 6 Perretti-Charrier, La Thuile, Paesaggi geologici e storici .....	31
Figure 7 8800 years of high-altitude vegetation and climate history at the Rutor.....	32
Figure 8 Rutor Serac Lake 1909 .....	33
Figure 9 Photo of summer 2021 .....	33
Figure 10 Rutor Glacier on summer 2021 .....	34
Figure 11 Rutor July 2021 .....	35
Figure 12 Rutor 1926 Archivio storico.....	35
Figure 13 Google Earth, Indren glacier .....	37
Figure 14 Indren glacier, July 2021 .....	38
Figure 15 Indren glacier summer 2021.....	40
Figure 16 Indren glacier in the 60s source: meteobook.it.....	40
Figure 17 Coordinates relationship (Kraus,1998).....	43
Figure 18 A Bundle adjustment (Inghilleri,1970) .....	44
Figure 19 Base station DIATI100.....	46
Figure 20 GCP first campaign .....	46
Figure 21 'Base' station DIATI88 .....	47
Figure 22 DIATI71IDROMETRO base station.....	48
Figure 23 Levelling the free surface of Serac lake .....	49
Figure 24 Levelling the free surface of Serac lake .....	49
Figure 25 Levelling the free surface of Serac lake .....	50
Figure 26 Levelling on Serac lake .....	50
Figure 27 Drone flight on glacier front.....	51
Figure 28 DIATI71IDROMETRO base stationFigure 29 Drone flight on glacier front.	51
Figure 30 GCPs around Serac lake .....	52
Figure 31 Marker on Gamma 'base' station .....	54
Figure 32 Probe sampling to measure ice thickness .....	55
Figure 33 Marker on the glacier to set a GCP 1m x 1 m .....	55
Figure 34 GCPs on upper Rutor glacier on Google Earth .....	56

Figure 35 Spectra Trimble receiver SP80.....	57
Figure 36 DJI Phantom 4 .....	58
Figure 37 DJI Phantom 4 use during the Rutor campaign at Serac Lake .....	59
Figure 38 ConveRgo software .....	60
Figure 39 Point 105, DJI drone pole.....	62
Figure 40 iXM-RS150F Camera.....	64
Figure 41 Aircraft and camera position .....	65
Figure 42 GCPs and CPs 2021 .....	67
Figure 43 Orthophoto from flight 2021 .....	68
Figure 44 DSM from flight 2021 .....	69
Figure 45 GCPs and CPs 2020 .....	73
Figure 46 Orthophoto from flight 2020 .....	74
Figure 47 DSM from flight 2020 .....	75
Figure 48 Differences between Geoportale DSM and 2021 DSM .....	76
Figure 49 Section of Geoportale and 2021 models on glacial foreheads .....	77
Figure 50 Section line .....	77
Figure 51 Difference of 2020 and 2021 DSM models.....	78
Figure 52 Section 1- on the glacier foreheads .....	81
Figure 53 Section 2- Central section.....	81
Figure 54 Section 4- Rutor's head section .....	82
Figure 55 Section 3- Longitudinal section North- South.....	82
Figure 56 Section 5- Zoom on east forehead.....	82
Figure 57 Section 6- Zoom on the west forehead.....	83
Figure 58 Orthophoto from DJI Phantom images of 9th and 21st July 2021 .....	84
Figure 59 Section 2 on Serac lake .....	85
Figure 60 Section 1 East glacier forehead .....	85
Figure 61 Monograph Rumiod station.....	87
Figure 62 Reference station positions.....	88
Figure 63 GNSS Calendar .....	89
Figure 64 Rinex convertes .....	90
Figure 65 RTKPost .....	90
Figure 66 Total trajectory with ambiguity fixed/not fixed .....	91
Figure 67 Output .pos RTKPost with the virtual reference station .....	91
Figure 68 Plot of the output on RTKPost with virtual reference station .....	92
Figure 69 Output .pos RTKPost with the RUMIOD base .....	93
Figure 70 Plot of the output on RTKPost with RUMIOD station .....	93
Figure 71 Flight trajectory on the Rutor glacier 2D .....	94
Figure 72 Full trajectory .....	94
Figure 73 Altimetric flight trajectory on the Rutor glacier.....	95

Figure 74 Flight trajectory on the Rutor glacier 3D .....	95
Figure 75 Flight trajectory with the Rumiod base station .....	96
Figure 76 Yay, Pitch, Roll angles .....	97
Figure 77 Camera and IMU positions onboard on the aircraft from DIgiSky.....	98
Figure 78 Matlab Script 'SCRIVI EVENT MARKER' .....	100
Figure 79 Cerca EVENT MARKER response .....	101
Figure 80 RTKPost .....	101
Figure 81 Output shots over time – interpolated GNSS antenna to shooter time.....	102
Figure 82 Flight trajectory with shots position in 2D .....	102
Figure 83 Flight trajectory with shots position in 3D .....	103
Figure 84 Eccentricity GNSS antenna – camera projection points .....	104
Figure 85 Comparison between the camera centres .....	106
Figure 86 Comparison between shots in 3D .....	107
Figure 87 Velocity between of the aircraft derived from GPS coordinates.....	107
Figure 88 Distance between height coordinates .....	108
Figure 89 Distance between East coordinates .....	108
Figure 90 Distance between North coordinates .....	108
Figure 91 Distance between TA and GPS shots .....	109
Figure 92 Offset between the TA and GPS coordinates .....	109
Figure 93 Selected shots .....	110
Figure 94 Aircraft velocity on 60 selected shots .....	111
Figure 95 Offset between TA and GPS on 60 shots selected .....	111
Figure 96 Shots comparison with 0.8s offset in 2D.....	112
Figure 97 Shots comparison with 0.8s offset in 3D.....	113
Figure 98 60 shots selected after the first iteration.....	113
Figure 99 Coordinates differences after the first iteration.....	114
Figure 100 Coordinate difference after the second iteration .....	114
Figure 101 Coordinate difference after the fourth iteration.....	115
Figure 102 Third iteration centres distance on the first shot .....	115
Figure 103 Planar distance between TA and GPS coordinates .....	116
Figure 104 Planar distance between TA and GPS coordinates .....	116
Figure 105 Linear trend in the second interval .....	117
Figure 106 Linear trend in the first interval.....	117
Figure 108 Linear trend in the fourth strip .....	118
Figure 107 Linear trend in the third strip.....	118
Figure 109 Linear trend in the fifth strip .....	119
Figure 110 Remote sensing process (Boccardo, s.d.) .....	121
Figure 111 Satellite images area.....	124
Figure 112 Residual Error Geomatica Banff .....	125

Figure 113 GCP, CP, TP used .....	127
Figure 114 Orthophoto 1 obtained from Pleiades.....	129
Figure 115 Orthophoto 2 obtained from Pleiades.....	130
Figure 116 Zoom to the original resolution on the glacier area on the Pleiades orthophoto (red square in Figure 115) .....	131
Figure 117 Zoom to the original resolution on the glacier area on the Aerial orthophoto (red square in Figure 116).....	132
Figure 118 DSM obtained with 6 GCPs ellipsoidal height .....	133
Figure 119 2017 Satellite DSM - 2021 Aerial DSM .....	135
Figure 120 Stable areas.....	136
Figure 121 Classification of the areas according to the slope .....	138
Figure 122 Mean and Standard Deviation difference values for each slope range .....	139
Figure 123 Reclassification according to exposure .....	141
Figure 124 Mean and standard deviation difference values for each exposure range ...	142
Figure 125 Section line on the glacier .....	143
Figure 126 Pleiades- DSM aerial section 1 .....	144
Figure 127 Pleiades- DSM aerial section 2 .....	144
Figure 128 RTK station INDREN 1 base station .....	146
Figure 129 Marker measurement during the campaign of July 2021 .....	148
Figure 130 Indren glacier GCPs .....	149
Figure 131 Indren orthophoto flights 2021 .....	151
Figure 132 Orthophoto from flights 2020.....	152
Figure 133 Differences on DSM models of 2020 and 2021 .....	153
Figure 134 AtlaScan model Indren 2020 .....	155
Figure 135 Multitemporal analysis of east glacial forehead retreat on orthophoto 2021 .....	159
Figure 136 Section on east and central glacial front.....	160
Figure 137 Zoom section on east glacial front .....	160
Figure 138 Section line of Figures 136-137 .....	160

# Table Index

Table 1 World Glacier Monitoring Services (WGMS), Surface glaciers in the world....	17
Table 2 Ice volume in European Alps and change, 2006 (Haeberli, et al., 2021) .....	28
Table 3 Villa, Tamburini et al, Volume reconstruction of Rutor Glacier.....	36
Table 4 Villa, De Amicis, Rutor glacier surface variation between LIA and 2004.....	37
Table 5 Front altitude (ComitatoGLaciologicoItaliano) .....	39
Table 6 DIATI88 coordinates .....	47
Table 7 DIATI 71 coordinates .....	48
Table 8 Compensation calculated outward and return.....	51
Table 9 Coordinates GCPs July 2021 .....	53
Table 10 Gamma 'base' coordinates.....	54
Table 11 GCPs upper part of Rutor glacier .....	56
<i>Table 12 Characteristic receiver TRIMBLE SP80</i> .....	57
Table 13 Characteristics of Phantom 4 camera .....	58
Table 14 GCPs drone flights of 9th July 2021 – Serac Lake.....	61
Table 15 Residual errors on GCPs drone model 9 <sup>th</sup> July.....	61
Table 16 Average camera location error on drone model 9 <sup>th</sup> July.....	61
Table 17 GCPs of drone Serac lake flight of 20th July 2021 – Serac Lake .....	62
Table 18 Pole DJI coordinates .....	62
Table 19 Average camera location errors on drone model 21 <sup>st</sup> July .....	63
Table 20 Residual error on GCPs drone model 21 <sup>st</sup> July.....	63
Table 21 GCP model 2021.....	66
Table 22 Residual errors on GCPs model 2021.....	70
Table 23 Residual errors on check points model 2021 .....	70
Table 24 Comparison between aerial and Geoportale .....	71
Table 25 GCP model 2020.....	71
<i>Table 26 Additional GCPs model 2020 from 2021 model</i> .....	72
Table 27 Residual error on GCPs model 2020 .....	72
Table 28 Residual errors on check points model 2020 respect 2021 model.....	72
Table 29 Comparison between 2020 and 2021 models on time invariant areas.....	79
Table 30 Sections legenda .....	81
Table 31 Legend of the sections .....	85
Table 32 IMU .me3 sample data at shooting time .....	97
Table 33 Lever Arm output to be add.....	105
Table 34 Coordinates .....	105
Table 35 Distance between TA and GPS coordinates of the first shot.....	116
Table 36 Linear trend.....	119
Table 37 Pleiades constellation characteristics (ESA, 2021) .....	123

Table 38 Residual errors .....	126
Table 39 Residual errors .....	128
Table 40 Statistics according to the slope range.....	139
Table 41 Statistics according to the exposure range.....	142
Table 42 Indren glacier GCPs.....	147
Table 43 Average camera location error.....	150
Table 44 Residual errors on GCP .....	150
Table 45 GCPs trial.....	154



# Chapter 1

## The Cryosphere and its Sensitivity to Climate Change

### 1.1 The Cryosphere and its components

The entirety of the frozen water present on the Earth's surface is called the **cryosphere**, and it's represented in the form of snow, sea ice, ice caps, ice covers, frozen lake and rivers and permafrost and occupies about 10 % of the Earth's surface(as shown in Table 1). The term "cryosphere" derives from the Greek word '**Kρύος**', kryos that means cold.

REGION	AREA (km <sup>2</sup> )
Africa	10
Antarctica	13593310
Asia and Eastern Europe	185211
Australasia (New Zealand)	860
Western Europe	53967
Greenland	1726400
North America (without Greenland)	276100
South America	25908
<b>World total</b>	<b>15861766</b>

Table 1 World Glacier Monitoring Services (WGMS), Surface glaciers in the world

The cryosphere on high mountain regions hosts roughly 10% of the global population (IPCC<sup>1</sup>) and is a key element of Earth's climate interactions and its global water balance. Changes to the cryosphere are closely connected to mountain ecosystems, which provide the water supply for agriculture and environments downstream as well as drinking water for society and fuel for hydropower production. The cryosphere is fundamental for both human and natural systems, and it balances in the climate conditions of the Earth.

In order to understand the essence of the cryosphere, the following paragraphs will briefly define its main components.

**Snow** forms when the air temperature of cloud condensation is under 0°C, and it combines into crystals of various shapes. Snow is a key element in the world's climate and is an essential habitat for fauna and flora in many parts of the world.

<sup>1</sup> Intergovernmental panel on climate change

When snow falls, it can be differently classified in different variously as firn, slush, sastrugi, or cornice. Firn is snow that has collected for more than a year with high density, slush refers to a snow-water mixture, cornices and sastrugi are of wind formations. Sastrugi occur when wind pushes the snow into jagged, irregular forms along its surface, whereas cornices, as the name implies, are overhangs of snow on ridges or cliff faces. The main elements of the Earth's cryosphere are sea ice, ice caps, ice sheets, permafrost and glaciers.

**Ice sheets** are the largest elements, continental-scale ice layered bodies created of years of snow accumulation that flow onto the ocean. They can develop under the sea level and be hundreds of meters thick. The two main ice sheets still present from the last Ice Age cover Greenland and the Antarctica region. The Antarctica ice sheet contains 91% of the world's freshwater ice.<sup>2</sup> The balance of ice sheets is controlled by snow precipitations, the melting of lateral parts, and the detachment of icebergs. Ice sheets are a key element in the study of past climate eras because they still contain trapped carbon dioxide molecules. **Sea ice** is different from the other types because it has its melting and freezing cycles entirely on the ocean. Sea ice sheets can be as thin as a few centimetres or be meters thick. Most sea ice forms in the Arctic and Antarctic oceans and has a fundamental role for the indigenous Arctic people. Sea ice influences Earth's climate and is a parameter for studying climate change.

**Ice shelves** are floating ice masses connected to the land that usually develops near the coastal areas and protect them. As for the ice sheets, the two mains still ones still in existence are the Greenland and Antarctic sheets. The mass of the ice shelves continuously evolves, and they increase and lose mass, especially with the 'calving' process, or **iceberg** detachment, which has increased in recent years.

**Permafrost** is defined as "*sub-surface earth materials that remain at or below 0°C continuously for two or more years, is widespread in the Arctic, sub-Arctic and high-mountain regions as well as in the ice-free areas of the Antarctic and sub-Antarctic.*"<sup>3</sup> It is a permanently frozen layer composed of soil, gravel, and sand surrounded by ice. Permafrost covers around 22.8 million km<sup>2</sup> in the Northern Hemisphere, and it's fundamental in studying the Earth's climate. The upper part of the permafrost is called the 'active layer,' and this layer melts during the summer and freezes during autumn.

**Glaciers** are a "*natural accumulation of ice with a stratified structure, due to the transformation of meteoric snow, soft and porous, first into granular snow (firn), then into boiling ice, and finally into the so-called 'glacier ice,' transparent, white or slightly*

---

<sup>2</sup> Glaciers , pp. 11 - 24

<sup>3</sup> WMO, World Meteorological Organization

*greenish[...];”<sup>4</sup> and are also defined as “a large mass of ice that moves slowly over land, esp. down the side of a mountain, often moving rocks with it and changing the shape of the land.”<sup>5</sup>* Glaciers are the remains of the last ice age when they represent the coverage of around 32% of the land and 30% of the oceans.

Glaciers are formed by a balance between ablation (mass loss) and accumulation (mass gain) of the perennial snow cover; the prevalence of one or the other phenomenon determines the glacier’s retreat or growth. The snow accumulated is compressed into the ice with sediments that accumulate, especially in high mountains zones and high latitudes. Glaciers are categorized into several types according to their shape, topography, or ice temperature; however, it’s also important to consider that glaciers are natural environments and that it is impossible to differentiate them into strict classifications.

According to the World Glacier Inventory (WGI), glaciers are classified according to their essential elements in their territorial context.

The primary classifications are continental caps, valley glaciers, mountain glaciers, or are divided by form, compound, cirque, plate, and by the characteristics of the front, which can be lobed or piedmont.<sup>6</sup> It can sometimes be difficult to clearly make these distinctions.

**Ice caps** are thin ice sheets distributed over 50000 km<sup>2</sup> and cover the land and the environment under them.

**Ice fields** are the spreading of glacial ice in different directions; unlike ice caps, they are not continuous, but they are divided by mountains that modify their flow.

**Tidewater glaciers** are glaciers whose boundaries extend directly into the ocean. Iceberg calving can occur with this type of glacier.

**Mountain or alpine glaciers** are formed in mountainous regions and have very different extensions.

**Piedmont glaciers** are created by steep iced valleys that slope into a flat plain and make particularly shaped formations similar to lobes.

**Rock glaciers** are formed by rock and debris with ice at their core. They are typically shaped like a tongue or lobe. Differently from the other types, they have fast-displacement that is visible from their landforms.

However, the types above are all global classifications, while sub-genres based on specific geographical areas are also common. According to the Castato dei ghiacciai italiani (The Registry of Italian Glaciers), European glaciers can be divided into three types: Pyrenean or mountainous type, alpine type and Himalayan type.

---

<sup>4</sup> (Vocabolario Treccani)

<sup>5</sup> Cambridge dictionary

<sup>6</sup> WGI

The Pyrenean or mountainous type does not have a tongue shape despite having a wide accumulation zone, while the alpine type has both a large tongue and a large accumulation zone, whereas the Himalayan type of glaciers are formed by the union of different melting basins and are often covered by moraine debris.

Glaciers are formed over many years, and even if they look like static masses, they are always mobile masses. Their movements create different characteristic environments. Glaciers move due to their weight and gravitational forces, and sometimes they slide either over a layer of water or on a sediment layer. Their movement shapes the surrounding environment, glaciated valleys being one of the most characteristic examples. The retreat of a glacier causes another characteristic environment. During their regression, glaciers leave the sand, mud, gravel, and other sediments changing their own shape and leaving clear traces of their past dimensions.

Glaciers characterize all continents that have emerged from the Earth's crust; in Europe, they are characteristic of high mountain areas where climatic conditions are favourable to the accumulation of snow. The alpine glaciers can have a different scale, and they vary from small areas to massive extensions through mountain peaks. Their size plays a key role in responding to mass changes that occur over time.

Glaciers are formed by an accumulation of snow in the so-called '**accumulation area**' in the area of the glacier highest in elevation. This then becomes ice, increasing the overall mass. Due to the effects of its increasing weight, the glacier is forced to flow down towards the '**ablation area**', where part of the glacier's mass thaws and then evaporates (Figure

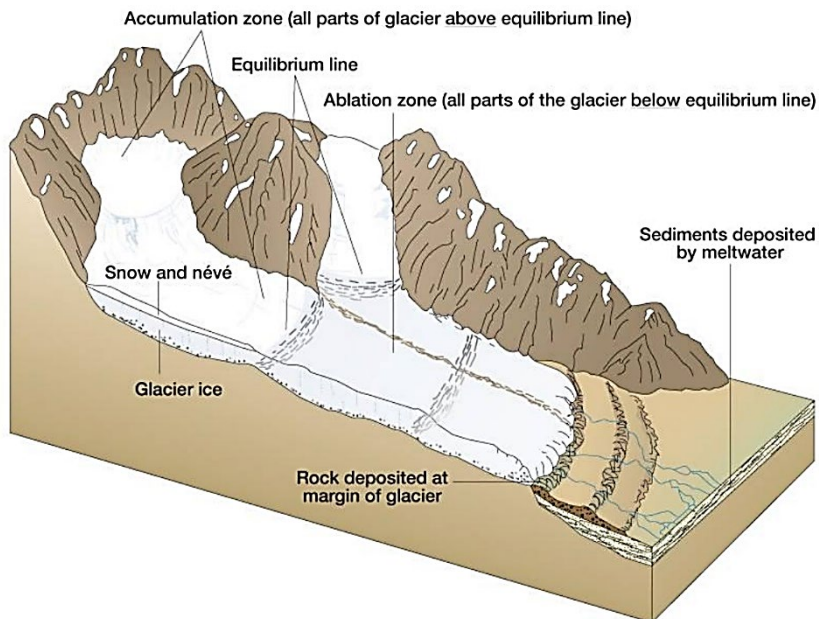


Figure 1 Glacier formation dynamics (Christopherson, 2010).

1). In the separation between the accumulation zone and the ablation zone, there is an ideal line called the ‘**equilibrium line**’ where melting and snowfall are balanced.

When there are no temperature variations, glacier mass tends to remain in the same shape and there are no significant size modifications. The balance of a glacier is always in a dynamic equilibrium. Winds and avalanches contribute to the displacement of snow masses and thus to a redistribution that may favour ablation or snow accumulation.

The continuous movement of the snow mass causes the formation of different features. During movements, the sliding forces create long cracks in the glacier called crevasses, which may be isolated or, when they intersect, they are called **seracs**. The ice mass forms long dark lines visible on the surface when moving, picking up rock debris and dirt and forming **moraines**. Moreover, when the snow melts, the formation of **supraglacial lakes** is possible, formed by surface meltwater basins and moulin, vertical fractures created by meltwater.

## 1.2 Cryosphere and climate change

The cryosphere is undergoing continuous changes, especially in mountainous environments, and these changes will continue, both locally and globally. In mountainous environments, changes will not only be caused by climate change but also by indirect causes with considerable environmental and socio-economic impacts. Glaciers are crucial elements in the water balance cycle in mountainous environments and sensitive indicators of climate change.

Each component of the cryosphere plays a specific role in the Earth’s ecosystem, and each change impacts several areas. Melting ice sheets and glaciers influence rising sea levels, and their melting alters marine ecosystems. Similarly, melting sea ice can alter general ocean circulation and marine ecosystems in terms of productivity and biodiversity. In climate terms, the reduction of the snow-white reflective surface increases global warming by reducing the earth’s albedo and promoting ice-albedo feedback. The thawing (and subsequent decrease) of the permafrost damages the delicate balance of the subsurface, changing the carbon cycle by increasing the release of methane into the air. (IPCC, 2013,2017)

In the European Alps, an increase of 0.3°C in air temperature on average per decade has been observed (IPCC, 2018), varying between the seasons, with more marked increases in summer and spring (Auer et al., 2007; Ceppi et al., 2012). This discontinuity of variation is also observed at a global scale in different elevations, as warming phenomena are generally enhanced above 500 m above sea level (e.g., Wang et al., 2016a; Qixiang et al., 2018). On the contrary, there is no uniform trend on a global scale for high elevations. An

observable trend clearly highlights the continuous decline in the mountain cryosphere: the European Alps have lost 54% of their ice area since 1850, and this trend is expected to continue. Projections indicate that, following this trend, around 4-13% of the original ice area will remain by 2100. (Rasul, et al., 2020) In recent decades, the snow line has crept upward, and snow cover days continue to diminish. The Representative Concentration Pathway 8.5 of the AR5 IPCC (Intergovernmental Panel on Climate Change) report predicts an 80% loss of the current mass of the European glaciers (Core Writing Team, 2014).

Snow cover is a key aspect in the glacier equilibrium because it is the most common component, and it helps the thermal regulation of the glacier by reflecting heat and shielding the ice, protecting the deeper layer from melting. Snowy precipitations are very sensitive to climate change, and they are characterized by severe fluctuation over the years and the decades. As the snow line shifts upward, liquid precipitation will be more frequent at low elevations. This will lead to a general rise in melting and, consequently, to the activation of forcing mechanisms connected to air temperature. Snow and, more generally, glacial areas are essential to the Earth's energy balance with their whiteish colours that interact with the Albedo effect, increasing reflective surfaces and reducing the absorption of the incoming solar radiations. The increase in temperature, and consequently, the reduction of the snow cover, leads to a reduction of the Albedo effect with the rise of radiation waves that increases the Earth's surface temperature by up to 2 degrees locally. This dramatic forcing feedback is less clear at lower altitudes where aerosols and particulate matter scatter waves and mitigate the effect but more pronounced at high altitudes. Moreover, the deposition of dark particulate matter such as dust and black carbon due to pollution will further increase melting by decreasing the reflectivity of the remaining snow and accelerating snow cover reduction. These feedback mechanisms are also important for permafrost in mountainous areas because of the carbon dioxide contained under it, which could consequently be released into the atmosphere.

The glacier types give different responses to climate change.

Due to rising temperatures, the Equilibrium Line Altitude of a glacier initially set to a certain height (ELA1) goes upward (ELA2) (Figure 2). This leads to an increase of melted snow and to a smaller accumulation area. With the passing of time, the glacier responds with the adjustment of the ELA, which becomes a different shape depending on the type of glacier. While small glaciers tend to disappear completely, mountain glaciers reduce their thickness, and valley glaciers lose their tongues.

For example, glaciers that are shallowly sloping with long tongues in valleys, such as in Alaska, Canada, and the Alps, reduce their mass, responding slowly to climate change-driven readjustment. This leads to a strong thinning of the glaciers, with the result that they retain their initial appearance even with heavy losses in mass. In contrast, small,

typically mountainous glaciers are quicker to adjust to climate change and reshape themselves by increasing their ablation area more quickly IPCC (Vaughan, et al., 2013).

For the European Alps, it seems that the industrial revolution was the key element in causing the retreatment of alpine glaciers, not due to climate change which became evident later, but because levels of black carbon soot increased. Despite the rise of temperatures and diminishing precipitation, the alpine glaciers increased their mass until 1910. However, the soot started to cover the snow from the late 1950s, decreasing the albedo and consequently accelerating the melting of the snow due to the increased solar radiation it received (Painter et al., 2013).

The evolution of the modification of snow cover is now being investigated in climate models, but it's clear that the increase in rainy precipitation in the alpine areas and the continuous increase in the temperature trend led to a 25% decrease in snow mass. In the

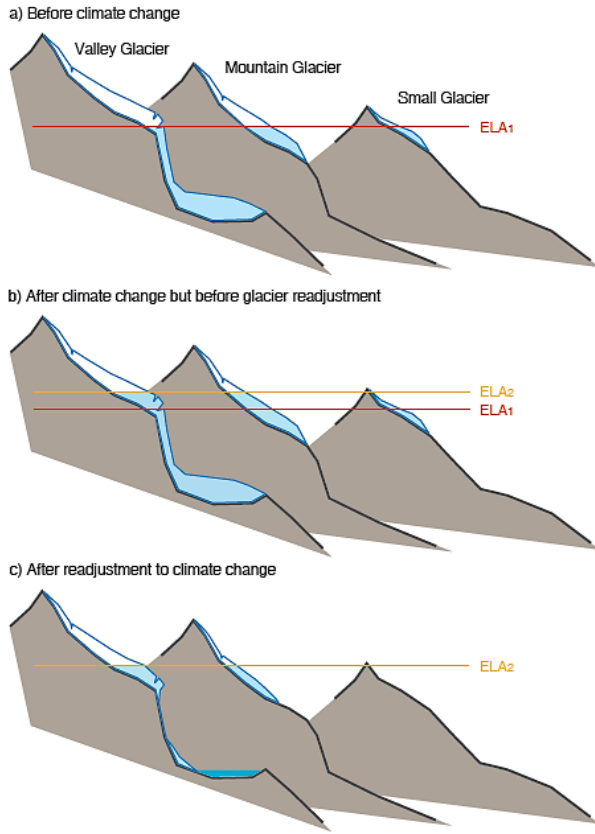


*Figure 2 IPCC AR5, Schematic of three types of glaciers located at different elevations, and their response to an upward shift of the equilibrium line altitude (ELA).*

IPCC scenarios, the prediction of reduction in snow cover is from 30% RCP 2.6 to up to 80% in the RCP 8.5 by the end of 2100(Figure 3).

The glacier extent covers an area of around 250 000 km<sup>2</sup> (except Antarctica, Greenland Region and Canadian and Russian Arctic) displaced in quite all regions of the world with different climate features. The evolution of a glacier, as said before, depends mainly on the balance between the accumulation and ablation of snow, and the temperature response of the glacier area is caused by atmospheric warming, an increase in longwave radiation, and changes in air moisture. Atmospheric warming is the main driver of the recession of glaciers worldwide, and the increase of greenhouse gases caused by human activities plays a big role in it (Marzeion et al., 2014).

Studies clearly show the high probability of a considerable loss of ice mass for all polar and high mountain regions (Figure 4). The IPCC 2100 projections underline the biggest impacts on mass losses in the regions where glaciers are small, like the situation of the European Alps.

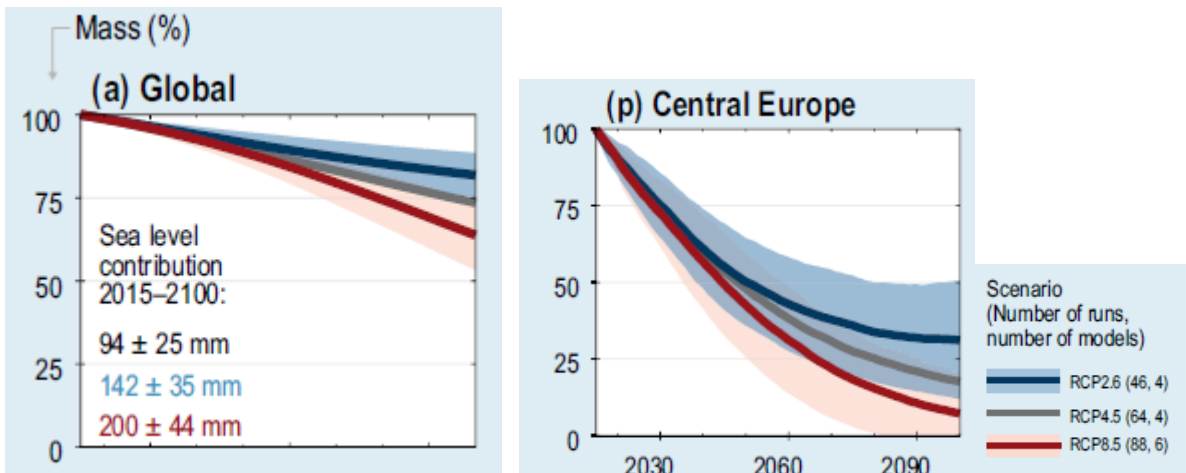


*Figure 3 Projected glacier mass evolution between 2015 and 2100 relative to each region's glacier mass in 2015 (100%) based on three Representative concentration pathways. (IPCC)*

A similar concept, not explored here, also applies to the modification of permafrost mass, lake and river ice, and all ecosystems connected to them.

Changes in this equilibrium may have multiple consequences for vulnerable mountain ecosystems and the people who live in them. Glaciers, and more generally, the whole cryosphere, regulate water resources for more than 600 million people worldwide, for the mountains themselves, and downstream regions. It is used for hydropower production, freshwater supply for agriculture, and for domestic and industrial use. Every change in the cryosphere balance can impact and even harshly modify both the human population and ecosystems.

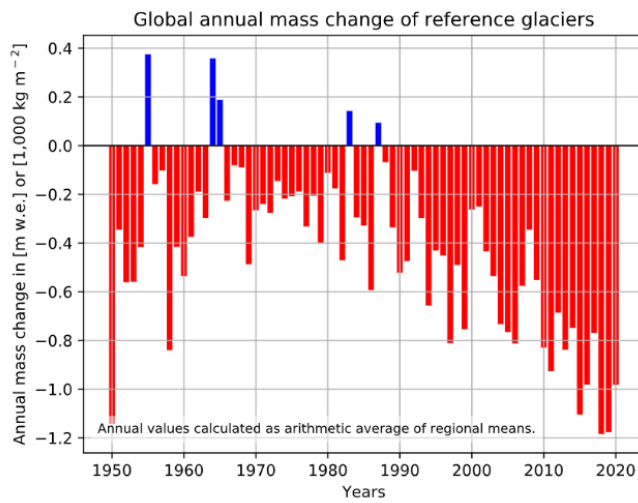


*Figure 4 World Glacier Monitoring Service (WGMS), Annual mass balance of reference glaciers with more than 30 years of ongoing glaciological measurements*

The melting of the glaciers, ice caps, ice sheets, and the cryosphere, in general, leads to rising sea levels. A clear estimation of the rise due to melting of big ice masses (due to global warming) is still the subject of numerous studies on the accurate estimation of mass balances, but it seems they account for 30% of the modification of the sea level during the last century. (NSIDC, 2015)

Moreover, the cryosphere, especially in alpine areas, is connected to the socio-economic livelihood of the mountain population and tourism-dependent communities.

Furthermore, the decrease of glaciers also impacts water quality due to the intensifying of anthropogenic pollutants that affect the ecosystems present downstream. It will also change the hydropower production both due to the change in runoff and the release of sediment and debris due to melting. Concerning agriculture, snow reduction led to changes in soil moisture in some areas and to changing water supply levels for irrigation. This, combined with the increase in temperature, may lead to the emergence of higher altitude crops.

Water security is an evident consequence of climate change in mountainous areas. Decreased water security combined with an increasing population, and thus increased demand for drinking water, will have huge consequences from the small scale to the regional scale, especially with the increase of dry periods.

Lastly, it's important to consider the increase of occurrence of natural hazards, landslides, avalanches and flooding strictly connected to the modification of areas formed eras ago and may become unstable slopes. For example, in the European Alps, for years, the debris flow fulfilled the glacier fronts, with the accelerating of melting and the increase of transport sediment, this can lead to an increase of instability of slopes and landslide occurrence. Moreover, unprecedented heatwaves in the high mountains can trigger melting and detachment phenomena from steep walls.

*'There is high confidence that the exposure of people and infrastructure to cryosphere hazards in high mountain regions has increased over recent decades, and this trend is expected to continue in the future (IPCC 2021).'* The increase of rainy precipitation will lead to an increase in wet snow and consequently an increase in avalanches, the increase of snowmelt will cause an increase in glacial lakes, an increase in flow, and possible avalanches in periglacial lakes with the possibility of floods are only some of the possible problems connected to the melting of glaciers. Furthermore, it is important to consider the economic importance of mountain areas in terms of tourism and economic spin-off. The European Alps are involved in the largest winter tourism and ski industry that depends mainly on atmospheric and snow conditions. Even if in recent years the ski resorts are increasingly engaged in proposing tourism that is not strictly related to skiing, the highest revenue still comes from the winter season and its related activities. Entire mountain communities depend on winter tourism and, especially in Alpine regions, temperature increase scenarios of 2°C would lead to considerable economic losses with a consequent general increase in costs and serious financial risk.

Not least, changes in the cryosphere create a loss in cultural values and human well-being all over the world. This is the case, for example, if the small island states in the Arctic region, the small indigenous communities of Annapurna Conservation Area of Nepal, but also small village inhabitants of the Italian Alps that have their cultural identities in the mountain environments will have serious damages connected to modification of mountain environment due to climate change.

Moreover, 46 out of the 247 UNESCO World Heritage natural sites include glacier areas, and 8 of these sites will be gone by 2100, according to both the 2.6 and RCP 8.5 projection scenarios. (IPCC, 2017,2021)

Unlike numerous other environments, the mitigation options are set only to reduce hazards caused by an increase in temperature, but adaptation options in this sector are not well

developed. They are mostly autonomous modifications of communities that, for example, modify the agricultural production and change the water management, but which may be insufficient over long periods.

Climate change in glacial environments will lead to an increase of cryosphere hazards and to a complete change in the balance, ecosystems, and habits of the populations that interact with them. Monitoring glaciers is one of the first steps towards mitigating and adapting to these new balances to protect population and biodiversity in these vulnerable areas.

## Chapter 2

# Valle d'Aosta glaciers: Rutor and Indren Glaciers

### 2.1 Valle d'Aosta glaciers

Situated in the northwest of the Italian peninsula, Valle d'Aosta is the least extensive region in Italy. Its territory is characterised entirely by the Alps, which reach their highest peaks in its territory. More than 30% of its territory exceeds an elevation of 2,500 m above sea level, which means that glaciers and periglacial environments are the main surroundings. Valle d'Aosta hosts 192 glaciers that with its 132.90 km<sup>2</sup> are the major snow-covered area in Italy. Small and medium glaciers characterise the Valle d'Aosta region, in fact in the 2-5 km<sup>2</sup> and 5-10 km<sup>2</sup> classes we can organize 55% of the region glaciers.

According to the Italian Glaciological Committee, every year since 1913, Italian glaciers have been monitored using strain-net networks estimating the distance from ground control points. (Villa, De Amicis, Maggi, 2007)

The Valle d'Aosta glaciers were monitored in 1975, 1999, and 2005 with coloured orthophoto digitized by hand used to determine the glacier borderlines.

Three different stations at different altitudes exist for recording meteorological data for Valle d'Aosta, with recorded data from 1975 to 2005 for Brusson (BR, 1332 m asl, Valtournenche (VT, 2526 m asl) and Pian Rosa (PR, 3488 m asl).

In the period between 1975 and 2005, the Aosta Valley Glaciers lost 44.3 km<sup>2</sup>; the small glaciers range wider area lost due to different altitudes of the glaciers and of the mountains that host them and much variability on their ELA (Equilibrium Altitude Line). A sensible reduction for glaciers of the region is estimated roughly at 27% in the period considered with a similar trend of the other Italian glaciers. However, it is evident that this reduction has substantially accelerated in the last few decades due to climate (Diolaiuti, et al., 2012).

	1850	1975	2000	2005
Volume (km <sup>3</sup> )	200	105	75	65
Relative volume change (%)	-	-47.5	-28.5	-12.5
Change rate (% decade <sup>-1</sup> )	-	-3.8	-11.4	-25.0

Table 2 Ice volume in European Alps and change, 2006 (Haeberli, et al., 2021)

During the Italian Glaciological Committee 2019 measurement campaign, 51 of the Valle d'Aosta glaciers were retreating (94% of those measured), 3 were stationary, and 0 glaciers were advancing. The snout fronts were similar to the previous year computed with some more dramatic situations. Another evaluation enhanced, there is a general increase of debris and sediment on the glaciers, a clear signal of their retreat. In the as-yet-unpublished data provided by ARPA Valle D'Aosta, 41 glaciers have been lost in 20 years, from 216 in 1999 to 184 in 2020, with a surface reduction of 16 km<sup>2</sup> per year.

In Italy, according to ARPA Valle D'Aosta (Agenzia Regionale Protezione Ambiente, or the Regional Agency for Environmental Protection), glaciers are monitored in several different ways:

- Organized regional monitoring activities on glaciers with mass balances: changes in the mass of a glacier are measured as the difference between the snow accumulated in winter and the mass lost through ablation in summer. The mass balance is expressed in millimetres of water equivalent and is estimated as an average value considering winter accumulation (generally checked in spring, at the end of May) and summer melting at the end of September. Accumulation is calculated by measuring the height of the snow and its density, while ablation is measured by inserting small-diameter aluminium rods into the snowpack
- Measuring mass balances of selected glaciers with the Secure Mountain Foundation (Fondazione Montagna Sicura)
- Measuring snout retreat: by taking a fixed reference point, it is possible to estimate the retreat of an ice front by measuring the distance between this point and the front and repeating the measurements over time, either in the field or using aerial images.
- Thickness measuring: unlike mass balances, the thickness of a glacier is more complicated to estimate. In order to take measurements, it is necessary to cross the glacier, either on foot or by helicopter, and to estimate the thickness indirectly by georadar, thus estimating the properties of the subsurface materials and the thickness of the ice.

All these measurements allow glaciers to be monitored and the impact of climate change on them to be estimated over time.

## 2.2 Rutor glacier

Rutor glacier is a glacier located in the north-western part of the Italian peninsula on the Italian French border (as shown in Figure 5), and with a surface of 8.4 km<sup>2</sup>, it is Valle d'Aosta's third largest glacier after Miage e Lys glaciers. It is also called 'Rutor' or 'Rhutor' and it derives its name from French-Provençal language '**Ru**' that means small river and '**Tors**', which means arduous to underline a path made of rocky jumps, levels



Figure 5 Google Earth, Rutor geographical overview

and precipices of the watercourse. It is 4.68 km long and extends from 2540 to 3486 m (head of the Rutor) above sea level (a.s.l.)

The extension of this glacier is from north to west with a quite regular shape without steep slopes, and it decreases from the peak to the lake's areas. The glacier is split by 'Vedrette del Rutor' peaks into two main parts. The glacial front is divided into three lobes by rocky areas and surrounded by moraines consisting of glacial deposits.

The glacier is characterised by a system of glacial lakes and cavities filled with sediments that have formed over the years. The New Lakes, Lago Marginale and Lago Superiore are lakes formed as proglacial lakes after the retreat of 1950 and fed by the meltwater of Rutor. These lakes are characterised by different colours due to varying percentages of silty sediments in the inland water. Lake Santa Margherita, of which only evidence of a peat bog remains today, is a wide depression at an altitude of 2400 m above sea level that extends perpendicularly to the glacier.

After 1820, the glacier front gradually receded and Lake Margherita underwent a process of emptying, slowly lowering its level by about ten metres.

During the Little Ice Age, Rutor had an immense extension and extended up to 2150 m a.s.l. until the Lac Du Glacier above La Thuile. The Lac du Glacier, now partially filled with sediment and in the past larger in size, extends over the plain known as the Plan de la Lière at 2145m above sea level. At the end of the plain, two moraine arches mark the boundaries Rutor's maximum extent during the Little Ice Age. The Rutor glacier has

retracted more than 2 km since the end of the Little Ice Age in the mid-19th century and till the 90s seems to have lost about 480 million cubic meters of ice.

The Rutor has been the subject of numerous floods, the most problematic and destructive of which are reported to have occurred between 1594 and 1598, several in the 17th century and two events in 1751 and 1752, but not all events have been documented as they were repeated annually. Some of these events occurred at the same time as regional flood events, such as the one in 1640 which also caused the flooding of the town of Aosta (Bonetto, 2015).

Numerous mass changes caused by violent floods have been documented (Bonetto et al, 2014). The floods were caused by the glacial tongue, which prevented the water from flowing into Lake Santa Margherita, and as the water pressure increased, the rock face collapsed, and flooding ensued. The last glacial flood took place in September 1864. In Figure 6 are reported some modifications of the glacier during the years.



Figure 6 Perretti-Charrier, La Thuile, Paesaggi geologici e storici

*“From 1975 to the present, another 50% of the remaining volume was lost. This calculates to a volume reduction rate of  $-0,5\% \text{yr}^{-1}$  from its maximum size during the Little Ice Age to 1975, a value of  $-1,1\% \text{yr}^{-1}$  between 1975 and 1991, and a volume reduction rate of  $-2,1\% \text{yr}^{-1}$  until 2006.<sup>7</sup>* (Figure 7)

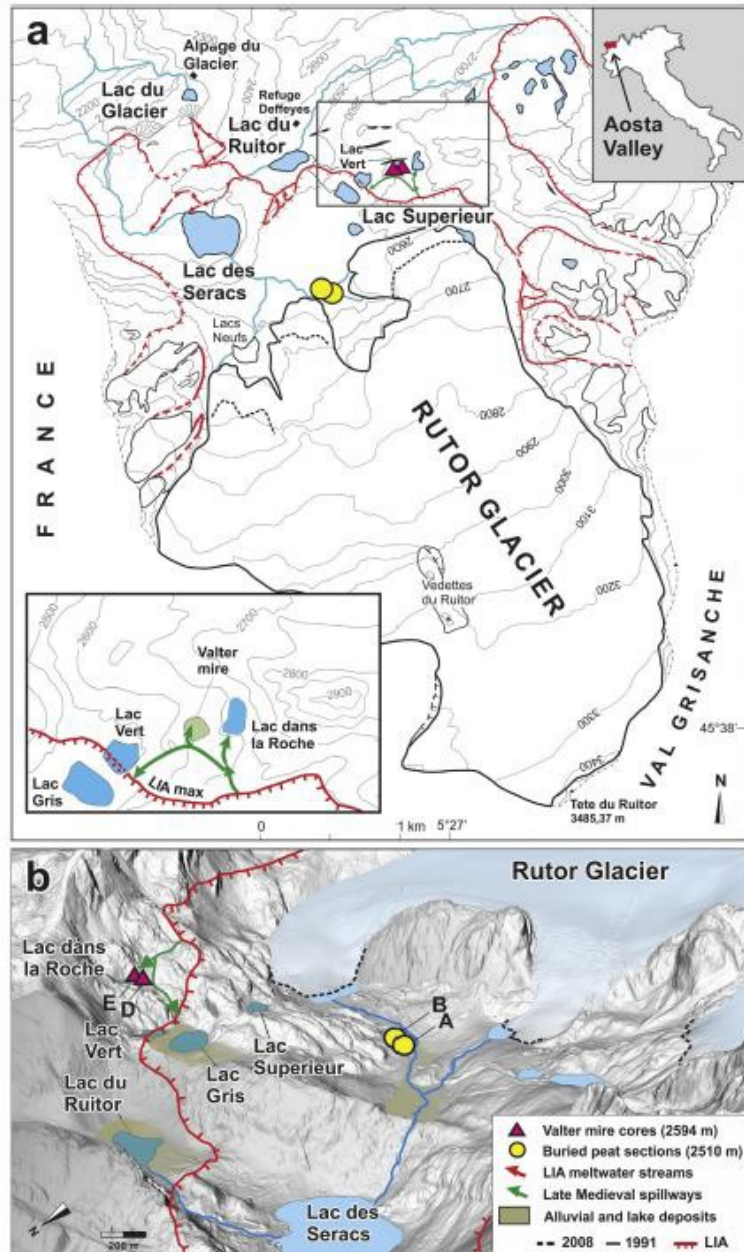


Figure 7 8800 years of high-altitude vegetation and climate history at the Rutor

<sup>7</sup> (Villa, et al., 2008)

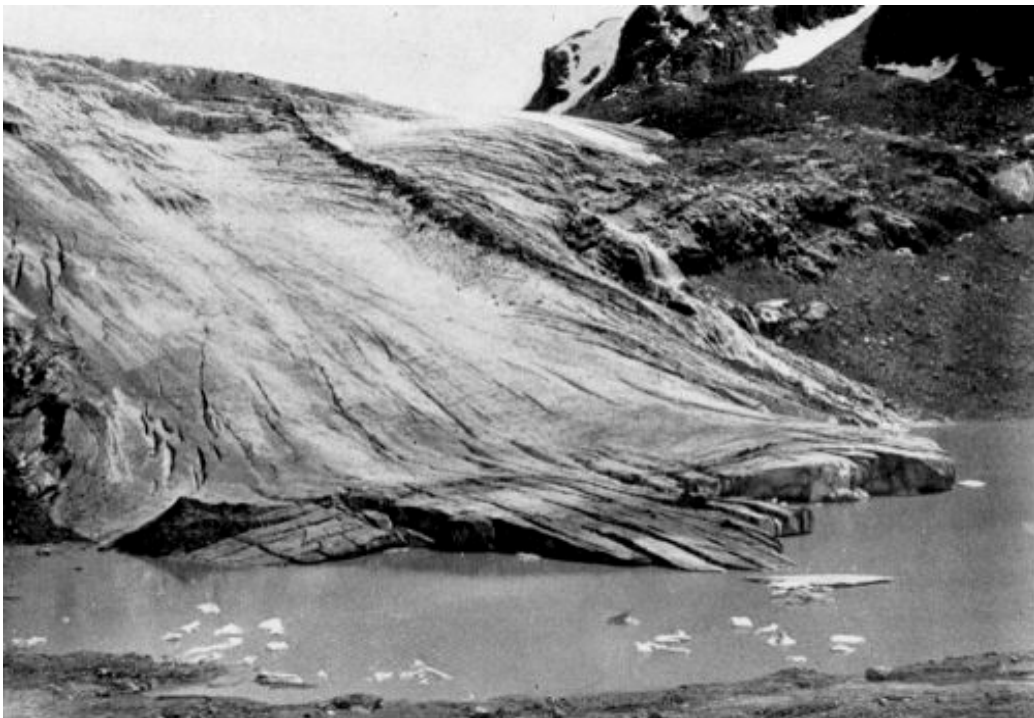


Figure 8 Rutor Serac Lake 1909

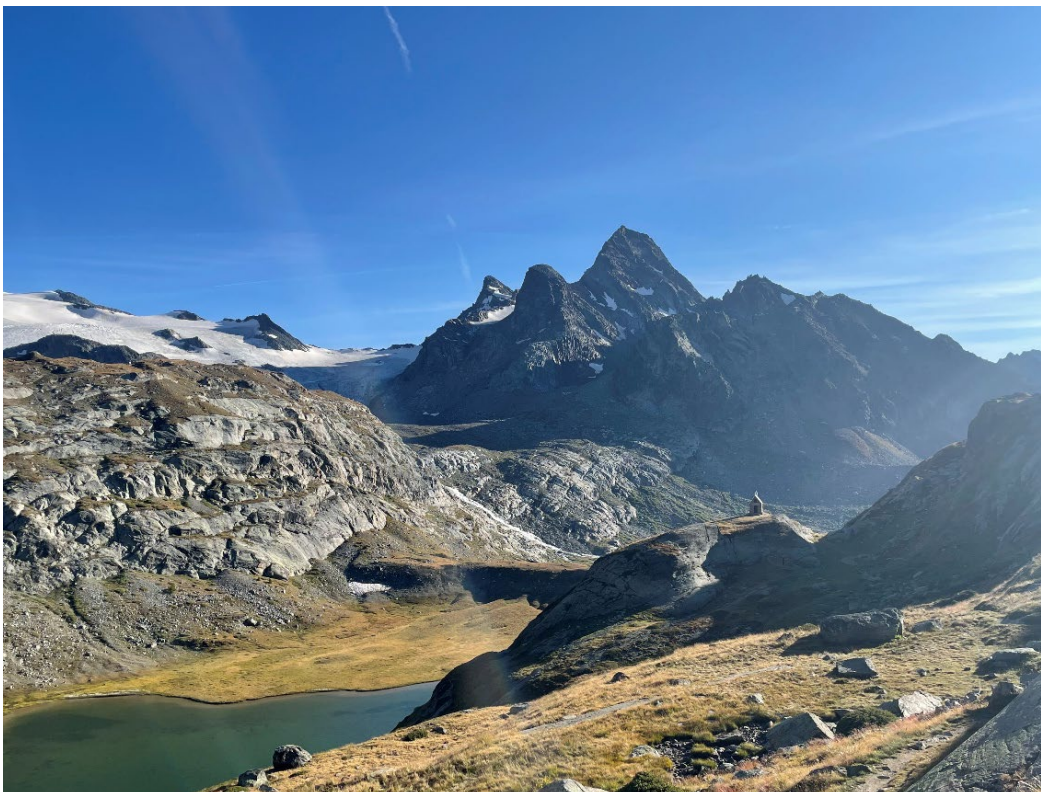


Figure 9 Photo of summer 2021



Figura 11 Brocherel, Rutor 1909



Figure 10 Rutor Glacier on summer 2021



Figure 12 Rutor 1926 Archivio storico



Figure 11 Rutor July 2021

## 2.2.1 Studies on the Rutor glacier

The position of the Rutor glacier has been monitored since 1916, but more regular surveys started in 1948. In 1917, 1928, and 1934 were published topographic surveys were published from Sacco, Bossolasco, and Peretti, respectively. In 2005 a work that reconstructs the Little Ice Age extension of the glacier was published by Orombelli. In 2007 a cartographic analysis was published based on a topographic map and morphological reconstruction (Villa et al., 2007).

In 2006 and 2008, GPR (Ground Penetrating Radar) and GPS surveys were performed both to correlate the data spatially and create a surface model (Villa, Tamburini, et al.). In comparison with the previous surveys, it was possible to reconstruct the volume of the glacier from the Little Ice Age to 2006. Data are reported in Table 3

Year	Volume	$\Delta$ Volume	$\Delta$ Volume / year
Little Ice Age	$690 \times 10^6 \text{ m}^3$	-	-
1975	$269 \times 10^6 \text{ m}^3$	-61%	$-0.5\% \text{ yr}^{-1}$
1991	$222 \times 10^6 \text{ m}^3$	-17%	$-1.1 \text{ yr}^{-1}$
2006	$150 \times 10^6 \text{ m}^3$	-31%	$-2.1 \text{ yr}^{-1}$

Table 3 Villa, Tamburini et al., Volume reconstruction of Rutor Glacier

The volume of the Little Ice Age is estimated through a morphological reconstruction, the 1975 and 1991 model is done by 1:10000 cartography, and the most recent 2006 is modelled thanks to data from the GPS survey, showing a significant reduction of the volume, about 75%, from the first period evaluated (Villa, Tamburini, et al., 2006).

In the 2007 work, the traditional methods are integrated with the GIS method to evaluate the volume modifications. The boundaries of the glacier were reconstructed according to different historical cartography and maps of different authors. From the data estimated, the glacier clearly shows a steady retreat except during the countertrend periods of 1916-1926 and 1975-1988 (Villa, et al., 2007).

Year	Surface Area	Variation %	Cumulative variation %
LIA	$12,47 \times 10^6 \text{ m}^2$	-	-
1864	$12,25 \times 10^6 \text{ m}^2$	-1.77%	-1.77%
1905	$10,757 \times 10^6 \text{ m}^2$	-6.71%	-13.74%
1926	$10,645 \times 10^6 \text{ m}^2$	+0.25%	-14.64%
1930	$10,529 \times 10^6 \text{ m}^2$	-0.97%	-15.57%
1954	$9,420 \times 10^6 \text{ m}^2$	-10.04%	-24.47%

1975	$9,123 \times 10^6 \text{ m}^2$	-0.86%	-26.83%
1988	$9,202 \times 10^6 \text{ m}^2$	+0.86%	-26.21%
1991	$9,110 \times 10^6 \text{ m}^2$	-1.00%	-26.95%
1998	$9,076 \times 10^6 \text{ m}^2$	-0.35%	-27.22%
2000	$8,794 \times 10^6 \text{ m}^2$	-3.19%	-29.48%
2004	$8,569 \times 10^6 \text{ m}^2$	-2.61%	-31.29%

Table 4 Villa, De Amicis, Rutor glacier surface variation between LIA and 2004

The morphological evolution of the surface was also elaborated, and it enhance the loss of mass everywhere with more evidence in the lower part of the glacier.

An interesting analysis was computed on the Equilibrium Line Altitude (ELA) that increased from 2775 m during the LIA to 2850 m in the 80s, a period in which the glacier advanced slightly. From the 1990s onwards, the juggernaut continued its retreat, increasing its speed considerably in recent years.

In 2018 deep research in the stratigraphy of the glacier was developed to reconstruct the climate variations and modification in vegetation and glacier extension from the Late Holocene until recent years. It was highlighted that during the middle Holocene, the glacier was in a contraction phase, and then with a decrease of 1.8 °C, the glacier regime changed. Before the Middle Ages, human activities in the glacier area are negligible, even if they are present since the Iron Ages (Badino, Ravazzi et al,2018).

The ARPA Valle D'Aosta in cooperation with CC-Glacier Lab of Politecnico of Turin monitor the glacier continuously since 2020.

## 2.3 Indren Glacier

The Indren glacier is located in the Northwest part of the Italian Alps (Figure 13), in the southern part of the Monte Rosa massif and extends between Piramide Vincent and Punta

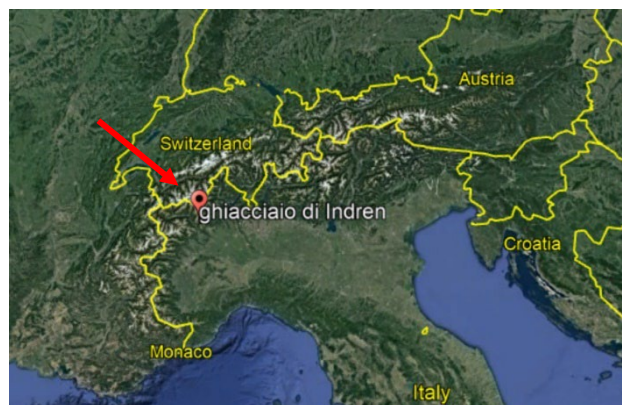


Figure 13 Google Earth, Indren glacier

Giordani, 4215 and 4046 m respectively. Monte Rosa massif is on the wider mountain areas of the Alps and backdrops the Gressoney Valley.

The Indren glacier has an average temperature of -2.3°C, and a snow cover from early October to July, with the main accumulation of snow being around 818 cm yearly and 400 mm of rainy precipitation. The massif area is involved in tectonic and erosional processes, and it hosts considerable geological and geomorphological diversity, thanks to basins and periglacial lakes (Tognetto, 2021).

Even if it is a high mountain area, human influence is present: the meltwater of the Indren glacier is involved in hydroelectric power production. The area is full of people and tourists all year long due to the ski resort of Monte Rosa station and various trekking routes.

The Indren glacier (Figure 14) is monitored by ARPA Valle D'Aosta, and since 2007 regular monitoring for mass balances has been carried out. The Indren glacier covers an area of 0.92 km<sup>2</sup> with a steeper upper part of accumulation that slopes down to a medium slope in the lower part.



Figure 14 Indren glacier, July 2021

The area of the glacier is fragmented, and the ablation zone is characterized by lots of crevasses and surface drainage thanks to different small rivers that go into a proglacial lake outflow by a narrow torrent (Freppaz, 2021).

An abrupt change of slope at about 3800 metres leads to a hanging serac, which causes frequent avalanches.

Indren is monitored as described above with an estimate between snow accumulation in winter and ablation in summer, with measurement campaigns in spring and late summer. Snow accumulation is estimated over the entire glacier surface by measuring snow thickness and density at some points, while for summer, ablation measurements are made at ablation posts at points in different sectors of the glacier. In the Italian Glacier Registry (Catasto dei Ghiacciai Italiano), it is identified as n. 306, and in the last measurement, its fluctuation was equivalent to -4m of water and the snout elevation is at 3091 m asl.

<b>Year campaign</b>	<b>Change [m]</b>	<b>Front Elevation</b>
1985-1986	-16 (1970-1986)	3155
1988-1989	-14 (1971-1989)	3180
1989-1990	-12	3180
1993-1994	-7 (1990)	3060
1996-1997	-4 (1994)	3060
1997-1998	-19	3060
1998-1999	-5	3060
2002-2003	-9 (2000)	3089
2003-2004	-1	3089
2004-2005	-3	3089

*Table 5 Front altitude (Comitato GLaciologico Italiano)*

As with other Alpine glaciers, the glacier mass is steadily decreasing, and despite winter accumulations, summer melting continues to result in a loss of thickness. Data on the front elevation and change of the glacier are reported in Table 5 and photo comparison on Figure 15 and 16.

The Indren glacier is also the focus of ARPA's radiometric analysis of cryoconite. Cryoconites are airborne dust deposits that settle on the glacial surface. By reducing the albedo of the snowpack, this dust increases the absorption of solar radiation, accelerating the melting of the glacier (Morra di Cella, 2021).



sciovia sul ghiacciaio di Indren (m. 3150-3350) - sullo sfondo: Stazione Funivia (m. 3260) - Piramide Vincent (m. 4215)

Figure 16 Indren glacier in the 60s source: meteobook.it

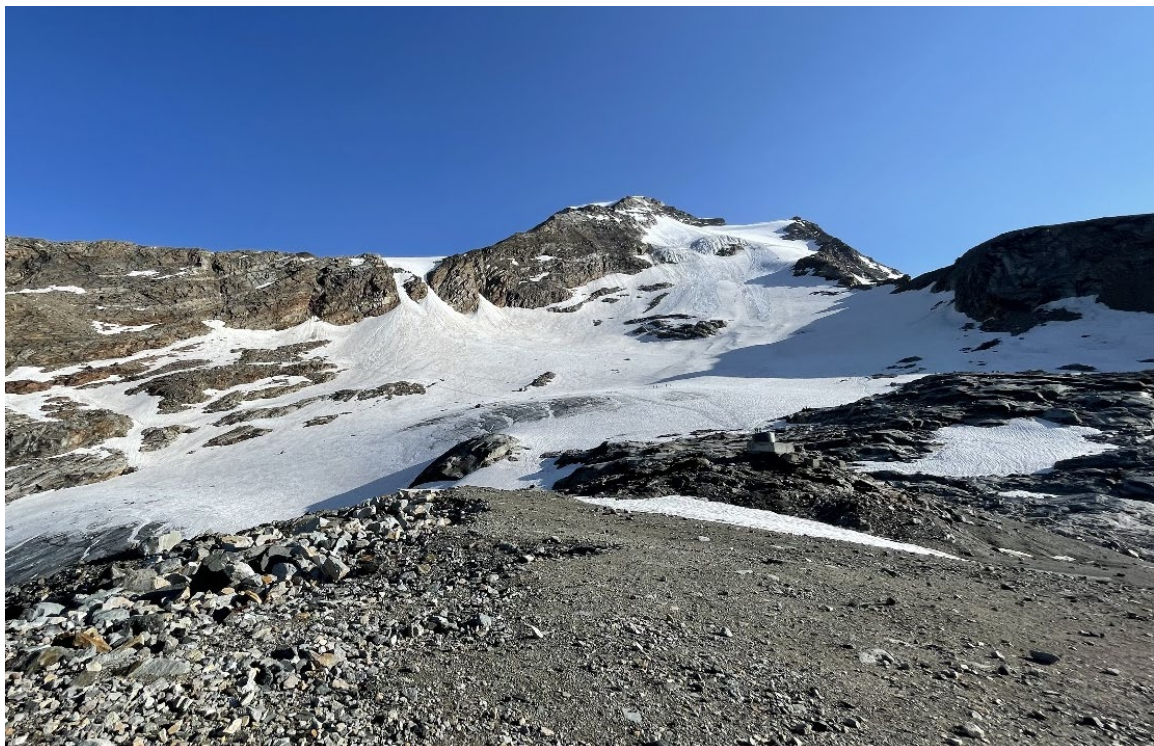


Figure 15 Indren glacier summer 2021

# Chapter 3

## Glacier monitoring techniques

Glacier monitoring techniques are usually developed in different phases. A preliminary programming phase is necessary to understand areas to be monitored, plan the activities, the instrument and the goals. Different monitoring techniques can be chosen by analysing the extension area and the accessibility of the places to be monitored. Generally, the high-mountain environment and in particular the glacial surface is characterised by uneven paths that can only be reached on foot or by helicopter, with considerable difficulty and cost. For these reasons, a valuable tool for monitoring a glacier is photogrammetry.

In the two cases examined, the conditions of accessibility are diametrically opposed. The Rutor glacier can only be reached by a two-hour footpath to the Deffeyes refuge and then another half hour to the glacial front, or by helicopter, making the transport of materials and tools tiring or expensive.

The Indren glacier can be reached directly from Gressoney via two successive cableways, allowing easy transport of people and instruments.

### 3.1 Photogrammetry, hints of theory

Photogrammetry is a science that, through the acquisition and processing of data and their subsequent interpretation, enables the measurement and obtaining of three-dimensional information from them without having physical contact with them. Photogrammetry is based on the concept of central perspective, which consists of the transformation of three-dimensional reality into a two-dimensional product employing a geometric transformation through a mathematical model. In fact, it is possible to construct a straight line between a point on the image, the point and the centre of grip O and the corresponding point A. The lines are called projection rays. Considering the same point in at least two central perspectives makes it possible to estimate its position in three-dimensional space.

When at least two different frames with two different acquisition centres of one object are considered, the lines connecting the same point with the frames and the two respective centres are called **homologous rays** and the points, homologous points.

It is possible to establish two types of orientation

- an **internal orientation** is given by the parameters  $\xi_0$ ,  $\eta_0$  and c which allow the geometry within the frame to be characterised and to restore the projectivity.  $\xi_0$ ,  $\eta_0$ , are the coordinates of the perspective centre in the 2D internal coordinate

system;  $c$  is the so-called **principal distance or focal length** and is the distance between the centre of the camera and the frame.

- an **external orientation** consists of estimated rototranslation parameters that allow estimating the position and attitude of the take point of the camera in three-dimensional space thus restoring the set-up of the catch. The external orientation can be estimated by considering 6 different parameters, 3 rotations and 3 translations and they usually are the coordinates of the perspective centre  $O (X_0, Y_0, Z_0)$  in the internal reference system and the three angles ( $\omega, \phi, \kappa$ ) of rotation around each axis in the time of acquisition.

The external orientation consists of two steps, **relative** and **absolute orientation**. The purpose of relative orientation is to cross pairs of homologous rays. It is generally done by collimating 6-8 spatially well-distributed homologous points (at least 6, but generally 12 and more, well distributed). To superimpose the model on the terrain, the rototranslation parameters are determined and the absolute orientation is determined. In this way, the model previously linked to its reference system is oriented, georeferenced and at the correct scale.

The image coordinates ( $\xi, \eta$ ) and the ground coordinates of the object represented ( $X, Y, Z$ ) are linked by a set of equations called **collinearity equations**.

$$\xi = \xi_0 - c \frac{r_{11}(X - X_0) + r_{21}(Y - Y_0) + r_{31}(Z - Z_0)}{r_{13}(X - X_0) + r_{23}(Y - Y_0) + r_{33}(Z - Z_0)}$$

$$\eta = \eta_0 - c \frac{r_{12}(X - X_0) + r_{22}(Y - Y_0) + r_{32}(Z - Z_0)}{r_{13}(X - X_0) + r_{23}(Y - Y_0) + r_{33}(Z - Z_0)}$$

These equations are the frame coordinates dependent on external and internal orientation and the XYZ coordinates of the object should be represented (Figure 17).

$$X = X_0 + (Z - Z_0) \frac{r_{11}(\xi - \xi_0) + r_{12}(\eta - \eta_0) + r_{13}c}{r_{31}(\xi - \xi_0) + r_{32}(\eta - \eta_0) + r_{33}c}$$

$$Y = Y_0 + (Z - Z_0) \frac{r_{21}(\xi - \xi_0) + r_{22}(\eta - \eta_0) + r_{23}c}{r_{31}(\xi - \xi_0) + r_{32}(\eta - \eta_0) + r_{33}c}$$

Where:

- ( $\xi, \eta$ ) are the coordinates of a point in the image coordinates;

- $\text{PP}(\xi_0, \eta_0)$  called Principal Point are the coordinates of the point O on the frame plane;
- $r_{ij}$  are the rotation matrix;
- $c$  is the principle distance or focal length.

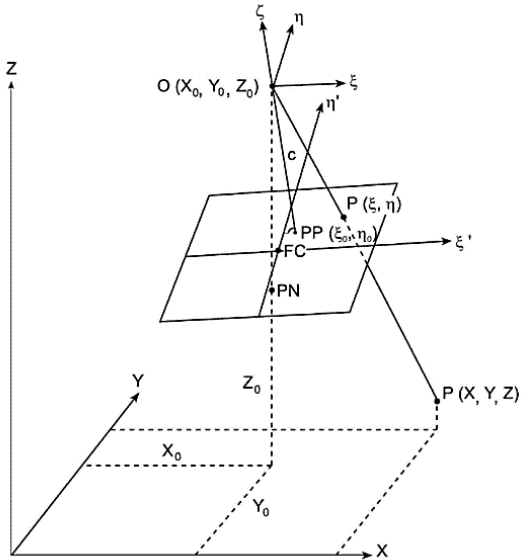


Figure 17 Coordinates relationship (Kraus, 1998)

When the relative and absolute orientation parameters are known, the coordinates of the homologous point are measured and through the collinearity equation, it is possible to measure the coordinates (X, Y, Z) of a point P.

The main steps of a photogrammetric process are:

- Acquisition of data phase, during which a two-dimensional image of the 3D object is acquired. It is necessary for reconstruction that the frames have a longitudinal coverage of at least 60% ( $>20\%$  transverse coverage, but today usually 60%).
- Selecting Ground Control Points to fix the reference system
- Orientation (internal and external):
  - Internal: to define the position of the projection centre utilizing the principal distance  $c$  and the coordinates of the point.
  - External: to define position and attitude parameters.
- Plotting phase: The product is restored to its true three-dimensional form during this process.
- Improving quality data with the integration and editing phase and comparing models obtained from different acquisitions.

In addition to the coordinates of the support points, it is also important to consider the coordinates of the camera centres. The frames are taken with an overlap of at least 60 per cent longitudinally and 60 per cent transversely. The collinearity equations can be used to calculate the relationships between the coordinates using the 'bundle adjustment' method (Figure 18 A,B).

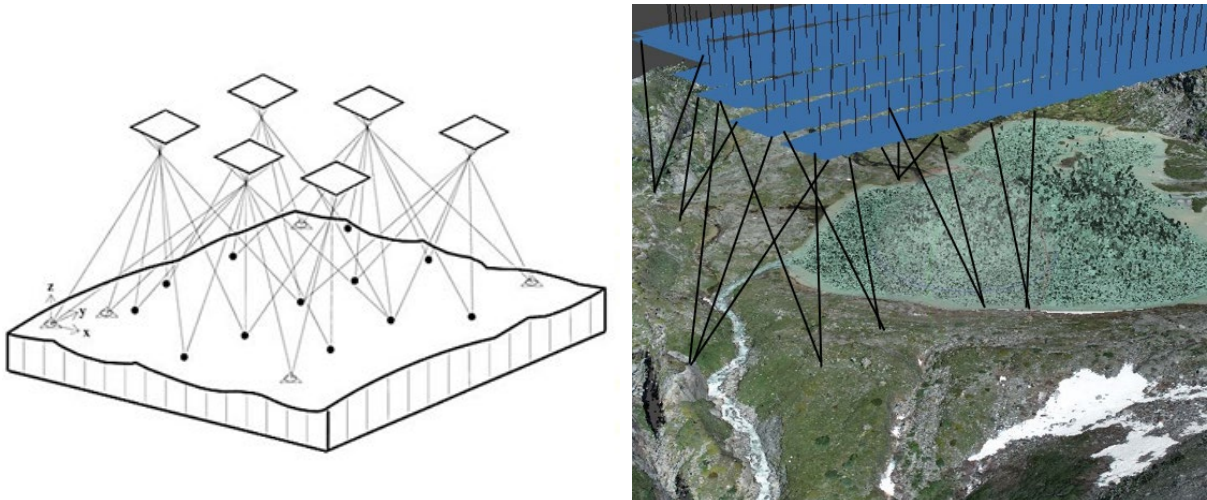


*Figure 18 A Bundle adjustment (Inghilleri, 1970)*

*B. Bundle adjustment on Metashape*

With a rototranslation operation, a closer match is achieved between the image coordinates of the Tie Points (TP) and the image and object coordinates of the GCPs. The aerial triangulation makes it possible to reduce GCP, allowing external orientation parameters to be obtained analytically from the same frames. It's important to consider not just the number, but also the distribution of the Ground Control Points. (M. Kasser, 2002)

### 3.2 Rutor monitoring campaigns and Ground Control Points

In order to proceed with the reconstruction of the photogrammetric model, the coordinates of points known as Ground Control Points (GCP) are required, which can be acquired in various ways. For both glaciers, Rutor and Indren, the position of the GCPs was surveyed using the Global Navigation Satellite Systems (GNSS) and different constellations.

Any position on the ground can be defined at any location on earth by sending signals with the satellite constellation. The position can be relative or absolute. The absolute positioning requires a long transmission between receiver and satellite and allows a metrical precision.

In the relative positioning, the receiver known point is called 'base', the unknown point to be determined is called the 'rover' and the vector between the two points is called the 'baseline'. The vector between the two points is determined, and the point's position is post-processed.

GPS positioning can be static or kinematic, the first requiring a stationary time on the point for several epochs. The kinematic positioning allows a centimetre accuracy with a short measuring time of less than one minute and centimetre accuracy.

Where possible due to network coverage, Network Real-Time Kinematic was used, but as is often the case in environments such as glaciers, this was not always possible. It was necessary to create 'base stations' to measure different points.

The Rutor glacier has been monitored by ARPA since 2005. Some points along the Rutor glacier were already set during the years. Still, the collaboration with the glacier lab polytechnic of Turin has resulted in a work aimed at monitoring the glacier and periglacial lakes in the lower and upper part during next years. To this end, GCPs have been set up in the proximity of the Serac lake in the month of July and then on the glacier above. After a preliminary analysis of the existing orthophotos, three measurement campaigns were carried out to determine the support points, two in July and one in September before the aerial photogrammetric flight.

- **First campaign 8-10/07/2021**

The positioning of the GNSS base station was placed in front of the Deffeyes hut on a vertex materialised with a DIATI100 (Figure 19) bolt and washer and coordinates were detected with the RTK network. The DIATI100 point was then used as a 'base' station to get the differential corrections at the other points not covered by the GSM signal. Twelve Ground Control Points were identified and marked with red paint on boulders, and markers were placed at some points later after photogrammetric drone flights. The GCPs identified (Figure 20) are numbered consecutively from 100.



Figure 19 Base station DIATI100

GNSS ‘base’ station DIATI100 – coordinates UTM ETRF2000 r RTK il 9th July 2021  
Est = 342979.659      Nord = 5059115.879  
h = 2621.306    H = 2567.337 pp: sommità bullone (N=53.969)

Hydraulic and hydrological activities were also carried out here and geophones were installed.

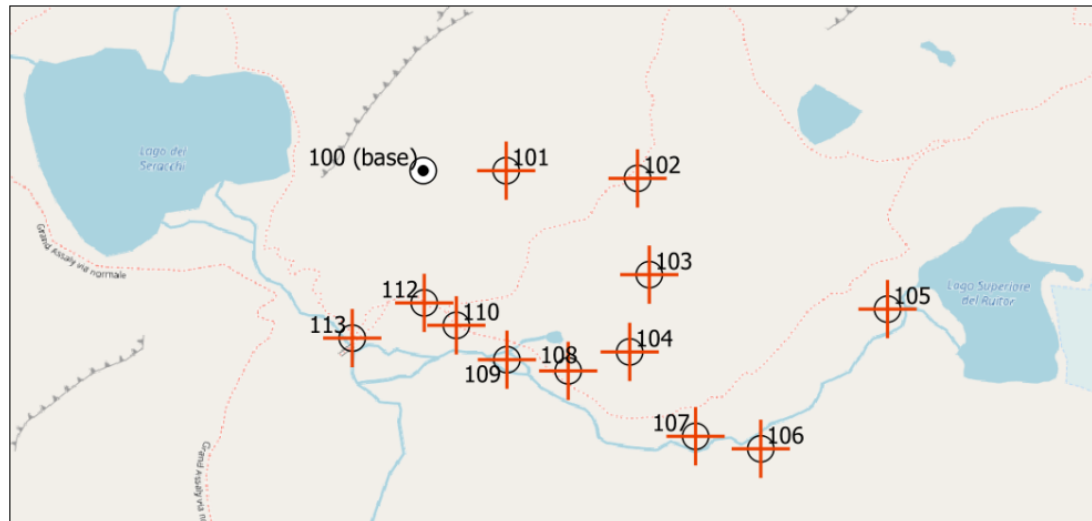


Figure 20 GCP first campaign

- **Second campaign 19-21/07/2021**

This campaign aimed to refine the GCPs around Serac Lake.

The second campaign, in which the writer also took part, was carried out by leaving on the morning of Monday 19<sup>th</sup> July from the Turin Polytechnic and then proceeding on foot from La Thuile to the Duffeyes refuge with equipment. Measurement operations began in the early afternoon.

On the 19<sup>th</sup> of July DIATI88 (Figure 21) point, materialised with bolt and washer, was used as a base to measure the serac lake with RTK mode. The coordinates of this point are detected with RTK (Real Time Kinematic) with centimetric precision thanks to the use of the GSM network using the ITALPOS network (ItalianPositioningService, s.d.).

Flow measurements were taken at the Serac Lake outfall.



*Figure 21 'Base' station DIATI88*

GNSS “base” DIATI88 - coordinates UTM ETRF2000 of RTK on 19th July 2021
---

Est = 342861.808	Nord = 5059729.085	h = 2557.756
------------------	--------------------	--------------

H = 2503.828 pp: sommità bullone (N=53.928)
---

*Table 6 DIATI88 coordinates*

The points selected on the raw orthophoto taken in the first campaign are reached and marked painted red. Each point is detected with RTK GNSS from the base station DIATI88. These points identified are numbered consecutively from 200.

On the 20th of July, using the DIATI71IDROMETRO point as the 'base' station, the hydraulic sections of the Serac Lake outfall were carried out (saved with progressive numbering from the number 2000) and the geometric levelling of the free surface of the lake was carried out after materialising the cornerstones with a 'DIATI71' washer (Figure 22).



Figure 22 DIATI71IDROMETRO base station

GNSS “base” DIATI71 Coordinate UTM ETRF2000 of RTK on 20 luglio 2021 ( $h_{\text{strum}}=1.136$  contrassegno antenna)  
Est = 342367.746      Nord = 5059296.364      h = 2442.075  
H = 2388.137 pp: sommità bullone (N=53.938)

Table 7 DIATI 71 coordinates

During this campaign geometric levelling (Figure 23,24,25 and 26) of the free surface of



Figure 24 Levelling the free surface of Serac lake



Figure 23 Levelling the free surface of Serac lake



Figure 25 Levelling the free surface of Serac lake

the Serac lake has been carried out, marking the cornerstones with a DIATI 17, 71,77 e 78 bolt and washer.

Within the hydraulic activities, RTK measured points with a 20 cm pitch were taken to reconstruct the section of the outfall of the Serac lake and on the upper lake, other points were taken to survey the trend of the stream bottom.



Figure 26 Levelling on Serac lake

Levelling was carried out with a Leica Na2002 level ( $\text{emk} = 2 \text{ mm/km}$ ) and a fibre stadia with braces, round trip to check the closure error and make a compensation. By bringing the foot of the staff to the free surface, the height was determined and at the same time the GNSS RTK recorded the position. Near point DIATI 78 (PELO3=0), the height of the free surface was equalled to zero, and the results of the line compensation were calculated Outward and return. Results are reported in Table 8:

<b>Station</b>	<b>Elevation [m]</b>	<b>St Deviation [m]</b>	<b>95%</b>
PELO3	0.0000	0.000000	0.000000
DIATI71	1.2000	0.002007	0.003934
DIATI77	0.6010	0.002849	0.005584
DIATI78	0.2074	0.002275	0.004460
DIATI79	0.1745	0.001855	0.003636
PELO1	0.0018	0.002140	0.004194
PELO2_IDROMETRO	-0.0240	0.002172	0.004257
PELO4	-0.0042	0.002950	0.005782
PELO5	0.0012	0.003331	0.006529

Table 8 Compensation calculated outward and return

The closing error between forward and backward level line on the DIATI71 terminal is 0.0003 mm. The only significant gradient was found in the vicinity of the PELO2\_IDROMETRO point, which was -2.4 cm.



Figure 27 Drone flight on glacier front

Following the identification of GCPs, two photogrammetric drone flights (in Figure 27) were identified, the first over Serac Lake, and the second at the glacier front.

At the end of the campaigns of July, GCPs are set along all around the lake area and lower glacier part (Figure 30).



Figure 30 GCPs around Serac lake

POINT	EST	NORD	h ELLIPSOIDAL	LONG	LAT	H ORTOMETRIC
<b>DIATI71 idrometro</b>	342367.784	5059296.409	2442.042	6.97530816	45.66747763	2388.105
<b>DIATI79</b>	342341.192	5059279.430	2441.039	6.97497252	45.66731884	2387.102
<b>201</b>	342304.308	5059374.129	2458.975	6.97446860	45.66816229	2405.045
<b>204</b>	342667.248	5059317.573	2445.777	6.97914324	45.66773609	2391.831
<b>206</b>	342275.253	5059182.328	2447.586	6.97415808	45.66643038	2393.646
<b>DIATI78</b>	342340.675	5059161.750	2441.090	6.9756717	45.66807482	2387.145
<b>207</b>	342373.252	5059008.779	2450.933	6.97547162	45.66489158	2396.981
<b>DIATI77</b>	342446.643	5058980.292	2441.501	6.97642236	45.66465203	2387.545
<b>208</b>	342581.677	5058979.782	2442.147	6.97815484	45.66467814	2388.187
<b>104</b>	343311.199	5058821.599	2593.567	6.98756470	45.66342063	2539.576
<b>105</b>	343717.153	5058872.667	2598.342	6.99275606	45.66397170	2544.339
<b>106</b>	343585.115	5058742.797	2584.734	6.99110399	45.66277368	2530.731
<b>107</b>	343414.532	5058683.127	2575.548	6.98893492	45.66219839	2521.549
<b>108</b>	343208.488	5058795.695	2565.480	6.98625543	45.66316437	2511.492
<b>109</b>	343111.677	5058812.825	2559.079	6.98500797	45.66329655	2505.095
<b>110</b>	343026.117	5058867.692	2562.365	6.98389265	45.66377071	2508.386
<b>111</b>	343026.098	5058867.686	2562.354	6.98389241	45.66377065	2508.375
<b>112</b>	342978.138	5058904.335	2563.441	6.98326531	45.66408945	2509.464
<b>113</b>	342861.706	5058841.121	2561.233	6.98179209	45.66349442	2507.258
<b>114</b>	343414.527	5058683.133	2575.556	6.98893485	45.66219845	2521.557
<b>115</b>	343658.193	5058869.207	2605.054	6.99200080	45.66392727	2551.053
<b>116</b>	343716.409	5058967.115	2594.689	6.99271615	45.66482112	2540.689
<b>117</b>	343866.232	343866.232	2594.011	6.99461764	45.66543062	2540.008

Table 9 Coordinates GCPs July 2021

- Third campaign 6-8/09/2021**

This campaign was aimed to set GCPs identified by 1m<sup>2</sup> markers in the upper part of the glacier.

The third campaign, in which the writer also took part, started on the morning of Monday 6<sup>th</sup> September from the Turin Polytechnic, with an overnight stay in Aosta and a meeting at 7.30 a.m. in La Thuile to climb the glacier by helicopter.

On the 7<sup>th</sup> of July divided into three teams and accompanied by mountain guides, the helicopter dropped the teams off at three different points on the glacier to allow the 1m x 1m markers to be placed (Figure 32) at well-distributed points previously agreed upon with ARPA.



Figure 31 Marker on Gamma 'base' station

The base station was made at the 'GAMMAITALPOS' (Figure 31) point and surveyed with a GNSS RTK network.

GNSS "base" GAMMA Coordinates UTM ETRF2000 of RTK of 7 September 2021 N=5057564.580 m, E=343289.730 m h= 2880.235m
---

Table 10 Gamma 'base' coordinates



Figure 33 Marker on the glacier to set a GCP 1m x 1 m



Figure 32 Probe sampling to measure ice thickness

During the placement of the GCPs and the placement of the markers for the subsequent

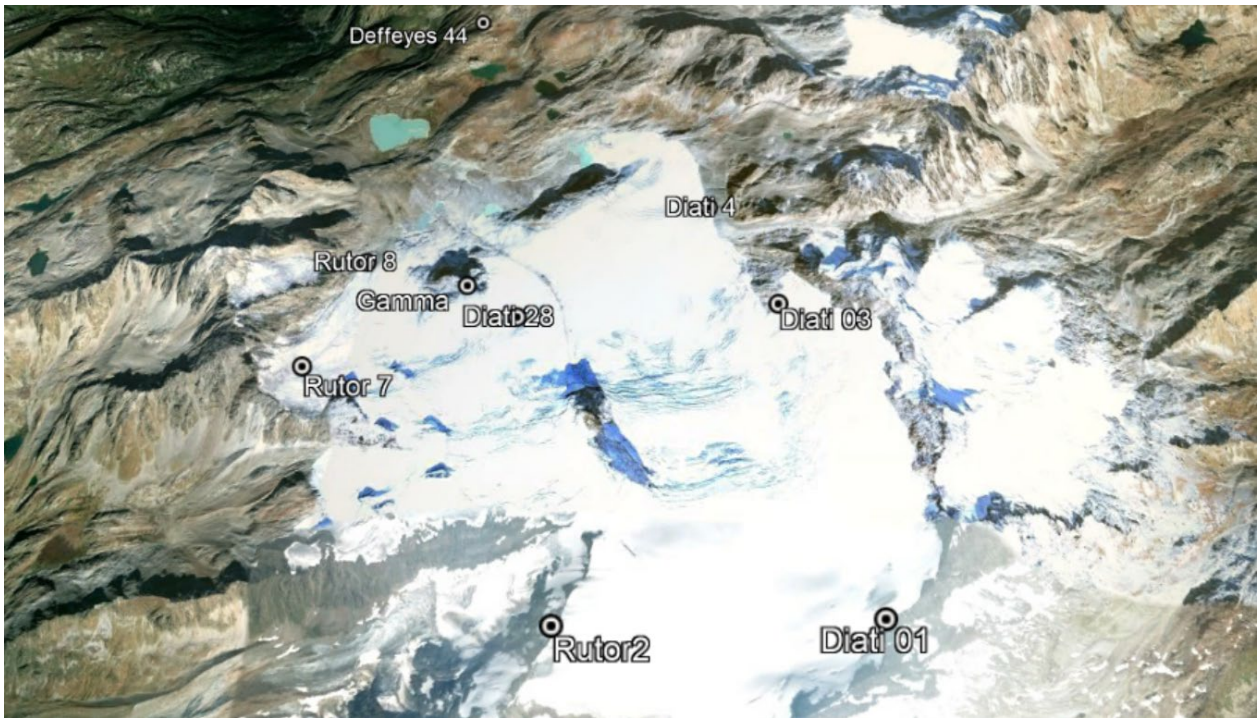


Figure 34 GCPs on upper Rutor glacier on Google Earth

Point	Nord	Est	h ell	Long °	Lat °	H orto
<b>Gamma</b>	5057564.005	343293.081	2885.525	6.98870143	45.65391850	2831.488
<b>Rutor 7</b>	5056930.069	342412.407	2905.426	6.97761059	45.64801656	2851.392
<b>Rutor 8</b>	5057774.980	342623.509	2691.688	6.98004474	45.65566470	2637.679
<b>Diati04</b>	5058236.014	344729.662	2794.485	7.00691458	45.66028651	2740.441
<b>Deffeyes44</b>	5060023.265	343055.184	2573.299	6.98485610	45.67598651	2519.383
<b>Rutor 6</b>	5056182.460	343399.113	3236.109	6.99050608	45.64151496	3182.023
<b>Diati 01</b>	5055411.245	345669.828	3408.882	7.01987133	45.63508612	3354.725
<b>Diati03</b>	5057424.267	345159.501	3028.005	7.01268715	45.65308057	2973.931
<b>Testa</b>	505433.637	345248.55	3523.774			

Table 11 GCPs upper part of Rutor glacier

photogrammetric flight, the snow thickness was measured at various points by sampling (Figure 33).

At the end of the glacier descent, the three groups rejoined the Duffeyes hut and split up. One group descended towards the valley while another remained to continue the work of setting up GCPs in the lower part of the glacier, the part characterised by the lake system.

TRIMBLE SP80 (Figure 35) receivers were used for all measurements in the Rutor campaigns, care was taken to mark the instrumental height each time, which varied according to whether the pole was used and subtracting it from the measured height to get the height of the point. The TRIMBLE SP80 receiver characteristics are reported in the Table 12.

*Table 12 Characteristic receiver TRIMBLE SP80*

<b>Characteristics SP80 Spectra Precision</b>	
<b>Dimensions</b>	
<b>GNSS constellations and channels</b>	GPS L1C/A, L1P(Y), L2P(Y), L2C, L5 GLONASS L1C/A, L2C/A - BeiDou B1 (phase 2), B2 Galileo E1, E5a, E5b QZSS L1C/A, L2C, L1SAIF, L5 SBAS
<b>Precision Real-Time RTK</b>	Horizontal 8 mm+1ppm Vertical 15 mm+1ppm



*Figure 35 Spectra Trimble receiver SP80*

### 3.3 UAV (Unmanned Aerial Vehicles):

A drone was also used to carry out thorough surveys of the glacier font and the lakes below.

#### 3.3.1 Drone photogrammetry

UAV (Unmanned Aerial Vehicles) includes vehicles that do not require a pilot on board, are created for military purposes, are lightweight and easily transportable, allow low-altitude flight and are rapidly spreading into many fields and are commonly referred to as 'Drones'.



Figure 36 DJI Phantom 4

In geomatics, they make it possible to carry out photogrammetric flights and detect areas that are difficult to reach in other ways. Drones fall into two broad categories: 'fixed-wing' drones and multi-rotor drones, such as those used in the campaigns under review. The drone used on the Rutor glacier is the **DJI PHANTOM 4** (Figure 36), with an integrated RTK GNSS receiver that provides the position in real-time.

Weighing 1380 g and its limited size, this drone was carried easily up the glacier and thanks to the favourable weather conditions and the absence of wind at altitude, it was able to fly during the measurement campaign. The drone's built-in camera of 12.4 M pixels with 1" sensor and an Electronic Shutter Speed from 8 to 1/8000 s allowed photo sequence for Serac Lake and the glacier front.

Model	FC6310R
Focal Length	8,8 mm
Image size	4000×3000 pixel
Sensor	CMOS 1/2.3"
Capture mechanism	Electronic shutter

Table 13 Characteristics of Phantom 4 camera

It is important to consider when planning and organising the operating temperature range ranging from 0° to 40° C, temperatures in glacier monitoring can often be below this range even in summer periods. Furthermore, although the estimated maximum flight time is

approximately 28 minutes, low temperatures can significantly reduce this duration, requiring frequent battery changes. During the campaign, it was necessary to bring 4 batteries to be changed as needed.

(DJI, s.d.)



*Figure 37 DJI Phantom 4 use during the Rutor campaign at Serac Lake*

In order to survey with a drone, it is necessary to plan the obstacles and the area to be covered in terms of space and flight time, as well as the conditions for planning the use of the batteries.

The two photogrammetric flights on the Rutor (Figure 37), on the serac lake and at the glacier front. The flight over Lake Seracs was repeated in both July campaigns. In the first one, the rocky wall adjacent to the lake was not surveyed, so in the second one, it was repeated with an accurate scan of the entire lake with a nadiral view and of the adjacent wall with an inclined view.

Concerning the flight at the front of the glacier on 20 July 2021, with an RTK positioning to have camera centre with centimetric precision. It was essential to assist the pilot in controlling obstacles and the presence of animals that could have attacked the drone. The

flight was also made over the lower serac part of the glacier. Maximum attention was paid to the temperature and wind conditions, limiting battery life. The flight was made respecting an overlap of at least 70% between one shot and the next, both in longitudinal and transversal direction with a time interval of about every second.

The Rutor glacier was flown over by three different drone flights:

- a first flight on 9<sup>th</sup> July 2021 between 12 and 17 over the Serac lake with 995 images with flight altitude of 125 m and a ground resolution of 2.86 cm/pix and a covered area of 3.71 km<sup>2</sup>.
  - On 20<sup>th</sup> July 2021 the same location, over the same Serac lake, another flight was made at a lower altitude to allow a GSD of 5 cm and include the rock wall adjacent to the lake not included in the previous flight with RTK precision. This flight produces 369 images.
  - On the 20<sup>th</sup> July 2021 later, 17:20 to 17:40 with RTK poles to survey the glacier front and lower part. The flight produced 364 images.
- Both these two flights have a ground resolution of 3.46 cm/pix, covers together an area of 4.6 km<sup>2</sup> flying at an altitude of 127 m.

### 3.3.2 Drone Model

For the elaboration of the drone, images are used **Agisoft Metashape**.

The DJI Phantom 4 drone saves images in folders and switches to a second folder when it reaches number 999. So first, it is necessary to rename files of different folders to ensure to have no problem during the import process (Service, s.d.).

The coordinates of the drone camera are geographic coordinates ETRF2000 (longitudinal, latitudinal, ellipsoidal height), the reference system is set on ‘Rete Dinamica Nazionale RDN2008 (EPSG:6706)’. It is necessary to convert the ellipsoidal height into the

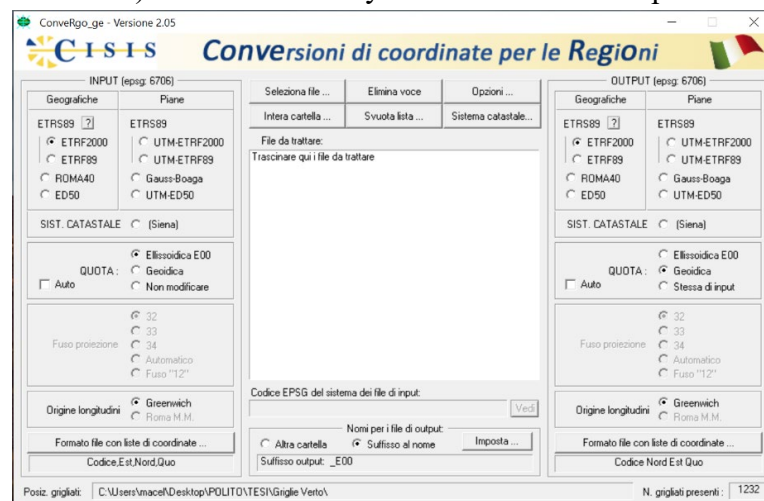


Figure 38 ConveRgo software

orthometric height. The coordinates are exported from the software and thanks to a notepad text file they are converted with grids through **ConveRgo**, (Conversioni di coordinate per le Regioni) (Figure 38). ConveRgo provides the Geoid ondulation N

$$H = h - N$$

These steps are necessary for all drone flights.

For the model of the 9<sup>th</sup> July 2021 images are imported and height converted with the process described before. The flight covers Serac lake and all the area until marginal lake and glacial front. 10 GCPs are used on the ground all set in the central part, between the two lakes and coordinates reported in Table 14.

POINT	EST	NORD	H ORTOMETRIC	ESTIMATED EST	ESTIMATED NORD	ESTIMATED H
105	343717.153	5058872.667	2544.339	343717.157	5058872.661	2544.334
106	343585.115	5058742.797	2530.731	343585.119	5058742.782	2530.734
108	343208.488	5058795.695	2511.492	343208.453	5058795.691	2511.494
109	343111.677	5058812.825	2505.095	343111.666	5058812.802	2505.139
111	343026.098	5058867.686	2508.375	343026.092	5058867.683	2508.391
112	342978.138	5058904.335	2509.464	342978.105	5058904.372	2509.482
113	342861.706	5058841.121	2507.258	342861.705	5058841.111	2507.247
114	343414.527	5058683.133	2521.557	343414.520	5058683.104	2521.551
115	343658.193	5058869.207	2551.053	343658.193	5058869.207	2551.053
116	343716.409	5058967.115	2540.689	343716.401	5058967.123	2540.689

Table 14 GCPs drone flights of 9th July 2021 – Serac Lake

and allows faster identification of any errors.

Computed the model, the residual error is estimated on the GCPs:

N. Points	RMSE X [cm]	RMSE Y [cm]	RMSE Z [cm]	RMSE XY [cm]	RMSE TOT [cm]
9	1,675	1,849	1,786	2,4956	3,069

Table 15 Residual errors on GCPs drone model 9<sup>th</sup> July

The average camera location error is estimated:

X error [cm]	Y error [cm]	Z error [cm]	XY error [cm]	TOT error [cm]
0,667	0,950	1,098	1,161	1,598

Table 16 Average camera location error on drone model 9<sup>th</sup> July

For the model of the flights at end of July 20th, images of the two flights are elaborated together to have a complete and better resolution of the Serac lake area and the glacial front. The markers collected during the campaign are in UTM-ETRF2000 coordinate, so into the software, a different system for them is set. Superimpose in QGIS the DSM models an altimetric shift probably due to pole height in the glacial front was detected.

So, it was decided to run the models again separately. The Serac lake flight model runs using 7 GCPs with no pole correction.

POINT	EST	NORD	H ORTOMETRIC	ESTIMATED EST	ESTIMATED NORD	ESTIMATED H
<b>201</b>	342304.308	5059374.129	2405.045	342304.308	5059374.129	2405.045
<b>204</b>	342667.248	5059317.573	2391.831	342667.154	5059317.508	2392.052
<b>207</b>	342373.252	5059008.779	2396.981	342373.289	5059008.765	2397.016
<b>208</b>	342581.677	5058979.782	2388.187	342581.580	5058979.830	2388.268
<b>DIATI 71</b>	342367.784	5059296.409	2388.105	342367.739	5059296.370	2388.161
<b>DIATI 77</b>	342446.643	5058980.292	2387.545	342446.618	5058980.272	2387.556
<b>DIATI 79</b>	342341.192	5059279.430	2387.102	342341.185	5059279.449	2387.138

Table 17 GCPs of drone Serac lake flight of 20th July 2021 – Serac Lake

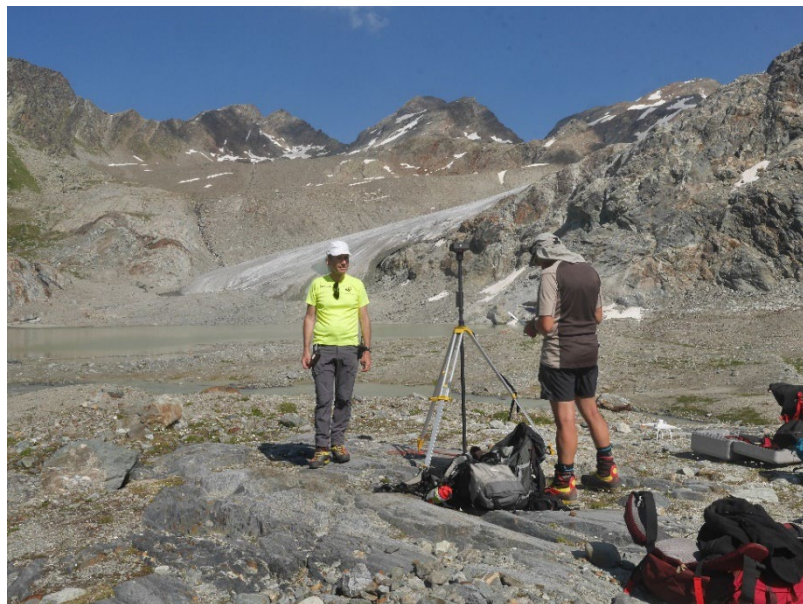


Figure 39 Point 105, DJI drone pole

For what concerns the flight on the glacial front the only point detected was point 105 used as GNSS base station for the RTK fly (Figure 39).

POINT	EST	NORD	ELLIPSOIDAL H	LONGITUDE	LATITUDE	ORTOMETRIC H
<b>105</b>	3437172.153	5058872.667	2598.342	6°99372039	45°.66578606	2405.045

Table 18 Pole DJI coordinates

Unfortunately, this point was not detected by drones' images, so no GCPs are used for the model, but only coordinates of projection centre by RTK. Therefore, to elaborate the model are used only the camera centre position.

The post-processing process provided by drone photogrammetry is more straightforward and allows faster identification of any errors.

The average camera location errors are estimated and reported in Table 19:

X error [cm]	Y error [cm]	Z error [cm]	XY error [cm]	TOT error [cm]
2,568	3,062	3,862	3,995	5,558

*Table 19 Average camera location errors on drone model 21<sup>st</sup> July*

The residual errors on the GCPs are estimated and reported in Table 20:

N. Points	RMSE X [cm]	RMSE Y [cm]	RMSE Z [cm]	RMSE XY [cm]	RMSE TOT [cm]
7	4,94	3,726	6.76	6,192	9,16

*Table 20 Residual error on GCPs drone model 21<sup>st</sup> July*

The drone models thanks to the low flight height and the RTK position return very accurate 3D models with centimetric precision.

### 3.3.3 Discussion

As far as the application on a large glacier like Rutor is concerned, it is possible to use drone surveys only for portions to be accurately analysed, integrated and in addition with a global model from an aircraft. The centimetric precision make the drone an excellent tool for analysis of specific portions, such as the glacier front on which the retreat is evaluated.

It is important to remember the limitations of drone surveys due to battery life, even for a small portion of the glacier such as the one desired, several flights had to be carried out. Moreover, it should always consider the difficulty and the need for personnel and bring the drone to the site. Although small in size, the physical effort of carrying a drone for hours on a mountain path is not always easy and problem-free. Finally, it must be considered that the places where glacier monitoring takes place are often remote places without a network. Therefore, it is often impossible to use the RTK positioning system of the drone camera.

# Chapter 4

## Photogrammetric flight of Rutor glacier

### 4.1 Aircraft, IMU, camera characteristics

The photogrammetric flights over the Rutor glacier, in September 2020 and repeated a year later in September 2021, were both carried out by DigiSky, a Turin-based EASA certified company. The company has over 20 years' experience in aerial mapping for various purposes, surveillance, large-scale infrastructure and environmental risk management. The company based at Turin Aeritalia Airport (LIMA) allowed the flights to last about one hour with take-off and landing in Turin. (Digisky, 2021)

The aircraft that carried out the photogrammetric flights are equipped with a GNSS antenna, an IMU inertial unit, and the PhaseOne camera under the right wing.

The PhaseOne camera (iXM-RS150F) in Figure 40, is a medium format camera, with a focal length of 50 mm, a sensor size of 40 x 53.5mm and a resolution of 151.3 MPx. The aircraft features a dual camera, but only frames from PhaseOne were used for processing. (PhaseOne, 2021)

The aircraft has two low-quality IMUs, one on the wing and one on the aircraft body (Figure 41).



Figure 40 iXM-RS150F Camera



Figure 41 Aircraft and camera position

## 4.2 Photogrammetric flight data

The Rutor glacier was flown over by three different photogrammetric flights:

- The first flight on 30 September 2020 from 10:30 a.m. to 11:30 a.m. (GMT +2), in this first flight the examination area had not yet been exactly delineated, the 818 images cover the entire glacier from the Rutor head to 3500 m asl but exclude the area of the Serac lake and the Deffeyes refuge. The flight altitude was 946 m off the ground with a ground resolution of 0.7m/pix and an area covered of 25.2 km<sup>2</sup> with frame average scale 1/20 000.
- The photogrammetric flight was repeated one year later, on 13 September 2021 from 9:40 a.m. to 11:10 a.m., following the 6-8 September campaign for the placement of markers at the summit. This flight produced 848 images and covers a larger area than the previous year, covering the area from the Duffeyes refuge and the Serac and Margherita lakes to the head of the glacier. The flight altitude was 877 m off the ground with a ground resolution of 0.6m/pix and a covered area of 34.5 km<sup>2</sup>(1/18 000).
- Due to the presence of clouds over the glacier's summit, a partial flight was carried out again on 30 September 2021 from 9:20 a.m. to 9:40 a.m. and produced 202 images.

### 4.3 2020 and 2021 models of Rutor glacier

The glacier models were made using the AgiSoftware MetaShape using the reference system RDN2008 / UTM zone 32N (N-E) (EPSG: 6707).

The 2021 model was created by importing the photograms of the flights (of 13<sup>th</sup> and 30<sup>th</sup> September 2021). After aligning the photos, the coordinates of the markers (reported in Table 21) measured on the field used as GCPs (Figure 42) were imported and collimated. The markers were searched for in the various images and associated with the coordinates as a first step.

GCPs set during the 2021 September campaign (see p. 3.2) before the flight were used to support the photogrammetric flight.

POINT	EST	NORD	H ORTOMETRIC	ESTIMATED EST	ESTIMATED NORD	ESTIMATED H
<b>DELTA_ITALPOS</b>	343402.457	5056181.871	3187.372	343402.496	5056181.898	3187.403
<b>DEFFEYES_44</b>	343055.184	5060023.265	2519.383	343055.171	5060023.276	2519.420
<b>DIATI71_IDROMETRO</b>	342367.784	5059296.409	2388.105	342367.746	5059296.406	2388.120
<b>DIATI79</b>	342341.192	5059279.430	2387.102	342341.192	5059279.430	2387.102
<b>DIATI88</b>	342861.808	5059729.085	2503.829	342861.812	5055411.235	3354.771
<b>DIATI_01</b>	345669.828	5055411.245	3354.725	345669.741	5055411.235	3354.771
<b>DIATI_04</b>	344729.662	5058236.014	2740.441	344729.640	5058235.942	2740.412
<b>JEEP</b>	343376.188	5059430.130	2539.520	343376.256	5059430.136	2539.383
<b>GAMMA</b>	343293.081	5057564.005	2831.488	343293.073	5057563.981	2831.507
<b>DIATI28</b>	343628.886	5057306.819	2841.446	343628.886	5057306.797	2841.454
<b>106</b>	343585.115	5058742.797	2530.731	343585.096	5058742.782	2530.750
<b>RUTOR_7</b>	342415.786	5056929.465	2856.811	342415.766	5056929.480	2856.754
<b>RUTOR_8</b>	342623.509	5057774.980	2637.679	342623.492	5057775.019	2637.638
<b>TESTA</b>	345256.689	5054934.338	2530.731	343585.096	343585.096	2530.750

Table 21 GCP model 2021

These points were founded on the images taken from PhaseOne to insert in each image to georeferenced it. This part takes a long time due to the wide area covered by the flight and the high number of images.

Once the camera centres and georeferentiation were done, the dense cloud was built. After the cleaning of the cloud, the mesh was created interpolating the dense point cloud. The model was completed and the orthophoto and digital surface model (DSM) were generated and exported.

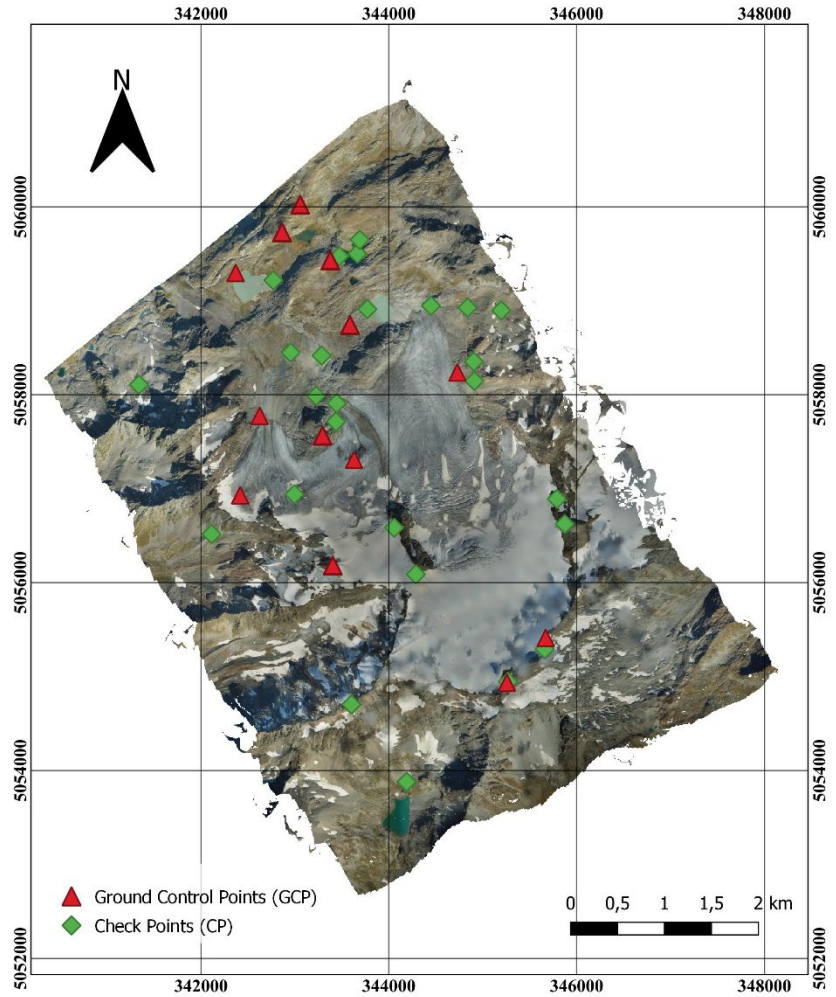


Figure 42 GCPs and CPs 2021

With the 2021 model has been produced at the end:

- An Orthophoto with a GSD<sup>8</sup> equal to 0.06 m in Figure 43.
- A DSM with a GSD equal to 0.24 m in Figure 44.
- A Dense Cloud of 3.338.453.261 points.

---

<sup>8</sup> Ground Sample Distance

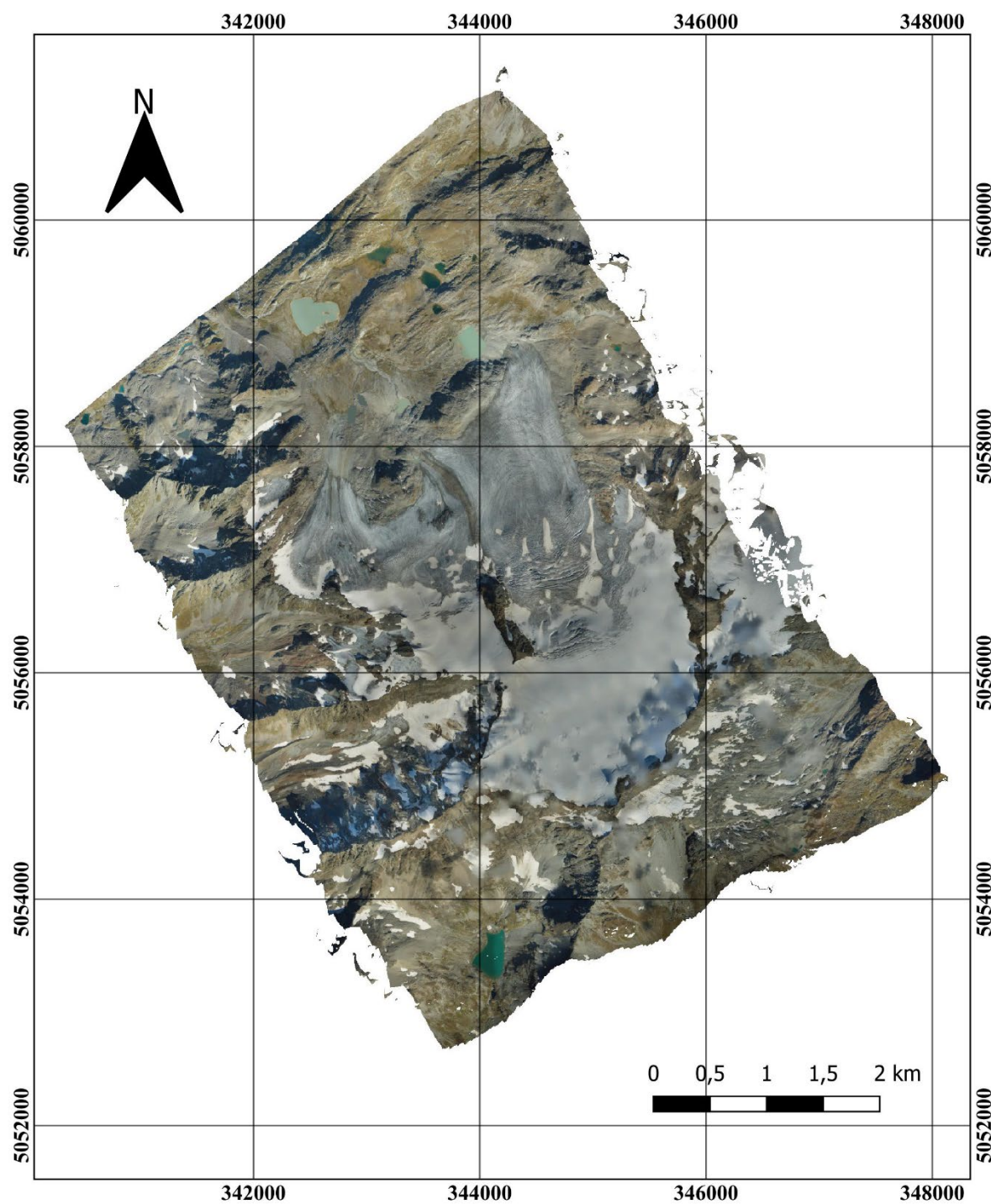


Figure 43 Orthophoto from flight 2021

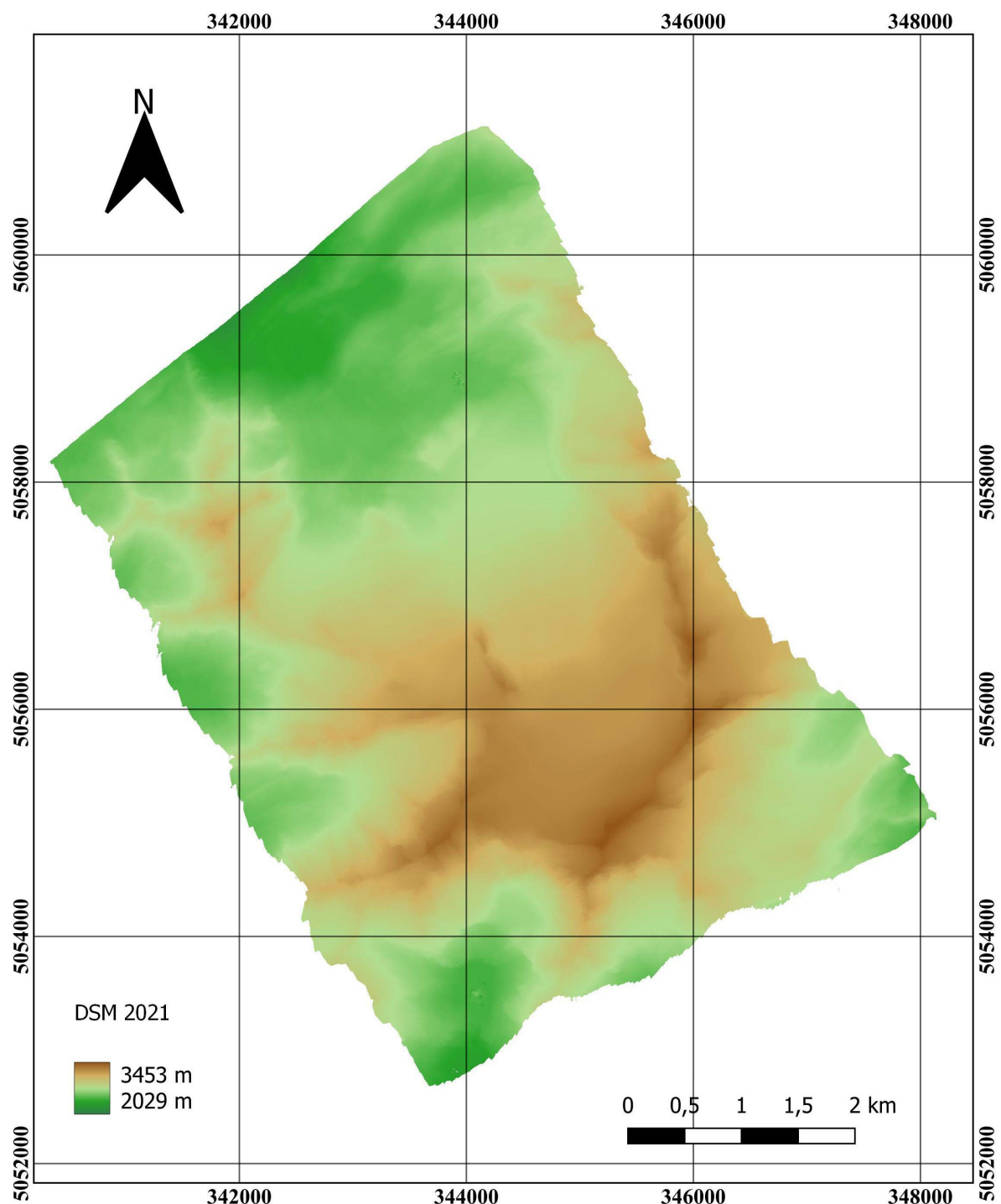


Figure 44 DSM from flight 2021

The total error of the 2021 model is 0.10 m on the East, 0.02 m on the North and 0.05 on the height. The root mean square error (RMSE) is computed in 3D directions shown in Table 22:

N. Points	RMSE X [cm]	RMSE Y [cm]	RMSE Z [cm]	RMSE XY [cm]	RMSE TOT [cm]
13	4,699	2,776	5,585	5,45876	7,810

Table 22 Residual errors on GCPs model 2021

To check the goodness, the quality and reliability of the model a series of Check Points (CP) are identified on the model and estimates the coordinates and the relative errors. This was not an easy step due to the difficulty to find stable and horizontal stable points well identifiable (Table 23). Some CP are surveyed in the July 2021 during drone campaign, other CP are obtained from GCPs 2020 photogrammetry model.

N. Points	RMSE [cm]	X [cm]	RMSE [cm]	Y [cm]	RMSE [cm]	Z [cm]	RMSE [cm]	XY [cm]	RMSE TOT [cm]
34	6,041		7,112		13,751		9,331		16,618

Table 23 Residual errors on check points model 2021

The points entered are collimated to help the program recognise homologous points in the various frames. This is followed by aerial triangulation to determine the camera centres. The model obtained from the 2021 photogrammetric flight will be considered the 'Zero Model' against which monitoring in subsequent years will be compared. Mass balances will be calculated from this model, and the other models will be coregistered if necessary. Due to the reliability of the model and the lack of GCPs, this procedure was applied to the 2020 model.

The 2021 model represents a fundamental step in monitoring the Rutor glacier and its environment. From the work done, it will be possible over time to carry out a periodic annual monitoring activity in collaboration between the Glacier Lab of the Politecnico di Torino and ARPA Valle D'Aosta without necessarily having to continuously walk along the glacier. The network of GCPs, especially in the upper part, will have to be checked before each photogrammetric flight. It will be possible to plan a thickening of the markers distributed on the glacier to improve the accuracy of future models.

To a further comparison the model is evaluated against the DSM of 2008 of the Geoportale Piemonte- Valle D'Aosta executed with a laser scanner. A rocky stable area on the lower part of the glacier was considered to use the raster calculator on QGIS, make the DSM difference and estimate the zonal statistic on it. The value obtained are reported in table 24:

Mean [m]	Standard Deviation [m]
-0,244	0,428

Table 24 Comparison between aerial and Geoportale

The analysis is computed on 790 000 elements (pixels) on the stable zones reported in Figure 120 (chapter 6). As expected, the difference is around 0.25 m. This can also be used to a qualitative comparison between the two DSM to estimate the snow melting.

For the 2020 model, the process has been longer and more complex than for the 2021 model. A first aerial triangulation was done with 6 measured points and 6 coregistered points from the 2021 model. In 2020 the upper part of the glacier has no marker set, so, for this reason, was necessary to find some known stable points clearly identifiable, for example, the jeep garage and the small pillar on the top of the glacier. Unfortunately, due to snowfall and the accumulations of snow on the area was difficult to find another stable point along the glacier upper part. Due to the difficulty in finding clearly distinguishable

POINT	EST	NORD	H ORTOMETRIC	ESTIMATED EST	ESTIMATED NORD	ESTIMATED H
TESTA	345256.689	5054934.338	2530.731	345256.764	5054934.368	3481.443
JEEP	343376.188	5059430.130	2539.520	343376.422	5059429.966	2539.342
206	342275.253	5059182.328	2393.646	342275.454	5059182.192	2393.582
207	342373.254	5059008.767	2396.982	342373.068	5059008.959	2397.017
208	342581.677	5058979.782	2388.187	342581.129	5058980.078	2388.360
POINT 2	344061.100	5059073.237	2548.485	344061.073	5059073.261	2548.509
POINT 3	342255.400	5059178.701	2390.757	342255.531	5059178.663	2390.752
POINT 7	342900.246	5058255.734	2554.692	342900.292	5058255.607	2554.762
AC1	342110.853	5056516.686	2559.464	342111.309	5056516.531	2724.111
AC2	344189.480	5053879.475	2724.145	344189.537	5053879.452	2559.462
AC3	344288.151	5056088.120	3259.533	344287.884	5056088.050	3259.502
AC4	341338.593	5058107.171	2634.974	341338.670	5058107.254	2634.940

Table 25 GCP model 2020

points, a post-collimation refinement process was also necessary to precisely identify the images in which was present a high error in pixels during the collimation due to the difficulties to well see the exact pixel of the marker chosen. Removing these images to have a more precise estimation led to a better estimation of the coordinates.

The GCP found in the first estimation was not well distributed and after the triangulation, the model result was well set on the west part but not correct in the central and east part. This led to an estimation of 4 new points on the 2021 model, on the centre and the east border of the area and on an iterative process to improve point collimations point by point by removing markers on images where due to an unclear definition the marker had been roughly collimated. By also trying the exclusion of some GCPs and triangulating the

camera again, giving a weight of 0.02m as accuracy, with 5 measured points and 7 co-registered points from the 2021 model well distributed the model came up with a total error of 0.13 m in the East, 0.24 in the North and 0.07 m in height.

After an initial comparison of the DSMs, the possibility of a systematic error in certain model parts was noted in the sections. In order to eliminate this error, we proceeded to search for other photographic points on the 2021 model which were also visible in the frames of the September 2020 flight.

From the GIS analysis of the section of the DSM models, significant sections that could be affected by error were identified and additional GCPs were distributed.

To improve the accuracy, it is decided to add 5 more GCPs well distributed (all GCPs and CPs are reported in Figure 45), especially in areas affected by the error and around the glacier area.

POINT	EST	NORD	H ORTOMETRIC	ESTIMATED EST	ESTIMATED NORD	ESTIMATED H
GCP2020	344838.234	5058926.412	2728.306	344838.295	5058926.398	2728.327
GCP2020_1	344911.169	5058146.298	2831.135	344910.981	5058146.326	2831.177
GCP_2020_2	345873.749	5056623.356	3323.905	345873.747	5056623.213	3323.698
GCP_2020_3	343600.944	5054702.418	3305.543	343600.906	5054702.404	3305.369
GCP_2020_4	345790.213	5056890.141	3238.675	345790.243	5056890.332	3238.864
GCP_2020_5	344448.179	5058946.713	2623.434	344448.175	5058946.728	2623.403

Table 26 Additional GCPs model 2020 from 2021 model

The residual error on the GCPs is computed and reported in Table 27:

N. Points	RMSE X [cm]	RMSE Y [cm]	RMSE Z [cm]	RMSE XY [cm]	RMSE TOT [cm]
18	20,410	13,105	10,605	24,255	26,618

Table 27 Residual error on GCPs model 2020

And to check the precision the residuals on the check points are evaluated and reported in table 28:

N. Points	RMSE X [cm]	RMSE Y [cm]	RMSE Z [cm]	RMSE XY [cm]	RMSE TOT [cm]
10	18,034	18,343	26,2633	25,724	36,762

Table 28 Residual errors on check points model 2020 respect 2021 model

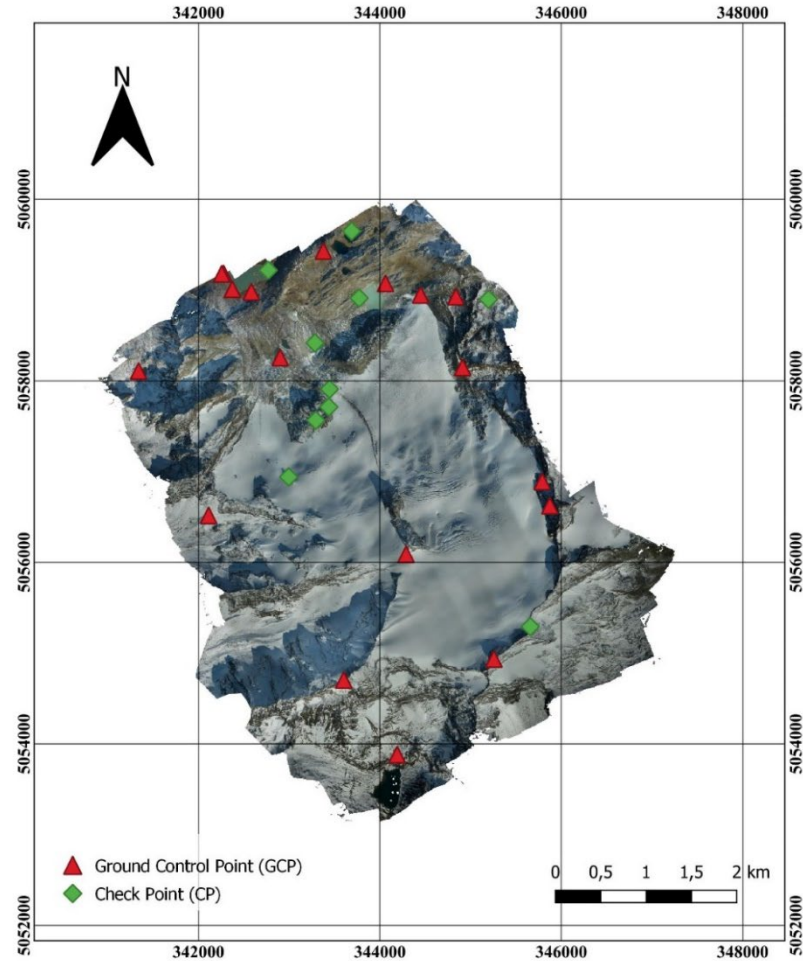


Figure 45 GCPs and CPs 2020

With the 2020 model has been produced at the end:

- An Orthophoto with a GSD equal to 0.07 m in Figure 46.
- A DSM with a GSD equal to 0.14 m in Figure 47.
- A Dense Cloud of 1.871.761.605 points

This further step emphasised the importance of the distribution and precision of the support points for the model's success. With this additional addition, the model appears to be free of systematic errors, however, the error estimates reached for the 2021 model cannot be achieved. This procedure also underlines the need for well-distributed GCPs detected throughout the study area to obtain a reliable and truthful model with which to monitor the glacier over time.

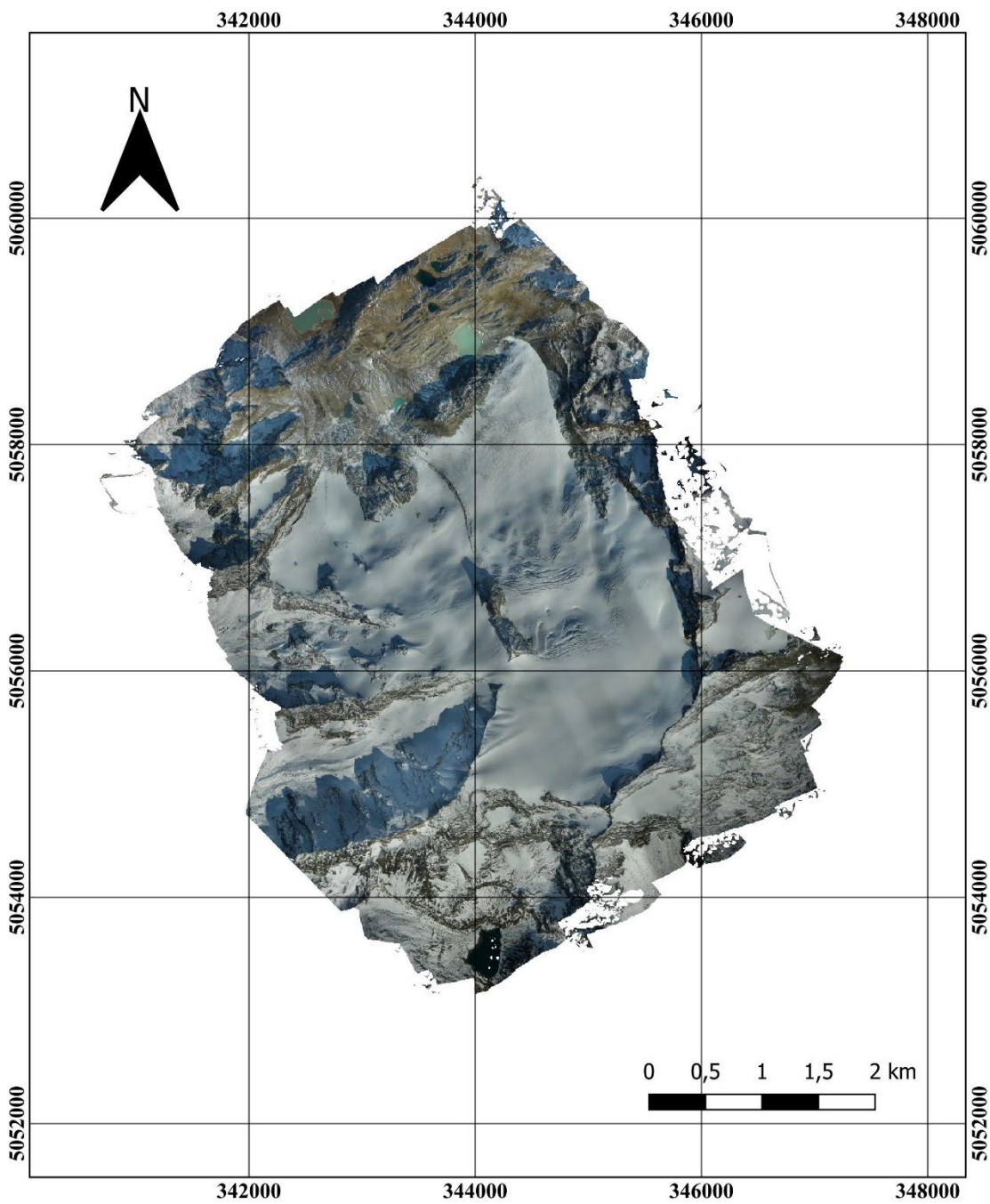
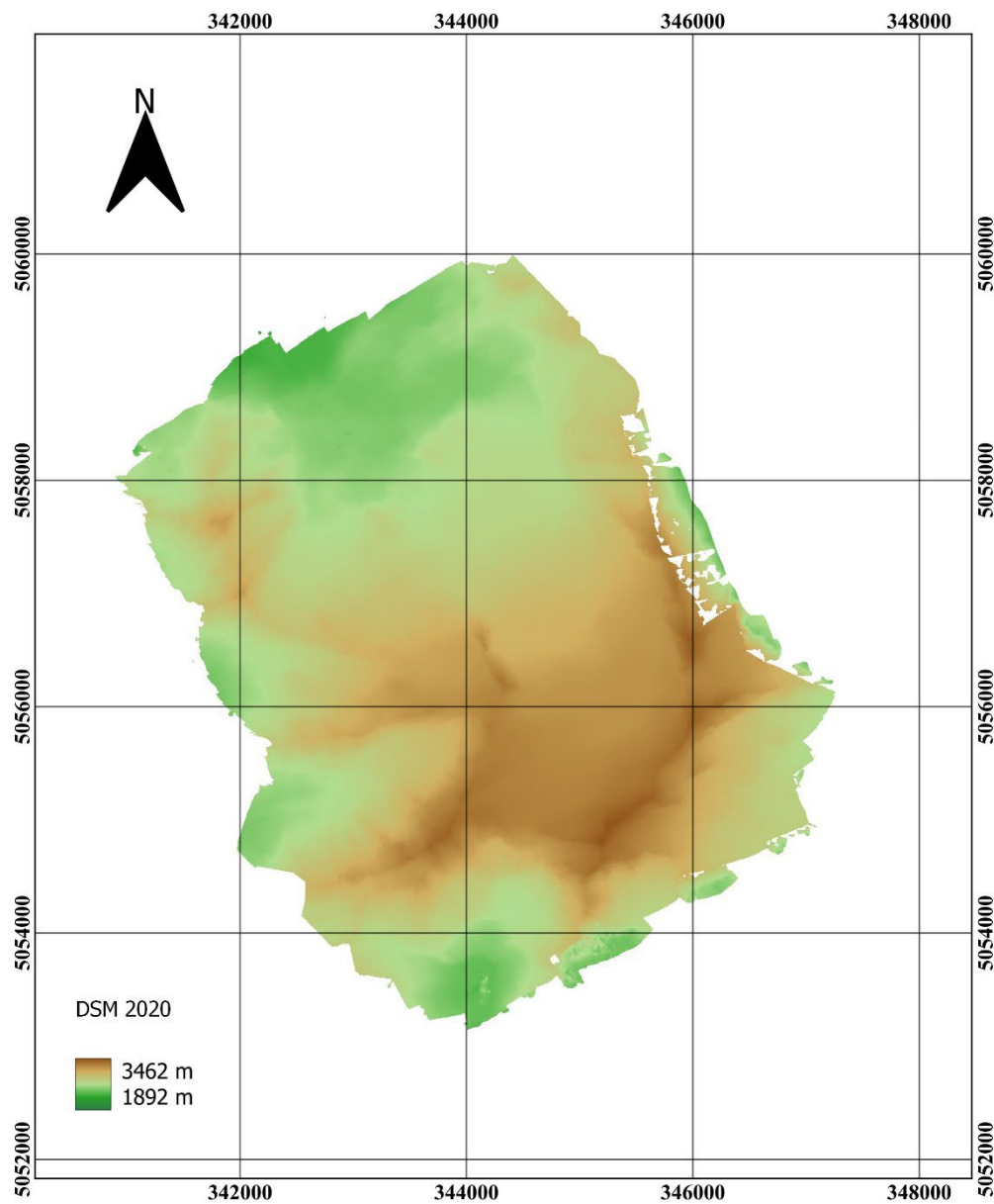


Figure 46 Orthophoto from flight 2020



*Figure 47 DSM from flight 2020*

To compare the models and compute the modification of the glacier, the orthophoto and the DSM model are imported in the open-source software **QGIS (Geographic Information System)**. GIS is able to read raster and vectorial files, georeferenced and compare them. To compare the mass balance of the glacier during the years, check the

precision of the model and have a better resolution in some areas, also the drones DSM are imported.

First of all, the comparison is done between the Geoportale model of 2008 and the 2021 photogrammetric model with the difference of the two DSM (Figure 48) and the qualitative section on the glacial fronts (Figure 49).

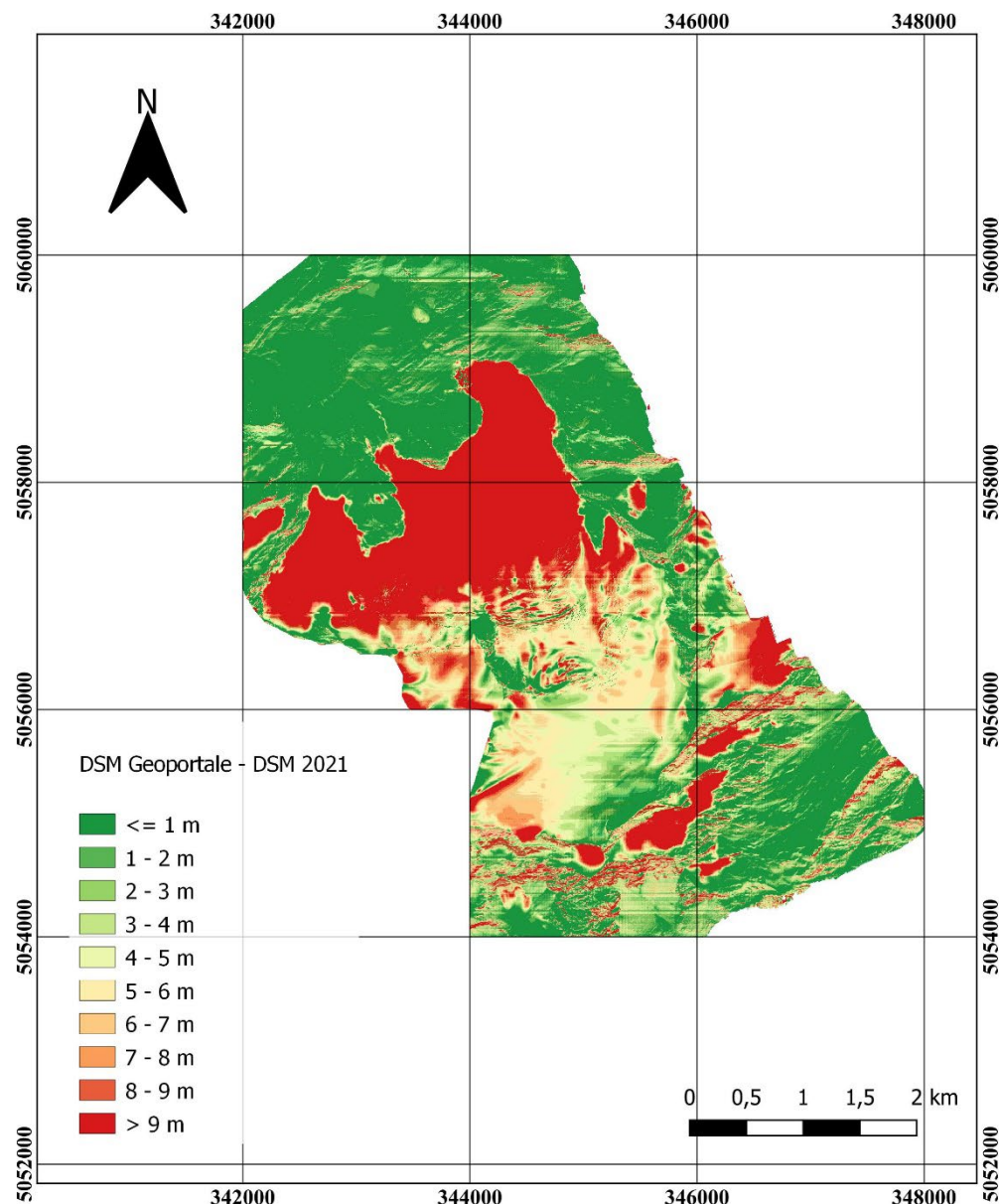


Figure 48 Differences between Geoportale DSM and 2021 DSM

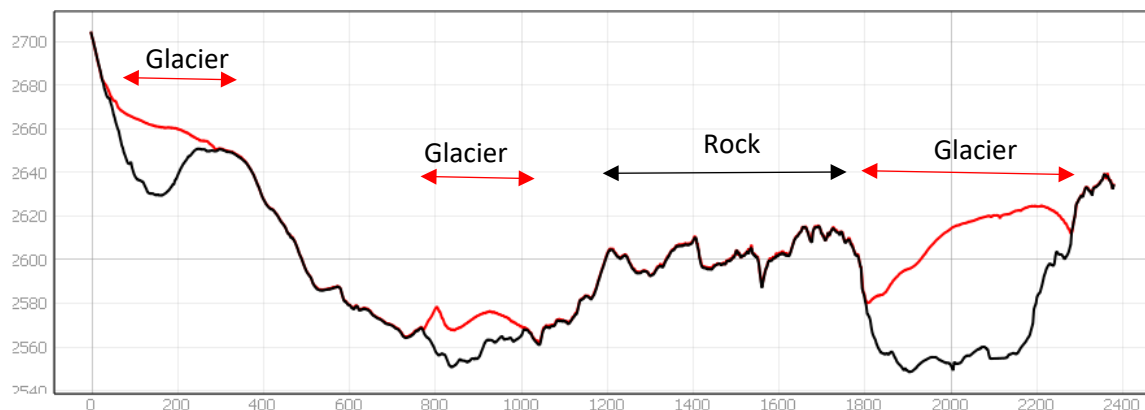


Figure 49 Section of Geoportale and 2021 models on glacial foreheads

**LEGEND:**

- Geoportale DSM model 2008
- Photogrammetric DSM model 13<sup>th</sup> September 2021

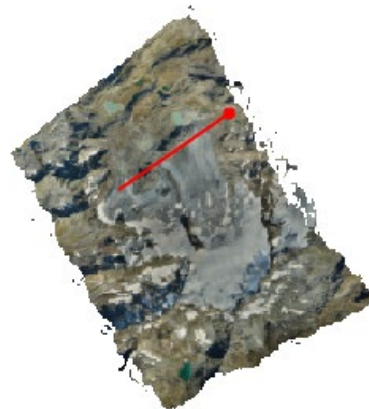


Figure 50 Section line

The shape underlines the accuracy of the model on the stable zones that are overlapped and enhance the level of the snow 13 years before. With the comparison between the two DSM the glacial front is now more than 60 meters below the 2008 estimation on the East front. The ablation reaches 80 metres in some points, but in the lower part of the glacier is globally around 60 metres. The retreat estimated is coherent to the snow melting evaluated in one year by the comparison of 2020 and 2021 models.

The mass balance of the glacier one year later is made by subtracting the 2021 model from the 2020 model (Figure 51) and checking the precision of the models evaluating the stable points (for example the rocks).

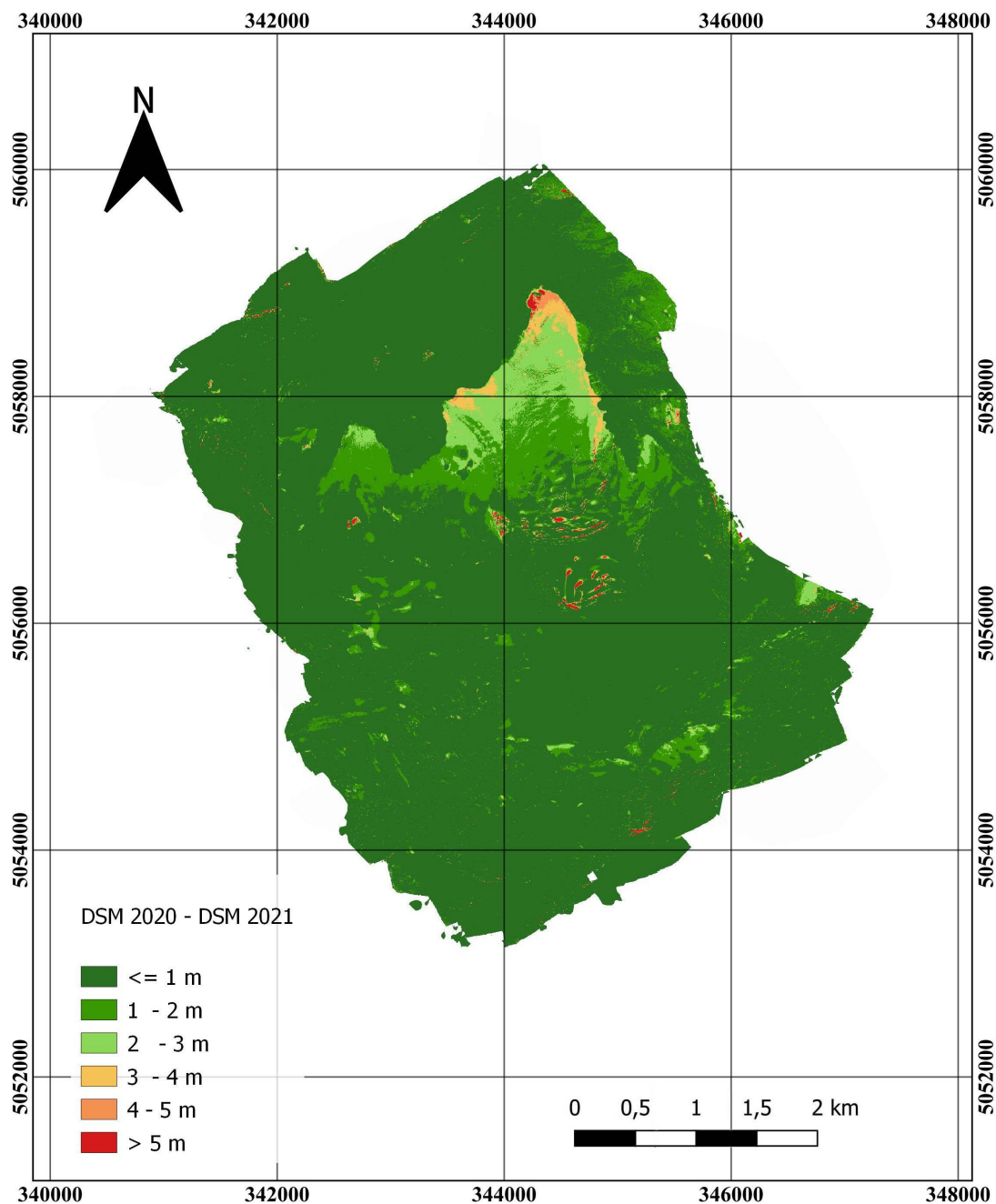


Figure 51 Difference of 2020 and 2021 DSM models

<b>Mean [m]</b>	<b>Standard Deviation [m]</b>
0.028	0.117

*Table 29 Comparison between 2020 and 2021 models on time invariant areas*

The centimetric accuracy of the model makes it possible to estimate glacier melt from a couple of metres at the summit to peaks of over 4 metres/year at the front. The east front thickness lost is around 4m/year, 2m/year on the west front and 3-4m/year on the central front.

Thanks to the QGIS software was possible to cut some specific sections to cross-compare the models, both photogrammetric and drones and estimate glacier melting during the last year.

These models are elaborated as part of the Glacier Lab glacier monitoring project collaborating with ARPA Valle d'Aosta.

In November 2021, after elaborating the Rutor models, the orthophotos and the DSM were given to ARPA to elaborate the mass balance.

It resulted that the east glacial front is the zone in which the major ablation is verified, central and west fronts are melting, even if one order of magnitude is less than the east one. The cartographic products of the photogrammetric processing of the Rutor glacier and the data obtained were provided to ARPA to support the monitoring activities of the impacts of climate change on the cryosphere. Changes in permafrost and meteorological changes with references to snowfall and average temperatures are also included in the annual assessments. The mass loss during the hydrological year (October to September of the following year) is calculated from the state of the ice surface deduced from the DSM at the end of the ablation period and allows a multi-temporal analysis for comparison between years. The negative mass balance term representing total ablation is then included in national, European and international reports. The elaborations are part of ARPA's glacier reporting and in particular the Rutor data will be included in the global database of the World Glacier Monitoring Service. (WMO)

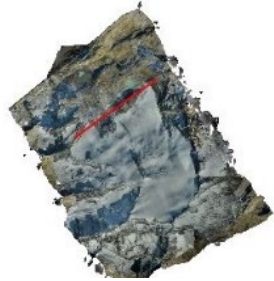
Rutor is one of the five sites monitored by ARPA in Valle D'Aosta and, in line with the average of the other glaciers, the average value of front retreat in the period 2000-2020 is -21 m, -15 m estimated in 2020 with a mass balance of -603 mm water equivalent. (ARPA Valle D'Aosta)

To underline the ablation are reported some sections (Figures 52-57) where the difference in the ice thickness between the two years is clear.

---

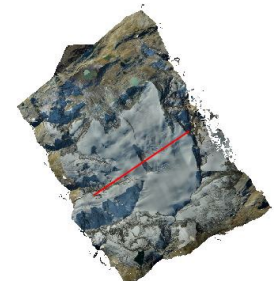
**SECTION 1**

Front section



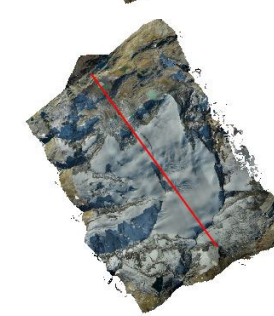
**SECTION 2**

Central section



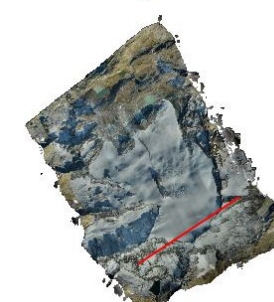
**SECTION 3**

Longitudinal section



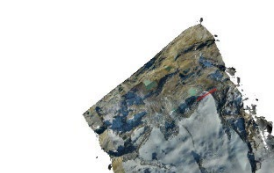
**SECTION 4**

Section on Rutor's head



**SECTION 5**

Zoom on east glacial front



## SECTION 6

Zoom on west glacial front

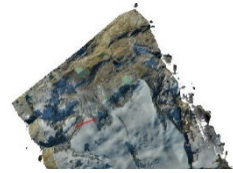


Table 30 Sections legenda

**LEGEND:**    Photogrammetric DSM model 13<sup>th</sup> September 2021  
              Photogrammetric DSM model 30<sup>th</sup> September 2020

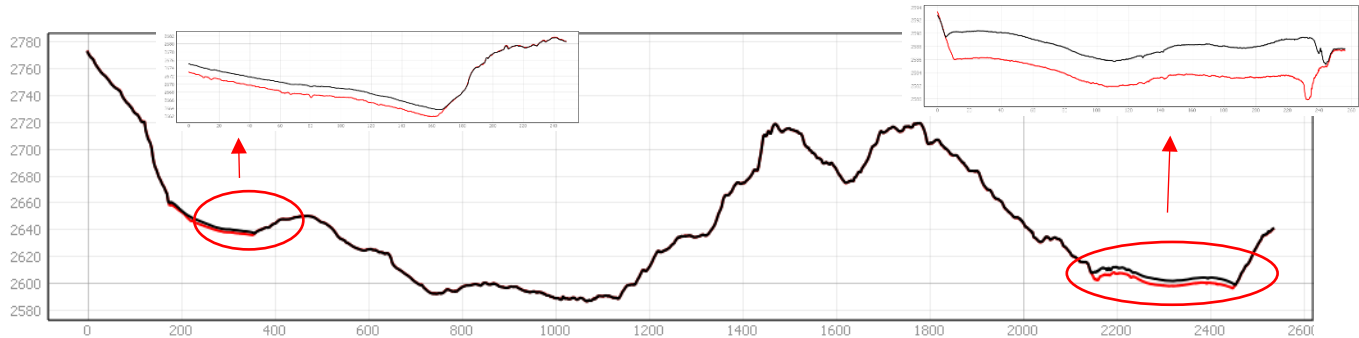


Figure 52 Section 1- on the glacier foreheads

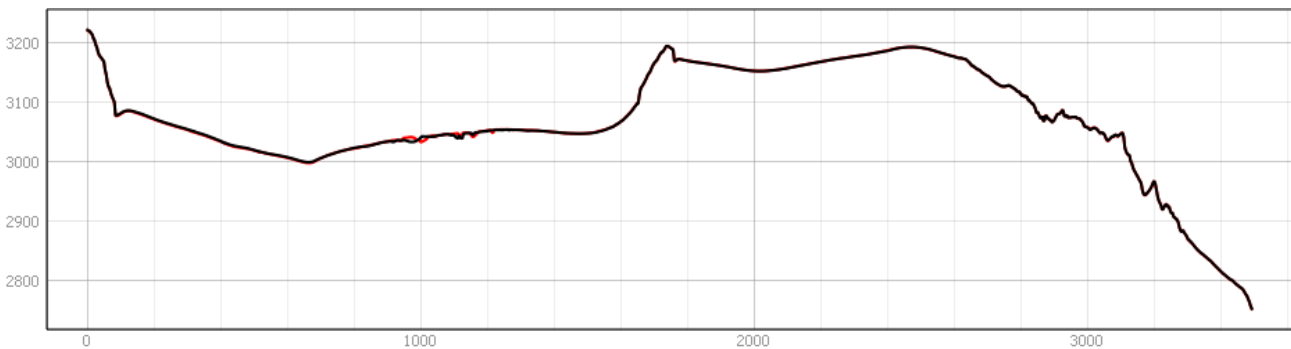
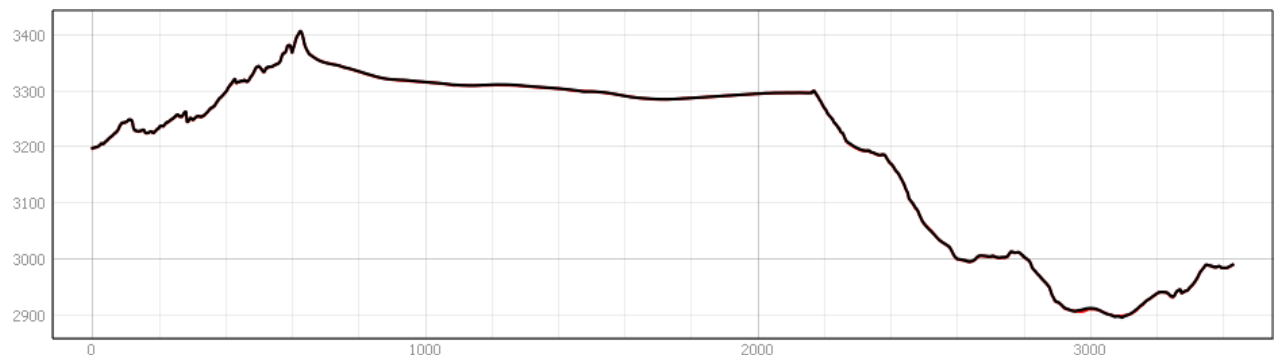
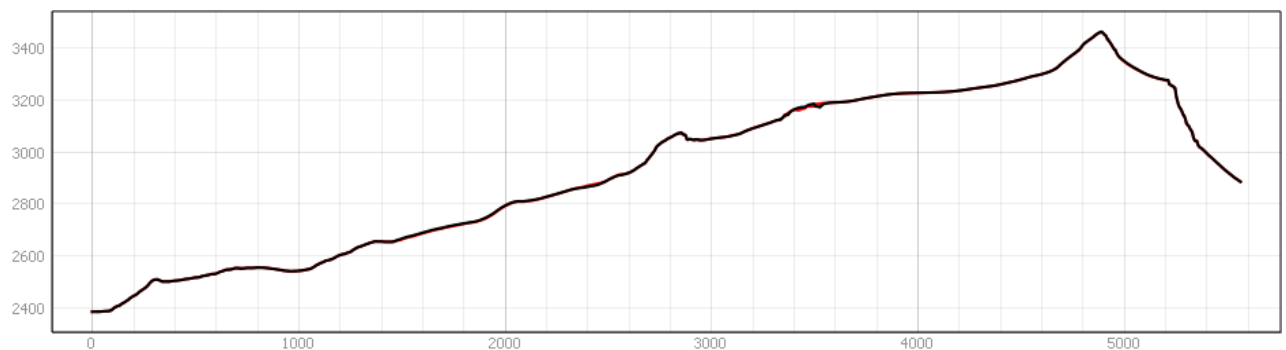


Figure 53 Section 2- Central section



*Figure 55 Section 3- Longitudinal section North- South*



*Figure 54 Section 4- Rutor's head section*

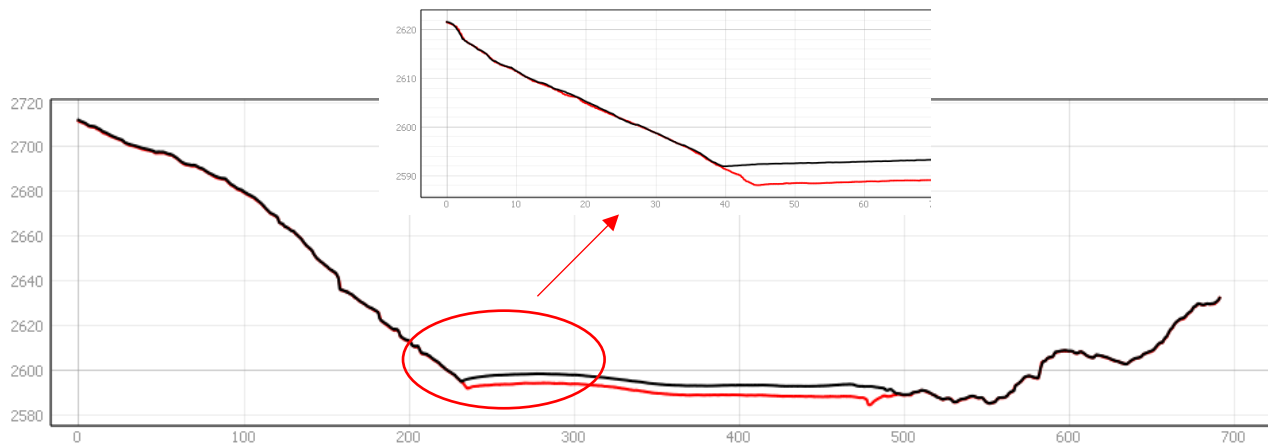


*Figure 56 Section 5- Zoom on east forehead*

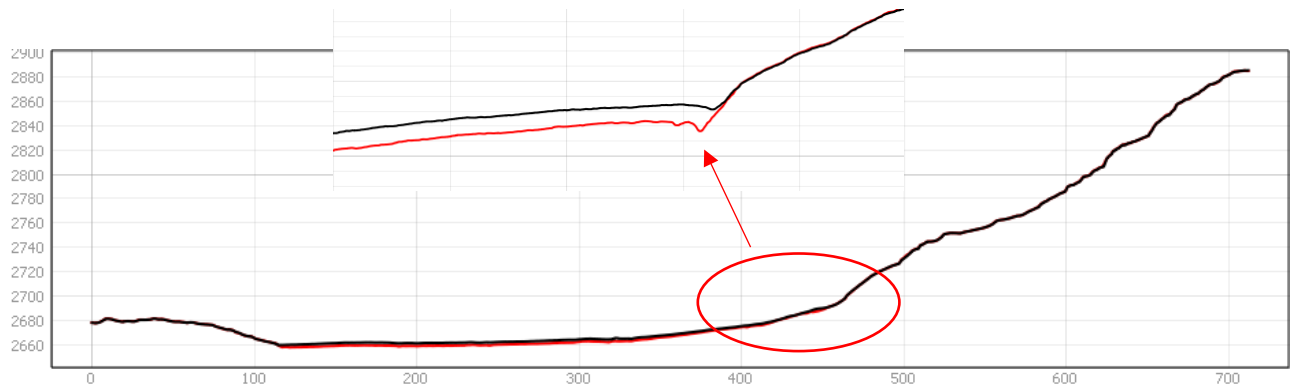


Figure 57 Section 6- Zoom on the west forehead

## 4.4 Drones cartographic products

The drone cartographic products are, for the Serac lake and glacial front from the survey on 9<sup>th</sup> July 2021:

- An Orthophoto with a GSD equal to 0.03 m.
- A DSM with a GSD equal to 0.057 m.
- A Dense Cloud of 540.444.284 points.
- 

And for the model built on the flight on the 21<sup>st</sup> July 2021;

- An Orthophoto with a GSD equal to 003 m in Figure 58.
- A DSM with a GSD equal to 0.069 m
- A Dense Cloud of 443.651.436 points.

Moreover, the sections on the East glacial front and on the Serac lake are reported in Figure 59 and 60 to cross compare the different DSM models of the aerial photogrammetry. It is clear the correspondence on the rocky areas and the mass ablation on the glacial front.

In the section on the Serac lake in Figure 59 on the lake there are peaks correspondent to the water surface. The software has problem to find correlations so it returns this strange behaviour on the model.

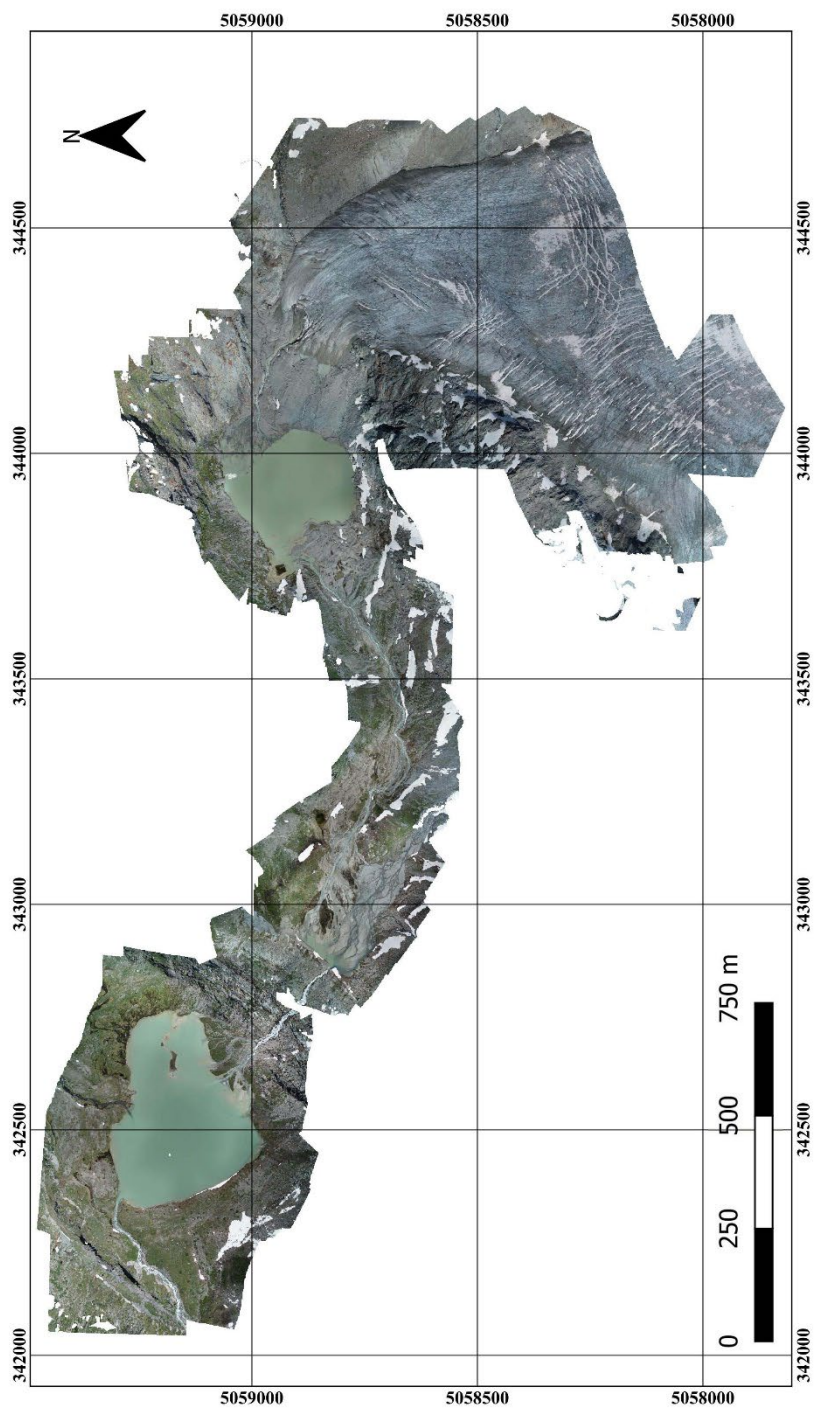
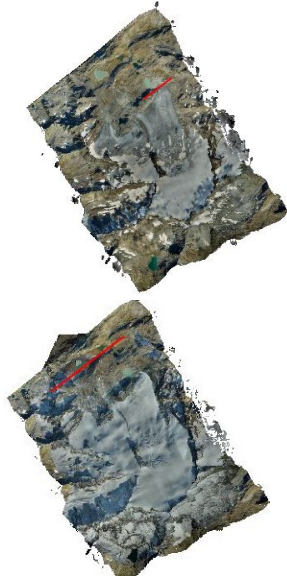


Figure 58 Orthophoto from DJI Phantom images of 9th and 21st July 2021

---

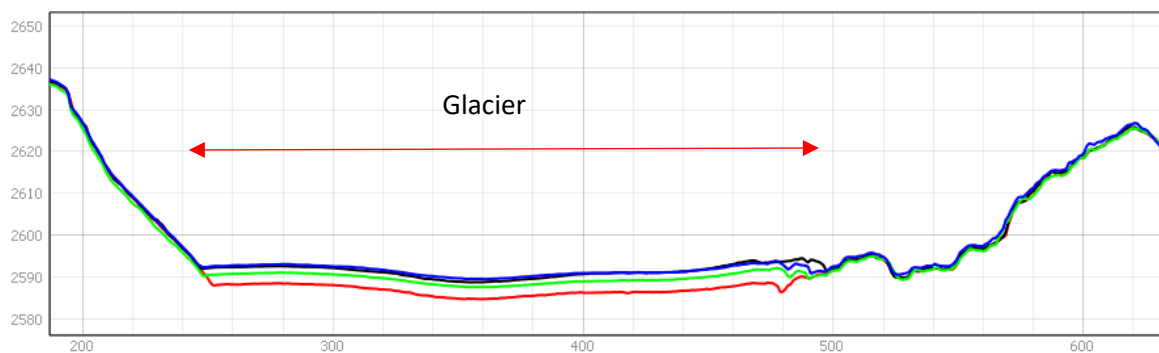
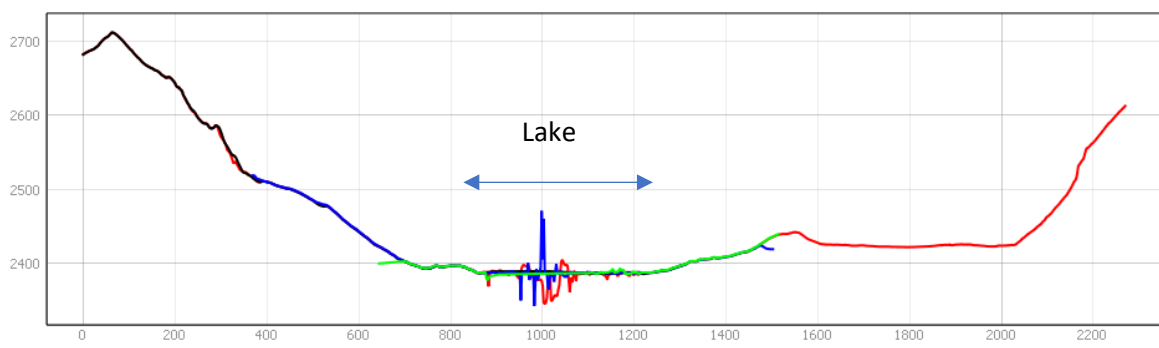
**SECTION 1**

Front west section

**SECTION 2**

Serac lake

---

*Table 31 Legend of the sections**Figure 60 Section 1 East glacier forehead**Figure 59 Section 2 on Serac lake*

LEGEND:

	Photogrammetric model 13 <sup>th</sup> September 2021
	Photogrammetric model 30th September 2020
	DJI drone model 9 <sup>th</sup> July 2021
	DJI drone model 21 <sup>st</sup> July 2021

# Chapter 5

## GNSS Data Post Processing

The GNSS data processing was elaborated to reconstruct the trajectory of the flight on the Rutor glacier and the camera's position at each shot.

### 5.1 Flightpath reconstruction

The GNSS data processing was only performed for the 2020 flight due to lack of data, but the procedure could be similarly applied on the 2021 flight.

The flight was carried out on 30<sup>th</sup> September 2020 from GPST time 08:16:37.1230 to 10:16:09.6430 taking 823 photos.

To postprocessing, the GNSS data was necessary to use a base station. From SPIN GNSS Portal - Servizio di Posizionamento INterregionale della Lombardia, Piemonte, Valle d'Aosta (Geoportale, s.d.), has been downloaded the RINEX of the base station of the 30<sup>th</sup> of September 2020. Unfortunately, there are no nearby stations to the Rutor Glacier, so the nearest base station was selected in RUMIOD, 18 km from the central part of the glacier considered. The monograph of the real base station is reported in Figure 61.

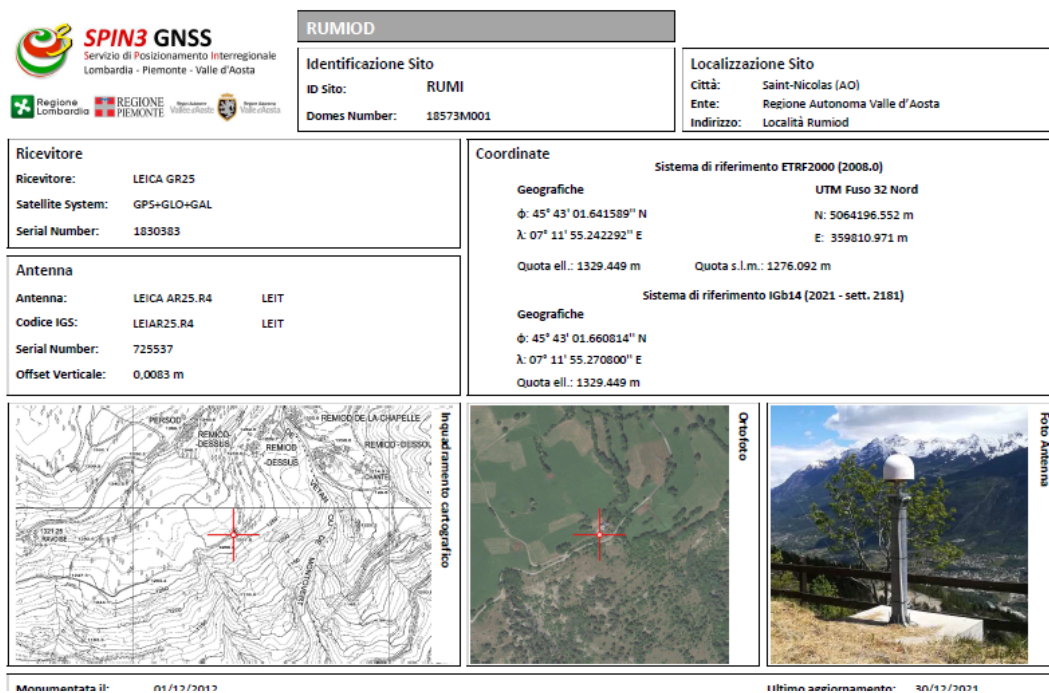


Figure 61 Monograph Rumiod station

Since the Rutor glacier is far from the nearest station, a virtual reference station nearer to the considered area was also used to reach a more precise fix ambiguity. The two station locations are reported in Figure 62.

Unfortunately, the glacier is out of the network, so the nearest possible virtual base station used is quite far. The location in geographic coordinates  $\varphi$ : 45.616666666,  $\lambda$ :

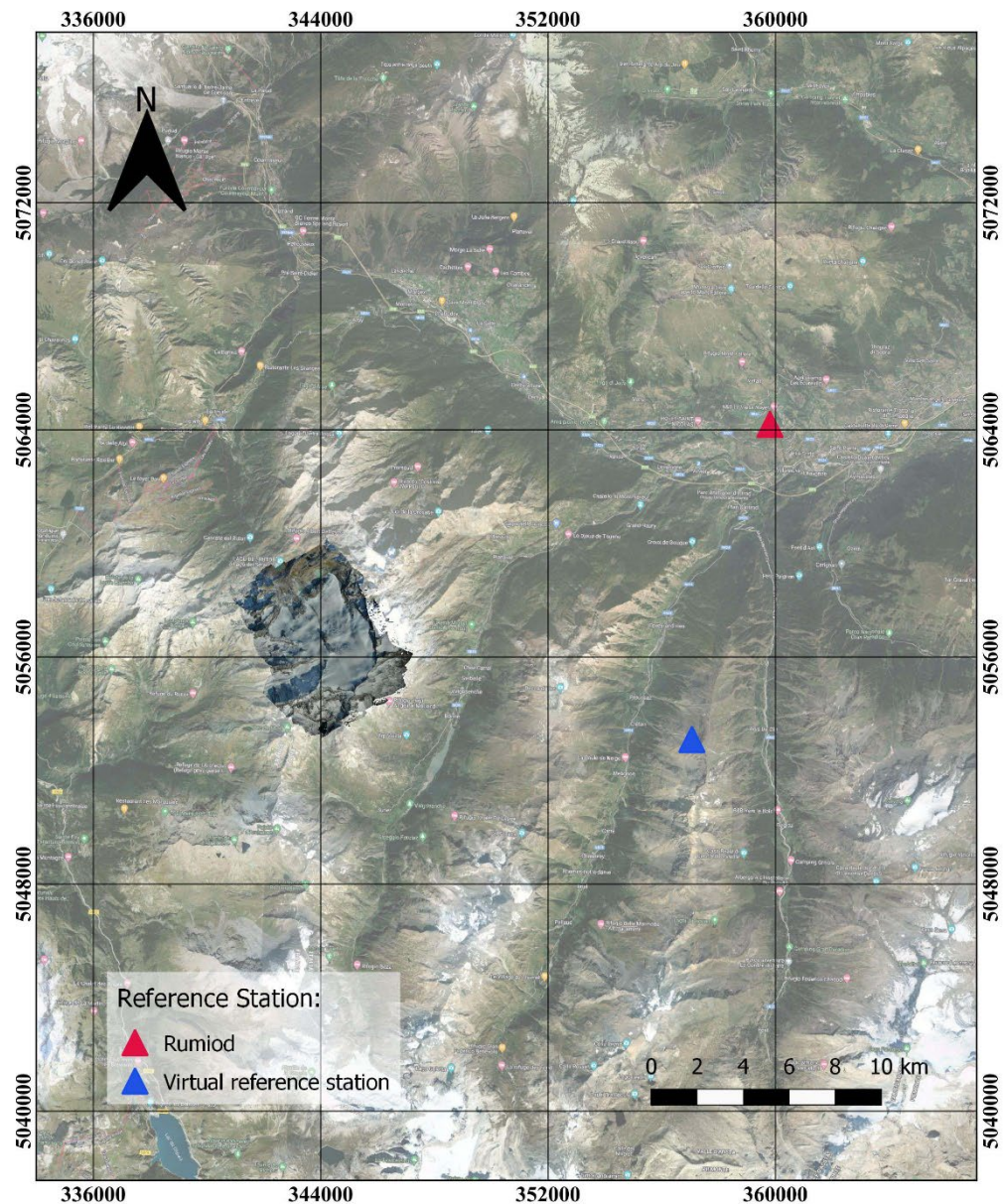


Figure 62 Reference station positions

7.166666667, h:3000.0083; in UTM-ERTF200 N: 5053092.571, E: 357064.129, H: 2945.859.

To calculate the trajectory, it is necessary to know the ephemeris. In this case, to have a more precise data processing, precise ephemerides were used, where the parameters of the orbits of the satellite trajectory are included.<sup>9</sup>

Precise ephemerides were downloaded from the GNSS Calendar portal (GNSSCALENDAR) for the flight data (Figure 63).

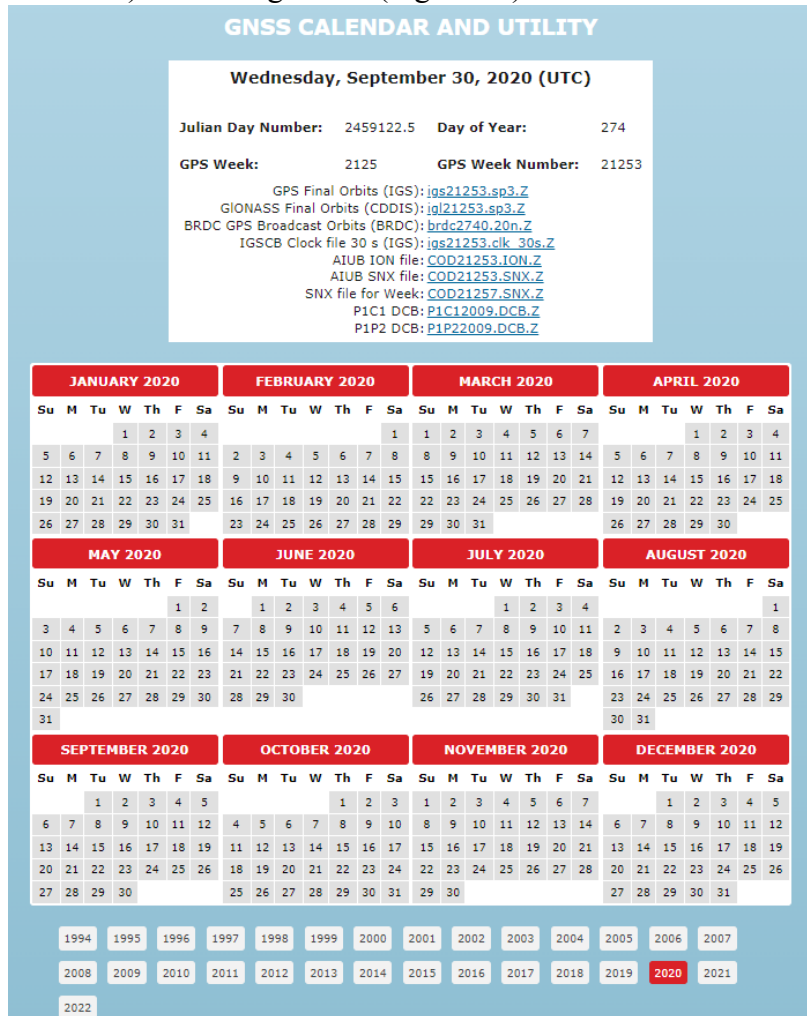


Figure 63 GNSS Calendar

The UBX data provided by DIGISKY have converted thanks to the RINEX converter (Figure 64).

<sup>9</sup> Alternatively, it is possible to use Broadcast ephemerides where ephemerides are calculated by interpolating to get real-time or predicted positions.

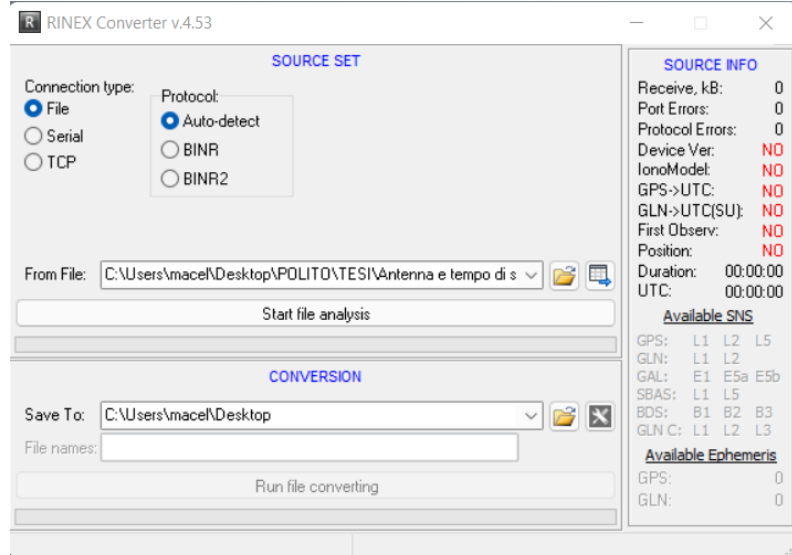


Figure 64 RINEX converteres

RTKLib software (Figure 65) was used to post-process the data and establish the trajectory, particularly the RTKPost software part.

In the software are inserted the observation (.o) RINEX file of the antenna on the aircraft (GPS and GLONASS), precise ephemerides (.sp3) downloaded as written above (GPS and GLONASS) and the observation file of the permanent virtual reference station.

The output file .pos gives the geographical coordinates ETRF2000 of the antenna position during the time. A first iteration is computed for the whole flight from Torino, the first part and the last are out of the interest of the data processing.

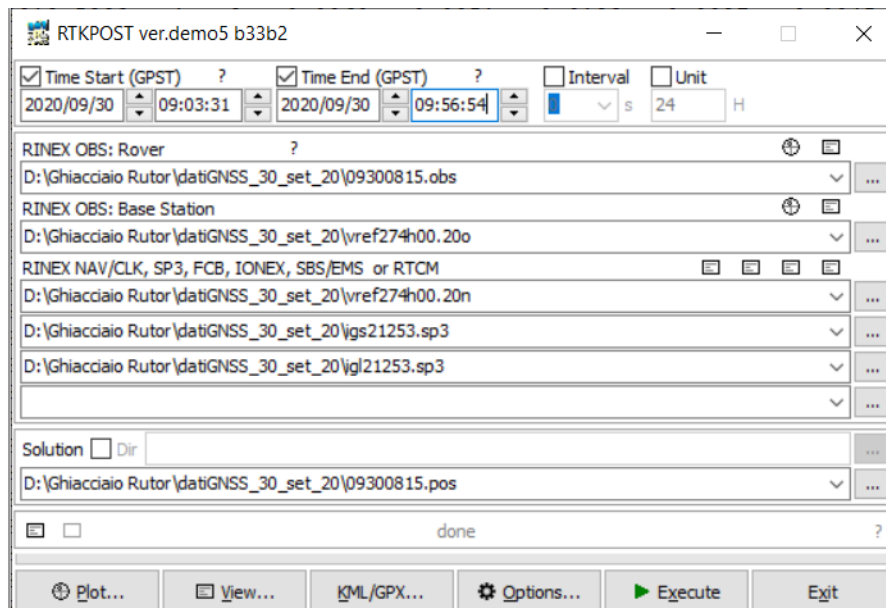


Figure 65 RTKPost

Hence, it is repeated to cut the part out of the interest with the time start from 09:03:31 and the time ends at 9:56:54 of the 30/09/2020 (Figure 68).

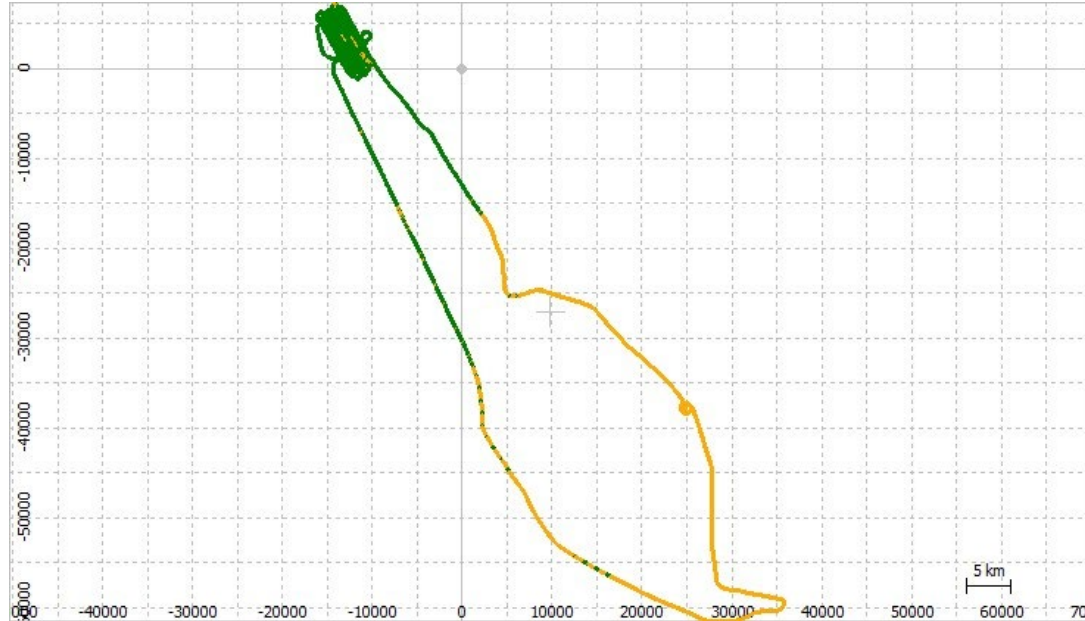


Figure 66 Total trajectory with ambiguity fixed/not fixed

The fixed ambiguity is given for the solution of Q=1(green dots) for the 55% (4214 positions) and not for the first part of the flight from Torino and the way back, as shown in Figure 66, with Q=2 and yellow dots in the image for 45% (3452 positions).

	program : RTKPOST ver.demo5 b33b2
2	% inp file : D:\Ghiacciaio Rutor\datiGNSS_30_set_20\09300815.obs
3	% inp file : D:\Ghiacciaio Rutor\datiGNSS_30_set_20\wref274h00.200
4	% inp file : D:\Ghiacciaio Rutor\datiGNSS_30_set_20\wref274h00.20n
5	% inp file : D:\Ghiacciaio Rutor\datiGNSS_30_set_20\igs21253.sp3
6	% inp file : D:\Ghiacciaio Rutor\datiGNSS_30_set_20\ig121253.sp3
7	% obs start : 2020/09/30 09:03:31.0 GPST (week2125 291811.0s)
8	% obs end : 2020/09/30 09:56:54.0 GPST (week2125 295014.0s)
9	% pos mode : kinematic
10	% freqs : L1+L2/ESb
11	% solution : combined
12	% elev mask : 15.0 deg
13	% dynamics : on
14	% tidecorr : off
15	% ionos opt : broadcast
16	% tropo opt : saastamoinen
17	% ephemeris : precise
18	% navi sys : gps glonass galileo beidou
19	% amb res : fix and hold
20	% amb glo : fix and hold
21	% val thres : 4.0
22	% antenna1 : ( 0.0000 0.0000 0.0000)
23	% antenna2 : LEIAR25.R4 LEIT ( 0.0000 0.0000 0.0083)
24	% ref pos : 45.616666666 7.166666667 3000.0083
25	%
26	(lat/lon/height=WGS84/ellipsoidal,Q=1:fix,2:float,3:sbas,4:dgps,5:single,6:ppp,ns=# of satellites)
27	% GPST latitude(deg) longitude(deg) height(m) Q ns sdn(m) sde(m) sdu(m) sdne(m) sdeu(m) sdu(m) age(s) ratio
28	2020/09/30 09:03:31.0000 45.618391456 7.043990404 3962.9693 1 10 0.0051 0.0041 0.0106 -0.0011 0.0024 -0.0021 0.00 6.0
29	2020/09/30 09:03:32.0000 45.618717216 7.043667542 3961.5921 1 10 0.0051 0.0041 0.0106 -0.0011 0.0024 -0.0021 0.00 6.0
30	2020/09/30 09:03:33.0000 45.619044672 7.043340474 3960.2090 1 10 0.0051 0.0041 0.0106 -0.0011 0.0024 -0.0021 0.00 6.0
31	2020/09/30 09:03:34.0000 45.619373519 7.043009329 3958.7626 1 10 0.0051 0.0041 0.0106 -0.0011 0.0024 -0.0021 0.00 6.0
32	2020/09/30 09:03:35.0000 45.619703973 7.042674942 3957.3918 1 10 0.0051 0.0041 0.0106 -0.0011 0.0024 -0.0021 0.00 5.9
33	2020/09/30 09:03:36.0000 45.620036988 7.042339230 3956.1385 1 10 0.0051 0.0041 0.0106 -0.0011 0.0024 -0.0021 0.00 5.9
34	2020/09/30 09:03:37.0000 45.620372640 7.042003276 3955.0726 1 10 0.0051 0.0041 0.0106 -0.0011 0.0024 -0.0022 0.00 5.9

Figure 67 Output .pos RTKPost with the virtual reference station

This is reasonable because Turin, take off area, is very far from the Rutor glacier. And it is possible also to see the cut plot of the path of the flight on the Rutor Glacier where is detected the central part with the float ambiguity.



*Figure 68 Plot of the output on RTKPost with virtual reference station*

The fixed ambiguity is given for the solution of Q=1(green dots) for the 88.5% (2802 positions) and not the central part of the glacier (yellow dots) for the 11.5% (363 positions), as shown in Figure 68.

The procedure was repeated using the RUMIOD base station to check the better option (Figure 70).

The output shows the phase ambiguity fixed for almost 98.3 % of the positions with the Rumiod base station. This is due to the fact that the virtual reference station is the result of interpolation and because the Rutor glacier is out of the network, and also the virtual reference station is far from the area considered. Considering the similar distance of the stations from the area, the permanent base station is therefore better. However, a more

accurate solution could be if there was the possibility to put the virtual reference station at the centre of the glacier.

For the data processing procedure, the Rumiod station was used as it is able to guarantee a fixed phase ambiguity for almost all, 98.3% (3110 positions) and floating for 1,7% (55 positions) of the flight over the glacier.

The antenna position is computed for each second.

```

1 % program : RTKPOST ver.demo5 b33b2
2 % inp file : D:\Ghiacciaio Rutor\datiGNSS_30_set_20\09300815.obs
3 % inp file : D:\Ghiacciaio Rutor\datiGNSS_30_set_20\vref274h00.20o
4 % inp file : D:\Ghiacciaio Rutor\datiGNSS_30_set_20\vref274h00.20n
5 % inp file : D:\Ghiacciaio Rutor\datiGNSS_30_set_20\igs21253.sp3
6 % inp file : D:\Ghiacciaio Rutor\datiGNSS_30_set_20\igl21253.sp3
7 % obs start : 2020/09/30 09:03:31.0 GPST (week2125 291811.0s)
8 % obs end : 2020/09/30 09:56:54.0 GPST (week2125 295014.0s)
9 % pos mode : kinematic
10 % freqs : L1+L2/E5B
11 % solution : combined
12 % elev mask : 15.0 deg
13 % dynamics : on
14 % tidecorr : off
15 % ionos opt : broadcast
16 % tropo opt : saastamoinen
17 % ephemeris : precise
18 % navi sys : gps gionass galileo beidou
19 % amb res : fix and hold
20 % amb glo : fix and hold
21 % val thres : 4.0
22 % antennal : ( 0.0000 0.0000 0.0000)
23 % antenna2 : LEIAR25.R4 LEIT ( 0.0000 0.0000 0.0083)
24 % ref pos : 45.616666666 7.166666667 3000.0083
25 %
26 % (lat/lon/height=WGS84/ellipsoidal,Q=1:fix,2:float,3:sbas,4:dgps,5:single,6:ppp,ns#= of satellites)
27 % GPST latitude(deg) longitude(deg) height(m) Q ns sdn(m) sde(m) sdw(m) sdne(m) sdeu(m) sdun(m) age(s) ratio
28 2020/09/30 09:03:31.0000 45.618391456 7.043990404 3962.9693 1 10 0.0051 0.0041 0.0106 -0.0011 0.0024 -0.0021 0.00 6.0
29 2020/09/30 09:03:32.0000 45.618717216 7.043667542 3961.5921 1 10 0.0051 0.0041 0.0106 -0.0011 0.0024 -0.0021 0.00 6.0
30 2020/09/30 09:03:33.0000 45.619044672 7.043340474 3960.2090 1 10 0.0051 0.0041 0.0106 -0.0011 0.0024 -0.0021 0.00 6.0
31 2020/09/30 09:03:34.0000 45.619373518 7.043009329 3958.7626 1 10 0.0051 0.0041 0.0106 -0.0011 0.0024 -0.0021 0.00 6.0
32 2020/09/30 09:03:35.0000 45.619703973 7.042674942 3957.3918 1 10 0.0051 0.0041 0.0106 -0.0011 0.0024 -0.0021 0.00 5.9
33 2020/09/30 09:03:36.0000 45.620036988 7.042339230 3956.1385 1 10 0.0051 0.0041 0.0106 -0.0011 0.0024 -0.0021 0.00 5.9
34 2020/09/30 09:03:37.0000 45.620372640 7.042003276 3955.0726 1 10 0.0051 0.0041 0.0106 -0.0011 0.0024 -0.0022 0.00 5.9

```

Figure 69 Output .pos RTKPost with the RUMIOD base

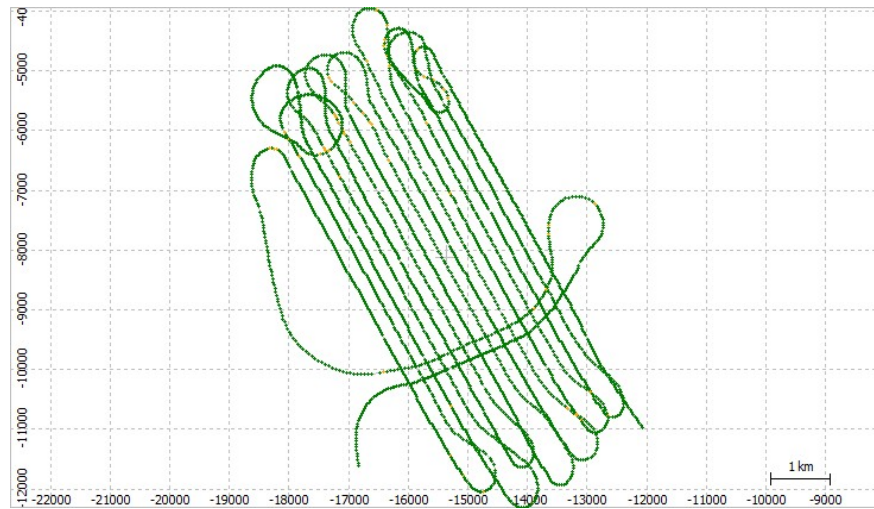
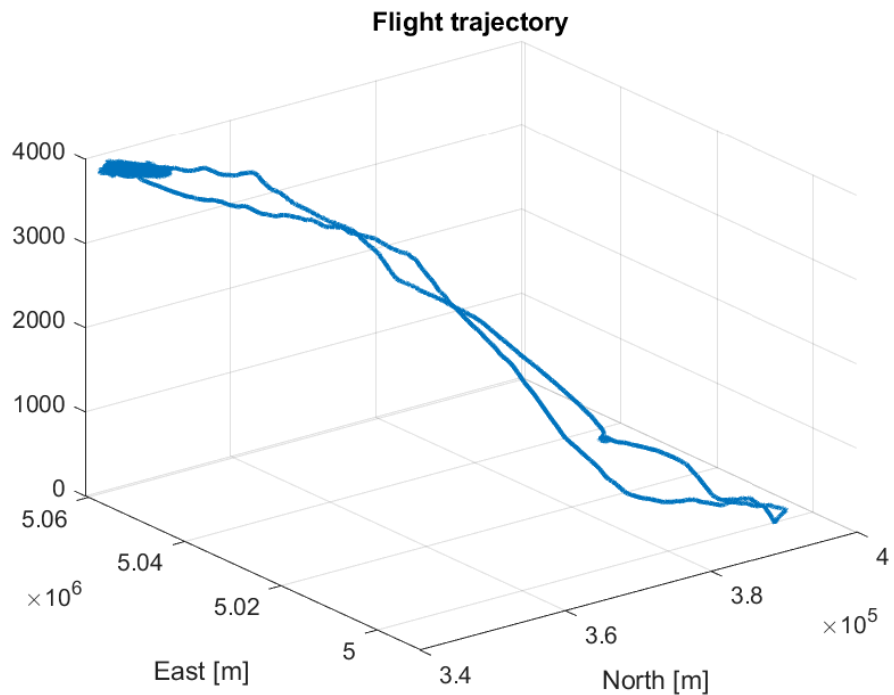
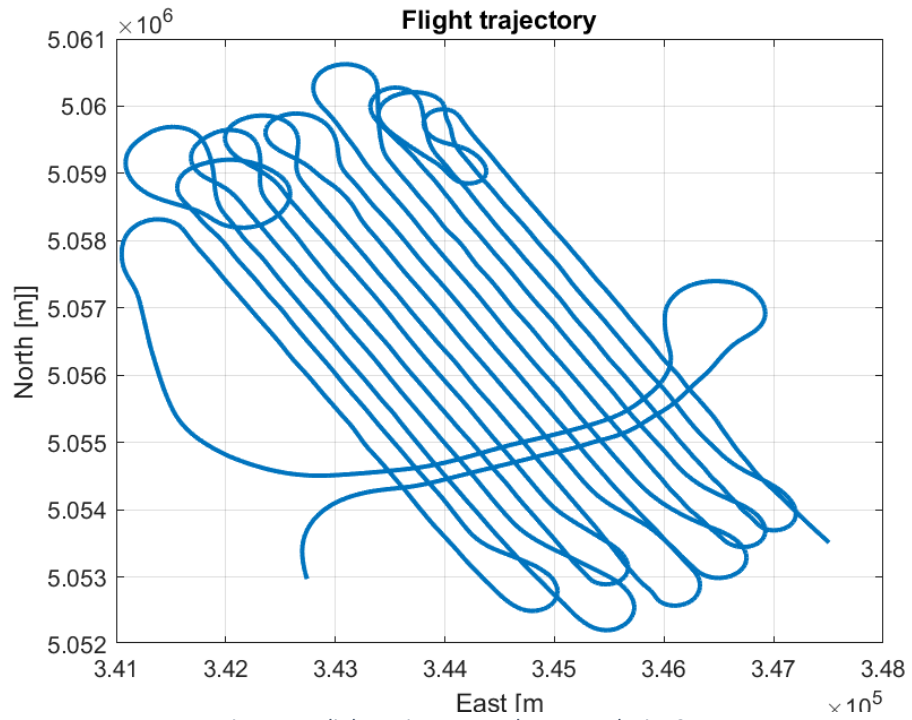


Figure 70 Plot of the output on RTKPost with RUMIOD station



*Figure 72 Full trajectory*

The flight path is plotted in 2D (Figure 71,72,73) and 3D (Figure 74) and with Matlab



*Figure 71 Flight trajectory on the Rutor glacier 2D*

software.

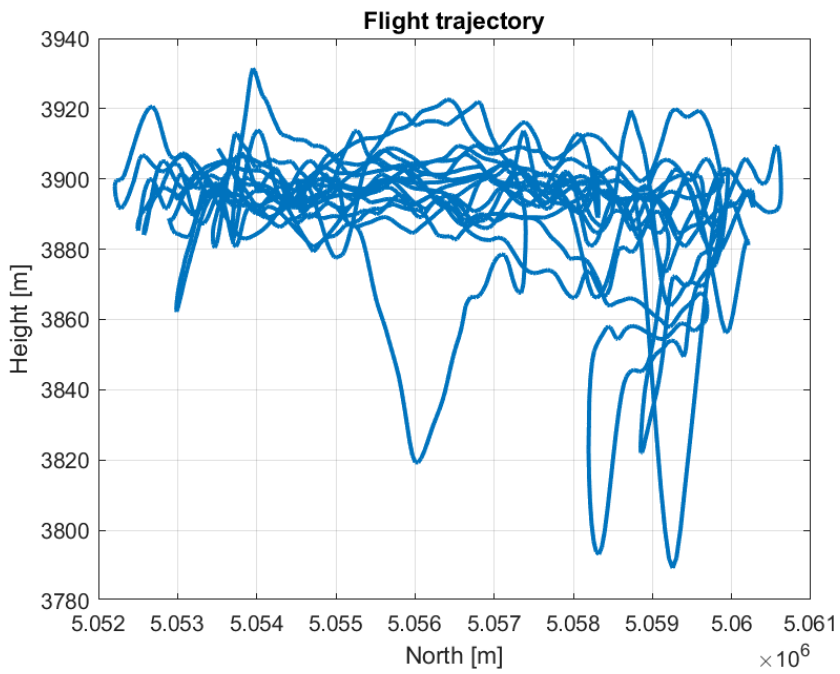


Figure 73 Altimetric flight trajectory on the Rutor glacier

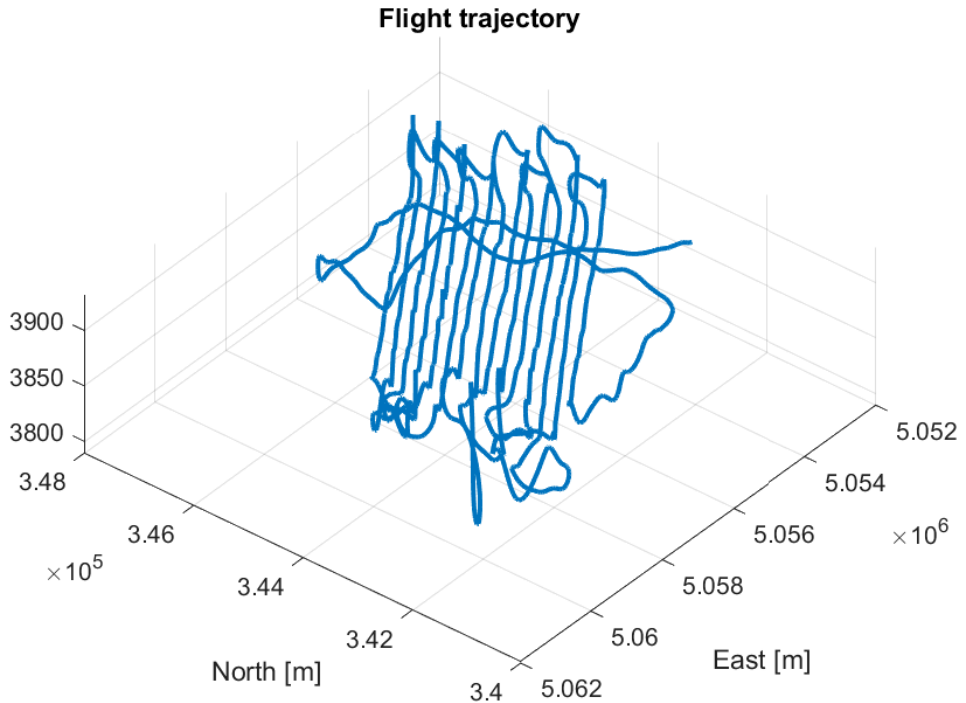


Figure 74 Flight trajectory on the Rutor glacier 3D

The trajectory of the flight computed is reported over the orthophoto in Figure 75. Both the orthophoto and the trajectory have their independent orientation, they are just imported in QGIS.

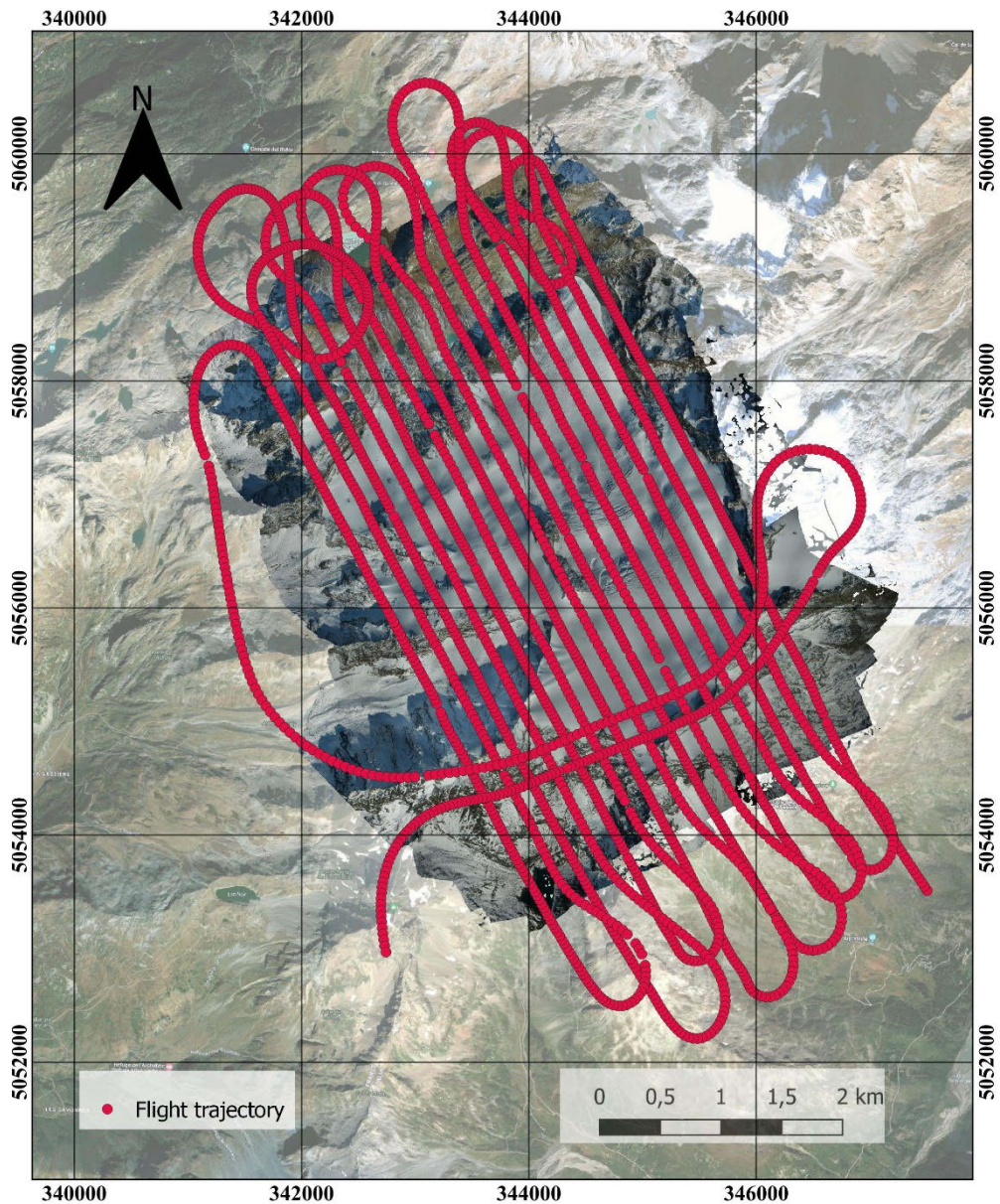


Figure 75 Flight trajectory with the Rumiod base station

## 5.2 IMU Data

The aeroplane was equipped with 2 IMU<sup>10</sup> platforms, one mounted on the body of the aircraft and one on the wing aligned with the camera vertically, about 40 cm above the camera (figure 77). The angles  $\omega, \phi$  and  $\kappa$  (as shown in Figure 76) of rotation along the three axis are registered.

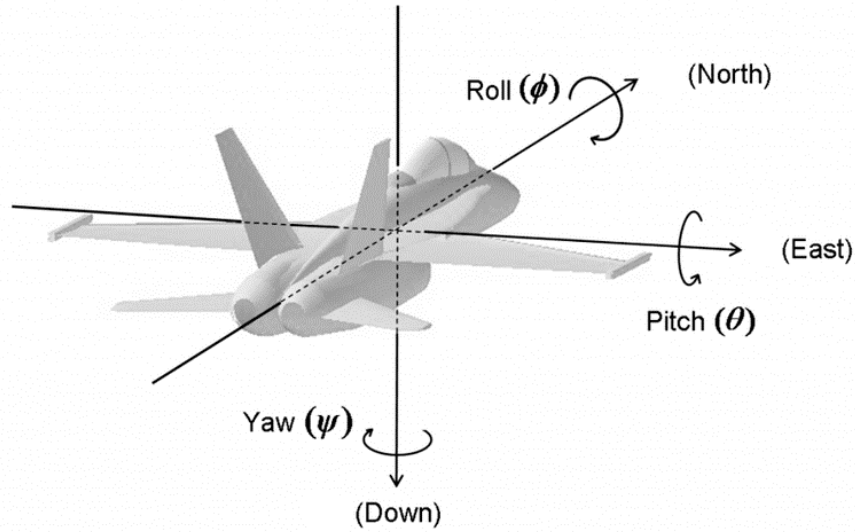


Figure 76 Yaw, Pitch, Roll angles

Digisky, together with the flight frames, provided the files containing the data recorded by the IMUs in .me3 format. Here are reported in the Table 32 a few lines of the first nine columns of data of the file:

UNIX Time [ms]	ID	Counter	H [m]	Lat [°]	Long [°]	Roll [°]	Pitch [°]	Yaw [°]
1631522382809	12554	1	281.1	45.0841638	7.6108634	-0.4	-4.4	-159
163152242229	12554	2	280.90	45.0841627	7.6108641	-0.2	-4.4	-159.8
1631525727517	12554	3	3720.90	45.6254.93	7.0137053	0.5	-4.5	167.8
1631525731167	12554	4	3723.70	45.6268869	7.0124737	0.4	-4.9	164.2
1631525734767	12554	5	3724.90	45.6283747	7.0113192	-1.1	-3.4	165.5
1631525738347	12554	6	3723.10	45.6295059	7.0104457	-0.1	-3.6	165.1
1631525741887	12554	7	3722.60	45.6310327	7.0092857	-1.7	-4.5	167.6
1631525745437	12554	8	3723.40	45.6321668	7.0084002	-0.6	-3.3	169.9
...	..	..	..	..	..	..	..	..

Table 32 IMU .me3 sample data at shooting time

The coordinates in the .me3 file are standalone approximate coordinates with metric precision, therefore there were not used.

<sup>10</sup> Inertial Measurement Unit

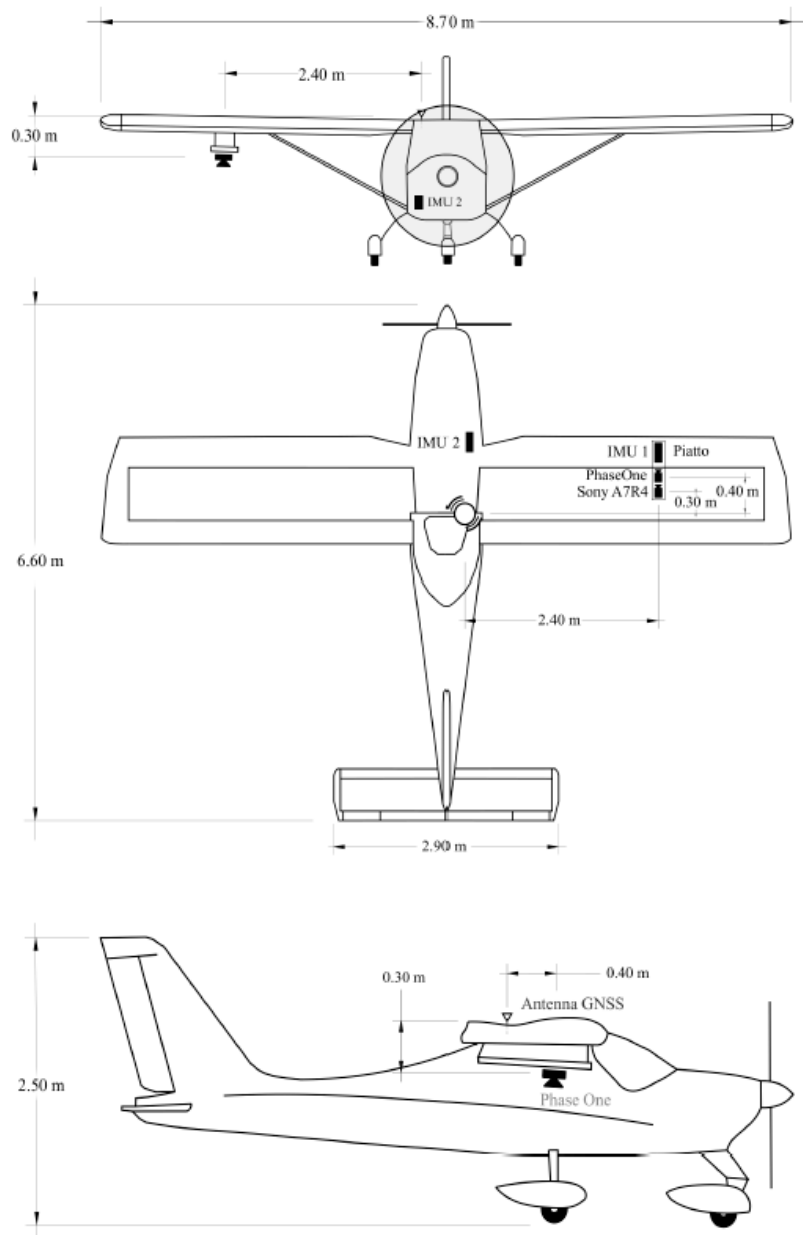


Figure 77 Camera and IMU positions onboard the aircraft from DigiSky

### 5.3 Antenna position at the time of the shooting

First of all, to calculate the antenna position at the shooting time is necessary to unify the scales of the recorded times. The trajectory obtained is in **GPS time**, while the time tag of the recorded shot is in **Unix time**.

The Unix time is a time computed in seconds starting from the Unix Epoch on January 1<sup>st</sup>, 1970, at UTC. (UnixTime)

On the other hand, the GPS time is a continuous time scale based on the atomic clock on the satellites and the Monitor Station established by the GPS control segment. It starts at 00:00 on January 6<sup>th</sup>, 1980. (ESA)

Both time scales were converted into Modified Julian Date to unify the time scales.

The Modifies Julian Date is a date obtained subtracting 2400000.5 days from the Julian date, so it is defined as

$$\text{MJD} = \text{JD} - 2400000.5$$

In this way, the number of the days is obtained starting from the 17<sup>th</sup> of November 1858. (Science World)

From the Time Tag in the Unix time, the time is converted into MJD, and it is expressed in seconds multiplying for 86400 (seconds in a day). In this way, the snapshots are added to the zero-time calculated. From the GPS time of the trajectory is also possible to convert it in MJD. With this procedure, all the time are expressed in the same timescale and comparable. All the procedure is done in Matlab according to the formulas and script of prof. A. Cina. (Cina, 2014)

To find the antenna position at each shot time it is necessary to insert into the Rinex file the ‘EVENT MARKER’ pulse elaborating the shot times in the .me3 file. The leap seconds between the two times is neglected because the time considered is GPS.

The procedure is done in Matlab.

The presence of these new lines is checked with the ‘cerca\_event\_marker.m’ script (partially reported in Figure 78).

```

% legge file rinex e file digisky e scrive event marker nel formato:
% > 2018 2 16 14 38 22.4296370 5 0 all'interno del file rinex. Essi vengono interpretati e interpolati con
RTKpost e le posizioni scritte nel file event.post generato da RTKLIB leggi_me3_digisky.m, date2j.m
%%%%%%%%%%%%%%%
flinp='D:\Ghiacciaio Rutor\datiGNSS_30_set_20\09300815.obs' %file rinex su cui scrivere Event marker
flevent='D:\Ghiacciaio Rutor\datiGNSS_30_set_20\09300815.me3'; %file con time stamp foto
flout='D:\Ghiacciaio Rutor\datiGNSS_30_set_20\09300815_EM.obs' %file rinex con Event marker
leapsecond=0; %nel caso particolare .me3 digisky il tempo unix parte già dal tempo GPS e non UTC
rate=1; %rate campionamento GNSS in secondi
sincro=0.0; %secondi sincronismo tempo camera e GPS
%%%%%%%%%%%%%%%
fid = fopen(flinp, 'r');
fid1 = fopen(flout, 'w');
[eventi]=leggi_me3_digisky(flevent); %legge file digisky .me3
EM=1; %contatore righe file .me3 timestamp
while feof(fid)==0
    tline = fgetl(fid);
    fprintf(fid1,tline);
    fprintf(fid1,'\n');
    carattere=tline(1,1);
    if strcmp(carattere,'>')
        y=str2num(tline(2:6));
        m=str2num(tline(8:9));
        d=str2num(tline(11:12));
        h=str2num(tline(14:15));
        min=str2num(tline(17:18));
        s=str2num(tline(20:29));
        nsat=str2num(tline(34:35));
        [t_unix,jd,mjd,gpsweek,n,sec_gpsweek]=date2jd(y,m,d,h,min,s);
        t_unix=t_unix+leapsecond+sincro; %passa da scala utc a gps
        if EM<size(eventi,1);
            if (eventi(EM,1)/1000-t_unix)<rate
                for i=1:1:nsat
                    tline1 = fgetl(fid);
                    fprintf(fid1,tline1);
                    fprintf(fid1,'\n');
                end
                t=(eventi(EM,1)/1000-t_unix); %decimali tempo scatto
                secondi=str2num(tline(20:21)); %secondi interi Rinex
                sec=secondi+t; % time stamp
                string1=(tline(1:18));
                string2=' 5 0           EVENT MARKER';
                fprintf(fid1,"%18s %10.7f %6s\n",string1,sec,string2);
                EM=EM+1;
            end
        end
    end
    fclose(fid);
    fclose(fid1);
    disp('il file rinex con event marker è');disp(flout);

```

Figure 78 Matlab Script 'SCRIVI EVENT MARKER'

The output is a modified Rinex file where the line EVENT MARKER is inserted for each time shot. In the examined case there are 823 lines inserted. It is possible to check the procedure with another script to search and check in the Rinex file the actual writing of the lines corresponding to the shots inserted under the name of 'EVENT MARKER' (Figure 79).

2020 9 30 8 16 37.1229799 5 0	EVENT MARKER
> 2020 9 30 8 16 38.1349852 5 0	EVENT MARKER
> 2020 9 30 8 19 28.5240166 5 0	EVENT MARKER
> 2020 9 30 8 19 29.5179818 5 0	EVENT MARKER
> 2020 9 30 9 3 58.9180033 5 0	EVENT MARKER
> 2020 9 30 9 4 1.6389794 5 0	EVENT MARKER
> 2020 9 30 9 4 4.4429958 5 0	EVENT MARKER
> 2020 9 30 9 4 7.3140118 5 0	EVENT MARKER
> 2020 9 30 9 4 10.2439935 5 0	EVENT MARKER
> 2020 9 30 9 4 13.2450042 5 0	EVENT MARKER
> 2020 9 30 9 4 16.2630205 5 0	EVENT MARKER
> 2020 9 30 9 4 19.2729967 5 0	EVENT MARKER
> 2020 9 30 9 4 22.3700128 5 0	EVENT MARKER

Figure 79 Cerca EVENT MARKER response

The file obtained is processed in RTKPost (Figure 80) software with the input file of the modified Rinex \_EM.obs and the same other parameters as before.

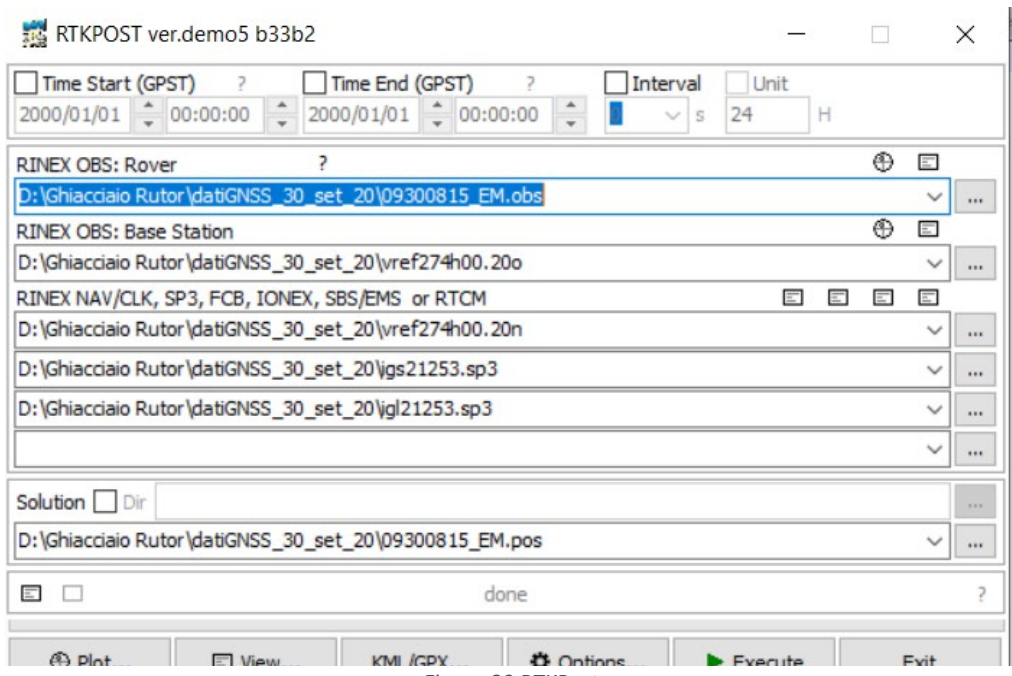


Figure 80 RTKPost

The output file (Figure 81) contains the time and the coordinates of each time shot in ETRF2000 that are converted with the Convergo Software into UTM-ETRF2000.

```

1 $ program : RTKPOST ver.demo5 b33b2
2 $ inp file : D:\Ghiacciaio Rutor\datIGNSS_30_set_20\09300815_EM.obs
3 $ inp file : D:\Ghiacciaio Rutor\datIGNSS_30_set_20\vrref274h00..20n
4 $ inp file : D:\Ghiacciaio Rutor\datIGNSS_30_set_20\vrref274h00..20n
5 $ inp file : D:\Ghiacciaio Rutor\datIGNSS_30_set_20\ig121253..gp3
6 $ inp file : D:\Ghiacciaio Rutor\datIGNSS_30_set_20\ig121253..gp3
7 $ obs start : 2020/09/30 08:16:03.0 GST (week2125 288963.0s)
8 $ obs end : 2020/09/30 10:25:07.0 GST (week2125 286707.0s)
9 $ pos mode : kinematic
10 $ freqs : L1+L2+ESB
11 $ solution : combined
12 $ elev mask : 15.0 deg
13 $ dynamics :
14 $ receiver : off
15 $ ionos opt : broadcast
16 $ tropo opt : saastamoinen
17 $ ephemeris : precise
18 $ navi sys : gps glonass galileo beidou
19 $ amb res : fix and hold
20 $ amb glo : fix and hold
21 $ val thres : 4.0
22 $ antennal : ( 0.0000 0.0000 0.0000)
23 $ antennal : LEIAR25.R4 LEITT ( 0.0000 0.0000 0.0083)
24 $ ref pos : 45.616666667 7.166666667 3000.0083
25 $
26 ($lat/ion/height=WGS84/ellipsoidal,Qsl:fix,2:float,3:sbas,4:dgps,5:single,6:ppp.ns=# of satellites)
27 $ GPST latitude(deg) longitude(deg) height(m) Q ns sdn(m) sde(m) sdu(m) sdne(m) sdeu(m) sduu(m) age(s) ratio
28 2020/09/30 08:16:02.9996 45.084135220 7.610826427 331.6774 2 8 0.0063 0.0050 0.0120 0.0022 0.0022 -0.0027 -0.00 0.0
29 2020/09/30 08:16:04.9995 45.084135225 7.610826424 331.6742 2 8 0.0063 0.0050 0.0120 0.0023 0.0022 -0.0027 -0.00 0.0
30 2020/09/30 08:16:05.9995 45.084135233 7.610826440 331.6785 2 8 0.0063 0.0050 0.0120 0.0023 0.0022 -0.0027 -0.00 0.0
31 2020/09/30 08:16:06.9995 45.084135242 7.610826441 331.6776 2 8 0.0063 0.0050 0.0120 0.0023 0.0022 -0.0027 -0.00 0.0
32 2020/09/30 08:16:08.9995 45.084135250 7.610826450 331.6793 2 8 0.0063 0.0050 0.0120 0.0023 0.0022 -0.0027 -0.00 0.0
33 2020/09/30 08:16:09.9995 45.084135215 7.610826440 331.6609 2 8 0.0063 0.0050 0.0120 0.0023 0.0022 -0.0027 -0.00 0.0
34 2020/09/30 08:16:09.9995 45.084135219 7.610826459 331.6753 2 8 0.0063 0.0050 0.0120 0.0023 0.0022 -0.0027 -0.00 0.0
35 2020/09/30 08:16:10.9995 45.084135224 7.610826444 331.6798 2 8 0.0063 0.0050 0.0120 0.0023 0.0022 -0.0027 -0.00 0.0
36 2020/09/30 08:16:11.9995 45.084135218 7.610826462 331.6773 2 8 0.0063 0.0050 0.0120 0.0023 0.0022 -0.0027 -0.00 0.0
37 2020/09/30 08:16:12.9995 45.084135212 7.610826462 331.6809 2 8 0.0063 0.0050 0.0120 0.0023 0.0022 -0.0027 -0.00 0.0
38 2020/09/30 08:16:13.9995 45.084135216 7.610826451 331.6817 2 8 0.0063 0.0050 0.0120 0.0023 0.0022 -0.0027 -0.00 0.0
39 2020/09/30 08:16:14.9995 45.084135221 7.610826455 331.6786 2 8 0.0063 0.0050 0.0120 0.0023 0.0022 -0.0027 -0.00 0.0
40 2020/09/30 08:16:15.9995 45.084135210 7.610826468 331.6804 2 8 0.0063 0.0050 0.0120 0.0023 0.0022 -0.0027 -0.00 0.0
41 2020/09/30 08:16:16.9995 45.084135227 7.610826479 331.6790 2 8 0.0063 0.0050 0.0120 0.0023 0.0022 -0.0027 -0.00 0.0
42 2020/09/30 08:16:17.9995 45.084135204 7.610826462 331.6789 2 8 0.0063 0.0050 0.0120 0.0023 0.0022 -0.0027 -0.00 0.0

```

Figure 81 Output shots over time – interpolated GNSS antenna to shooter time

In this case, an accessory file (EVENT\_) is created which contains the interpolated position of the centre of the antenna at the instant the camera is shot. These must then be brought back to the centre of the camera take-up by rotation of the lever arms.

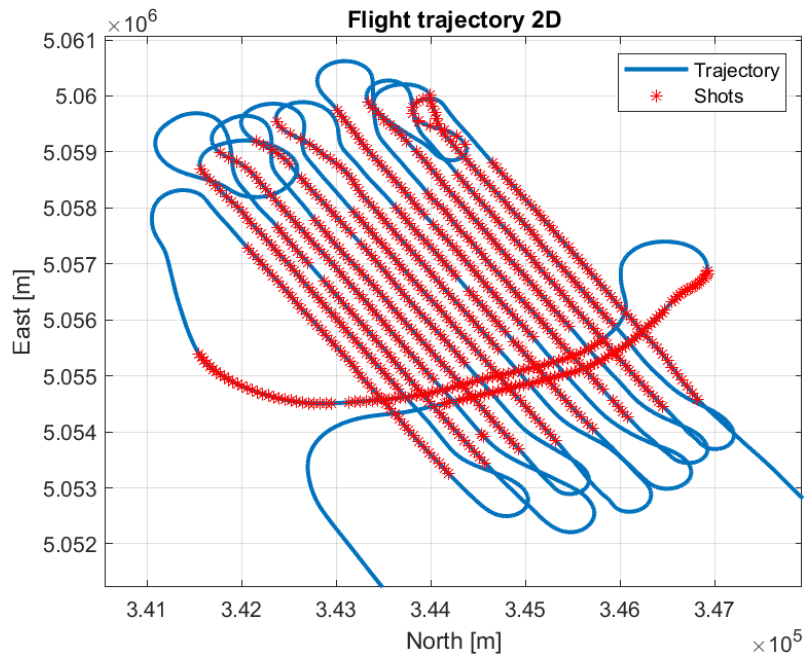


Figure 82 Flight trajectory with shots position in 2D

Unfortunately, in this system the GPS time is not synchronised with the strobe time given by the on-board clock. Any achievable interpolation goes through the offset estimation to align the time scales.

For the first double-check is now possible to plot the trajectory of the aircraft with the shot position for each frame both in 2D (Figure 82) and in 3D (Figure 83). It is possible in this way to avoid gross errors.

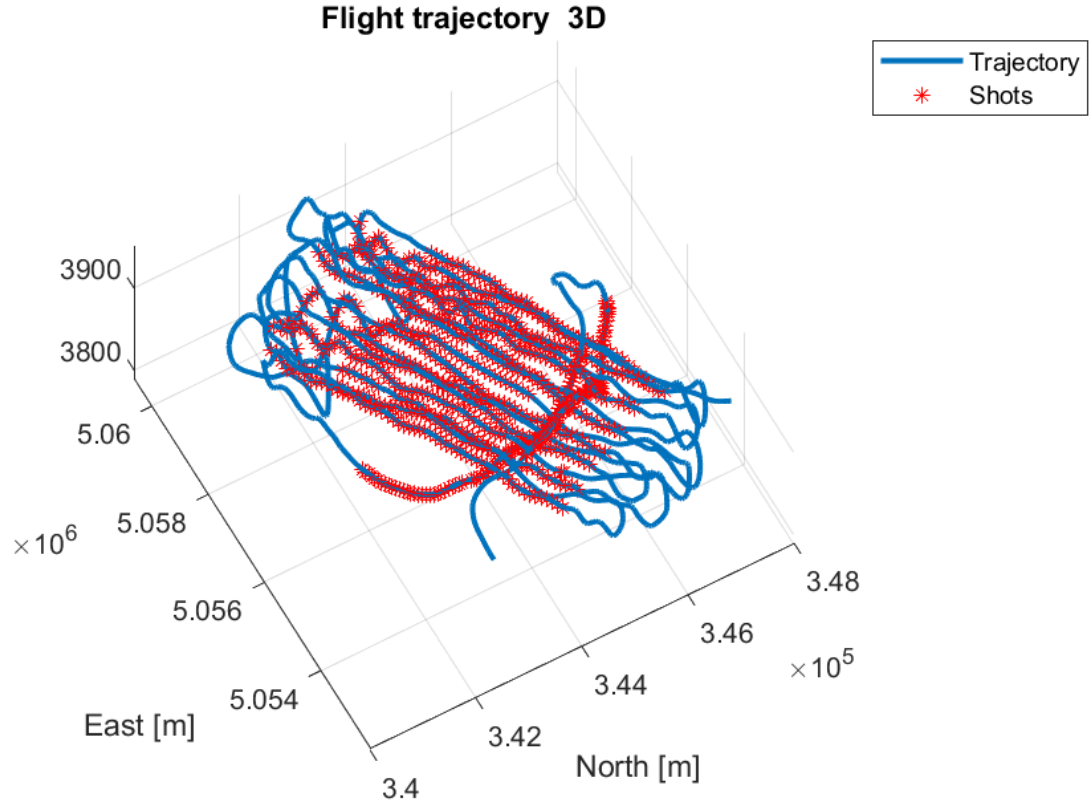


Figure 83 Flight trajectory with shots position in 3D

To estimate the exact camera position, it is necessary to compute the rototranslation matrix between the phase centre and the camera centre with the three angles around the three axes of the coordinate system using the aircraft IMU angles registered. The data of the camera are subjected to a translation due to the delay between the time and the registration and a rotation due to the IMU angles:

$$(E, N, h)^T_{camera} = (E, N, h)^T_{antenna} + [R] * (e_N, e_E, e_h)^T$$

The rotation matrix is composed by the rotation registered around the three angles,  $\omega$  angle, roll around the X-axis, the  $\phi$  angle, pitch around the Y-axis and  $\kappa$  angle, yaw around the Z-axis.

Then, the 'LEVER ARMS' (eccentricity between the centre of the GNSS antenna and the grip centre) will be rotated by the attitude angles 'yaw', 'pitch' and 'roll' to bring the centre of the GNSS antenna to the grip centre.

The GPS antenna, as said before, is positioned on the wing of the aircraft vertically aligned with the camera if the aircraft is in a nadiral position. Therefore, it is necessary to consider the eccentricity between the camera and antenna centres measured and given from Digisky.

$$\mathbf{e} = (0.10, 0, -0.40).$$

Thus, it is necessary to compute the eccentricity, called 'lever arm' for each position during the flight in Matlab (Figure 86).

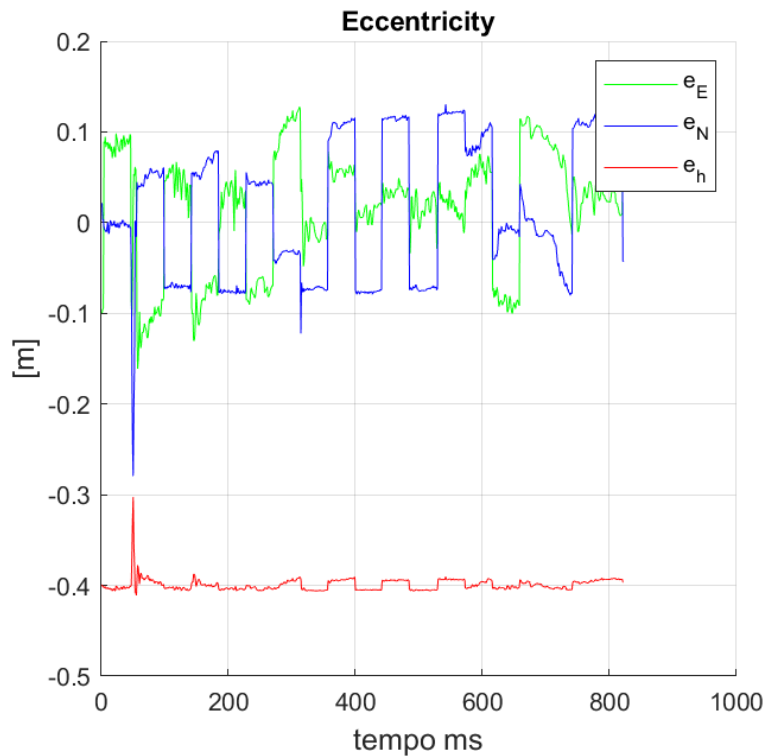


Figure 84 Eccentricity GNSS antenna – camera projection points

The lever arm output file (Table 33) returns the coordinates East, North and H at each Unix time. These coordinates are then added as a correction to the coordinates obtained from the processing of shooting times in RTKPost described above after the conversion from ETRF-2000 into UTM- ETRF2000.

Unix Time	E [m]	N [m]	H [m]
1601453798121	-0.10	0.02	-0.40
1601453799133	-0.10	0.02	-0.40
1601453969523	-0.10	0.00	-0.40

...	...	...	...
<i>Table 33 Lever Arm output to be add</i>			

In the end, the antenna position coordinates are computed with the lever arm correction: in Table 34:

<b>GPS time</b>	<b>Unix time [s]</b>	<b>E [m]</b>	<b>N [m]</b>	<b>H [m]</b>
09:03:58.9180	16014566389	346820.766	5054585.079	3883.590
09:04:01.6390	16014566416	346765.633	5054698.648	3879.449
09:04:04.4430	16014566444	346706.875	5054811.846	3881.505
09:04:07.3140	16014566473	346650.412	5054925.426	3883.222
09:04:10.2440	16014566502	346599.464	5055042.395	3884.561
09:03:58.9180	16014566389	346820.766	5054585.079	3883.590
...	...	...	...	...

*Table 34 Coordinates*

The times of the GPS position registered and the real shooting time do not coincide. Although, in fact, the sensor attached to the camera records the moment of maximum shutter opening when the shot is sent, while the sensor attached to the aircraft records the time when the frame is written, it is necessary to calculate this time interval attributable to the storage of the frame.

## 5.4 Comparison between GPS and AT camera centres

After processing the camera centres from direct photogrammetry, it is possible to compare them with those obtained by aerial triangulation to crosscheck and compare the procedures and the products obtained with two independently solutions.

In order to understand the temporal delay between the impulse of the camera and the registered shot time and correct the bias between the two systems, some steps are developed.

In this first step, the obtained result is based on the synchronicity of the two systems to recalculate each shot with the offset corrected and compare the two methods again.

The model of aerial triangulation is the one previously described model developed in Metashape. It is possible to download the coordinates of the camera centres obtained by aerial triangulation. Then, the comparison is made between these coordinates and those obtained by processing the GPS data processing.

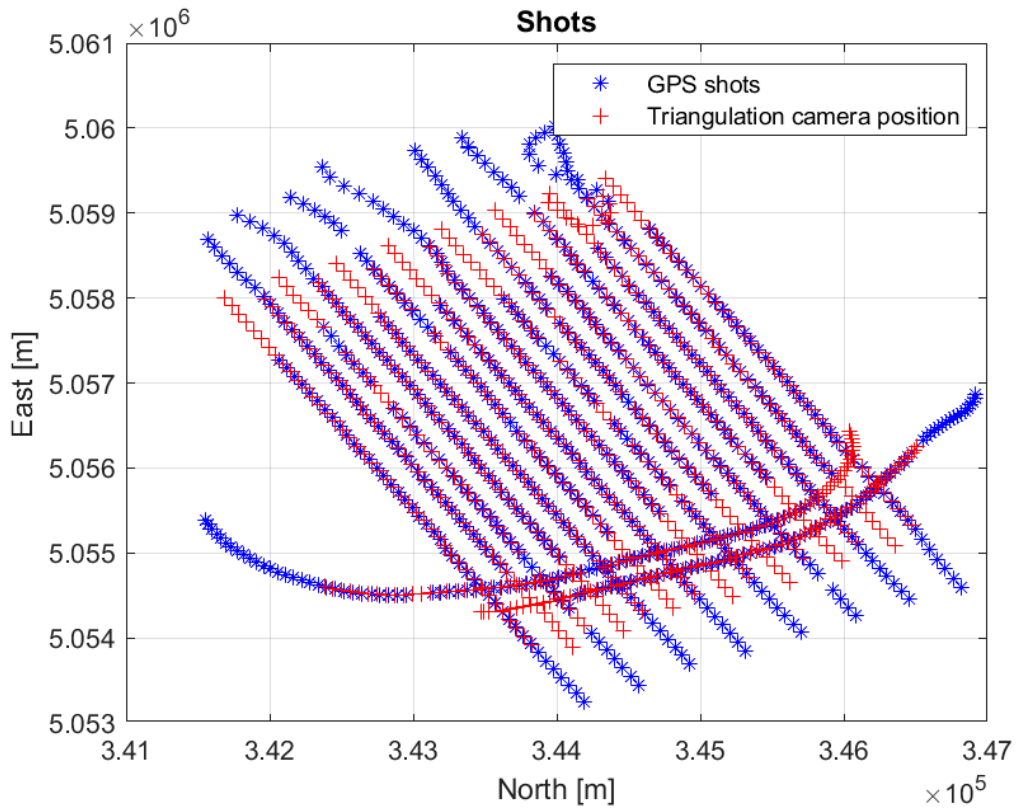


*Figure 85 Comparison between the camera centres*

Plotting the two sets of coordinates, as shown in Figure 85 and 86, is evident in the asynchronism between the camera centre derived from the aerial triangulation in red and the GPS shot time in blue.

First of all, it is necessary to compute the aircraft's velocity during the shooting time. For this reason, a coordinate is calculated starting from the coordinates of the 797 shots computed as described above CFR. Par. 5.4.

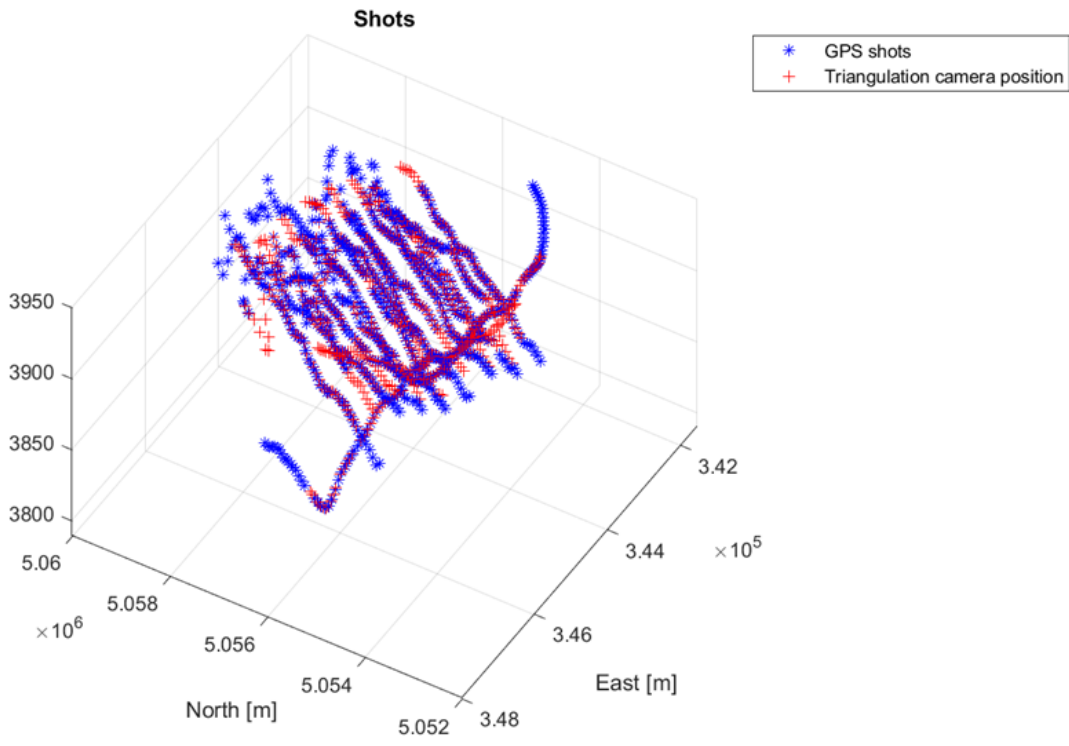


Figure 86 Comparison between shots in 3D

The s coordinate is calculated as follow:

$$s_{GPS} = \sqrt{(x_{i+1} - x_i)^2_{GPS} + (y_{i+1} - y_i)^2_{GPS} + (z_{i+1} - z_i)^2_{GPS}}$$

And for each  $\Delta t$  of two consecutive shots, the punctual velocity is computed and plotted in Figure 87:

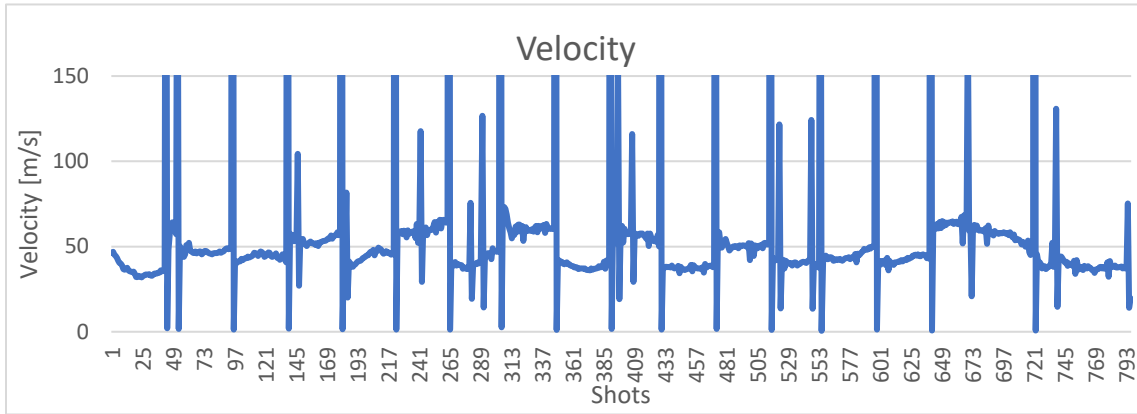


Figure 87 Velocity between of the aircraft derived from GPS coordinates

$$v = \frac{x_{i+1} - x_i}{\Delta t}$$

The curvilinear coordinates are also computed for the triangulation to compare them

$$s_{TA} = \sqrt{(x_{i+1} - x_i)^2_{TA} + (y_{i+1} - y_i)^2_{TA} + (z_{i+1} - z_i)^2_{TA}}$$

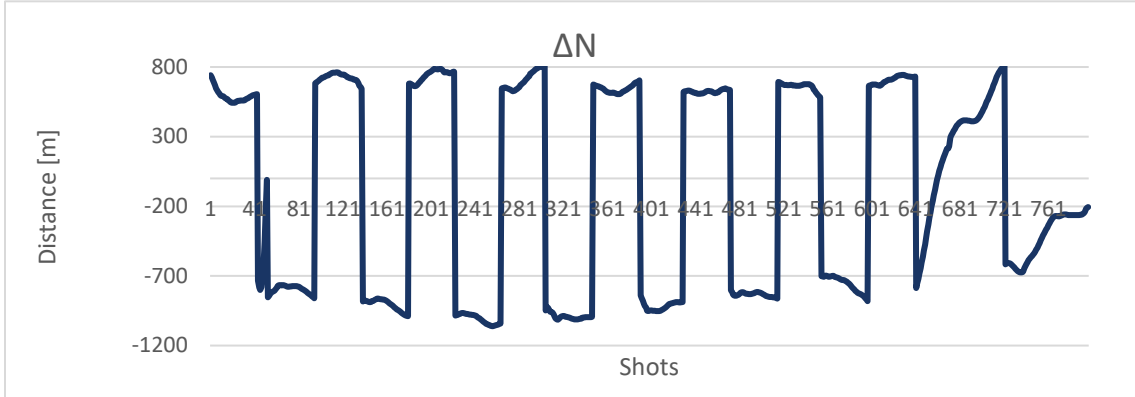


Figure 90 Distance between North coordinates

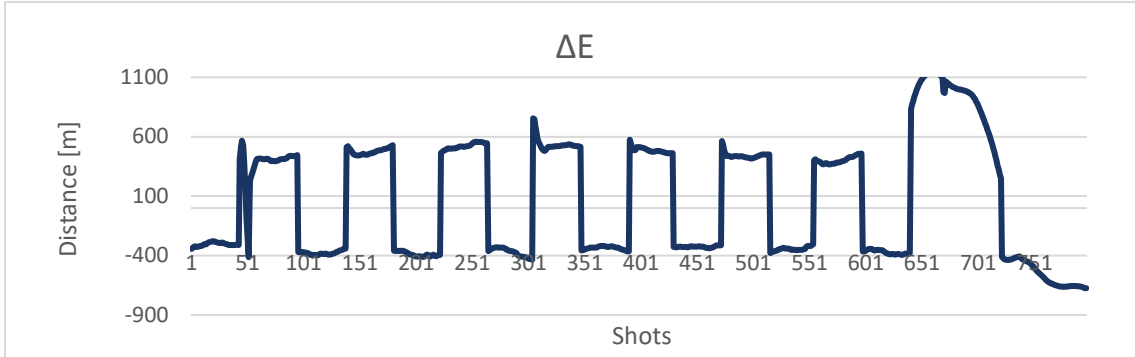


Figure 89 Distance between East coordinates

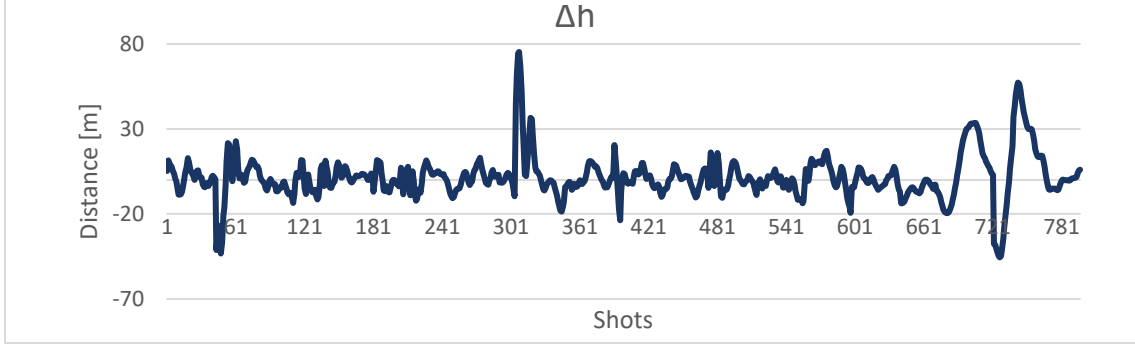


Figure 88 Distance between height coordinates

The distance between the north, east and height components of the two sets of coordinated is plot respectively in Figure 88-89-90. It is possible to recognize each strip on the glacier

and the final curvilinear part. The main differences are in the north component of the coordinates, while the altimetric component is quite constant.

The total distance between each shot coordinate is computed and plotted in Figure 91:

$$d_{TA-GPS} = \sqrt{(x_{TA} - x_{GPS})^2 + (y_{TA} - y_{GPS})^2 + (z_{TA} - z_{GPS})^2}$$

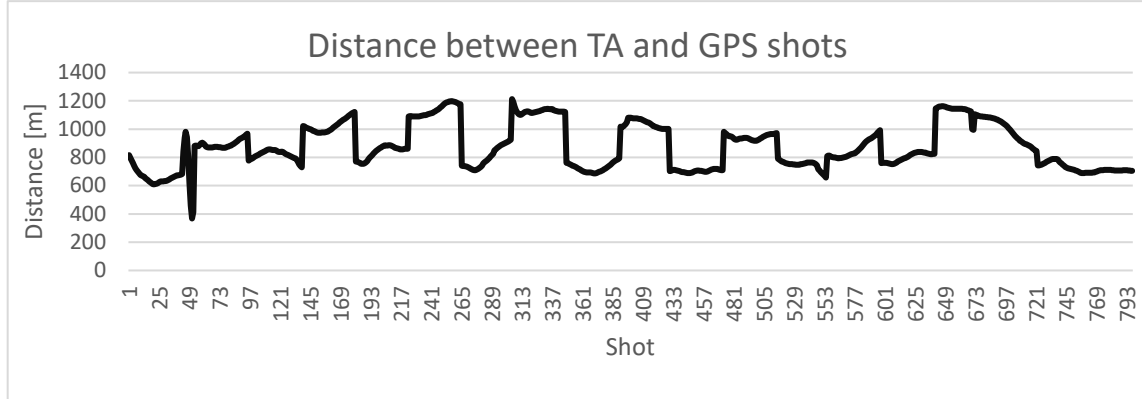


Figure 91 Distance between TA and GPS shots

and the delta offset (Figure 92) is

$$\delta = \frac{d}{\Delta t}$$

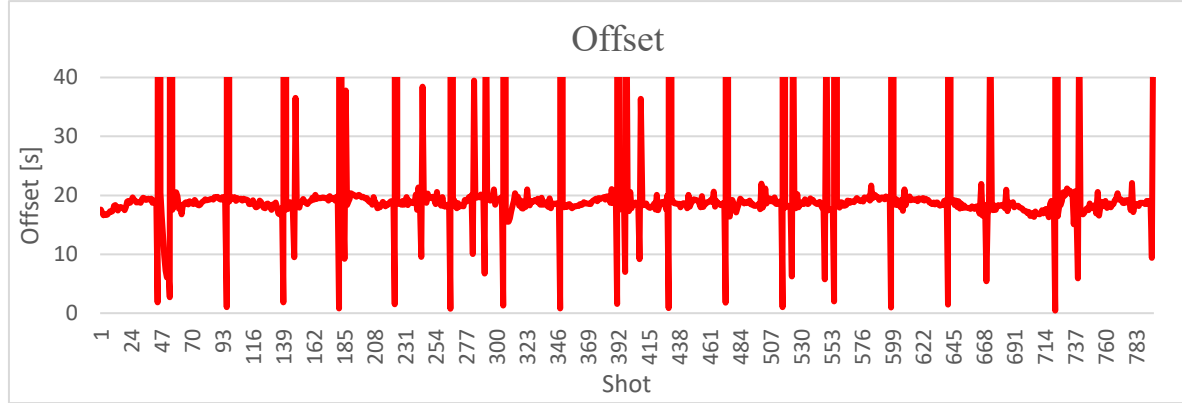


Figure 92 Offset between the TA and GPS coordinates

The velocity of the flight is not constant, probably due to the type of the aircraft and the wind. Nevertheless, it is possible to read the difference in velocity and the distance between each of the 15 strips from the graph. Moreover, the peak clearly shows the different turns at the end of each strip on the glacier.

Due to the presence of the turns, it is not possible to proceed with an average velocity and offset on the entire flight. For this reason, 60 different shots are selected (Figure 93), being careful to be at the centre of the strips and far from the turning points.

The selected point's coordinates are reported in 4 and entirely reported in the table in Annex 2.

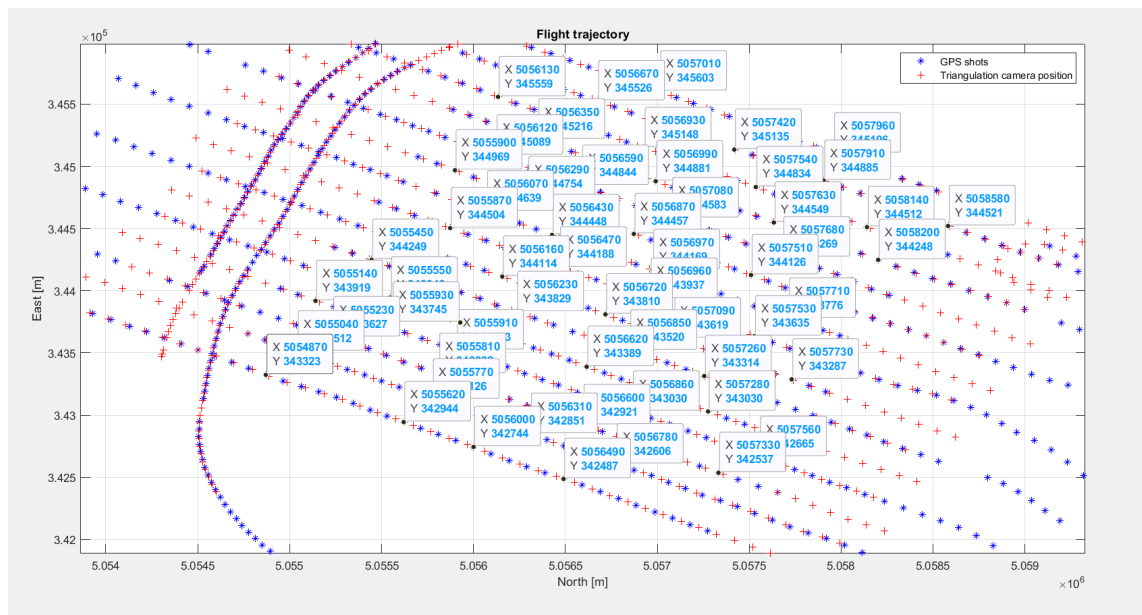


Figure 93 Selected shots

The velocity computed and the offset between the two sets of coordinates as described above is computed and equal to 46.84714 m/s with an offset of 18.88909 s.

The plots show that the velocity still oscillates on the different strips in the forward and backward trajectory (Figure 94) and also the offset oscillates (Figure 95).

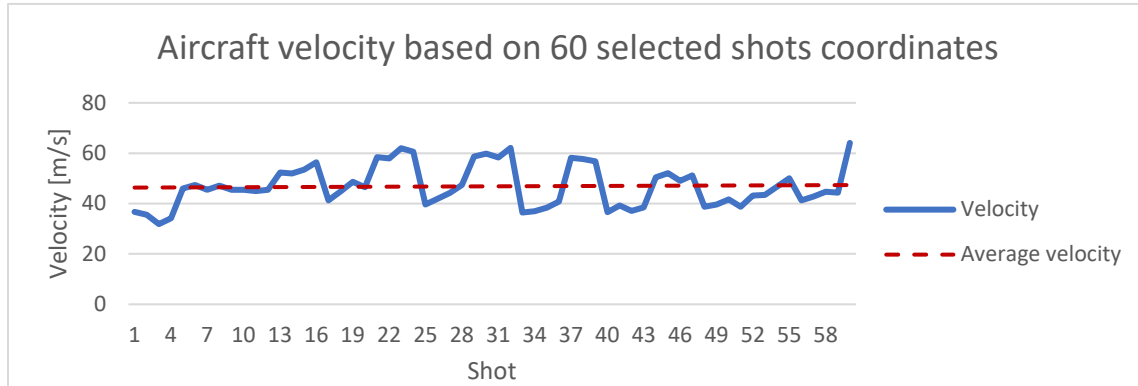


Figure 94 Aircraft velocity on 60 selected shots

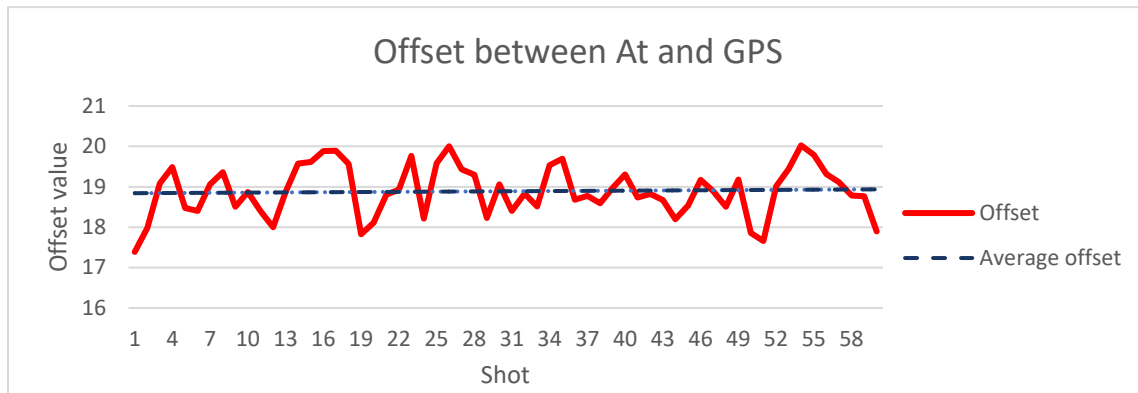


Figure 95 Offset between AT and GPS on 60 shots selected

With this delay computed between the time in the GPS shots and the coordinates from the aerial triangulation, the procedure is iterated.

The 18 seconds are the leap second between the GPS and the UTC time, so they are inserted in the leap second line (red line in Matlab script in Figure 78), the offset considered is 0.88 s.

The coordinates obtained are again converted in the ConveRgo software and estimated with the contribution of the lever arm previously computed.

To estimate the effective superposition of the two camera positions, the plot of the two sets coordinated is repeated in two (Figure 96) and three dimensions (Figure 97).

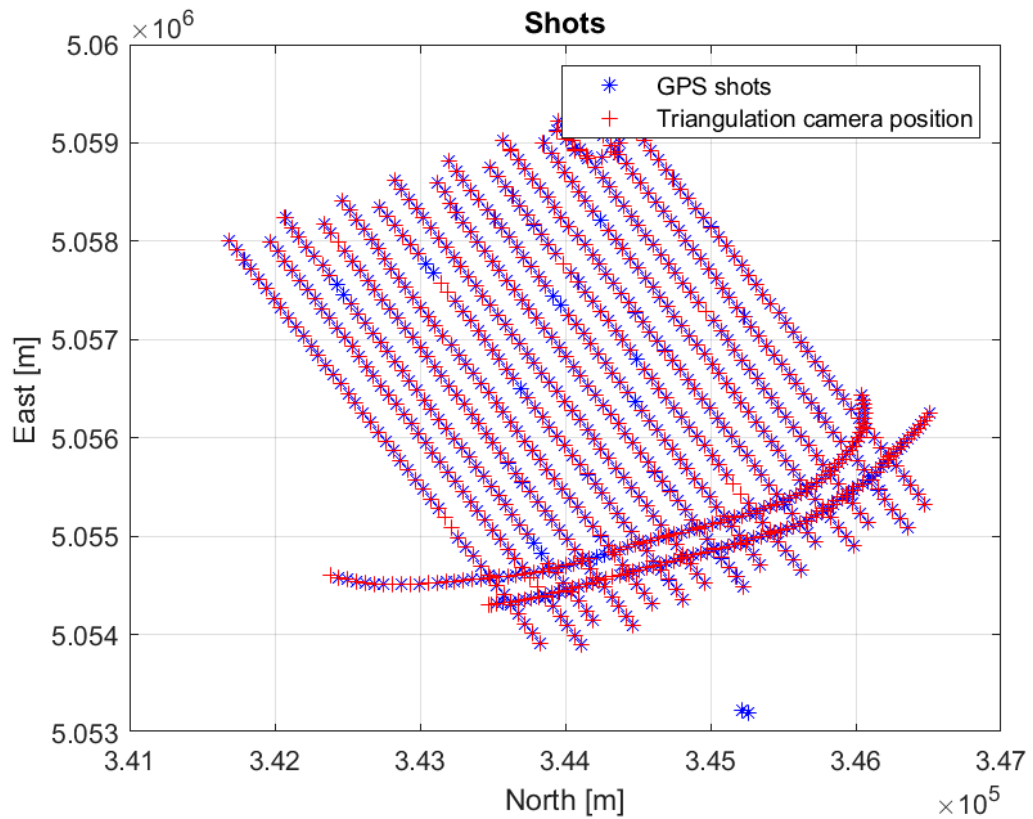


Figure 96 Shots comparison with 0.8s offset in 2D

From the plot, it is possible to see how the coordinates of the camera centres coincide for all the shots along the trajectory on the glacier.

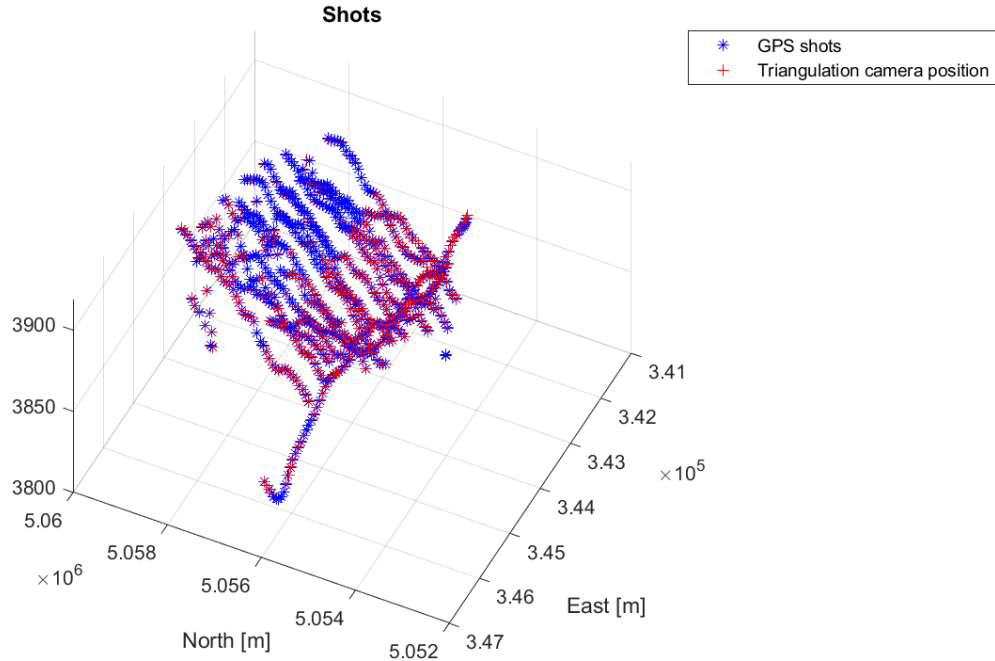


Figure 97 Shots comparison with 0.8s offset in 3D

The procedure is iterated to compute the exact offset between the two camera centres. Other 60 points (Figure 98) are extracted to estimate the difference of coordinates.

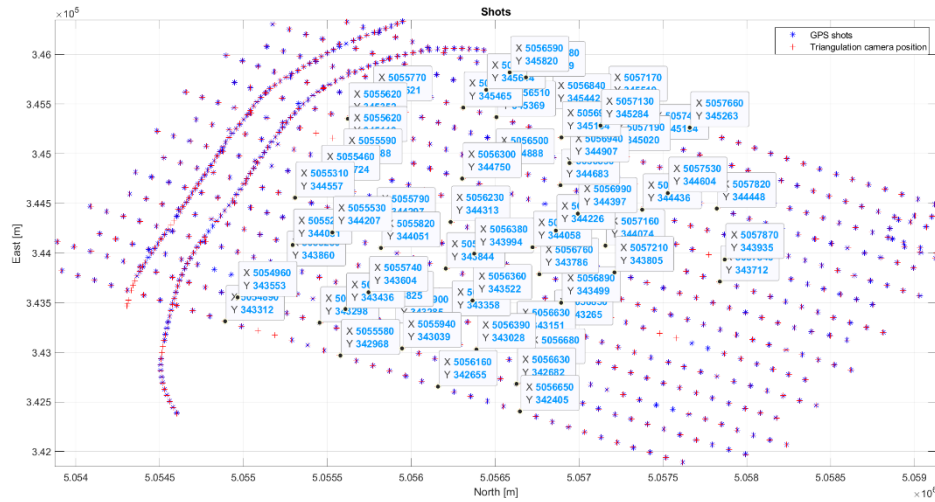


Figure 98 60 shots selected after the first iteration

After the first iteration, the difference in the north, east, and height coordinates enhance a quite constant shift in the different strips with less than 5 meters between the centres (Figure 99). The error is dominant in the north component.

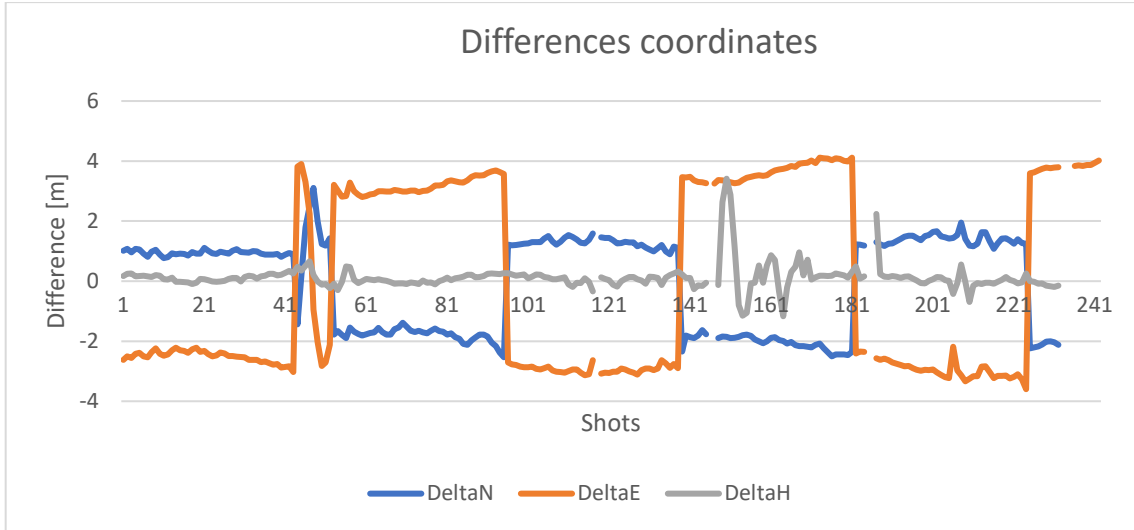


Figure 99 Coordinates differences after the first iteration

Another iteration is performed to further reduce the shift adding 0.01 s to the offset. The shift between the camera centres is now under 1 m (Figure 100). The north direction is still the most problematic.

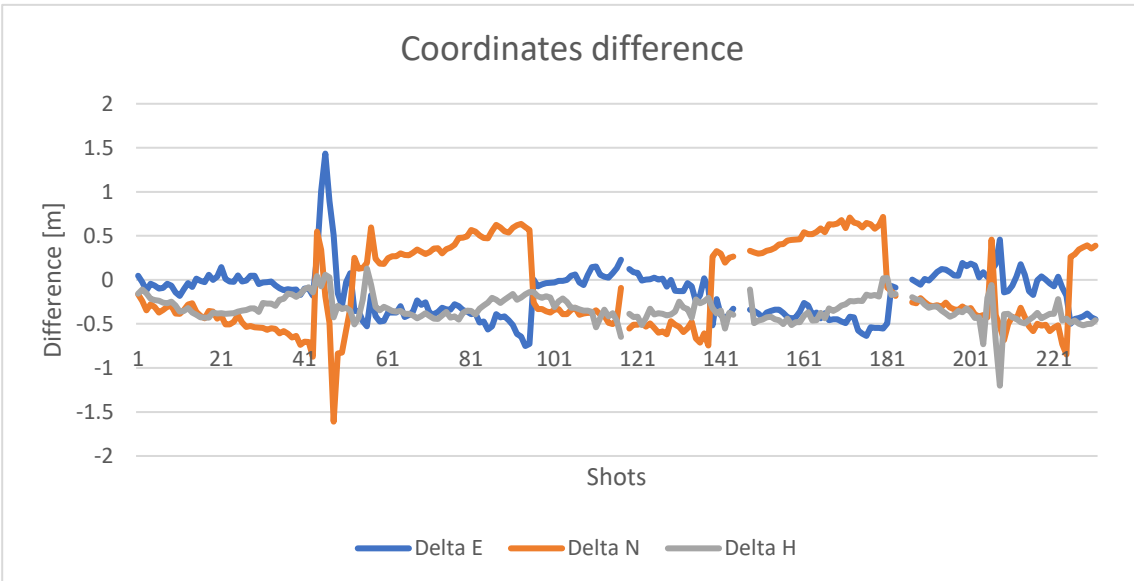


Figure 100 Coordinate difference after the second iteration

With the offset equal to 0.731 s, the coordinates difference is computed. It is halved as shown in the plot in Figure 101:

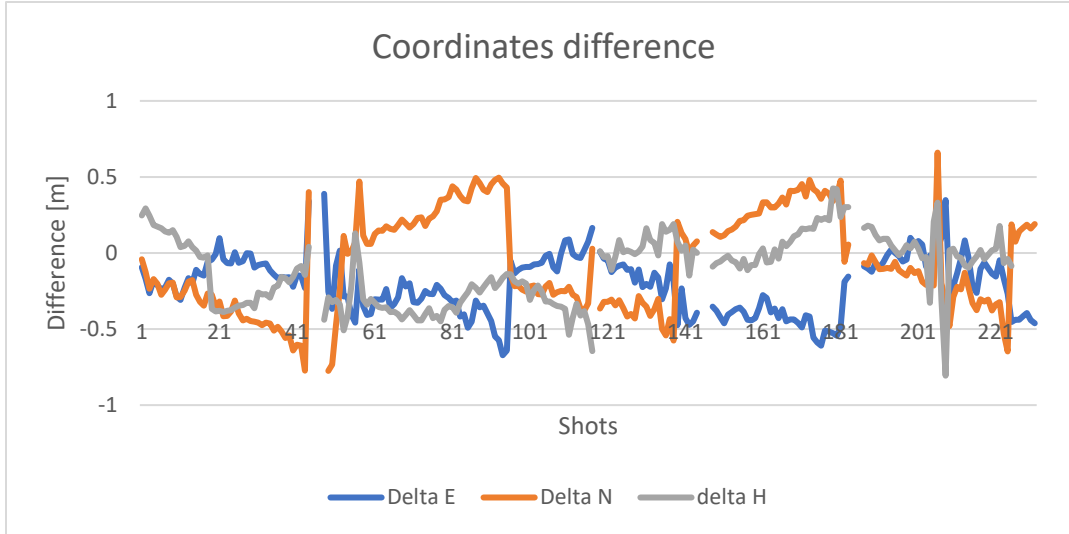


Figure 101 Coordinate difference after the fourth iteration

The analysis of the data underlines some not correspondent shots both on the aerial triangulation and on the GPS, probably due to the failure to register the shot. These data are missing, so the graph presents discontinuities.

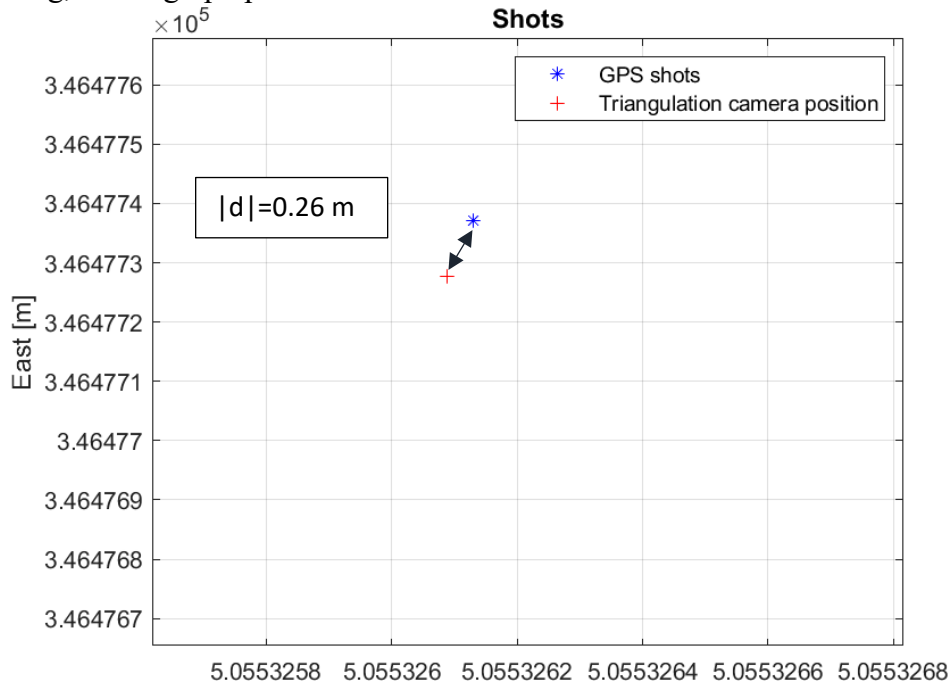


Figure 102 Third iteration centres distance on the first shot

After other iteration, the difference is reduced under 0.5 m, and the absolute value of the distance between the two centres is 0.26 m on the first shot is computed (Figure 102).

On the first shots coordinates the difference is computed:

$\Delta E$ [m]	$\Delta N$ [m]	$\Delta H$ [m]	D [m]
-0.093	-0.041	0.24641	0.266548

Table 35 Distance between TA and GPS coordinates of the first shot

Analysing the planar distance of the North and East coordinates and plotting it, it is clear that there is a jump after a certain interval of shots. Confirmed from Digisky, the time clock is synchronized with NMEA time around every 90 shots (Figure 103).

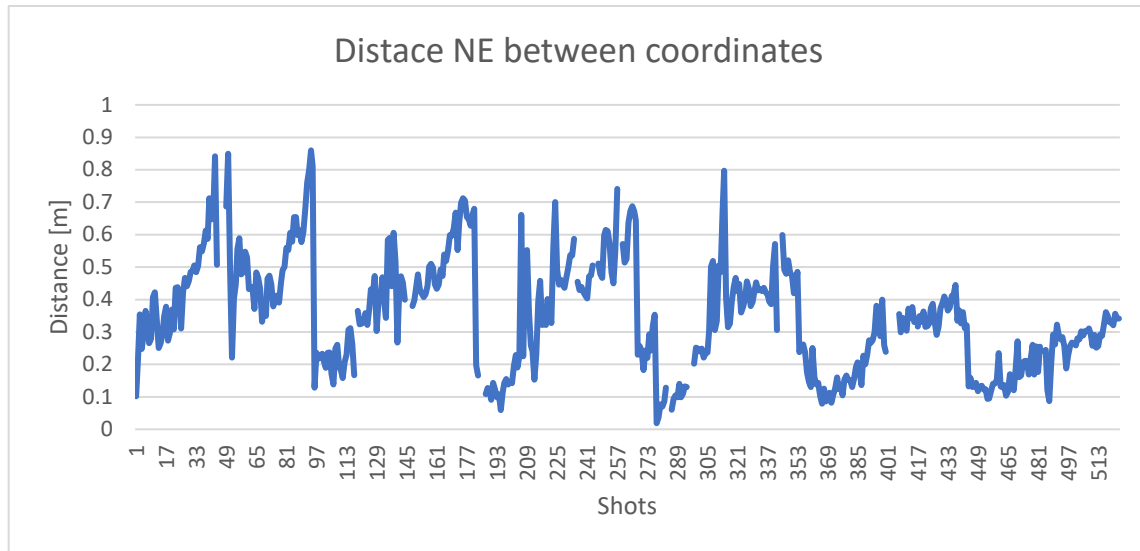


Figure 103 Planar distance between TA and GPS coordinates

To better interpret this linear trend, it is analysed considering 41 shots divided in 5 different plots for the interval of 41 shots considered (Figure 105-109).

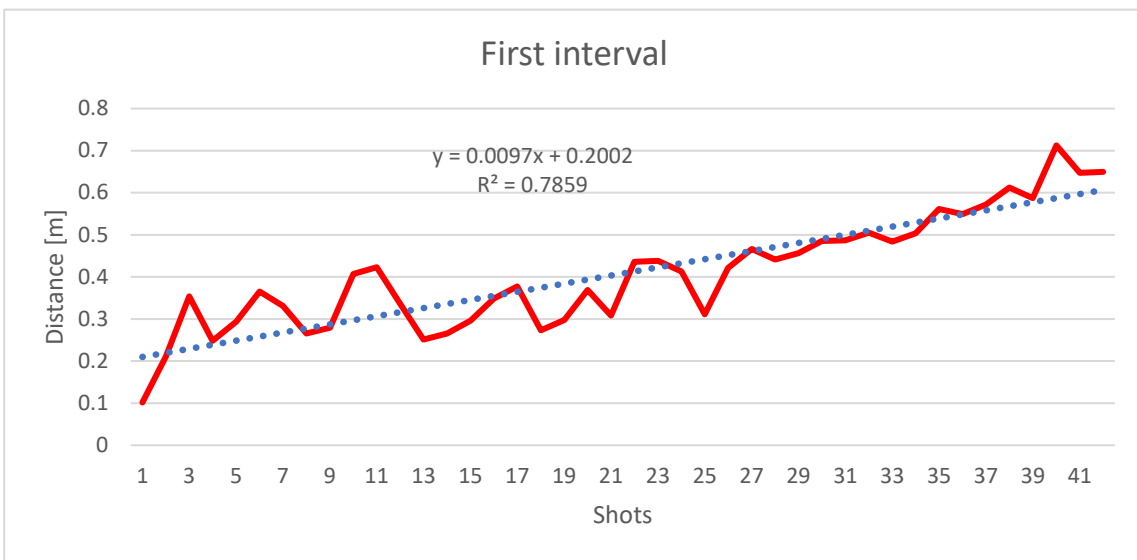


Figure 106 Linear trend in the first interval

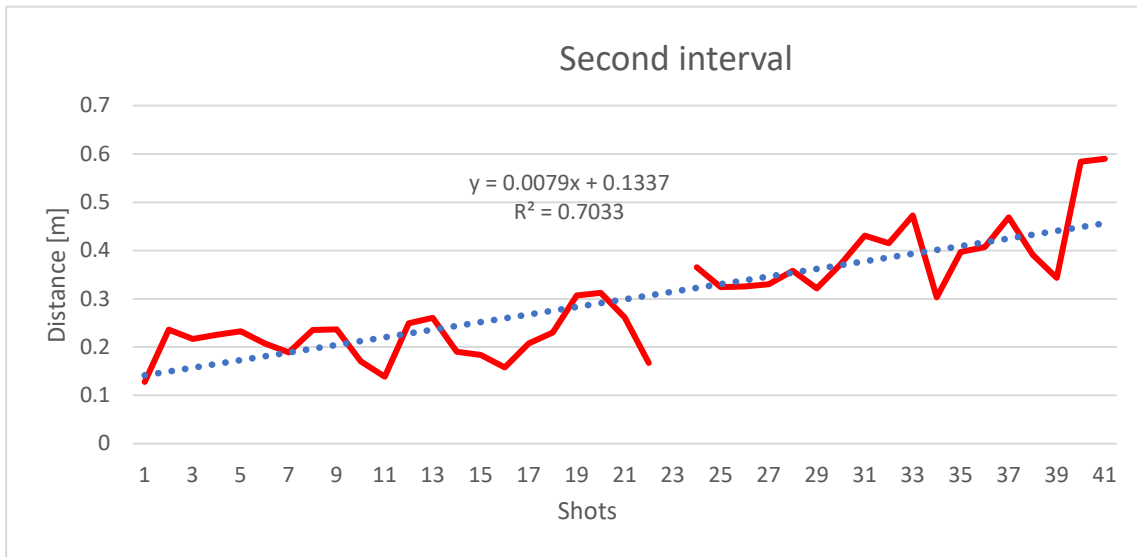


Figure 105 Linear trend in the second interval

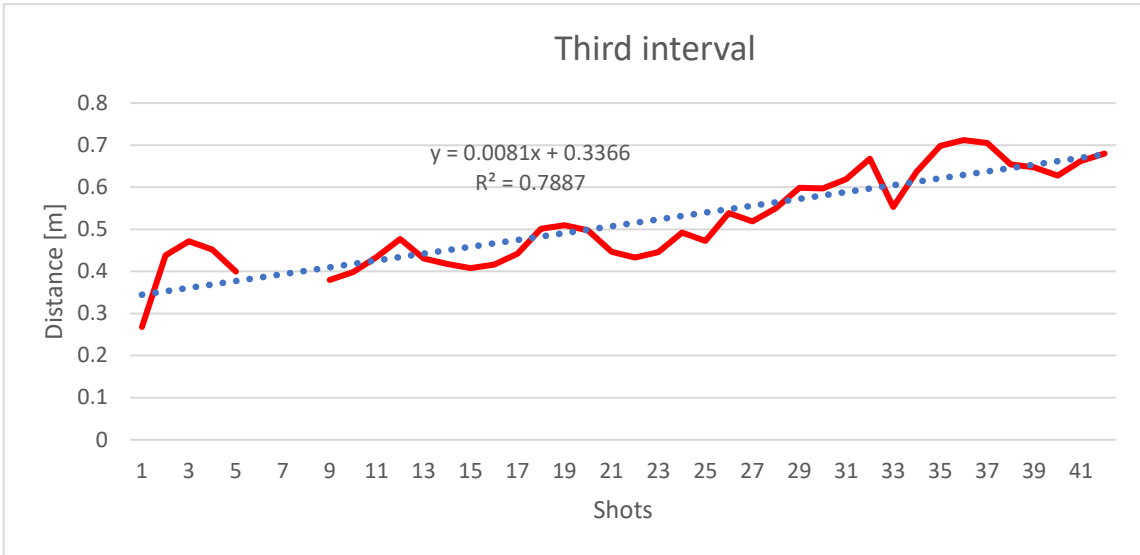


Figure 108 Linear trend in the third strip

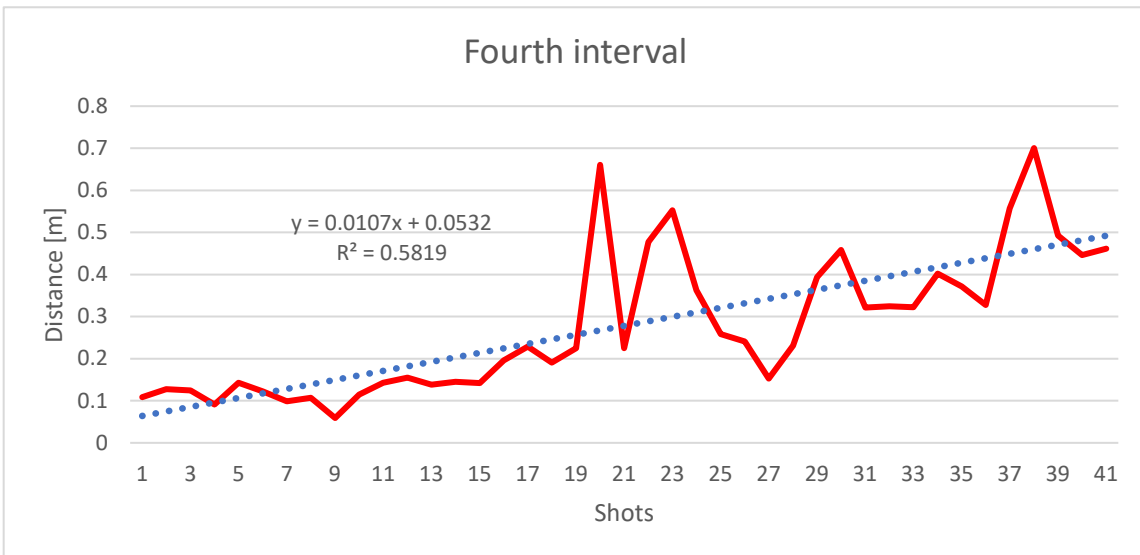


Figure 107 Linear trend in the fourth strip

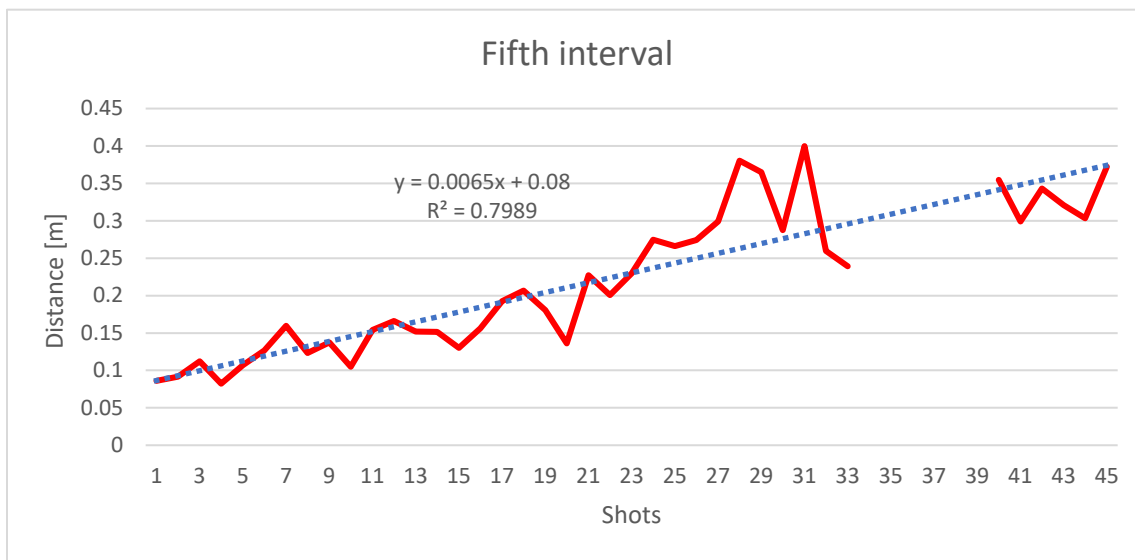


Figure 109 Linear trend in the fifth strip

The trend is:

First set considered	0,0097 x	+ 0,200
Second set considered	0,0079 x	+ 0,133
Third set considered	0,0081 x	+ 0,336
Fourth set considered	0,01 x	+ 0, 053
Fifth set considered	0,0065 x	+ 0, 08
<b>Mean: 0,0084</b>		<b>St. Dev: +/- 0,00143</b>

Table 36 Linear trend

Considering one shot around every 3 s, we can consider this trend over 40 shots, so around every 120s with the mean value of 0,0084 s and a standard deviation of 0,00143 s. For each second, the offset is 0,0281 and the standard deviation is 0,00048. Every three seconds, so every shot the delay increase by 0,3376 s with an uncertainty of +/- 0,05724 s. Considering 3117 s as the time of the entire flight over the glacier, the linear offset is equal to **8,76 s**. The estimated average velocity of 40 m/s at the end of the survey the precision is around 0,25 m.

It is now possible to compute the real offset to estimate the antenna position at the shot time, adding the linear increase of the offset over time.

$$\partial = \partial_0 + \partial' * (t - t_o)$$

Where the  $t_0$  considered is the epoch of the first shot and  $\partial_0$  is equal to 0.731 s estimated with the procedure described above.

Obtaining the camera centres for each shot is possible to import them into the software AgiSoftware Metashape to compute the model again.

This can be a rough estimation of the linear trend considering one shot every 3 seconds. Unfortunately, the shots interval is not constant, so to be rigorous is necessary to build the trend line associating to the initial and final point of the interpolating line the respective epoch and proceeding with the union of the successive lines.

## 5.5 Discussion

This procedure led to the possibility to build the model of the Rutor glacier (or whatever glacier) not only on the GCPs on the ground but also on the camera centres just computed. The centres derived are linked to the GCPs, but this is an important result, especially in monitoring difficult and wide environments, like the difficult accessible ones like the glacier, where the possibility to limit the GCPs could be fundamental. Unfortunately, the low cost and low-quality equipment provided does not allow for direct and accurate processing. The use of better quality equipment, but more important two synchronized clocks would allow for rapid and valid data processing that could improve model processing.

Furthermore, the possibility of having the camera centres can give robustness to the solution and the model and lead to the opportunity to limit the number of in-situ campaign GCPs because the high number of camera centres are added to the number of the GCPs surveyed.

# Chapter 6

## Photogrammetric processing of stereoscopic satellite images

### 6.1 Satellite imagery

The remote sensing techniques is made of three steps:

- Data acquisition
- Data processing
- And data interpretation.

The process is made up of different steps (shown in Figure 110) that can be schematically described as:

- Emission from an energy source;
- Interaction of the electromagnetic radiation with the atmosphere;
- Interaction with the Earth surface;
- Detection and measurement of the electromagnetic radiation by sensors;
- Data processing and interpretation.

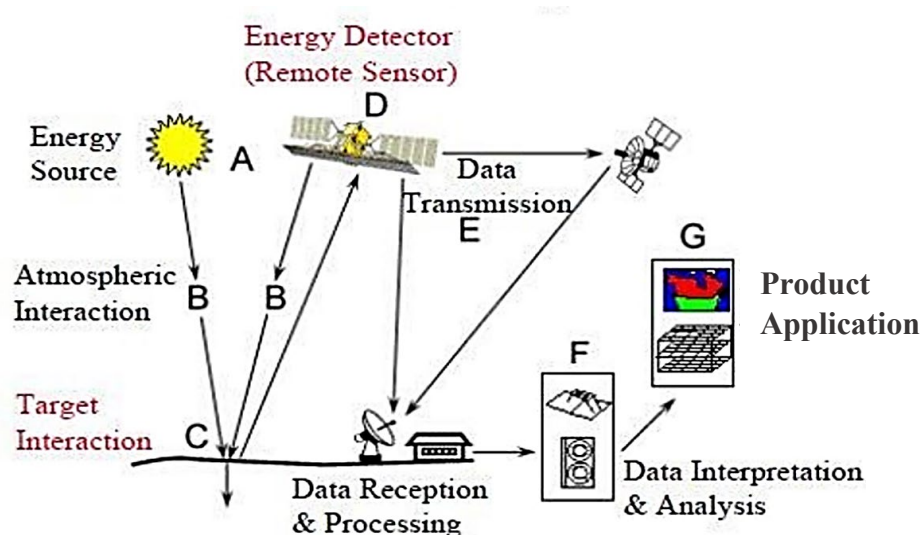


Figure 110 Remote sensing process (Boccardo, s.d.)

The digital sensors mounted on board of a satellite are able to convert the electromagnetic energy emitted or reflected from the earth surface into useful data. The acquisition is made through devices called ‘scanners’. A digital image is the output of the scanning process. The measurement can be done in two different modes, namely whiskbroom and pushbroom scanners. Whiskbroom scanning devices are the first type developed, now outdated. A rotating mirror with an angle of  $\pm 45^\circ$  with respect to the orbit direction redirects the radiation to the optical system, acquiring a single cell of the image matrix. The pushbroom scanners collect the image with line detectors mounted approximately at  $90^\circ$  with respect to the flight direction, acquiring a whole line of the image matrix.

The sensors are composed of an optical part to let the radiance reach the detector, a series of spectral filters, an analogue to digital converter that is the detector and, finally, a media that records the data. (Boccardo, s.d.)

Nowadays, remote sensing techniques are routinely adopted for the cryosphere evolution monitoring. Satellites images are powerful tools supporting the hazard estimation and the impact assessment of climate change in mountain areas. Recently the acquisition of the satellite imagery over the mountain areas improved in terms of resolution both spatially and radiometrically. (Taylor, et al., 2021)

## 6.2 Pleiades constellation

The cooperation between different European national space agencies (France, Austria, Sweden, Spain and Belgium) under the supervision of CNES (Centre National d’Études Spatiales) had led to the Pléiades program. The two optical satellites of one ton each make up the constellation developed for defence and civil use with a high spatial resolution of 0.7 m and a 20 km swath. The agreement was signed in 2001 and the first satellite was launched at the end of 2011, and it started the calibration phase until March 2012. In November 2012, the second satellite was sent off and the constellation was completely operative from 2013. The Pleiades satellites covering the visible<sup>11</sup> and NIR<sup>12</sup> spectral bands are positioned at 695 km of altitude in a Sun-synchronous orbit. (M. Benoit Boissin, 2012) The characteristics of these small satellites are the agility with a condensed design with high location accuracy thanks to a hexagonal structure equipped with three fixed solar panels (Light Panel Structures) installed at  $120^\circ$ . They have a swat field of view of 20 km in a nadiral position, a spatial resolution of 0.7 m for the panchromatic spectral band and 2.8 m for the multispectral band. The Pleiades optical system has a 0.65 m diameter and an f/20, 12.905 m of focal length. The location accuracy of the image is 1, with GCP and 20 m without GCPs (ESA, 2021)

---

<sup>11</sup> Blue, green and red spectral bands

<sup>12</sup> Near- infrared spectral band

The satellite characteristics are summarized in the Table 37:

Pleiades constellation	
Optical System	0.65 m diameter Focal length of 12.905 m f/20
Spatial resolution	0.7 m for Panchromatic 2.8 m for MS bands
Bands	Pan 480-820 nm MS bands: B0= 450-530 nm (blue) B1= 510-590 nm (green) B2= 620-700 nm (red) B3=775-915 nm (NIR)
Swat width	20 km at nadir
Instrument size	L > 1.594 m W < 0.98 m H < 2.235 m

Table 37 Pleiades constellation characteristics (ESA, 2021)

### 6.3 Data processing

The imagery used for the 3D analysis of the case study area is a Pleiades stereo pair acquired on 20/08/2017 at 14:57:30, kindly made available by ARPA Valle D'Aosta, characterised by an **actual GSD of 0.71 m** and an **off-nadir angle of +/- 8°**.

The surface covered from these images is **268.468 km<sup>2</sup>** in the Aosta Valley region close to the borders among Aosta Valley, Piedmont, and France, with different mountainous areas, the Gran Paradiso area and the Rutor glacier (the analysed case study) as shown in Figure 111.

The software used for the elaboration is PCI Geomatica Banff<sup>13</sup> version 2019.

---

<sup>13</sup> Now Catalyst



Figure 111 Satellite images area

## 6.4 Reference data

The reference data are the cartographic products resulting from the aerial photogrammetry process described in Chapter 4:

- an orthophoto from aerial photogrammetry with 50 cm of GSD with planar accuracy of 9 centimetres.
- a photogrammetric DSM with 24 cm of GSD with altimetric accuracy of 13 centimetres.

They are based on the 2021 aerial flight using 13 GCPs.

Both products are referenced with respect to the reference system RDN2008 / UTM zone 32N (N-E) (EPSG: 6707) in orthometric height.

## 6.5 Model Used and steps

According to the software, the model used is a Rational Function Model, RFM (or RPC<sup>14</sup>), a non-parametric math-based model that relates ground 3D coordinates to image 2D coordinates.

The process starts with the image pansharpening. This procedure led to join a low-resolution multispectral image and a high-resolution panchromatic image to merge them into a high-resolution multi-spectral image. In this process, the spectral characteristics of the original images are retained and conveyed in the high-resolution RGB image. (Banff, 2022)

After the pansharpening step, it is necessary to identify suitable Ground Control points in the images. Since the image covers a very large area, much larger than the area of interest, the search for GCPs is limited to the glacier area, located in the northwest area of the original satellite image. After a first attempt to manually find some recognizable points, the difficulty of distinguishing stable (over the time) and unique points with acceptable precision, it was considered appropriate to extract GCPs automatically from the orthophotos obtained from the processing of the aerial survey described in 6.4.

The software identifies the same stereo GCPs in both pan-sharpened images. After an analysis of the GCPs, a selection was carried out to remove those with larger residual errors. This resulted in a model with 6 GCPs well distributed in the area around the glacier. The height of these 6 points was derived from the DSM generated from the aerial survey. The software allows Tie Points (TP) to be automatically identified on both images, extracting the related image coordinates. After three iterations, the model was able to extract 27 stereos TP.

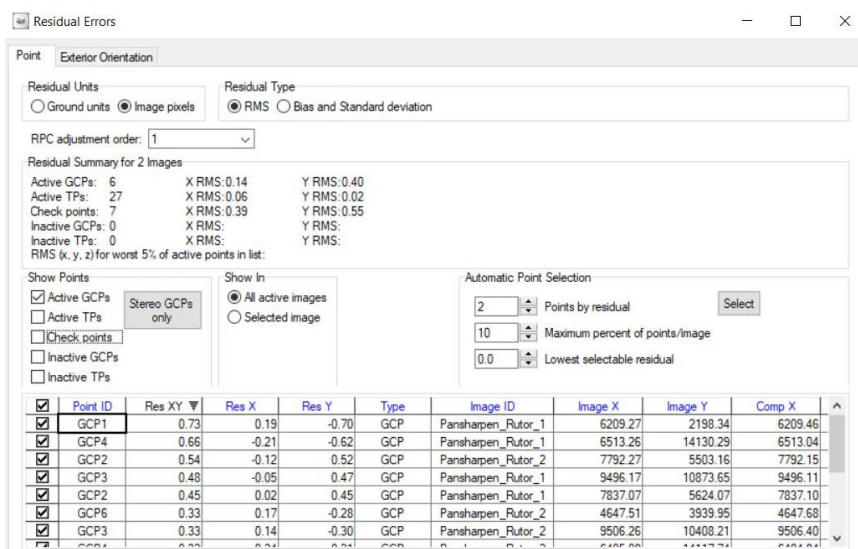


Figure 112 Residual Error Geomatica Banff

<sup>14</sup> Rational Polynomial Coefficients

To establish the 3D model accuracy some check points are necessary, i.e. points with known ground coordinates that are not used as GCP to calculate the model parameters. 7 stereo CPs are selected and used in the model.

The residuals derived from the model calculation are calculated for the differences between North, East and height coordinates calculated by the RPC model and measured from the reference cartographic products, indicated as XRMS, YRMS, ZRMS, respectively. The report (in Figure 112) shows the residual errors of the GCP and the CP calculate as:

$$X\text{ RMS} = \sqrt{\frac{\sum_i^n (\text{Res } X)_i^2}{n}}$$

$$Y\text{ RMS} = \sqrt{\frac{\sum_i^n (\text{Res } Y)_i^2}{n}}$$

$$Z\text{ RMS} = \sqrt{\frac{\sum_i^n (\text{Res } Z)_i^2}{n}}$$

The software also calculates the residual XY as the quadratic sum of the residuals.

Residual Summary for the 2 images is reported in the table:

N. of points	Type	X RMS	Y RMS	Z RMS
6	GCP	0.05 m	0.15 m	0.43 m
7	CP	0.18 m	0.19 m	1.04 m
27	TP	0.03 m	0.00 m	0.00 m

Table 38 Residual errors

To proceed with the DSM extraction, it is necessary to proceed with two different steps, the extraction of the epipolar images and the DSM generation from the epipolar images. The reprojection of the two epipolar images is done so that it is possible to find the matching component between the stereo pairs along a common x-axis. (Catalyst, 2022) After the epipolar images generation is possible to proceed with automatic extraction of the Digital Surface Model. The vertical datum of the DSM is left as ellipsoidal, to be consistent with the RPC model.

An evaluation to compare the model was done at the end of the process. The DSM was compared with the aerial DSM (2021) and the DSM of the Aosta Valley region (2008) available on the Geoportale website (Valle D'Aosta Region), performing a pixel-by-pixel difference over time-invariant areas. This comparison made on the stable zones was carried out to determine the accuracy of the model and on the estimation of the glacial ablation of the mass. Unfortunately, this comparison enhances a systematic error with

respect to the Geoportale DSM that leads to a vertical precision of +/-3,5 m and accuracy of around -2,5 meters.

To obtain a better product and try to eliminate the systematic error, possibly due to the automatic conversion from orthometric to ellipsoidal elevation in the generation of the DSM, it was decided to use the model in the Geomatica Banff in ellipsoidal height by converting the heights of GCPs and CPs with the grids in Convergo software (ConveRgo, s.d.) without the support of the aerial DSM. The CPs were also converted and due to the difficulty of manually collimating them, those with too high residuals were eliminated. The automatic Tie Point research has problems without the DSM in the glacial area, so it

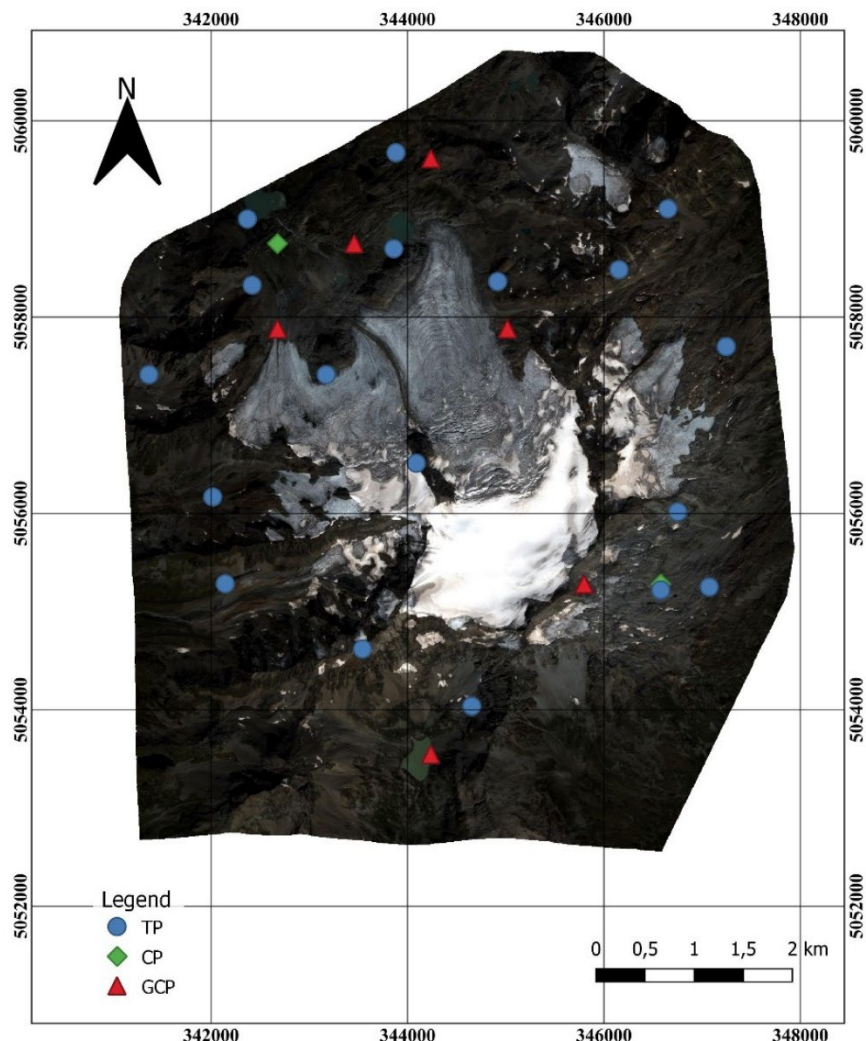


Figure 113 GCP, CP, TP used

was decided to manually collect exploiting only the image coordinates. The GCPs, CPs and TP used are reported in Figure 113.

At the end of the procedure, the model was computed again, and the residual errors were estimated, achieving comparable results.

They are reported in Table 39.

N. of points	Type	X RMS	Y RMS	Z RMS
6	GCP	0.05 m	0.15 m	0.43 m
2	CP	0.12 m	0.00 m	0.00 m
18	TP	0.10 m	0.02 m	0.00 m

Table 39 Residual errors

## 6.6 Cartographic products

At the end of the procedure orthophoto and DSM cartographic products are extracted:

Cartographic products obtained are

- 2 Orthophotos (one for each image of the stereo pair) with 50 cm of GSD in Figures 114 and 115.
- 1 DSM with 0.5 m of GSD in Figure 118.

In Figure 116 is reported a 1:1 zoom on the glacial area to show the level of detail of the Pleiades orthophoto. In Figure 117 is reported a 1:1 zoom on the glacial area to show the level of detail of the DigiSky aerial orthophoto.

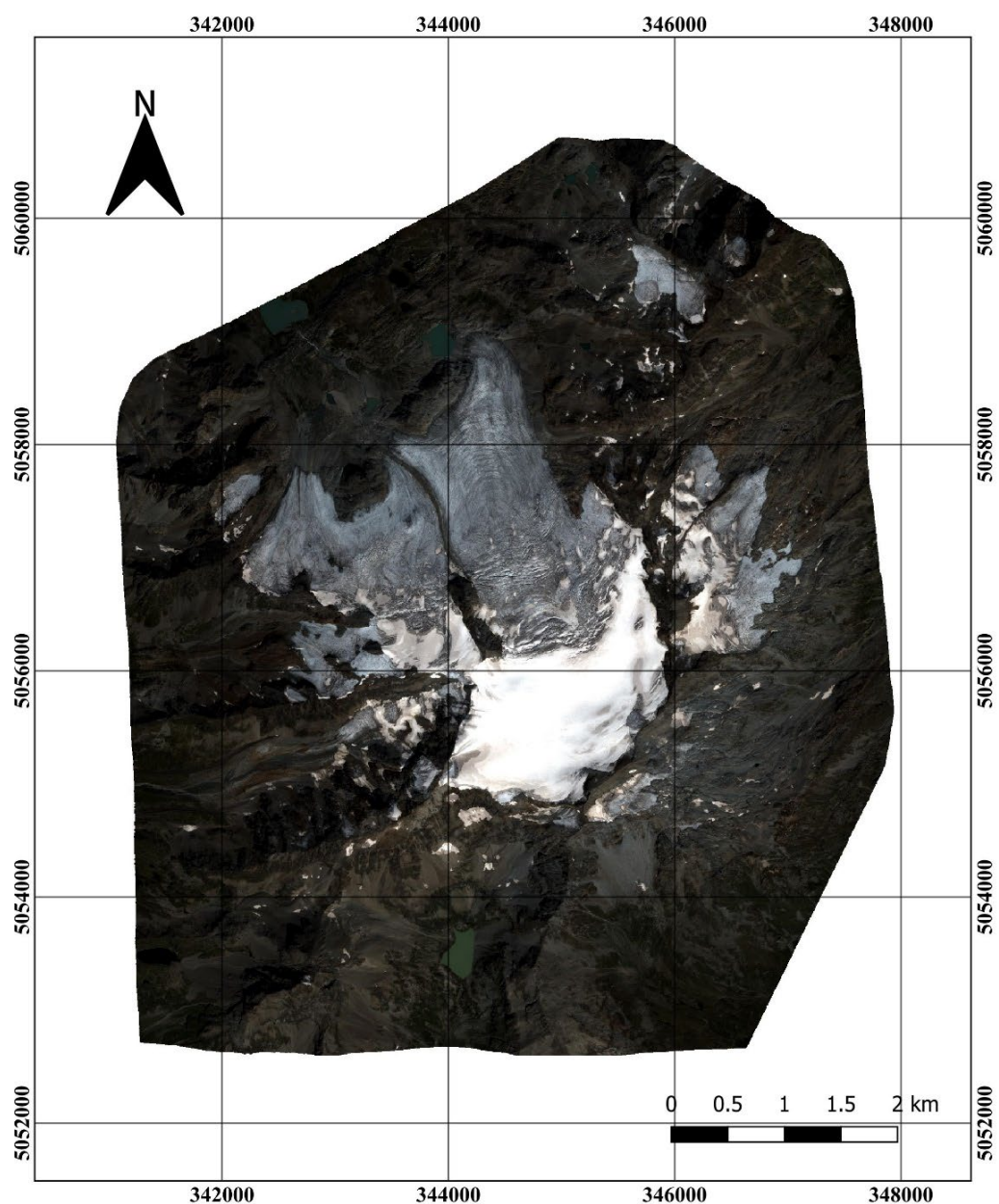


Figure 114 Orthophoto 1 obtained from Pleiades

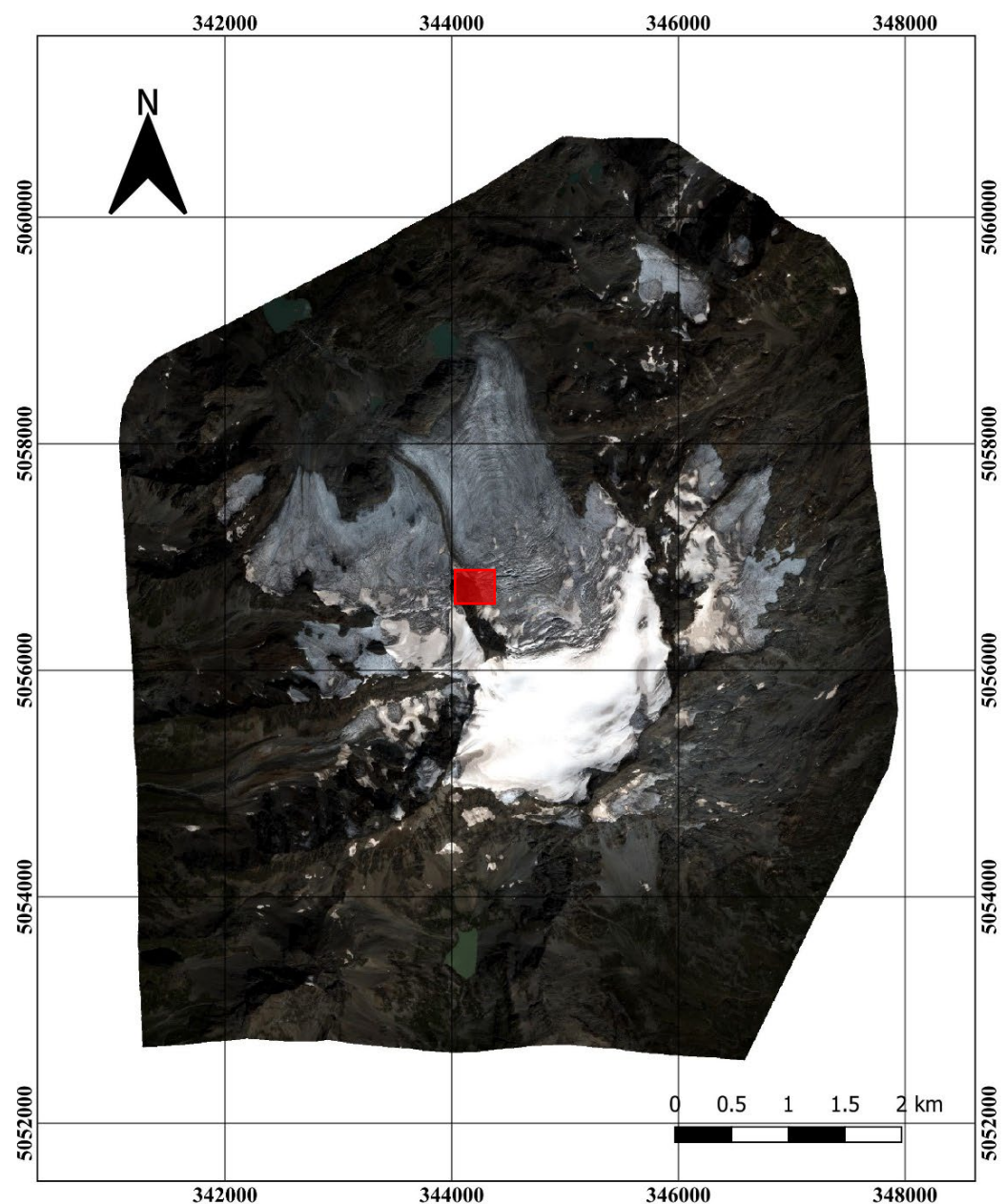


Figure 115 Orthophoto 2 obtained from Pleiades

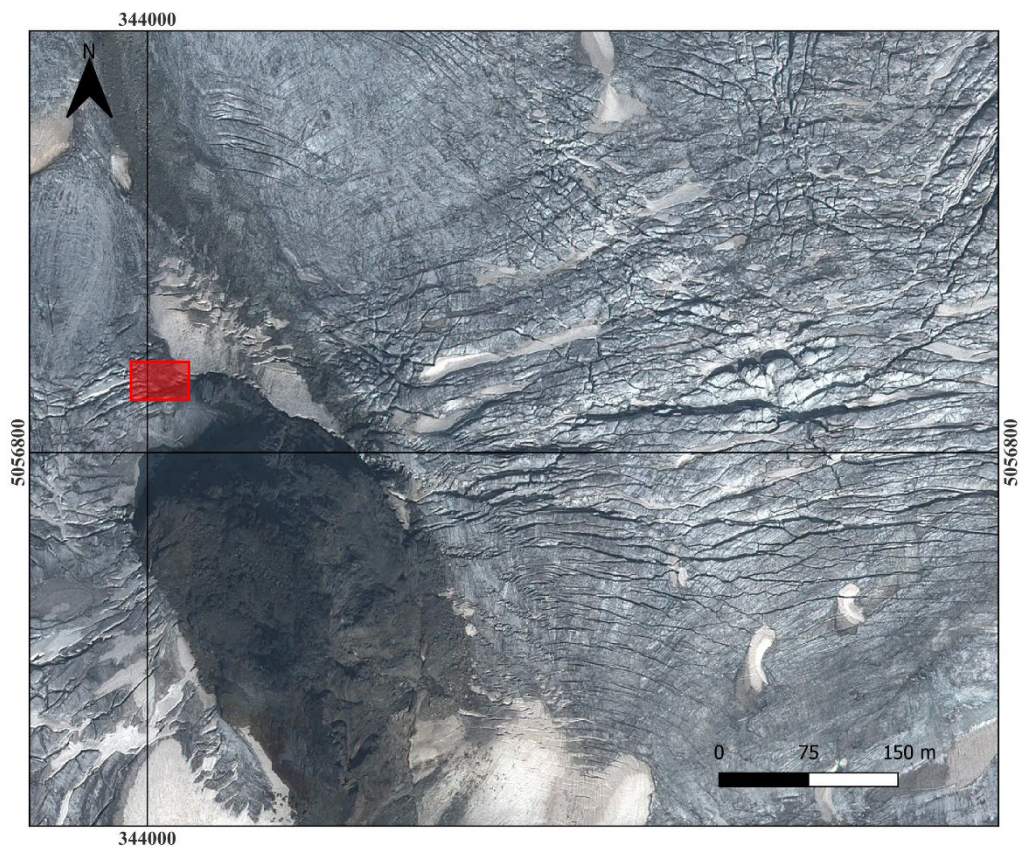


Figure 116 Zoom to the original resolution on the glacier area on the Pleiades orthophoto (red square in Figure 115)

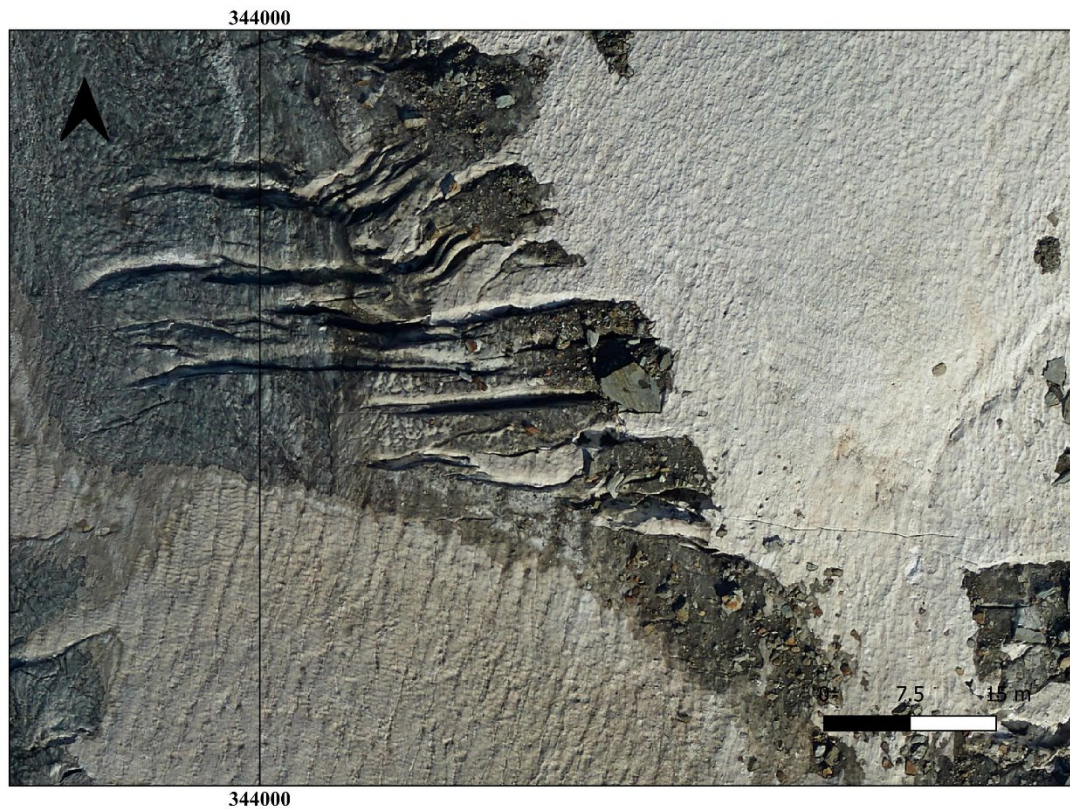


Figure 117 Zoom to the original resolution on the glacier area on the Aerial orthophoto (red square in Figure 116)

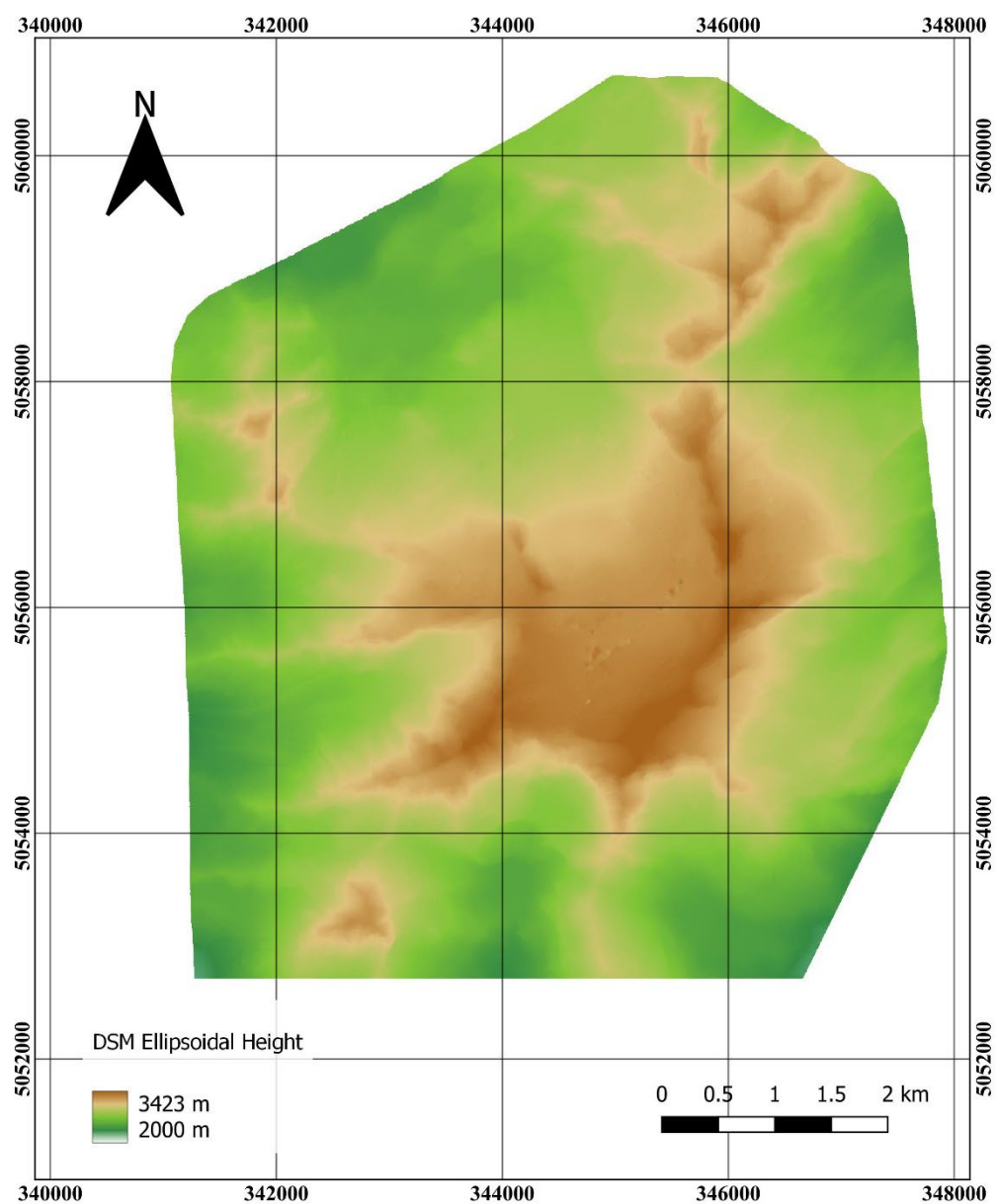


Figure 118 DSM obtained with 6 GCPs ellipsoidal height

## **6.7 2021 aerial DSM and 2017 satellite DSM comparison**

The goal is now to compare the aerial and the satellite DSM to estimate the model's accuracy and the snow melting. In order to make comparisons, it is necessary to convert the DSM from ellipsoidal to orthometric height. The size of the DSM produced does not allow for direct export to convert the coordinates. The DSM is split into tiles smaller than 4 GB and exported in XYZ file. The conversion id is performed in Convergo software. Then the data file is imported and converted into a raster file. The files are merged in a virtual raster file at the end of the procedure.

After the conversion of the Pleiades DSM to the orthometric height the difference between the Pleiades digital surface model and the aerial one is computed thanks to the raster calculator in QGIS (Figure 119). The mean difference on the whole area (both glacier and stable areas) is 0.10 m and the standard deviation is 7.71 m. The main differences are on the lower part of the glacier, on the glacial fronts with the three tongues where the mass ablation are over 6,8 meters as expected. The main problematic parts are on the west rocky areas around the glacier in the southern part as shown in red, in Figure 119.

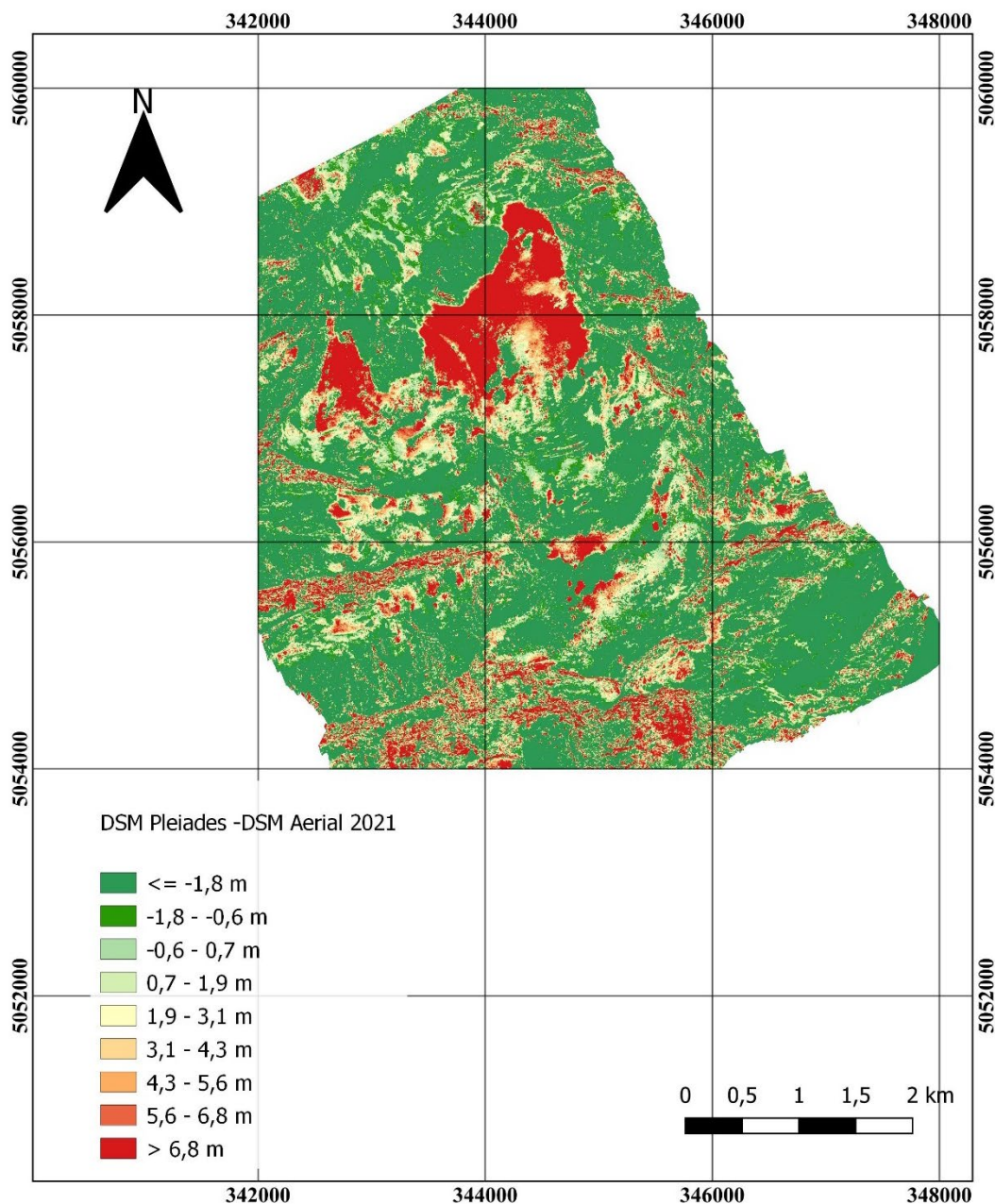


Figure 119 2017 Satellite DSM - 2021 Aerial DSM

The evaluation on the comparison of the satellite model and the aerial DSM is computed by selecting some 'stable areas' in Figure 120, which are supposed to remain unchanged over time. These areas are identified in the rocky lateral parts of the glacier and on the central "Vedette", a rocky area in the centre of the glacial mass. On these stable areas, the height differences between the two DSMs are calculated to be sure of comparing areas not

subject to change over time in order to estimate the precision and accuracy of the DSM obtained from the satellite images.

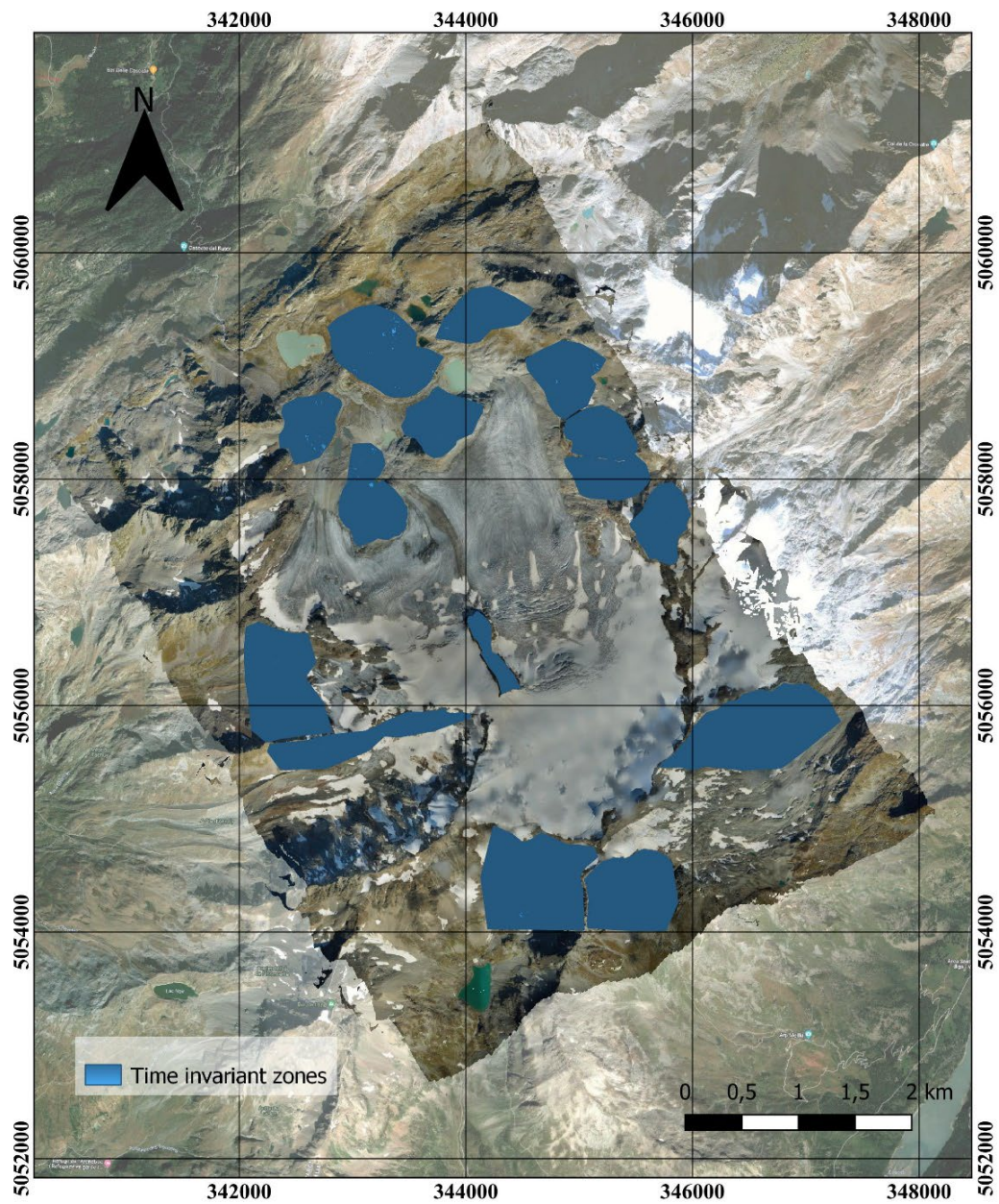


Figure 120 Stable areas

The outcome of the qualitative analysis of the results highlighted that the DSM difference has varying accuracy depending on the slope. Therefore, it was decided to analyse the differences on different slope classes. More specifically, as already highlighted in a similar analysis over the Belvedere glacier, although the morphology of the two glaciers is different, the altimetric accuracy seems to decrease with the slope's increase. (Giulio Tonolo, et al., 2020)

The slope on the ‘stable zones’ considered was calculated from the aerial DSM and discretized into 5 slope classes reported in Figure 121:

- $S < 18^\circ$
- $18^\circ < S < 36^\circ$
- $36^\circ < S < 54^\circ$
- $54^\circ < S < 72^\circ$
- $S > 72^\circ$

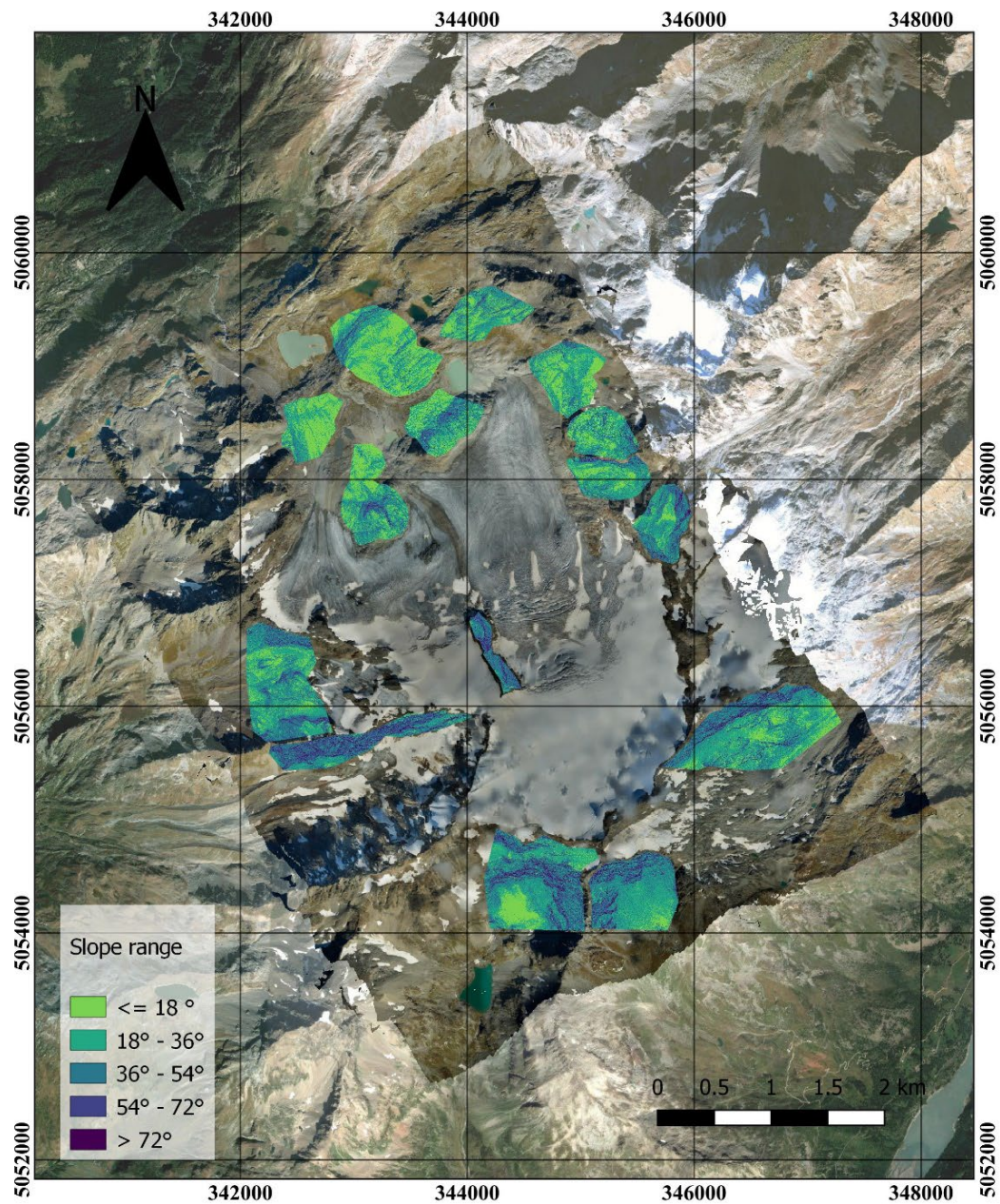


Figure 121 Classification of the areas according to the slope

With the analysis of the differences between the DSMs for each class considered the goal is to estimate the influence of the slope on the elevation differences and therefore the precision of the satellite DSM versus the slope. Thus, the areas considered were reclassified according to each slope class identified and then analysed.

The procedure consists of the following steps:

- the aerial DSM produced is analysed according to the slope, dividing into 5 classes listed above;
- the stable areas considered on the rocky parts are selected;
- each class is reclassified according to Digital Number (DN) 1 to 5, each associated with a class of slope;
- The reclassified areas were combined into a single multi-polygon for each class by means of a “dissolve” geoprocessing.
- statistics were calculated on each slope class applied to the difference between the aerial DSM and that obtained from satellite imagery.

Slope Range	DN	Count	Mean [m]	Standard Deviation [m]
$S < 18^\circ$	1	4631745	-2.89	3.88
$18^\circ < S < 36^\circ$	2	8574643	-2.26	6.00
$36^\circ < S < 54^\circ$	3	5625899	-1.41	7.58
$54^\circ < S < 72^\circ$	4	2087941	0.75	9.86
$S > 72^\circ$	5	544735	5.13	12.47

Table 40 Statistics according to the slope range

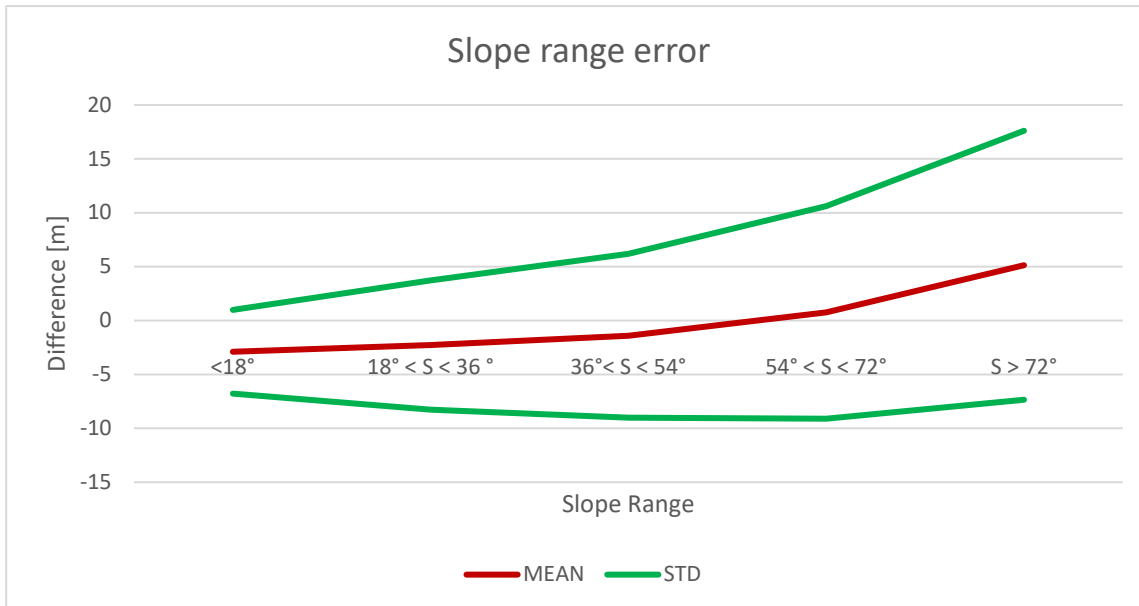


Figure 122 Mean and Standard Deviation difference values for each slope range

The mean values and the standard deviation are reported in Table 40 and plotted in Figure 122. The mean value of difference between the two DSM increases significantly between the slope classes, but more significant is the increase in the standard deviation from 3.8 m to over 12 m for the steepest parts. The most notable differences are on the steepest slopes. As a general result, it seems fair to say that the DSM obtained from the satellite images tend to smooth the elevation differences with respect to the reference DSM. Additionally, a non systematic error is also affecting mean values.

Using a similar procedure, the analysis was repeated on the exposure of the areas considered to understand if the illumination condition as well as the relative position of the satellite with respect to the aspect of the areas could impact on the photogrammetric processing of the stereo-pair.

The exposure on the ‘stable zones’ considered was detected from the aerial DSM and discretized into 8 classes:

- $-22.5^\circ < E < 22.5^\circ$ , North
- $22.5^\circ < E < 67.5^\circ$ , North-East
- $67.5^\circ < E < 112.5^\circ$ , East
- $112.5^\circ < E < 157.5^\circ$ , South-East
- $157.5^\circ < E < 202.5^\circ$ , South
- $202.5^\circ < E < 247.5^\circ$ , South-West
- $247.5^\circ < E < 292.5^\circ$ , West
- $292.5^\circ < E < 337.5^\circ$ , North-West

The map generated, in Figure 123, is an aspect map where the measured angle from North associates values from 0 to  $360^\circ$ .

The eight classes were evaluated in a procedure similar to that described above.

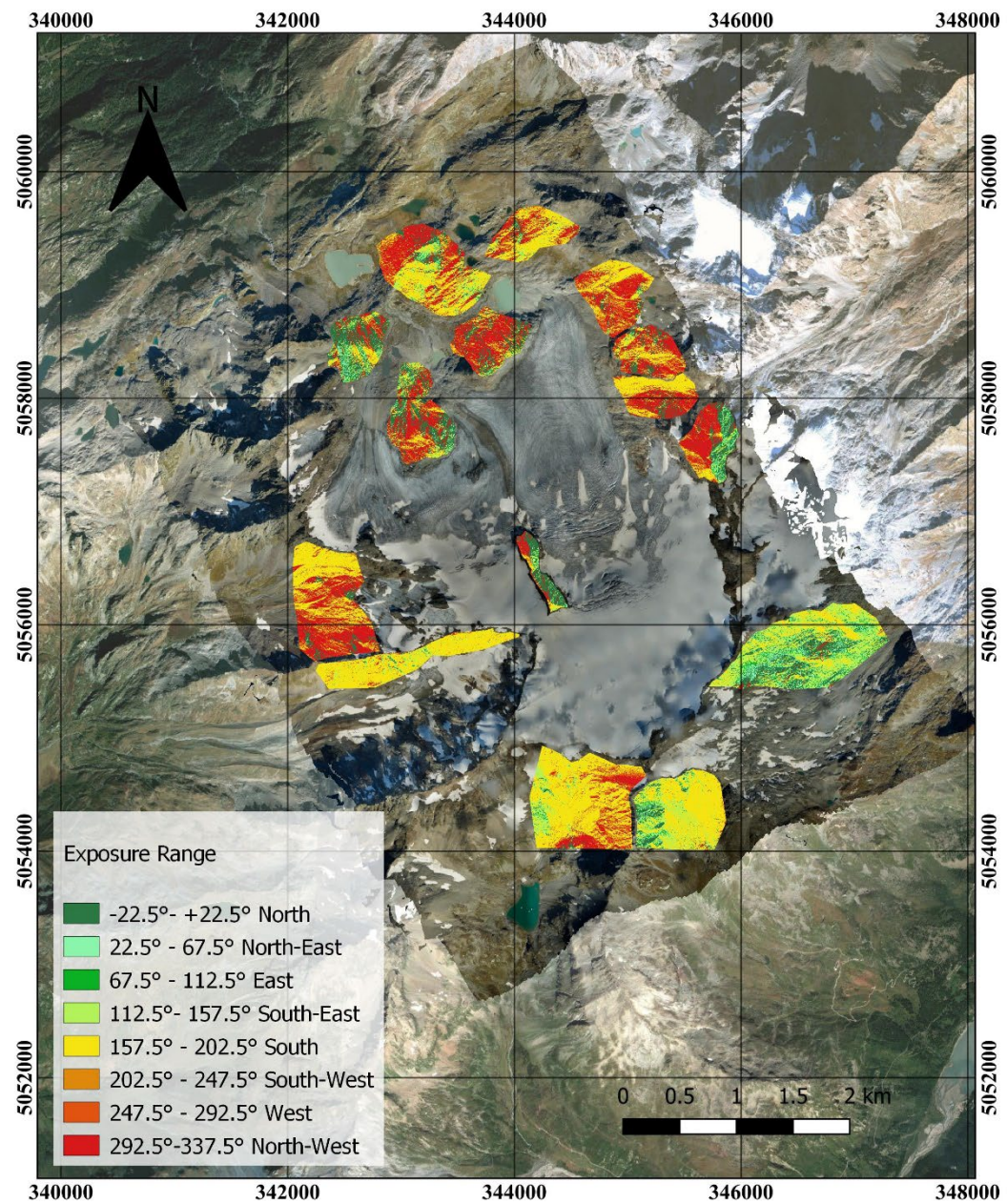


Figure 123 Reclassification according to exposure

Exposure Range	Direction	DN	Count	Mean [m]	Standard Deviation [m]
-22.5°<E < 22.5°	North	1	7000022	-5.09	4.76
22.5°<E < 67.5°	North-East	2	969933	-3.26	5.51
67.5°<E < 112.5°	East	3	470927	-1.98	6.22
112.5° < E < 157.5°	South-East	4	1027201	-0.87	6.49
157.5° < E < 202.5°	South	5	9087075	1.54	7.70
202.5° < E < 247.5°	South-West	6	1352347	-2.21	5.28
247.5° < E < 292.5°	West	7	700060	-3.10	4.926
292.5° < E < 337.5°	North-West	8	1436766	-3.95	4.58

Table 41 Statistics according to the exposure range

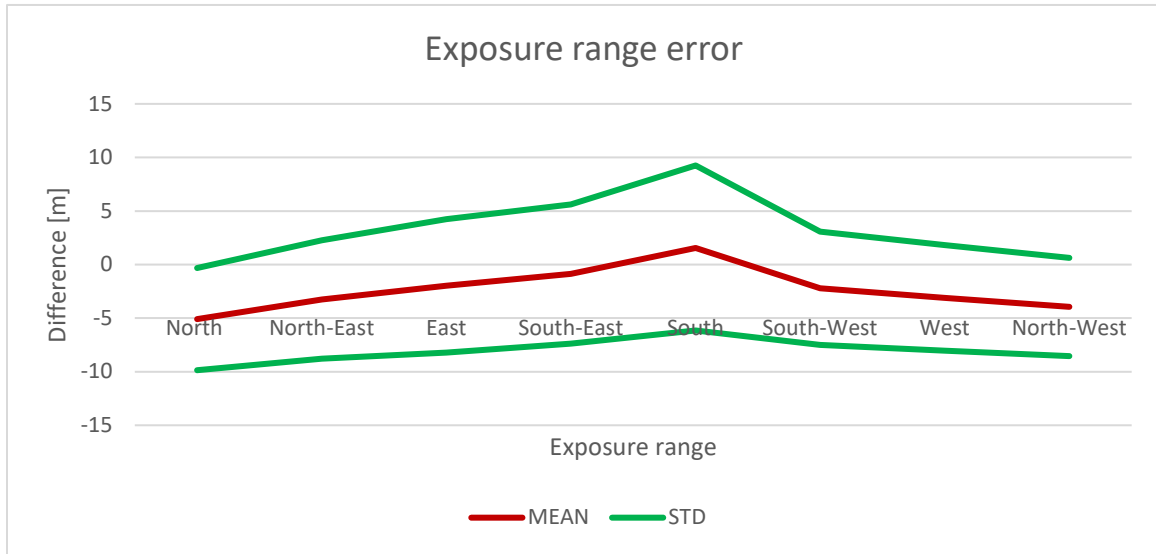


Figure 124 Mean and standard deviation difference values for each exposure range

The values of the mean and standard deviation are reported in the Table 41 and plotted in Figure 124.

With this classification it is possible to observe the exposition of the area considered. There is a clear correlation between the DSM difference error obtained from the satellite images and the exposure slope due to possible interference during the acquisition of the images and the sunshine of the areas considered. Moreover, it can be also due to the relative satellite/versant position, which leads to occluded areas in the stereoscopic pair. The azimuth angle of acquisition is 180°, North- South along the orbit results in a greater fault on east and west facing slopes that may be occluded. During acquisition it is difficult to identify homologous points and consequently on shady slopes it is not possible to find

Tie Points. This results in a clear correlation between error and exposure. A planimetric error could generate an altimetric shift, so there is a need to coregister the reference DSM or insert an automatic TP coregistration.

Two cross-sections (in Figure 125, 126,127) are executed on the glacial front and on the central part of the glacier to assess the expected elevation decrease due to the glacier melting.

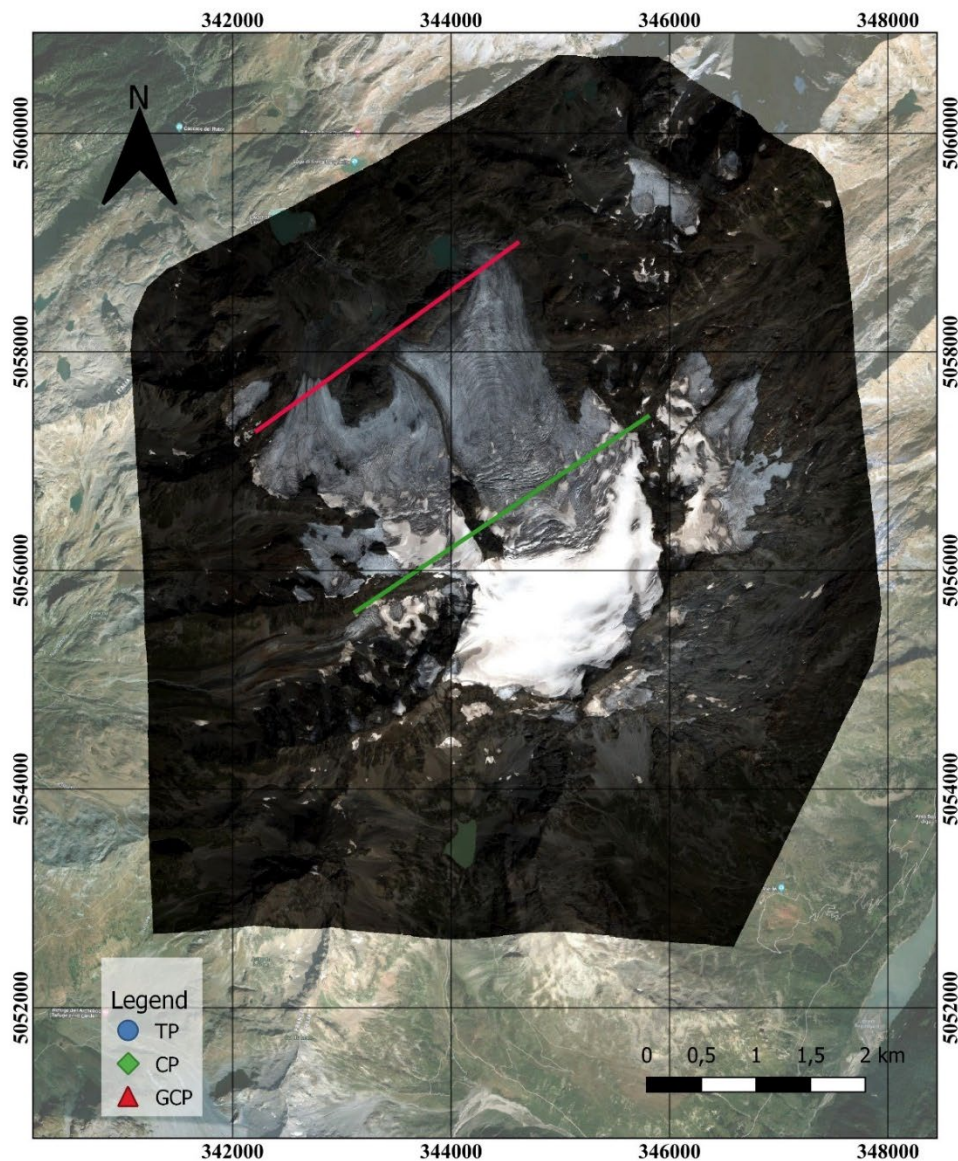


Figure 125 Section line on the glacier

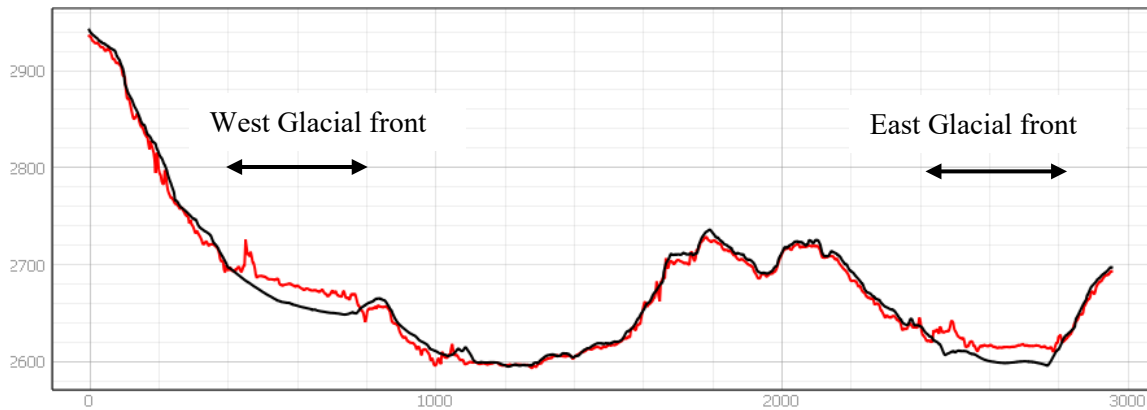
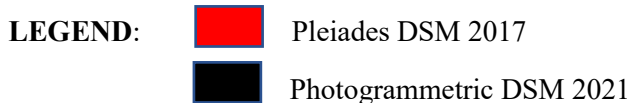


Figure 126 Pleiades- DSM aerial section 1



Figure 127 Pleiades- DSM aerial section 2



Although the error between the two DSMs is considerable, the glacial mass presents a gradual slope for almost all of its development, except for the summit, so it can be considered an estimate of ablation over time, especially the retreat of the fronts as shown in Figure 127. The satellite images date from August 2017 and the aerial images from September 2021. It is impossible to estimate the melting of the glacier accurately, but the lowering on the fronts is about 20 metres during 4 years. This result is consistent with the estimate made between the two aerial DSMs of 5 meters of thickness loss over a one-year period.

## 6.8 Discussion

The use of very high-resolution satellite imagery is a theoretically shorter process than processing aerial images, but it presents some problems that have not been fully solved. Despite two attempts to extract the DSM with both ellipsoidal heights and geodetic elevations, the bias is still present, thus leading to a lower accuracy than expected. Moreover, the automatic detection of GCPs and TPs is generally very effective on the satellite stereo pair while it shows difficulties over the glacier areas. On the other hand, precise manual detection of GCPs is very challenging. In planar terms, the result obtained allows an assessment of the retreat of the glacial fronts and a comparison with the other products, while altimetrically the assessment, although consistent with others analyses, is mostly a qualitative estimate, but still effective in identifying relevant ( $> +/- 5\text{m}$ ) elevation changes. Additionally, although rocky areas are considered to be stable over time, it could include areas subject to landslides or partial changes over time.

Satellite imagery photogrammetry is a valuable tool for qualitative glacier monitoring over large areas to identify hot spots where to focus ad-hoc aerial/drone surveys, but suitable reference data are required. A continuous monitoring over the time is certainly possible in order to assess seasonal variations in glacial mass. Both the influence of terrain slope and aspect as well as the azimuth of the available images should be carefully evaluated to assess the expected accuracy of a satellite based approach in glacier monitoring over a specific area of interest. More accurate results as model validation are expected on glaciers with smoother slopes, constant exposure and a proper satellite azimuth during the acquisition.

.

# Chapter 7

## Indren Glacier monitoring

The Indren glacier was considered in this work to show how the monitoring of a glacier can be done at different scales. The Indren is a much less extensive glacier, less than one square kilometre and easily accessible. Here two drone photogrammetric flights were carried out one year apart and a LIDAR scan in 2020.

### 7.1 Indren campaign

Indren campaign took place on 22<sup>nd</sup> and 23<sup>rd</sup> July 2021 starting from Gressoney-la-trinitè to verify the situation after around one year from the last campaign (done on 29<sup>th</sup> June 2020). On that occasion, some markers were set, and a first drone photogrammetric flight was executed.

The 2020 campaign was aimed to monitor the glacier in collaboration with the photographic campaign 'On the Trails of the Glaciers' by Fabiano Ventura.

The 2021 campaign consist of a first exploring part to check markers of the previous campaign and measure their coordinates and then to repeat the drone flight over the



Figure 128 RTK station INDREN 1 base station

glacier. The group was split into two climbing groups to go around different parts of the glacial area. Indren glacier covers a small area so in a few hours were possible to finish the procedure and go back to the cableway station. Both the flights of 2020 and 2021 were made with the DJI Phantom 4 drone described in chapter 3 (see 3.3.1).

First flights were taken on the 30<sup>th</sup> July 2020 from 9:58 to 13:15, covered an area of 3.46 km<sup>2</sup> and produced 1140 images with a flight altitude of 148 m and ground resolution of 0.03m/pix.

The Indren measurement campaign in the summer of 2021 took place after the Rutor measurement campaign described in chapter 3(3.2 Rutor monitoring campaigns and Ground Control Points) on 21<sup>st</sup>-23<sup>rd</sup> July 2021. On the afternoon of the 21st, after the descent from the Deffeyes refuge, the team, including the writer, moved from La Thuile to Gressoney-la-trinitè where they spent the remaining days of the campaign. Days 22<sup>nd</sup> and 23<sup>rd</sup> July were dedicated to monitoring the Indren glacier.

On 22 July, after the ascent by cable car, the group divided into two roped parties moved onto the glacier (Figure 129) to check the markers put in place in 2020 and recheck their positions and fix 4 new markers (INDREN12, INDREN13, INDREN14, INDREN15).

POINT	EST	NORD	<sup>h</sup> ELLIPSOIDAL	LONG	LAT	<sup>H</sup> ORTOMETRIC
INDREN1	411321.307	5082602.942	3333.918	45.891277438	7.856992978	3279.481
INDREN2	411374.931	5082561.155	3319.142	45.890908315	7.857691726	3264.711
INDREN3	411429.397	5082708.248	3359.940	45.891277438	7.858366476	3305.503
INDREN4	411427.912	5082707.197	3359.571	45.890908315	7.858347538	3305.134
INDREN5	411493.407	5082835.883	3375.553	45.892238987	7.859167851	3321.113
INDREN6	411547.255	5082980.852	3413.391	45.892229331	7.859835105	3358.945
INDREN7	411112.278	5083095.240	3406.858	45.893395771	7.854208172	3352.375
INDREN8	411093.964	5082967.139	3350.275	45.894707242	7.853995853	3295.800
INDREN9	411314.478	5083052.883	3391.072	45.895680507	7.856821895	3336.606
INDREN10	411254.389	5082580.097	3317.662	45.894525396	7.856134837	3274.660
INDREN11	411318.829	5082550.828	3329.094	45.895325452	7.856970656	3263.222
INDREN12	411210.993	5083050.489	3386.285	45.53430460	7.51197592	3331.812
INDREN13	411012.172	5083091.405	3415.864	45.53442790	7.51105075	3361.374
INDREN14	411045.711	5083114.165	3420.343	45.53450319	7.51120484	3365.854
INDREN15	411428.548	5083164.075	3438.374	45.53468267	7.51297773	3383.909

Table 42 Indren glacier GCPs

A pole with the base was positioned near the cableway, the only point covered by the network both in 2020 and 2021. Due to clouds, after the marker positioning was decided to wait for better weather conditions. Unfortunately, after three attempts to flight was not possible to continue with the flight due to clouds and strong wind. As a result, the attempts produce 191 images from 13:39 to 13:45 that will be not inserted in the model.

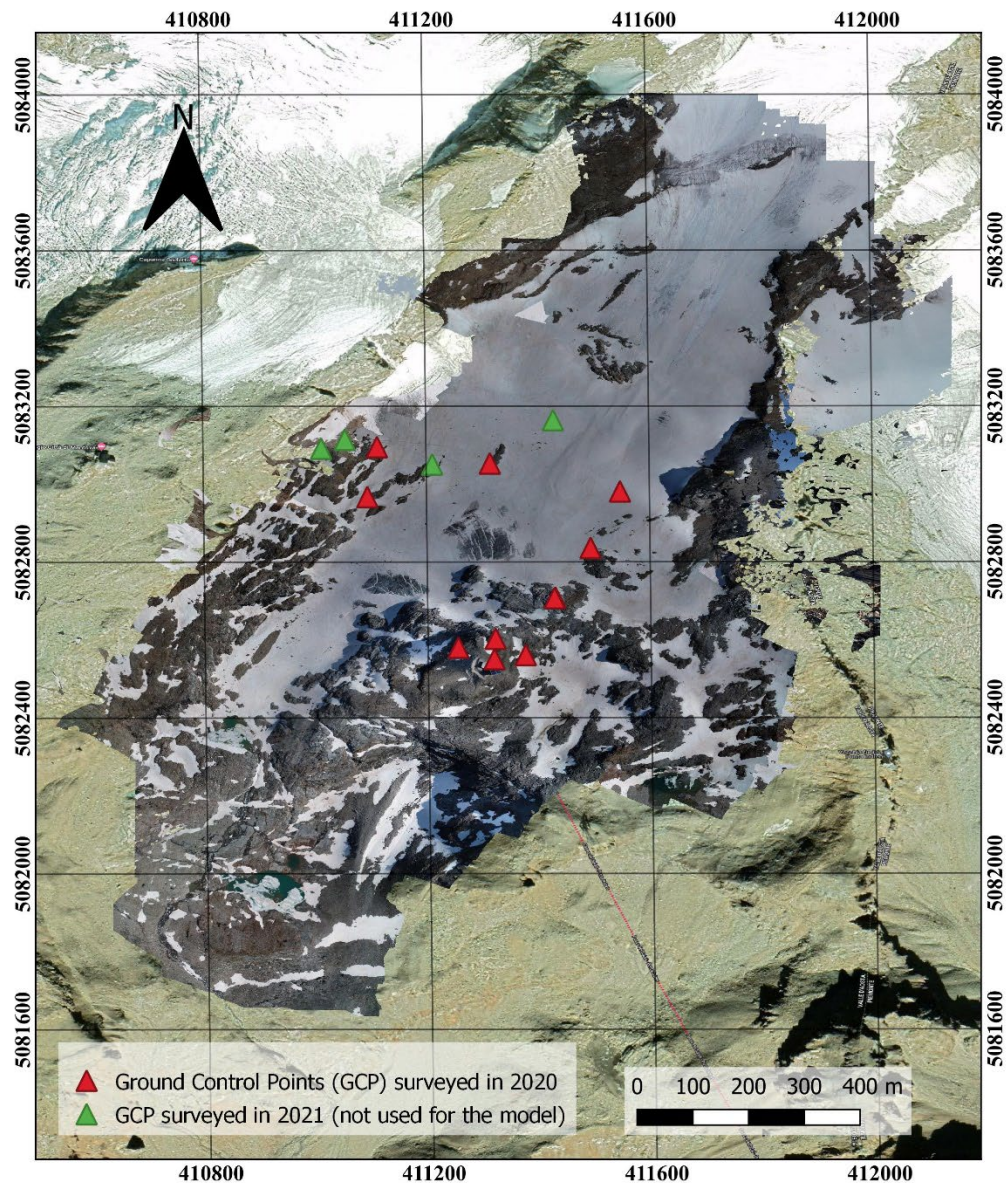
On the 23<sup>rd</sup> the better weather conditions, sunny and less wind allowed us to proceed with the drone flights. However, due to height and cold temperature that reduces the batteries autonomy, was necessary to proceed with different flights. During the photogrammetric flights, the problem of the low-altitude flight of the helicopter bringing supplies to the shelters occurs. Therefore, continuously monitor a second person supporting the piloting operator with binoculars was necessary. The pole RTK was set on INDREN 1 (Figure 128), so drone camera positions were estimated with the centimetric position. On 23<sup>rd</sup> July 2021 were acquired 1648 photos from 9:01 till 11:34 with a flight altitude of 149 m and a ground resolution of 0.03 m/pix and a coverage area of 13.2 km<sup>2</sup>.



Figure 129 Marker measurement during the campaign of July 2021

As described before for the photogrammetric flight of the Rutor glacier, the drone camera coordinates are collected with the ellipsoidal height. Thanks to the ConveRgo software, height is converted from ellipsoidal to orthometric, maintaining the same geographic coordinates ETRF2000.

Thanks to the camera location and to the GCPs (Figure 130) the model is georeferenced.



*Figure 130 Indren glacier GCPs*

For both the models, ended the data processing the residual error is calculated to estimate the precision of the products.

The camera average location error is computed in both models and reported in Table 44 :

Model	X error [cm]	Y error [cm]	Z error [cm]	XY error [cm]	TOT error [cm]
2020	0,588	0,512	1,467	0,780	1,661
2021	1,888	1,756	5,741	2,578	6,294

*Table 43 Average camera location error*

The average residual error is evaluated in both models are reported in Table 45:

Model	N. Points	RMSE X [cm]	RMSE Y [cm]	RMSE Z [cm]	RMSE XY [cm]	RMSE TOT [cm]
2020	10	3,57	2,790	4,105	4,531	6,114
2021	10	4,718	8,231	3,324	9,487	10,053

*Table 44 Residual errors on GCP*

The mesh is generated for both 2020 and 2021 models. Thanks to the dimension computational time are more than halved, processed from the machine in around 3 hours and 4.5 hours for 2020 and 2021 models, respectively.

## 7.2 Drone models: DSM and Orthophoto

The drone models of 2020 and 2021 are elaborated with the same procedure described for the Rutor glacier.

With the 2021 model has been produced at the end:

- An Orthophoto with a GSD equal to 0.03 m (Figure 131)
- A DSM with a GSD equal to 0.073 m

- A Dense Cloud of 583,278,042 points

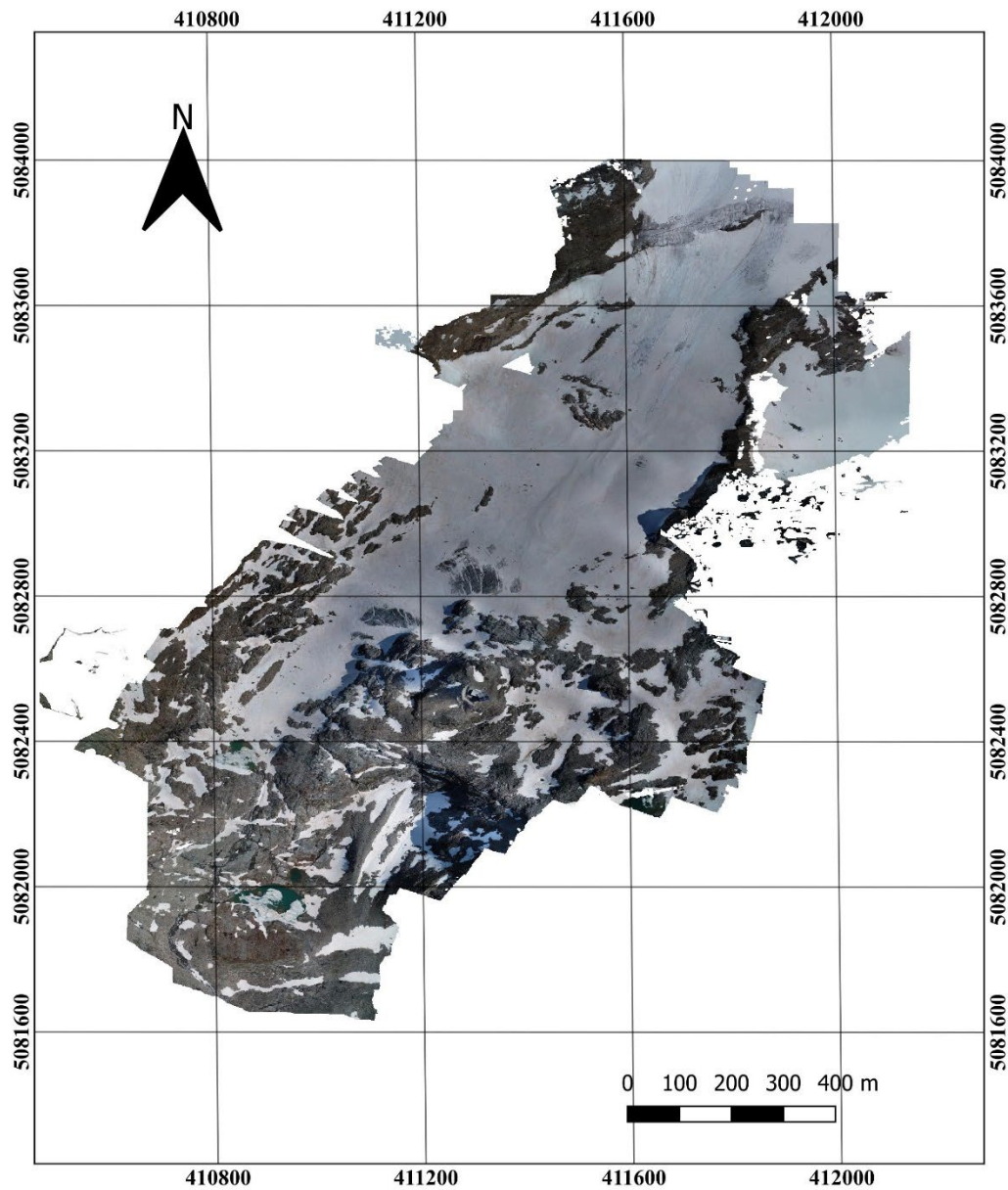


Figure 131 Indren orthophoto flights 2021

With the 2020 model has been produced at the end:

- An Orthophoto with a GSD equal to 0.03 m (Figure 132)
- A DSM with a GSD equal to 0.075 m
- A Dense Cloud with 298,988,434 points

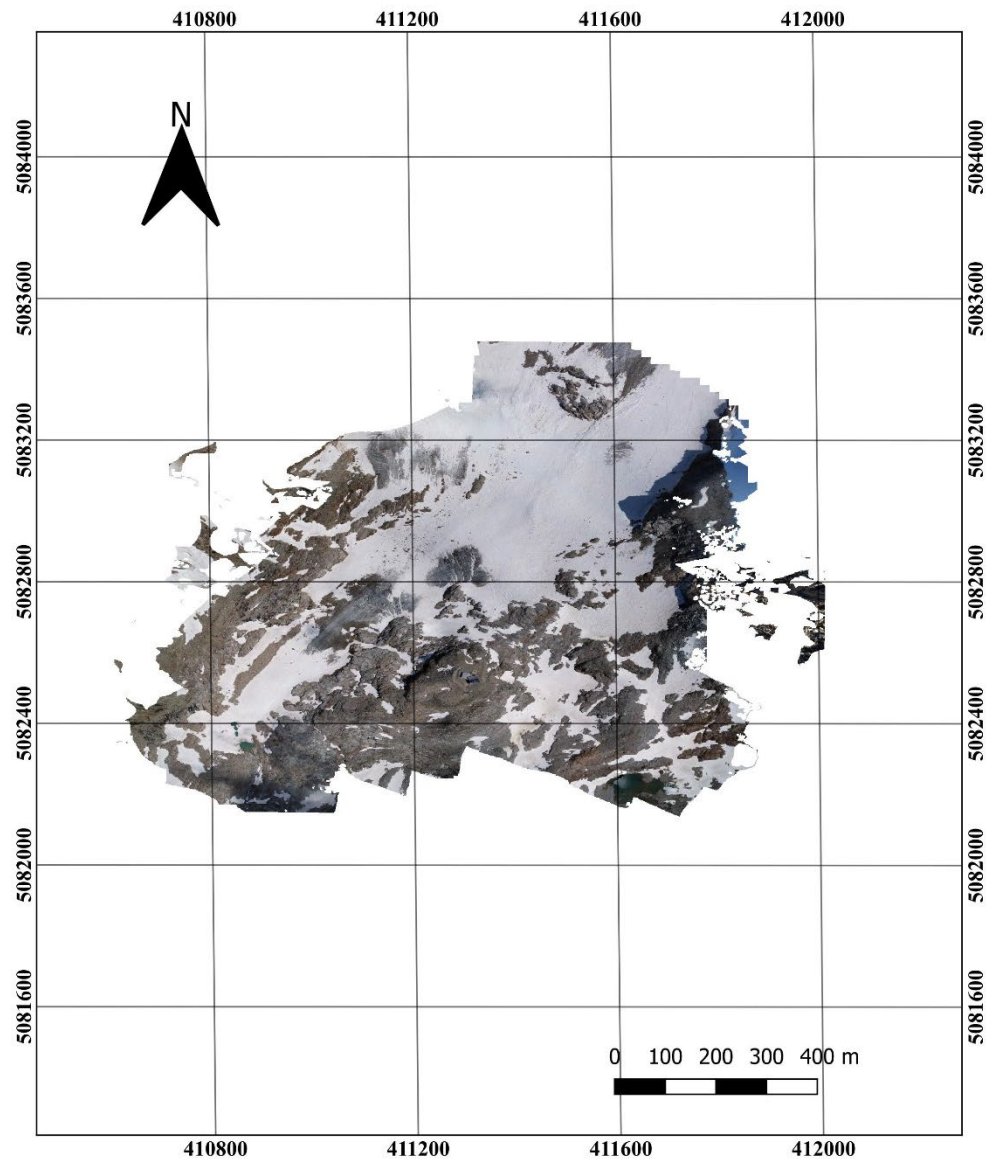
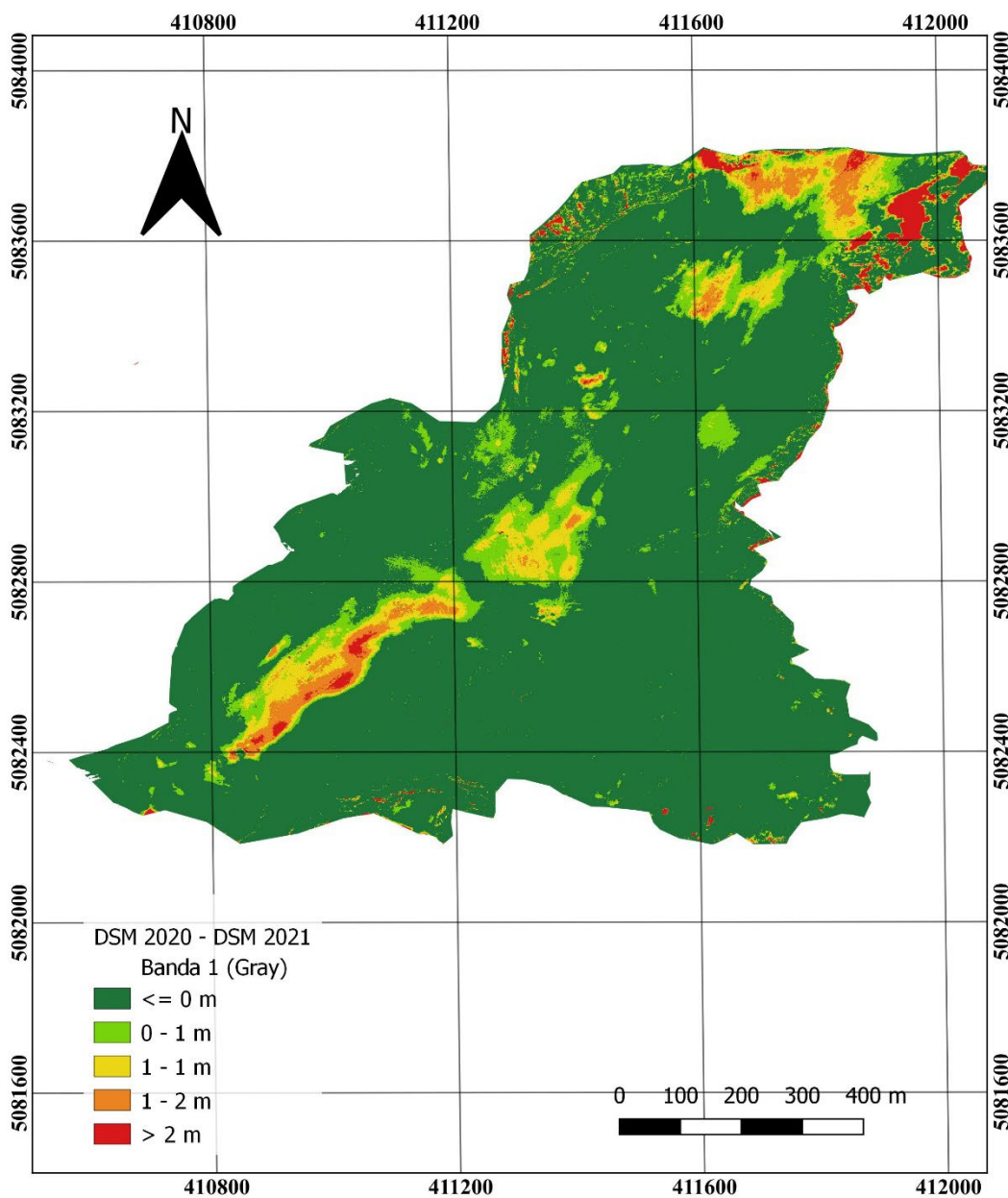


Figure 132 Orthophoto from flights 2020



*Figure 133 Differences on DSM models of 2020 and 2021*

From the difference between the two Digital Surface Models (Figure 133) is clear how the ablation area of the glacier is in the central part in an average thickness of 1 meter. It is

necessary to underline how the period considered is not the most relevant to monitoring the snow melting of a glacier. It is usually preferable to monitor when the melting is maximum at the end of the summer period. As said before, the period was chosen in collaboration with the photographic survey of the project 'On the Trails of the Glaciers' and repeated for consistency one year later at the same time.

### 7.3 GCP experiments

Due to the different scale of the Indren Glacier, it was possible to carry out GCP experiments on this glacier.

In order to test how the accuracy of the model varies, 4 different configurations were adopted for aerial triangulation by varying the weight of the camera intake centres and Ground Control Points:

1. the first not use the drone's camera projection centres and use only the GCPs;
2. the second using only the camera projection centres and using the markers as checkpoints;
3. the third using both GCPs and ground control points with the same weight;
4. a final configuration using the projection centres and only one GCP (INDREN1).

Case	Metashape Accuracy (m)	Long average error (m)	Lat average error (m)	Height average error (m)
1.	11GCP	0.005	0.0471	0.0823
	Cameras	10	0.0188	0.0175
2.	CP	10	0.4710	0.6650
	Cameras	0.02	0.0167	0.0164
3.	11GCP	0.02	0.0784	0.1235
	Cameras	0.02	0.0017	0.0161
4.	1 GCP	0.02	0.0032	0.0164
	Cameras	0.02	0.0167	0.0161

Table 45 GCPs trial

This trial was executed only with the primary point cloud and not proceeding with the dense cloud. The aim was only to underline the necessity of the GCPs on a monitoring drone application and to identify the best consideration. It is important to identify how this simple trial emphasises the need to place at least one marker. Although the possibility of not having any markers on the glacier would reduce monitoring costs and risks (mainly due to the use of a roped team that travels the glacier for the placement and survey of markers on the ground), it seems appropriate from an estimation by aerial triangulation not to use only the centres of the cameras, even if equipped with GPS receiver. The errors in case 2 in which only cameras are used are one order of magnitude in longitudinal,

latitudinal, and height coordinates. In the cases 1,3,4 the errors are centimetric with slight differences in the result.

## 7.4 LIDAR monitoring technique

As a further investigation, in 2020 on the Indren glacier a Lidar scan was executed. The Lidar (Light Detection and Ranging) technique measures distances by the time it takes a light signal to travel to and from the source to a chosen point. With a high-resolution camera and integrated GPS receiver, the Polaris scanner allows scanning in different environments and applications. However, when used in high mountains, the great weight and bulk are limiting, and it was only possible to carry out these scans because of the proximity of the area to the cable car. The 3D laser scans were processed using AtlaScan software.

The 3 scans were imported in the software and after the input sets, they are aligned. Unfortunately, there are important part on the glacial area missing, so it is impossible to compare them with the Metashape model computed.

An image of the point cloud visualisation obtained is reported in Figure 134.

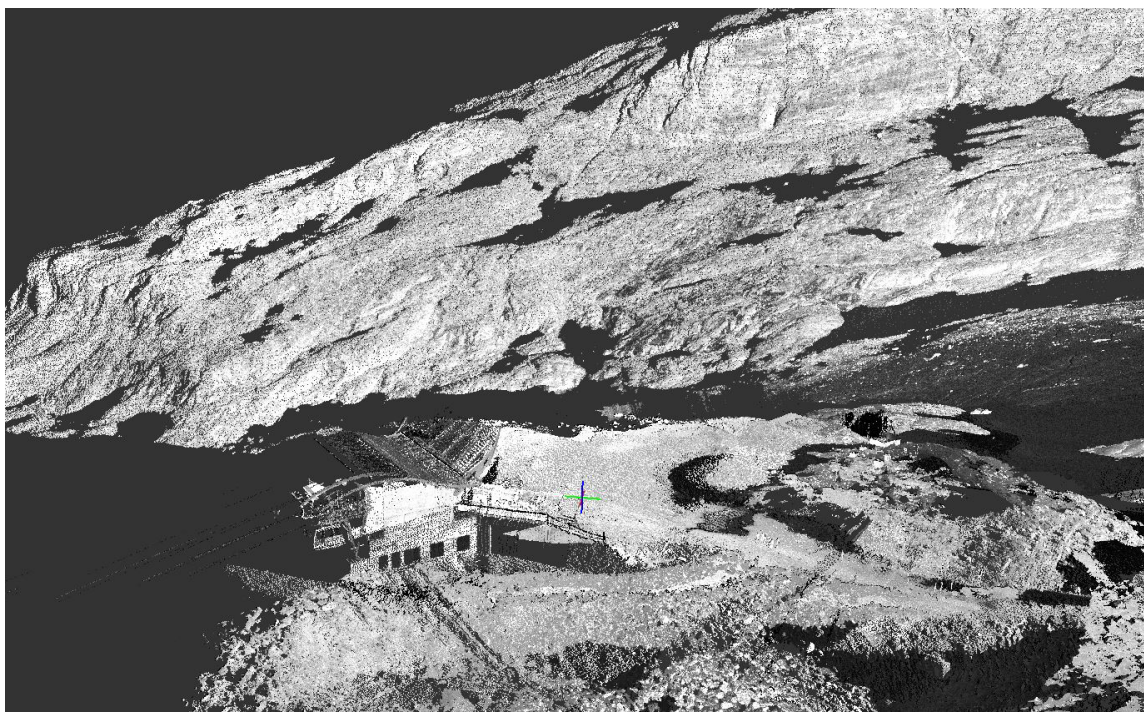


Figure 134 AtlaScan model Indren 2020

## 7.5 Discussion

As mentioned earlier (see p. 3.3.1), UAV are powerful tool in glacial environment and in particular drone photogrammetry is a valuable tool for smaller glaciers, such as the Indren Glacier, with more immediate post-production and model management. This case proved to be the best solution given the easy and direct accessibility and the possibility of a point with RTK connection to use as a base.

It is important to underline that it is clear that the end of July is not the right period for the glacier inspections. This is because the mass of snow accumulated during the winter on the glacier is still present and does not allow a proper evaluation of the updated mass balance and melted snow.

The model obtained with a centimetric precision can be used as a comparison for future inspection, it is a simpler drone application in a smaller and more accessible area than the Rutor one.

For the Lidar acquisition, more scans and more accurate detection of the snowy areas and a proper georeferentiation are necessary to carry out a comparison.

# Chapter 8

## Conclusions

Monitoring glacial environments is an application domain where several geomatic techniques can be effectively adopted. In this work, photogrammetric methods applied to imagery acquired from aerial, drone and satellite platforms were analysed for a multi-temporal 3D monitoring (i.e. 4D) of Rutor and Indren glaciers.

The different scales and accessibility of glaciers are crucial when choosing which instrumentation/technique to adopt.

On the Rutor glacier, whose extent is 8.4 km<sup>2</sup>, drone photogrammetry was used only to deepen the analysis and focus on priority areas or to support other hydraulic and geophysical analyses.

The photogrammetric approach exploiting a light aircraft was a necessary choice for the fast survey of the entire glacier and to enable a yearly monitoring. The GCPs, the excellent GSD of 0.06 m, and the centimetric accuracy allowed the production of an orthophoto with 6 cm GSD and a DSM with 24 cm GSD for the 2021 model.

3D co-registration of the 2020 model from the 2021 model was carried out with an accuracy of approximately 20 cm. Previous summer field surveying campaigns were necessary to support the photogrammetric flight.

Flight path processing for determining antenna position at the time of the image acquisition was carried out to make the model solution more robust and to limit in-situ surveys. The asynchronism between the time-stamp recording and the actual image acquisition, as well as the bias caused by NMEA time synchronization makes the direct photogrammetry approach possible but time/consuming and complicated. Post-processing with the insertion of the 'EVENT MARKER' GPS at the image acquisition time is necessary. However, the ability to estimate camera centre projection coordinates could limit the GCPs field surveys. Moreover, for large and poorly accessible environments such as glaciers ones, this would reduce costs and associated risks. Improvements and upgrades to the aircraft's onboard instrumentation could play a key role in containing the costs of measurement campaigns. The implementation of proper GNSS data processing could enable the monitoring of inaccessible glacial areas, although accuracy would become closely linked to the quality of the onboard instruments.

The use of very high-resolution satellite imagery is tested to assess the possibility of monitoring glaciers with this technique as well as to assess the 3D positional accuracy. Unfortunately, the elevation accuracy is lower than expected (with respect to previous

analyses) with a mean altimetric error on stable areas of 1-5 meters and precision proportional to the terrain slope. Nevertheless, satellite photogrammetry could be a valuable tool for monitoring glacial areas with gentle slopes thanks to the possibility of repeated monitoring over time and the avoidance of costly in-situ operations and ad/hoc aerial flights.

The terrain exposure with respect to the satellite position is a clear limitation in the use of satellite imagery in glacier monitoring. The influence of exposure could be overcome by combining targeted drone surveys in areas characterised by lower accuracy or, where possible, by choosing the optimal azimuth among the available archive satellite images covering the area under investigation.

From this multi-technique analysis of the Rutor glacier, the Rutor glacial front, as shown in the orthoimagery in Figure 135 and elevation cross section in Figures 136-137, is undergoing a constant annual retreat. Compared to the 2012 orthoimagery of the Geoportal of the Valle d'Aosta region, the eastern front, the most evident, is retreated over 250m. The vertical sections made it possible to compare the glacier with the DSM created in 2008 after verifying the accuracy on areas invariant over time. The glacier appears to have experienced an elevation loss up to 60 meters in the lower part of the fronts.

Unlike Rutor, drone photogrammetry is appropriate for the size of the Indren Glacier, which covers 0.92 km<sup>2</sup>. Furthermore, the interested area was imaged with a GSD up to of 0.03 m, and the related metric added/value products are characterised by a centimetric 3D accuracy and a very high level of detail.

Fundamental for all applications is the assessment of weather conditions and the presence of clouds, which, as was the case for the aerial campaigns, required the repetition of flights by both drone and aircraft. The presence of clouds can jeopardise the use of all the geomatic instruments considered, partially or totally covering the areas concerned and forcing postponement or repetition of flights, as in these cases. As far as drone flights are concerned, a crucial aspect is the air temperature and the presence of wind. Very low temperatures at glacial altitudes cause a considerable decrease in flight range and the consequent need to make many flights, increasing the overall time required. Drone photogrammetry, despite its limitations, provides a 3D centimetric accuracy and excellent spatial resolution. The lack of internet connection and the distance from GNSS permanent network stations \*or off-grid as in the case of Rutor) make post-processing of the data necessary, which reduces the use of such techniques for real/time applications

On the Indren glacier, it was possible to use also terrestrial laser scanning (Lidar Polaris) thanks to the proximity of the cable car that allowed its transport. However, the large size and weight of the Lidar does not make its use effective in most glacial environments.

Glacier monitoring is a complex procedure in which many variables have to be considered, considerable costs and inaccessible environments that are vast and changing.

The combination of several geomatics techniques has enabled the 4D monitoring of glaciers. Thanks also to the monitoring of the Rutor glacier carried out by the Aosta Valley region, was possible to compare both volumetrically, through qualitative sections and differences between DSM, and planimetrically (by means of orthoimagery visual interpretation) the glacier retreat. Some parts, such as the glacial fronts, underwent a considerable annual retreat.

Glaciers are a precious resource on which the economy and survival of many mountain communities often depend. The Rutor glacier, for example, provides a water supply for the areas below and is a resource to be monitored and protected over time.

The work carried out can be further developed, collaborating with ARPA Valle D'Aosta for increasingly accurate and multidisciplinary glacier 4D monitoring. In addition, another group of experts carried out geophysics and hydrological surveys not addressed in this work during the summer campaigns. The integration of these data in the 3D model allows a complete analysis of the evolution of the glacial environment.

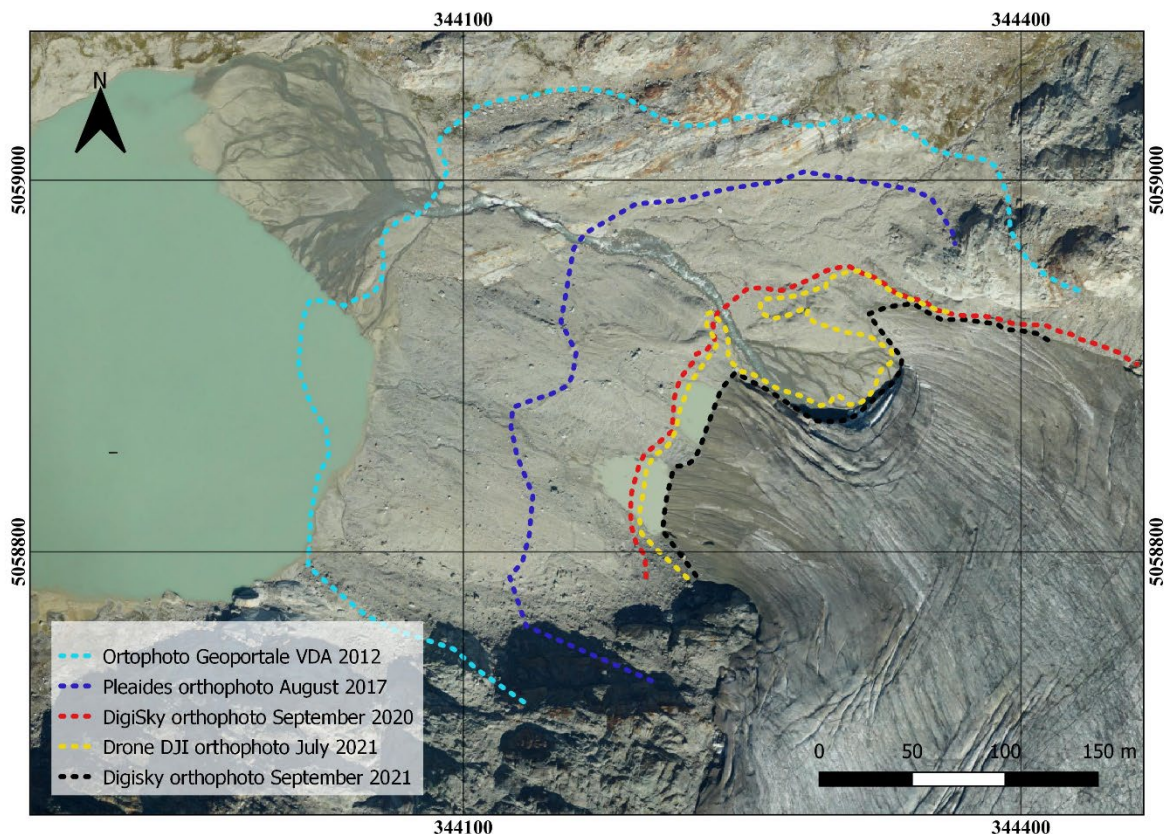


Figure 135 Multitemporal analysis of east glacial forehead retreat on orthophoto 2021

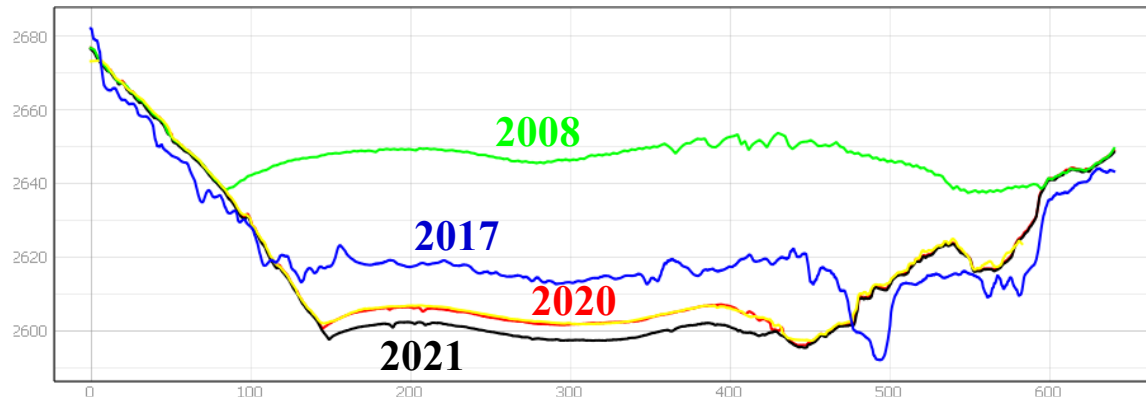


Figure 137 Zoom section on east glacial front

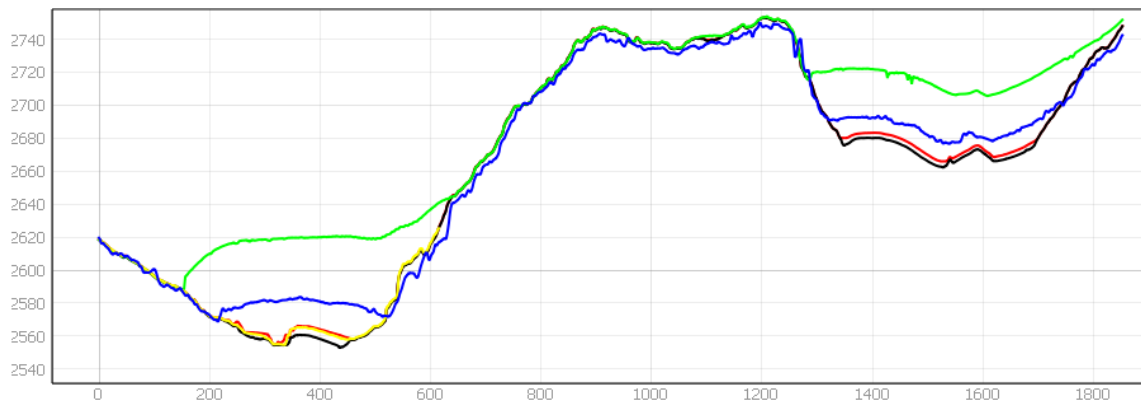


Figure 136 Section on east and central glacial front

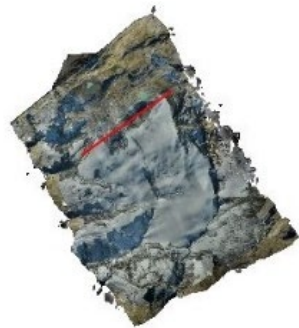


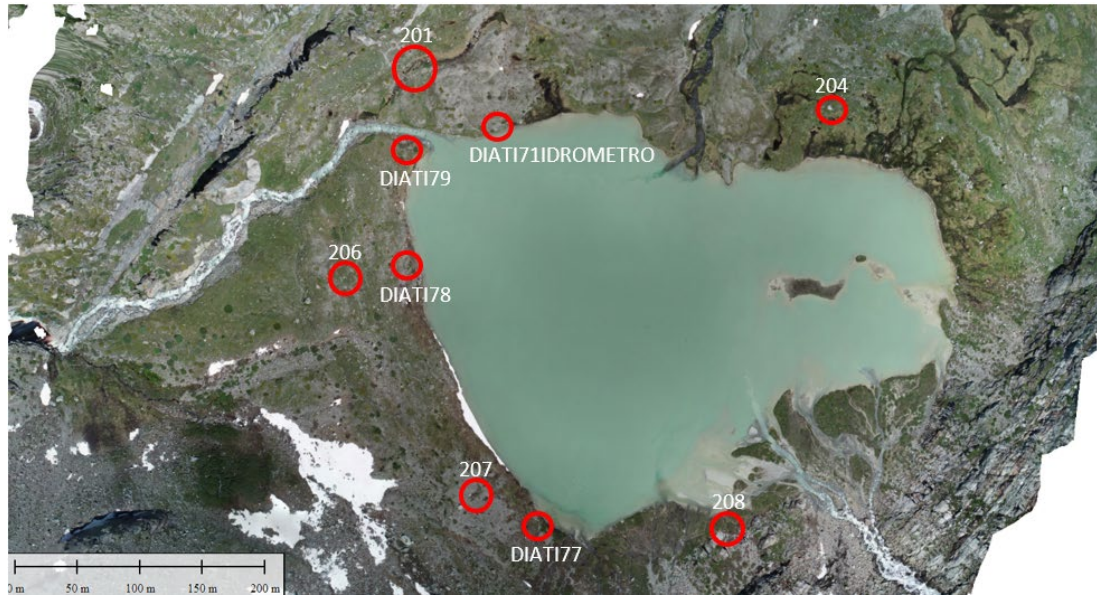
Figure 138 Section line of Figures 136-137

**LEGEND:**

-  DigiSky Photogrammetric DSM September 2021
-  Pleaides Satellite DSM August 2017
-  Drone Photogrammetric DSM July 2021
-  Geoportale DSM September 2008
-  DigiSky Photogrammetric DSM September 2020

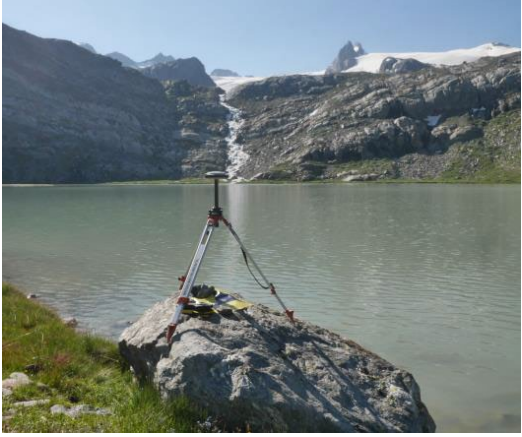
## ANNEX Chapter 4

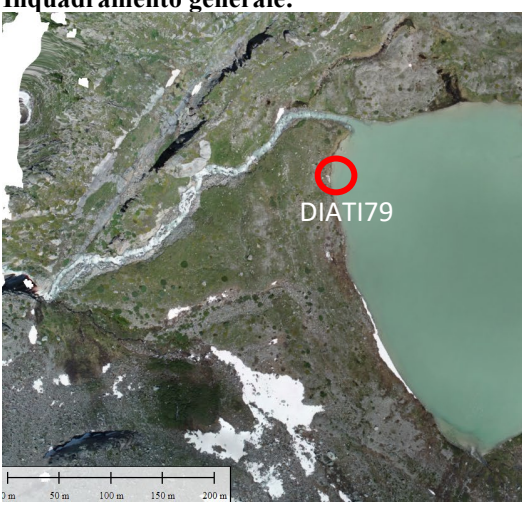
### Rutor Monographs Monografie lago Seracchi



PUNTO	EST	NORD	H ELLISSO IDICA	LONG	LAT	H ORTO METRI CA
<b>DIATI71 idrometro</b>	342367.784	5059296.4 09	2442.042	6.97530816	45.66747763	2388.105
<b>diati79</b>	342341.192	5059279.4 30	2441.039	6.97497252	45.66731884	2387.102
<b>201</b>	342304.308	5059374.1 29	2458.975	6.97446860	45.66816229	2405.045
<b>204</b>	342667.248	5059317.5 73	2445.777	6.97914324	45.66773609	2391.831
<b>206</b>	342275.253	5059182.3 28	2447.586	6.97415808	45.66643038	2393.646
<b>DIATI78</b>	342373.254	5059008.7 67	2450.934	6.97547165	45.66489147	2396.982
<b>207</b>	342373.252	5059008.7 79	2450.933	6.97547162	45.66489158	2396.981
<b>DIATI77</b>	342446.643	5058980.2 92	2441.501	6.97642236	45.66465203	2387.545
<b>208</b>	342581.677	5058979.7 82	2442.147	6.97815484	45.66467814	2388.187

<b>Località: LA THUILE</b> <b>Ghiacciaio RUITOR</b>		<b>Data: 20 LUGLIO 2021</b>
Nome: 201	Numero:	<b>Foto particolare:</b>
Descrizione:		
Ubicazione:		
<b>Coordinate ETRF2000 32N</b>		
<b>Est:</b> 342304.308	<b>Nord:</b> 5059374.129	
<b>long:</b> 6.97446860°	<b>lat:</b> 45.66816229°	
<b>H:</b> 2405.045	<b>h ell:</b> 2458.975	
<b>Inquadramento generale:</b>		<b>Foto generale:</b>
		
<b>Note:</b>		

<b>Località: LA THUILE</b> <b>Ghiacciaio RUITOR</b>	<b>Data: 20 LUGLIO 2021</b>
<b>Nome:</b> DIATI 71 <b>Numero:</b> idrometro	
<b>Descrizione:</b> GNSS "base" DIATI71 Coordinate UTM ETRF2000 rilevate RTK il 20 luglio 2021 Marker	<b>Foto particolare:</b> 
<b>Ubicazione:</b> Stazione base sul punto DIATI71 vicino all'idrometro posto all'emissario del lago dei seracchi	
<b>Coordinate ETRF2000 32N</b>	
<b>Est:</b> 342367.784	<b>Nord:</b> 5059296.409
<b>long:</b> 6.97446860°	<b>lat:</b> 45.66816229°
<b>H:</b> 2388.105	<b>h ell:</b> 2442.042
<b>Inquadramento generale:</b>	<b>Foto generale:</b>
	
<b>Note:</b>	

<p><b>Località: LA THUILE</b> <b>Ghiacciaio RUITOR</b></p>	<p><b>Data: 20 LUGLIO 2021</b></p>								
<p><b>Nome:</b> DIATI 79    <b>Numero:</b></p> <p><b>Descrizione:</b> Rondella DIATI</p> <p><b>Ubicazione:</b></p> <table border="1" style="width: 100%; border-collapse: collapse;"> <tr> <td colspan="2" style="text-align: center; background-color: #cccccc;"><b>Coordinate ETRF2000 32N</b></td> </tr> <tr> <td style="padding: 2px;"><b>Est:</b> 342341.192</td><td style="padding: 2px;"><b>Nord:</b> 5059279.430</td></tr> <tr> <td style="padding: 2px;"><b>long:</b> 6.97497252°</td><td style="padding: 2px;"><b>lat:</b> 45.66731884°</td></tr> <tr> <td style="padding: 2px;"><b>H:</b> 2387.102</td><td style="padding: 2px;"><b>h ell:</b> 2441.039</td></tr> </table>	<b>Coordinate ETRF2000 32N</b>		<b>Est:</b> 342341.192	<b>Nord:</b> 5059279.430	<b>long:</b> 6.97497252°	<b>lat:</b> 45.66731884°	<b>H:</b> 2387.102	<b>h ell:</b> 2441.039	<p><b>Foto particolare:</b></p> 
<b>Coordinate ETRF2000 32N</b>									
<b>Est:</b> 342341.192	<b>Nord:</b> 5059279.430								
<b>long:</b> 6.97497252°	<b>lat:</b> 45.66731884°								
<b>H:</b> 2387.102	<b>h ell:</b> 2441.039								
<p><b>Inquadramento generale:</b></p> 	<p><b>Foto generale:</b></p> 								

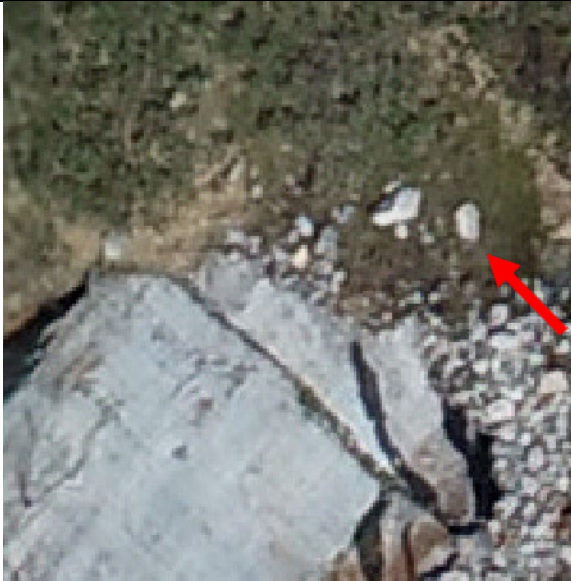
<b>Località: LA THUILE</b> <b>Ghiacciaio RUITOR</b>	<b>Data: 20 LUGLIO 2021</b>
<b>Nome:</b> 204 <b>Numero:</b> <b>Descrizione:</b> <b>Ubicazione:</b> <b>Coordinate ETRF2000 32N</b> <b>Est:</b> 342667.248 <b>Nord:</b> 5059317.573 <b>long:</b> 6.97914324° <b>lat:</b> 45.66773609° <b>H:</b> 2391.831 <b>h ell:</b> 2445.777	<b>Foto particolare:</b>
<b>Inquadramento generale:</b> 	
<b>Note:</b>	

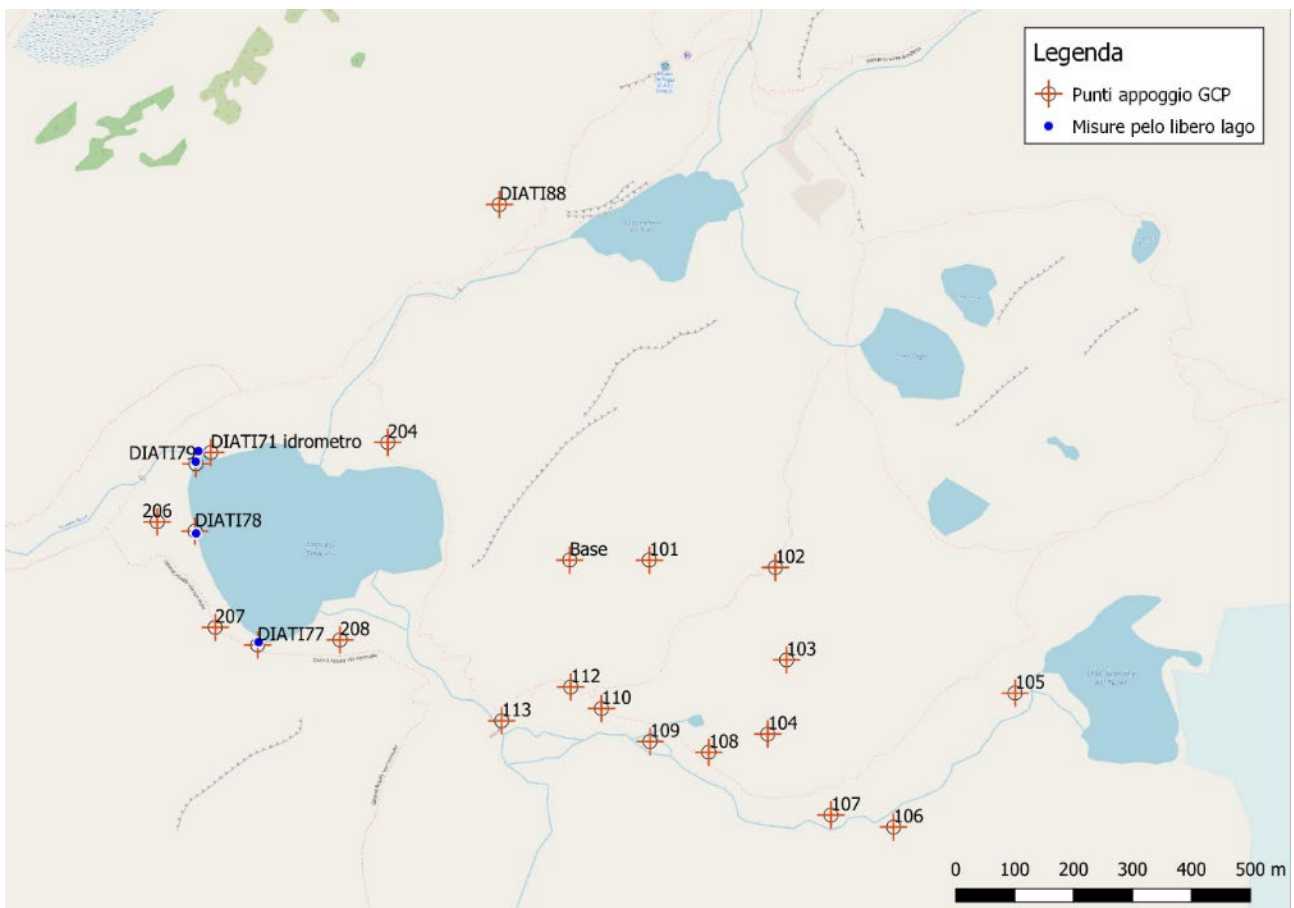
<p><b>Località: LA THUILE</b> <b>Ghiacciaio RUITOR</b></p>	<p><b>Data: 20 LUGLIO 2021</b></p>
<p><b>Nome:</b> 206      <b>Numero:</b></p>	<p><b>Foto particolare:</b></p>
<p><b>Descrizione:</b></p>	
<p><b>Ubicazione:</b></p>	<p><b>Coordinate ETRF2000 32N</b></p>
<p><b>Est:</b> 342275.253</p>	<p><b>Nord:</b> 342275.253</p>
<p><b>long:</b> 6.97415808°</p>	<p><b>lat:</b> 45.66643038°</p>
<p><b>H:</b> 2393.646</p>	<p><b>h ell:</b> 2447.586</p>
<p><b>Inquadramento generale:</b></p> 	<p><b>Foto generale:</b></p> 

<p><b>Località: LA THUILE</b> <b>Ghiacciaio RUITOR</b></p>	<p><b>Data: 20 LUGLIO 2021</b></p>						
<p><b>Nome:</b> DIATI 78    <b>Numero:</b></p> <p><b>Descrizione:</b> Rondella DIATI</p> <p><b>Ubicazione:</b></p> <p style="text-align: center;"><b>Coordinate ETRF2000 32N</b></p> <table border="1" style="width: 100%; border-collapse: collapse;"> <tr> <td style="padding: 2px;"><b>Est:</b> 342373.254</td> <td style="padding: 2px;"><b>Nord:</b> 5059008.767</td> </tr> <tr> <td style="padding: 2px;"><b>long:</b> 6.97547165°</td> <td style="padding: 2px;"><b>lat:</b> 45.66489147</td> </tr> <tr> <td style="padding: 2px;"><b>H:</b> 2396.982</td> <td style="padding: 2px;"><b>h ell:</b> 2450.934°</td> </tr> </table>	<b>Est:</b> 342373.254	<b>Nord:</b> 5059008.767	<b>long:</b> 6.97547165°	<b>lat:</b> 45.66489147	<b>H:</b> 2396.982	<b>h ell:</b> 2450.934°	<p><b>Foto particolare:</b></p> 
<b>Est:</b> 342373.254	<b>Nord:</b> 5059008.767						
<b>long:</b> 6.97547165°	<b>lat:</b> 45.66489147						
<b>H:</b> 2396.982	<b>h ell:</b> 2450.934°						
<p><b>Inquadramento generale:</b></p> 	<p><b>Foto generale:</b></p>						
<p><b>Note:</b></p>							

<p><b>Località: LA THUILE</b> <b>Ghiacciaio RUITOR</b></p>	<p><b>Data: 20 LUGLIO 2021</b></p>														
<table border="1"> <tr> <td>Nome: 207</td> <td>Numero:</td> </tr> <tr> <td colspan="2"><b>Descrizione:</b></td> </tr> <tr> <td colspan="2"><b>Ubicazione:</b></td> </tr> <tr> <td align="center" colspan="2"><b>Coordinate ETRF2000 32N</b></td> </tr> <tr> <td>Est: 342373.252</td> <td>Nord: 5059008.779</td> </tr> <tr> <td>long: 6.97547162°</td> <td>lat: 45.66489158°</td> </tr> <tr> <td>H: 2396.981</td> <td>h ell: 2450.933</td> </tr> </table>	Nome: 207	Numero:	<b>Descrizione:</b>		<b>Ubicazione:</b>		<b>Coordinate ETRF2000 32N</b>		Est: 342373.252	Nord: 5059008.779	long: 6.97547162°	lat: 45.66489158°	H: 2396.981	h ell: 2450.933	<p><b>Foto particolare:</b></p> 
Nome: 207	Numero:														
<b>Descrizione:</b>															
<b>Ubicazione:</b>															
<b>Coordinate ETRF2000 32N</b>															
Est: 342373.252	Nord: 5059008.779														
long: 6.97547162°	lat: 45.66489158°														
H: 2396.981	h ell: 2450.933														
<p><b>Inquadramento generale:</b></p> 															
<p><b>Note:</b></p>															

<p><b>Località: LA THUILE</b> <b>Ghiacciaio RUITOR</b></p>	<p><b>Data: 20 LUGLIO 2021</b></p>						
<p><b>Nome:</b> DIATI 77    <b>Numero:</b></p> <p><b>Descrizione:</b> Rondella DIATI e vernice</p> <p><b>Ubicazione:</b></p> <p style="text-align: center;"><b>Coordinate ETRF2000 32N</b></p> <table border="1" style="width: 100%; border-collapse: collapse;"> <tr> <td style="padding: 2px;"><b>Est:</b> 342446.643</td><td style="padding: 2px;"><b>Nord:</b> 5058980.292</td></tr> <tr> <td style="padding: 2px;"><b>long:</b> 6.97642236°</td><td style="padding: 2px;"><b>lat:</b> 45.66465203°</td></tr> <tr> <td style="padding: 2px;"><b>H:</b> 2387.545</td><td style="padding: 2px;"><b>h ell:</b> 2441.501</td></tr> </table>	<b>Est:</b> 342446.643	<b>Nord:</b> 5058980.292	<b>long:</b> 6.97642236°	<b>lat:</b> 45.66465203°	<b>H:</b> 2387.545	<b>h ell:</b> 2441.501	<p><b>Foto particolare:</b></p> 
<b>Est:</b> 342446.643	<b>Nord:</b> 5058980.292						
<b>long:</b> 6.97642236°	<b>lat:</b> 45.66465203°						
<b>H:</b> 2387.545	<b>h ell:</b> 2441.501						
<p><b>Inquadramento generale:</b></p> 	<p><b>Foto generale:</b></p>						

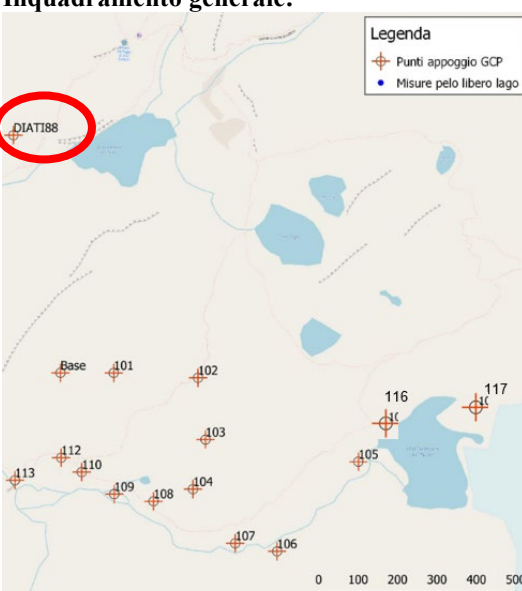
<p><b>Località: LA THUILE</b> <b>Ghiacciaio RUITOR</b></p>	<p><b>Data: 20 LUGLIO 2021</b></p>						
<p><b>Nome:</b> 208      <b>Numero:</b></p> <p><b>Descrizione:</b> freccia verniciata</p> <p><b>Ubicazione:</b></p> <p style="text-align: center;"><b>Coordinate ETRF2000 32N</b></p> <table border="1" style="width: 100%; border-collapse: collapse;"> <tr> <td style="padding: 2px;"><b>Est:</b> 342581.677</td><td style="padding: 2px;"><b>Nord:</b> 5058979.782</td></tr> <tr> <td style="padding: 2px;"><b>long:</b> 6.97815484°</td><td style="padding: 2px;"><b>lat:</b> 45.66467814°</td></tr> <tr> <td style="padding: 2px;"><b>H:</b> 2388.187</td><td style="padding: 2px;"><b>h ell:</b> 2442.147</td></tr> </table>	<b>Est:</b> 342581.677	<b>Nord:</b> 5058979.782	<b>long:</b> 6.97815484°	<b>lat:</b> 45.66467814°	<b>H:</b> 2388.187	<b>h ell:</b> 2442.147	<p><b>Foto particolare:</b></p> 
<b>Est:</b> 342581.677	<b>Nord:</b> 5058979.782						
<b>long:</b> 6.97815484°	<b>lat:</b> 45.66467814°						
<b>H:</b> 2388.187	<b>h ell:</b> 2442.147						
<p><b>Inquadramento generale:</b></p> 							

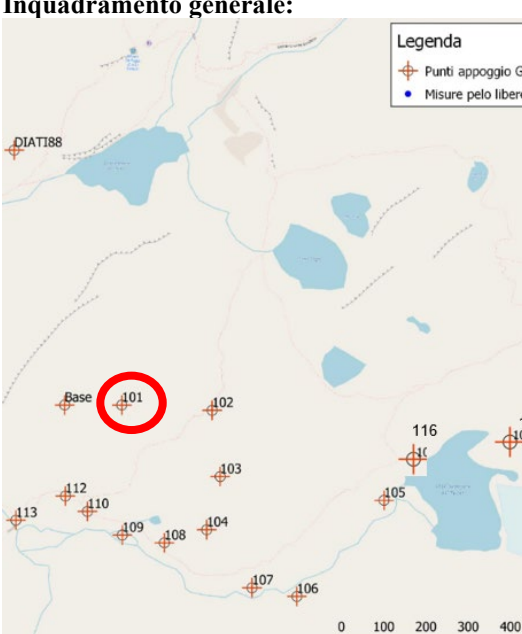


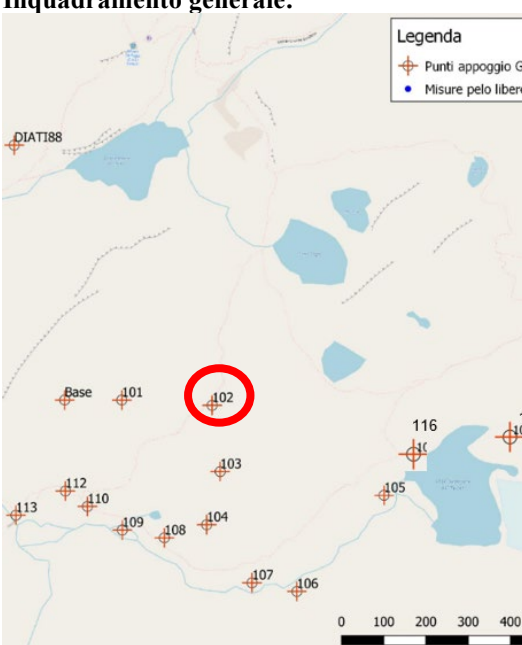
PUNTO	EST	NORD	H ELLISSOIDICA	LONG	LAT	H ORTOMETRICA
104	343311.199	5058821.599	2593.567	6.98756470	45.66342063	2539.576
105	343717.153	5058872.667	2598.342	6.99275606	45.66397170	2544.339
106	343585.115	5058742.797	2584.734	6.99110399	45.66277368	2530.731
107	343414.532	5058683.127	2575.548	6.98893492	45.66219839	2521.549
108	343208.488	5058795.695	2565.480	6.98625543	45.66316437	2511.492
109	343111.677	5058812.825	2559.079	6.98500797	45.66329655	2505.095
110	343026.117	5058867.692	2562.365	6.98389265	45.66377071	2508.386
111	343026.098	5058867.686	2562.354	6.98389241	45.66377065	2508.375
112	342978.138	5058904.335	2563.441	6.98326531	45.66408945	2509.464

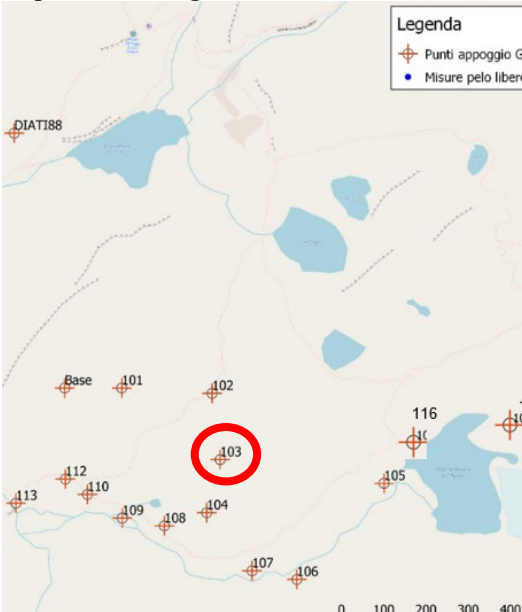
113	342861.706	5058841.121	2561.233	6.98179209	45.66349442	2507.258
114	343414.527	5058683.133	2575.556	6.98893485	45.66219845	2521.557
115	343658.193	5058869.207	2605.054	6.99200080	45.66392727	2551.053
116	343716.409	5058967.115	2594.689	6.99271615	45.66482112	2540.689
117	343866.232	5059031.117	2594.011	6.99461764	45.66543062	2540.008

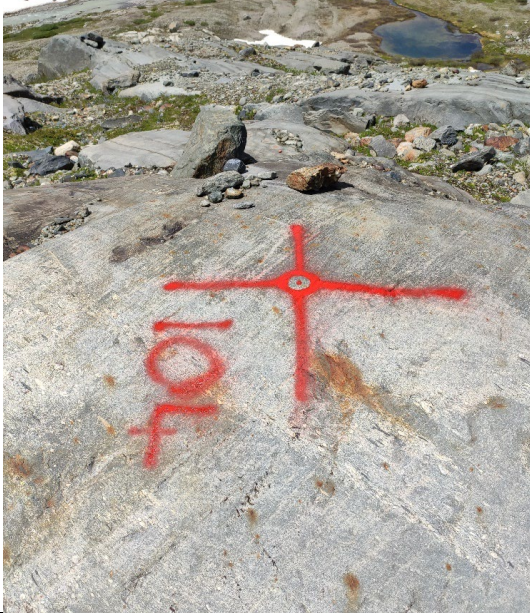
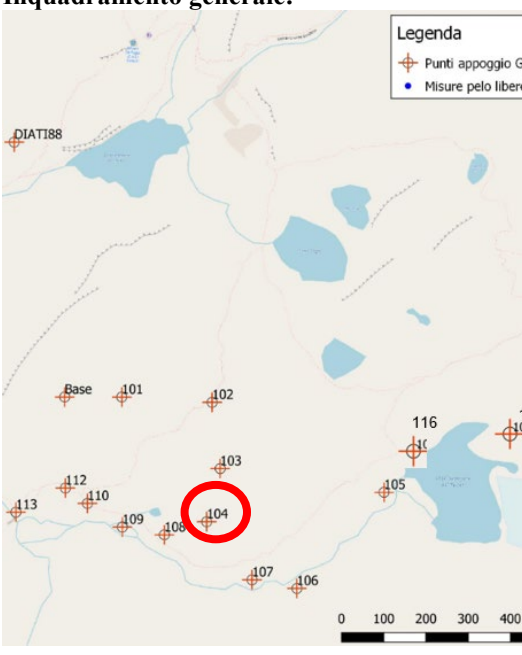
<b>Località: LA THUILE Ghiacciaio del RUITOR</b>		<b>Data:</b> 9 luglio 2021 materializzazione e rilievo
<b>Nome:</b> DIATI100 (BASE)	<b>Numero:</b>	<b>Foto particolare:</b>
<b>Descrizione:</b> bullone con rondella infisso su roccia		
<b>Ubicazione:</b> cima di fronte al rifugio Defeyes, raggiungibile in circa 30 min dal sentiero che porta al lago superiore		
<b>Coordinate ETRF2000 32N</b>		
<b>Est:</b> 411321.307	<b>Nord:</b> 5082602.942	
<b>long:</b> 7.856992978°	<b>lat:</b> 45.891277438°	
<b>H:</b> 3279.481	<b>h ell:</b> 3333.918	
<b>Inquadramento generale:</b>		<b>Foto generale:</b>
<b>Note:</b>		

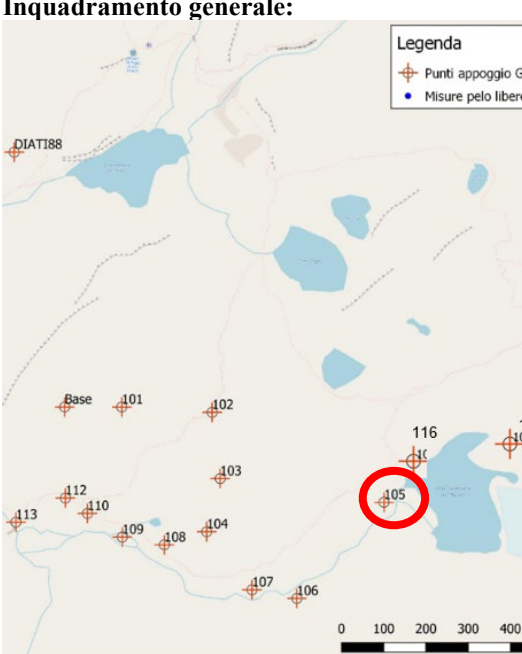
<p><b>Località: LA THUILE</b> <b>Ghiacciaio RUITOR</b></p>	<p><b>Data: 19 LUGLIO 2021</b></p>
<p><b>Nome:</b> DIATI 88    <b>Numero:</b></p>	<p><b>Foto particolare:</b></p>
<p><b>Descrizione:</b> Le coordinate DIATI88 sono state rilevate in modalità RTK con precisione centimetrica, sfruttando la presenza della rete GSM che ha permesso l'utilizzo dei prodotti di rete ITALPOS Rondella e 3 marker</p>	
<p><b>Ubicazione:</b></p>	<p><b>Coordinate ETRF2000 32N</b></p>
<p><b>Est:</b> 342861.808</p>	<p><b>Nord:</b> 5059729.085</p>
<p><b>long:</b> 6.98150628°</p>	<p><b>lat:</b> 45.67148192°</p>
<p><b>H:</b> 2503.829</p>	<p><b>h ell:</b> 2557.756</p>
<p><b>Inquadramento generale:</b></p> 	<p><b>Foto generale:</b></p>
<p><b>Note:</b></p>	

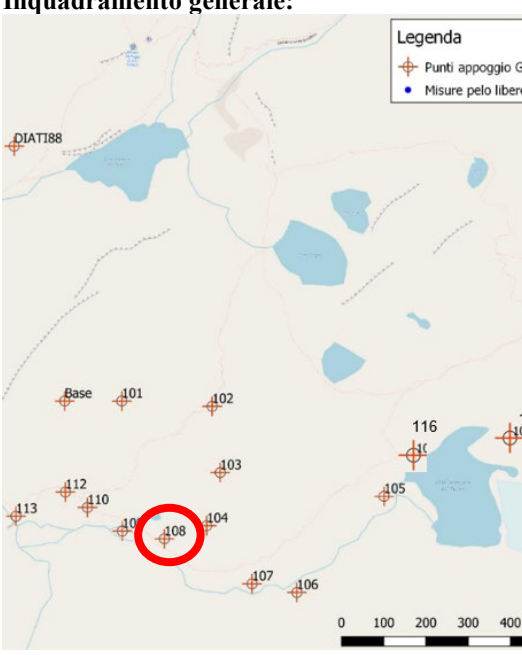
<b>Località: LA THUILE</b> <b>Ghiacciaio RUITOR</b>	<b>Data: 20 LUGLIO 2021</b>
<b>Nome:</b> 101 <b>Numero:</b> <b>Descrizione:</b> <b>Ubicazione:</b> <b>Coordinate ETRF2000 32N</b>	<b>Foto particolare:</b>
<b>Est:</b> <b>Nord:</b>	
<b>long:</b> ° <b>lat:</b> °	
<b>H:</b> <b>h ell:</b>	
<b>Inquadramento generale:</b> 	<b>Foto generale:</b>
<b>Note:</b>	

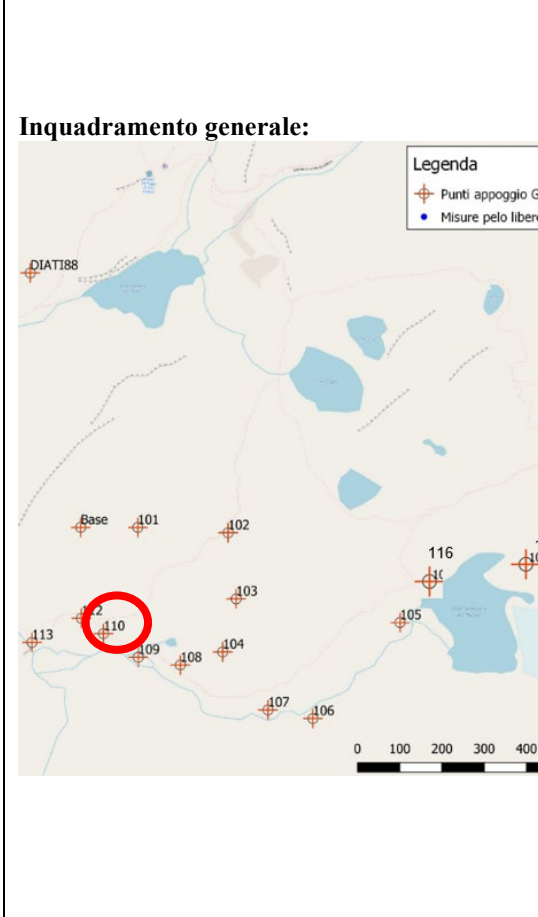
<b>Località: LA THUILE</b> <b>Ghiacciaio RUITOR</b>	<b>Data: 20 LUGLIO 2021</b>
<b>Nome:</b> 102 <b>Numero:</b>	<b>Foto particolare:</b>
<b>Descrizione:</b>	
<b>Ubicazione:</b>	
<b>Coordinate ETRF2000 32N</b>	
<b>Est:</b>	<b>Nord:</b>
<b>long:</b> °	<b>lat:</b>
<b>H:</b>	<b>h ell:</b>
<b>Inquadramento generale:</b> 	<b>Foto generale:</b>
<b>Note:</b>	

<b>Località: LA THUILE</b> <b>Ghiacciaio RUITOR</b>		<b>Data:</b> 20 LUGLIO 2021
Nome: 103	Numero:	
Descrizione:		
Ubicazione:		
<b>Coordinate ETRF2000 32N</b>		
Est:	Nord:	
long: °	lat: °	
H:	h ell:	
<b>Inquadramento generale:</b> +		
 <p>Legenda  <span style="color: orange;">+</span> Punti appoggio Go  <span style="color: blue;">●</span> Misure pelo libero</p> <p>DIATI88  Base 101 102  103  112 110 109 108 104  113 107 106  116 105 101  100 200 300 400</p>		
		<b>Foto generale:</b>
<b>Note:</b>		

<b>Località: LA THUILE</b> <b>Ghiacciaio RUITOR</b>	<b>Data: 20 LUGLIO 2021</b>
<b>Nome:</b> 104 <b>Numero:</b>	<b>Foto particolare:</b>
<b>Descrizione:</b>	
<b>Ubicazione:</b>	<b>Coordinate ETRF2000 32N</b>
<b>Est:</b> 343311.199	<b>Nord:</b> 5058821.599
<b>long:</b> 6.98756470°	<b>lat:</b> 45.66342063°
<b>H:</b> 2593.567	<b>h ell:</b> 2539.576
<b>Inquadramento generale:</b> 	<b>Foto generale:</b>
<b>Note:</b>	

<p><b>Località: LA THUILE</b> <b>Ghiacciaio RUITOR</b></p>	<p><b>Data: 20 LUGLIO 2021</b></p>														
<table border="1"> <tr> <td>Nome: 105</td> <td>Numero:</td> </tr> <tr> <td colspan="2"><b>Descrizione:</b></td> </tr> <tr> <td colspan="2"><b>Ubicazione:</b></td> </tr> <tr> <td colspan="2" style="text-align: center;"><b>Coordinate ETRF2000 32N</b></td> </tr> <tr> <td>Est: 343717.153</td> <td>Nord: 5058872.667</td> </tr> <tr> <td>long: 6.99275606°</td> <td>lat: 45.66397170°</td> </tr> <tr> <td>H: 2544.339</td> <td>h ell: 2598.342</td> </tr> </table>	Nome: 105	Numero:	<b>Descrizione:</b>		<b>Ubicazione:</b>		<b>Coordinate ETRF2000 32N</b>		Est: 343717.153	Nord: 5058872.667	long: 6.99275606°	lat: 45.66397170°	H: 2544.339	h ell: 2598.342	<p><b>Foto particolare:</b></p> 
Nome: 105	Numero:														
<b>Descrizione:</b>															
<b>Ubicazione:</b>															
<b>Coordinate ETRF2000 32N</b>															
Est: 343717.153	Nord: 5058872.667														
long: 6.99275606°	lat: 45.66397170°														
H: 2544.339	h ell: 2598.342														
<p><b>Inquadramento generale:</b></p>  <p><b>Legenda</b></p> <ul style="list-style-type: none"> <li>Punti appoggio GNSS</li> <li>Misure pelo libero</li> </ul>	<p><b>Foto generale:</b></p> 														
<p><b>Note:</b></p>															

<b>Località: LA THUILE</b> <b>Ghiacciaio RUITOR</b>	<b>Data:</b> 20 LUGLIO 2021
<b>Nome:</b> 108 <b>Numero:</b> <b>Descrizione:</b> <b>Ubicazione:</b> <b>Coordinate ETRF2000 32N</b> <b>Est:</b> 343208.488 <b>Nord:</b> 5058795.695 <b>long:</b> 6.98625543° <b>lat:</b> 45.66316437° <b>H:</b> 2511.492 <b>h ell:</b> 2565.480	<b>Foto particolare:</b> 
<b>Inquadramento generale:</b> 	<b>Foto generale:</b> 
<b>Note:</b>	

<p><b>Località: LA THUILE</b> <b>Ghiacciaio RUITOR</b></p>	<p><b>Data: 20 LUGLIO 2021</b></p>
<p><b>Nome:</b> 110      <b>Numero:</b></p>	<p><b>Foto particolare:</b></p>
<p><b>Descrizione:</b></p>	
<p><b>Ubicazione:</b></p>	<p><b>Coordinate ETRF2000 32N</b></p>
<p><b>Est:</b> 343026.117</p>	<p><b>Nord:</b> 5058867.692</p>
<p><b>long:</b> 6.98389265°</p>	<p><b>lat:</b> 45.66377071°</p>
<p><b>H:</b> 2508.386</p>	<p><b>h ell:</b> 2562.365</p>
<p><b>Inquadramento generale:</b></p> 	<p><b>Foto generale:</b></p> 

**Località: LA THUILE**  
**Ghiacciaio RUITOR**

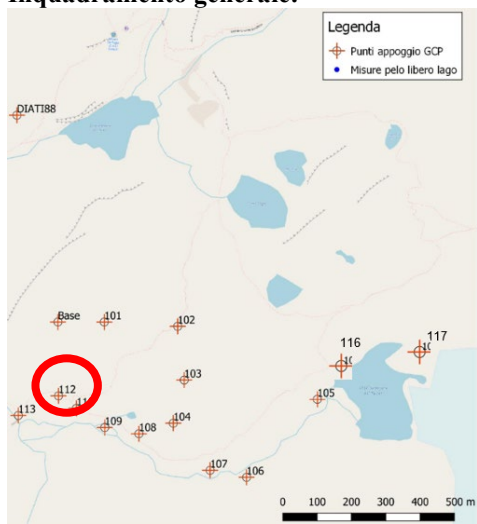
Nome: 112	Numero:
<b>Descrizione:</b>	
<b>Ubicazione:</b>	
<b>Coordinate ETRF2000 32N</b>	
Est: 342978.138	Nord: 5058904.335
long: 6.98389265°	lat: 45.66408945°
H: 2509.464	h ell: 2563.441

**Data: 20 LUGLIO 2021**

**Foto particolare:**



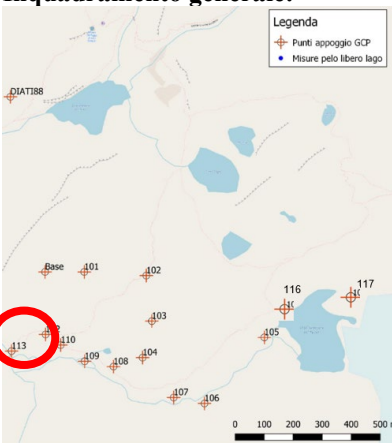
**Inquadramento generale:**



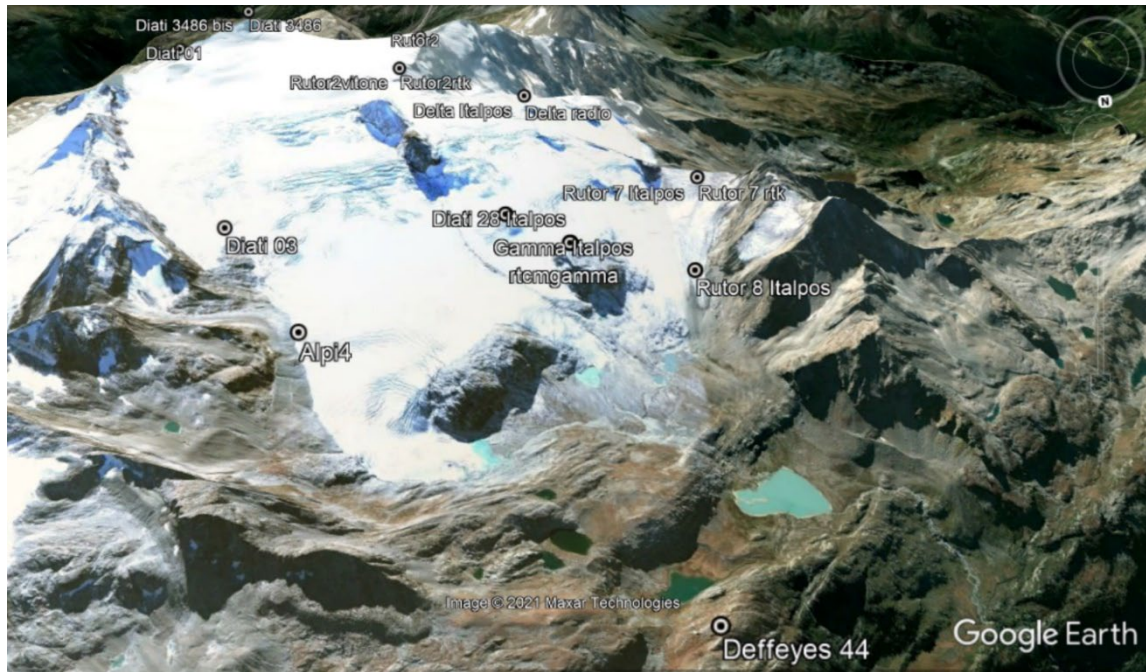
**Foto generale:**



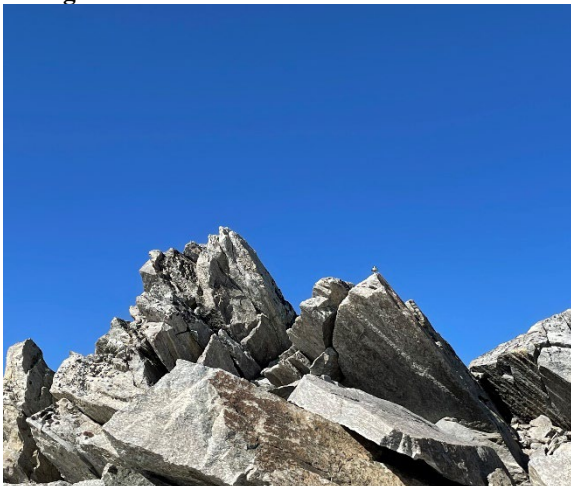
**Note:**

<p><b>Località: LA THUILE</b> <b>Ghiacciaio RUITOR</b></p> <table border="1"> <tr> <td><b>Nome:</b> 113</td><td><b>Numero:</b></td></tr> <tr> <td colspan="2"><b>Descrizione:</b></td></tr> <tr> <td colspan="2"><b>Ubicazione:</b></td></tr> <tr> <td colspan="2" style="text-align: center;"><b>Coordinate ETRF2000 32N</b></td></tr> <tr> <td><b>Est:</b> 342861.706</td><td><b>Nord:</b> 5058841.121</td></tr> <tr> <td><b>long:</b> 6.98179209°</td><td><b>lat:</b> 45.66349442°</td></tr> <tr> <td><b>H:</b> 2507.258</td><td><b>h ell:</b> 2561.233</td></tr> </table>	<b>Nome:</b> 113	<b>Numero:</b>	<b>Descrizione:</b>		<b>Ubicazione:</b>		<b>Coordinate ETRF2000 32N</b>		<b>Est:</b> 342861.706	<b>Nord:</b> 5058841.121	<b>long:</b> 6.98179209°	<b>lat:</b> 45.66349442°	<b>H:</b> 2507.258	<b>h ell:</b> 2561.233	<p><b>Data:</b> 20 LUGLIO 2021</p> <p><b>Foto particolare:</b></p> 
<b>Nome:</b> 113	<b>Numero:</b>														
<b>Descrizione:</b>															
<b>Ubicazione:</b>															
<b>Coordinate ETRF2000 32N</b>															
<b>Est:</b> 342861.706	<b>Nord:</b> 5058841.121														
<b>long:</b> 6.98179209°	<b>lat:</b> 45.66349442°														
<b>H:</b> 2507.258	<b>h ell:</b> 2561.233														
<p><b>Inquadramento generale:</b></p> 	<p><b>Foto generale:</b></p> 														

## Rutor Alto



<b>Località: LA THUILE</b> <b>Ghiacciaio RUITOR</b>		<b>Data: 07 Settembre 2021</b>
Nome:Marker 002 2	Numero:	<b>Foto particolare:</b> 
<b>Descrizione:</b> marker 1 m x 1m		
<b>Ubicazione:</b>		
<b>Coordinate ETRF2000 32N</b>		
Est: 344045.182	Nord: 5055306.918	
long: 6.99902857 °	lat: 45.63378016 °	
H ell: 3381.374	h orto: 3327.244	
<b>Inquadramento generale:</b>		<b>Foto generale:</b> 
		

<b>Località: LA THUILE</b> <b>Ghiacciaio RUITOR</b>	<b>Data:</b> 07 Settembre 2021
<b>Nome:</b> Rutor 2 vitone	<b>Numero:</b>
<b>Descrizione:</b> È presente un vitone 5/8 su uno spigolo. Non è stato materializzato marker perché già fotografico	<b>Foto particolare:</b>
<b>Ubicazione:</b> <b>Coordinate ETRF2000 32N</b> <b>Est</b> 344195.249 <b>Nord:</b> 5055808.939 <b>long:</b> 7.00083531° <b>lat:</b> 45.63833418° <b>H:</b> 3291.908 <b>h ell:</b> 3346.026	
<b>Inquadramento generale:</b> 	<b>Foto generale:</b> 
<b>Note:</b> Rilevo GNSS PP 15 min su prolunga Trimble. Fatto anche RTK radio e ITALPOS	

<b>Località: LA THUILE</b> <b>Ghiacciaio RUITOR</b>		<b>Data:</b> 07 Settembre 2021								
<b>Nome:</b> Rutor 6 delta	<b>Numero:</b>	<b>Foto particolare:</b>								
<b>Descrizione:</b> marker 1mx 1m										
<b>Ubicazione:</b> <table> <thead> <tr> <th colspan="2">Coordinate ETRF2000 32N</th> </tr> </thead> <tbody> <tr> <td><b>Est</b> 343402.457</td><td><b>Nord:</b> 5056181.871</td></tr> <tr> <td><b>long:</b> 6.99054915°</td><td><b>lat:</b> 45.64151042°</td></tr> <tr> <td><b>H:</b> 3187.372</td><td><b>h ell:</b> 3241.45</td></tr> </tbody> </table>		Coordinate ETRF2000 32N		<b>Est</b> 343402.457	<b>Nord:</b> 5056181.871	<b>long:</b> 6.99054915°	<b>lat:</b> 45.64151042°	<b>H:</b> 3187.372	<b>h ell:</b> 3241.45	
Coordinate ETRF2000 32N										
<b>Est</b> 343402.457	<b>Nord:</b> 5056181.871									
<b>long:</b> 6.99054915°	<b>lat:</b> 45.64151042°									
<b>H:</b> 3187.372	<b>h ell:</b> 3241.45									
<b>Inquadramento generale:</b>		<b>Foto generale:</b>								
										
<b>Note:</b> RTK Italpos e RTK Radio. Palina 2° e 3° pezzo hs=1.092m BAM										

--

<b>Località: LA THUILE</b> <b>Ghiacciaio RUITOR</b>	<b>Data: 07 Settembre 2021</b>	
<b>Nome:</b> Rutor 7 <b>Numero:</b>	<b>Foto particolare:</b> 	
<b>Descrizione:</b> marker 1mx 1m		
<b>Ubicazione:</b>		
<b>Coordinate ETRF2000 32N</b> <b>Est:</b> 342415.786 <b>Nord:</b> 5056929.465 <b>long:</b> 6.97765412° <b>lat:</b> 45.64801189° <b>H:</b> 2856.811 <b>h ell:</b> 2910.845		
<b>Inquadramento generale:</b> 		
<b>Foto generale:</b> 		
<b>Note:</b> RTK Italpos e RTK Radio. Palina 2° e 3° pezzo hs=1.092m BAM		

<b>Località: LA THUILE</b> <b>Ghiacciaio RUITOR</b>	<b>Data: 07 Settembre 2021</b>
<b>Nome:</b> Rutor 8 <b>Numero:</b>	<b>Foto particolare:</b>
<b>Descrizione:</b> marker 1mx1m	
<b>Ubicazione:</b>	<b>Coordinate ETRF2000 32N</b>
<b>Est</b> 342623.509	<b>Nord:</b> 5057774.980
<b>Long:</b> 6.98004474°	<b>lat:</b> 45.65566470 °
<b>H:</b> 2637.679	<b>h ell:</b> 2691.688
	<b>Foto generale:</b>
<b>Inquadramento generale:</b>	
	

**Note:** RTK Italpos e RTK Radio. Palina 2° e 3° pezzo hs=1.092m BAM

<b>Località: LA THUILE</b> <b>Ghiacciaio RUITOR</b>	<b>Data:</b> 07 Settembre 2021
<b>Nome:</b> Deffeyes	<b>Numero:</b>
44	
<b>Descrizione:</b> 3 marker 50x50 cm	
<b>Ubicazione:</b>	
<b>Coordinate ETRF2000 32N</b>	
<b>Est:</b> 343055.184	<b>Nord:</b> 5060023.265
<b>long:</b> 6.98485610	<b>lat:</b> 45.67598651 °
<b>o</b>	
<b>H:</b> 2519.383	<b>h ell:</b> 2573.299
<b>Inquadramento generale:</b> 	<b>Foto particolare:</b> 
	<b>Foto generale:</b> 

<b>Località: LA THUILE</b> <b>Ghiacciaio RUITOR</b>	<b>Data: 07 Settembre 2021</b>
<b>Nome:</b> Testa (Rutor 0) <b>Numero:</b>	<b>Foto particolare:</b>
<b>Descrizione:</b> marker 1m x 1m	
<b>Ubicazione:</b> (Marker vicino a IGM95)	
<b>Coordinate ETRF2000 32N</b>	
<b>Est</b> 345248.55	<b>Nord:</b> 505433.637
<b>long:</b> °	<b>lat:</b> °
<b>H:</b>	<b>h ell:</b> 3523.774
<b>Inquadramento generale:</b>	
<b>Note:</b> <b>testa del Rutor preso con il nome di DIATI 3486</b> <b>Adiacente</b> diati3486bis,5054934.077,345252.028,3529.094 diati3486bis 7.01466485 45.63070078 3583.262	<b>Foto generale:</b>

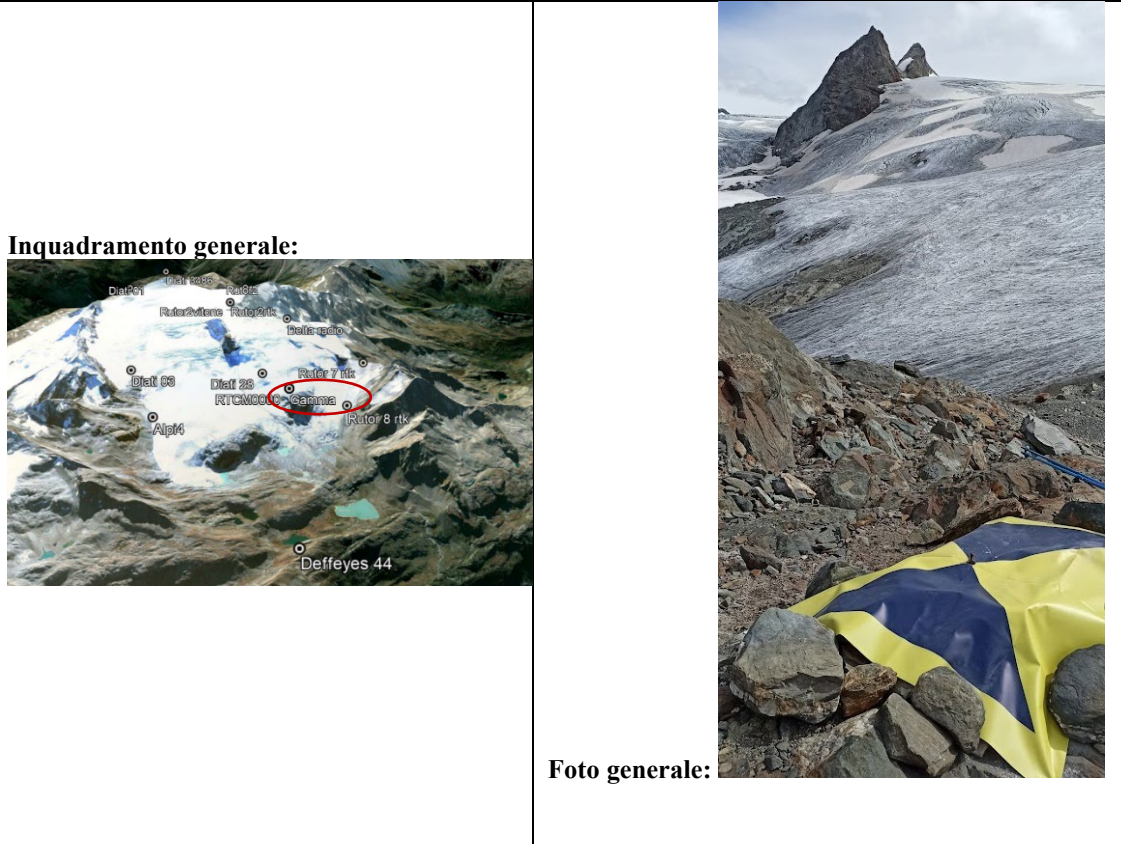
<b>Località: LA THUILE</b> <b>Ghiacciaio RUITOR</b>	<b>Data: 07 Settembre 2021</b>
<b>Nome:</b> DIATI 01 <b>Numero:</b>	<b>Foto particolare:</b>
<b>Descrizione:</b>	
<b>Ubicazione:</b>	
<b>Coordinate ETRF2000 32N</b>	
Est 345669.828	<b>Nord:</b> 5055411.245
<b>long:</b> 7.01987133°	<b>lat:</b> 45.63508612°
H: 3354.725	<b>h ell:</b> 3408.882
	
<b>Inquadramento generale:</b>	
	<b>Foto generale:</b>
<b>Note:</b>	
Ricalcolato in base alla GAMMA RTC000	

<b>Località: LA THUILE</b> <b>Ghiacciaio RUITOR</b>	<b>Data:</b> 07 Settembre 2021
<b>Nome:</b> DIATI 03 <b>Numero:</b>	<b>Foto particolare:</b>
<b>Descrizione:</b> marker 1m x 1m	
<b>Ubicazione:</b>	
<b>Coordinate ETRF2000 32N</b>	
<b>Est:</b> 345159.501 <b>Nord:</b>	
<b>5057424.267</b>	
<b>long:</b> 7.01268715°	<b>lat:</b> 45.65308057°
<b>H:</b> 2973.931	<b>h ell:</b> 3028.005
<b>Inquadramento generale:</b> 	<b>Foto generale:</b>
<b>Note:</b>	

<b>Località: LA THUILE</b> <b>Ghiacciaio RUITOR</b>	<b>Data: 07 Settembre 2021</b>
<b>Nome: DIATI 4</b>	<b>Numero:</b>
<b>Descrizione:</b>	
<b>Ubicazione:</b>	
<b>Coordinate ETRF2000 32N</b>	
<b>Est: 344729.662</b>	<b>Nord:</b> <b>5058236.014</b>
<b>long:</b> <b>7.00691458°</b>	<b>lat:</b> 45.66028651 °
<b>H: 2740.441</b>	<b>h ell:</b> 2794.485
<b>Inquadramento generale:</b>	
	<b>Foto generale:</b>
<b>Note:</b>	Preso con rtk radio nome 'Alpi4'

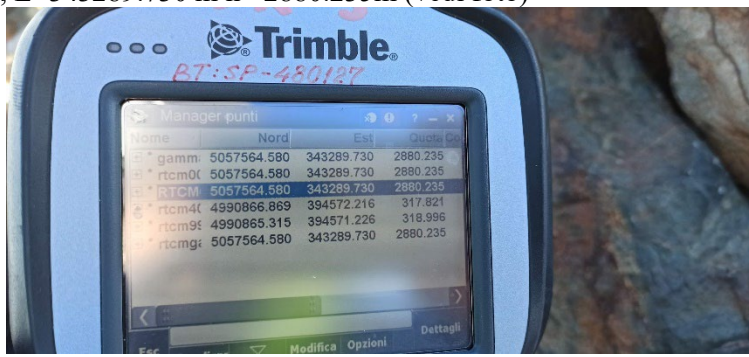
<p><b>Località: LA THUILE</b> <b>Ghiacciaio RUITOR</b></p>	<p><b>Data: 07 Settembre 2021</b></p>														
<table border="1"> <tr> <td>Nome: DIATI 28</td> <td>Numero:</td> </tr> <tr> <td colspan="2"><b>Descrizione:</b> tassello e marker 1m x 1 ,</td> </tr> <tr> <td colspan="2"><b>Ubicazione:</b></td> </tr> <tr> <td colspan="2" style="text-align: center;"><b>Coordinate ETRF2000 32N</b></td> </tr> <tr> <td>Est 343625.522</td> <td>Nord: 5057307.390</td> </tr> <tr> <td>long: 6.99304808°</td> <td>lat: 45.63509060°</td> </tr> <tr> <td>H: 2890.180</td> <td>h ell: 2944.235</td> </tr> </table>	Nome: DIATI 28	Numero:	<b>Descrizione:</b> tassello e marker 1m x 1 ,		<b>Ubicazione:</b>		<b>Coordinate ETRF2000 32N</b>		Est 343625.522	Nord: 5057307.390	long: 6.99304808°	lat: 45.63509060°	H: 2890.180	h ell: 2944.235	<p><b>Foto particolare:</b></p>  
Nome: DIATI 28	Numero:														
<b>Descrizione:</b> tassello e marker 1m x 1 ,															
<b>Ubicazione:</b>															
<b>Coordinate ETRF2000 32N</b>															
Est 343625.522	Nord: 5057307.390														
long: 6.99304808°	lat: 45.63509060°														
H: 2890.180	h ell: 2944.235														
<p><b>Inquadramento generale:</b></p>	<p><b>Foto generale:</b></p> 														
<p><b>Note:</b></p>															

<b>Località: LA THUILE</b> Ghiacciaio RUITOR		<b>Data:</b> 07 Settembre 2021
Nome: GAMMA/ RTCM0000/ rtcm0005/ RTCM0012	Numero:	<b>Foto particolare:</b>  
<b>Descrizione:</b> Stazione base radio RTK. <i>il pezzo si innestava parzialmente sul bullone quindi ai 25 cm della palina in carbonio vanno aggiunti 2.7 cm (stimati)</i>		
<b>Ubicazione:</b>		
<b>Coordinate ETRF2000 32N</b>		
Est 343293.081	Nord: 5057564.005	
<b>long:</b> 6.98870143°	<b>lat:</b> 45.65391850°	
<b>H:</b> 2831.488	<b>h ell:</b> 2885.525	



**Note: stazione base**

Coincide con il punto RTCM0000,5057564.580,343289.730,2880.235,  
 rtcm0005,5057564.580,343289.730,2880.235 e  
 RTCM0012,5057564.580,343289.730,2880.235  
 (notate discrepanze metriche rispetto a monografia ARPA); coordinate usate ETRF2000:  
 N=5056182.33 E=343400.89 h=3236.491) ATTENZIONE!: non abbiamo usate queste  
 coordinate ma quelle già inserite nel ricevitore e confermate via radio da Alberto, ovvero:  
 N=5057564.580 m, E=343289.730 m h= 2880.235m (vedi foto)



# ANNEX Chapter 5

## Antenna position at the shooting time

### Coordinates comparison to offset estimation of 60 selected shots

time	unix time (s)	N fotogramma	GPS		
			E	N	H
09:04:25.5280	16014566655	14	346337.947	5055597.732	3891.314
09:04:41.4100	16014566814	19	346068.257	5056107.500	3889.785
09:05:11.4270	16014567114	28	345603.045	5057012.168	3892.268
09:05:43.5330	16014567435	38	345105.676	5057958.447	3897.523
09:08:50.5680	16014569306	71	344520.885	5058582.575	3891.962
09:09:07.1500	16014569472	78	344885.568	5057905.212	3892.406
09:09:18.8770	16014569589	83	345134.859	5057418.803	3901.043
09:09:32.5100	16014569725	89	345430.977	5056857.718	3905.600
09:11:55.1980	16014571152	118	345558.649	5056133.644	3896.605
09:12:14.8170	16014571348	126	345148.157	5056928.114	3901.016
09:12:30.0850	16014571501	132	344833.905	5057536.170	3895.140
09:12:45.8640	16014571659	138	344511.982	5058141.026	3892.765
09:14:33.4900	16014572735	160	344248.318	5058202.188	3892.738
09:14:45.7670	16014572858	166	344548.603	5057634.688	3901.206
09:14:59.4900	16014572995	173	344880.590	5056991.515	3899.404
09:15:10.7740	16014573108	179	345168.381	5056440.815	3899.391
09:17:14.2390	16014574342	199	345420.088	5055490.719	3905.276
09:17:30.8930	16014574509	206	345089.153	5056121.452	3902.510
09:17:54.1330	16014574741	216	344583.140	5057077.589	3897.978
09:18:08.6050	16014574886	222	344269.274	5057682.404	3898.354
09:20:04.4530	16014576210	241	343586.418	5058557.128	3893.867
09:20:24.5270	16014576245	252	344126.339	5057510.181	3898.852
09:20:36.5640	16014576366	259	344457.117	5056872.403	3900.998
09:20:46.9860	16014576470	265	344753.836	5056294.791	3896.441
09:23:27.2840	16014578073	293	344638.918	5056070.426	3903.172
09:23:37.1990	16014578172	297	344448.373	5056427.542	3904.849
09:23:51.4490	16014578315	303	344168.466	5056974.358	3906.802
09:24:09.5870	16014578496	311	343776.135	5057713.055	3905.471

09:25:32.0410	16014579320	327	343199.392	5058413.591	3869.847
09:25:48.4480	16014579484	336	343634.709	5057528.018	3897.011
09:26:01.0530	16014579611	343	343987.778	5056861.477	3900.800
09:26:08.3090	16014579683	347	344187.758	5056467.327	3899.269
09:29:13.8730	16014581539	381	344113.862	5056156.325	3887.470
09:29:31.2900	16014581713	387	343810.113	5056717.933	3897.698
09:29:42.3890	16014581824	391	343618.835	5057089.002	3901.609
09:30:00.8400	16014582008	398	343287.429	5057731.077	3900.727
09:31:43.4850	16014583132	417	343048.385	5057750.049	3889.593
09:32:13.4400	16014583212	432	343828.857	5056233.359	3894.732
09:32:29.8730	16014583334	440	344249.401	5055446.042	3896.000
09:34:51.8790	16014583499	462	343945.625	5055547.441	3900.648
09:35:03.4970	16014584919	466	343744.990	5055927.819	3899.648
09:35:24.0650	16014585035	473	343389.038	5056616.230	3902.485
09:35:44.1340	16014585241	480	343029.534	5057276.665	3895.048
09:37:58.5940	16014585441	508	343029.620	5056863.520	3885.690
09:38:05.3260	16014586786	511	343184.093	5056563.812	3892.187
09:38:20.4400	16014586853	518	343522.552	5055906.671	3897.704
09:38:37.4770	16014587004	526	343919.015	5055140.415	3894.438
09:41:16.1910	16014587175	549	343626.607	5055233.994	3889.564
09:41:32.4320	16014588762	555	343331.763	5055810.680	3895.195
09:41:54.2370	16014588924	563	342920.980	5056595.398	3888.225
09:42:15.0690	16014589142	570	342536.689	5057333.174	3888.524
09:46:29.9100	16014589351	594	342605.731	5056775.512	3883.167
09:46:41.9420	16014591899	599	342850.777	5056308.911	3892.280
09:46:55.3550	16014592019	605	343125.645	5055774.950	3900.864
09:47:12.4340	16014592154	613	343512.426	5055040.434	3898.395
09:49:24.3800	16014592324	634	343323.574	5054869.872	3897.628
09:49:44.3270	16014593644	642	342944.185	5055619.964	3899.001
09:49:54.1680	16014593843	646	342744.358	5056000.699	3892.732
09:50:06.5460	16014593942	651	342487.405	5056490.054	3894.722
09:52:11.2570	16014594065	674	342112.523	5054740.423	3900.357

TA			D	V(m/s)	Delta offset
E	N	H			
346017.8	5056193	3887.074	675.7583	36.73475	17.38829
345770.2	5056681	3886.202	646.6503	35.50583	17.98138
345312.9	5057560	3894.472	619.57	31.85805	19.08335

344795.6	5058530	3893.227	650.7063	34.12715	19.4897
344935	5057816	3892.659	871.1211	46.00763	18.47645
345281.9	5057131	3903.005	870.1427	47.42016	18.40445
345540.7	5056645	3908.405	873.6184	45.45634	19.05736
345846.5	5056058	3904.272	900.8525	47.13177	19.35986
345165.2	5056892	3900.799	854.4277	45.41168	18.50673
344759.2	5057673	3892.748	840.2541	45.44025	18.86857
344452.7	5058254	3887.879	813.0147	45.02374	18.39862
344158.4	5058841	3889.419	784.2351	45.44557	17.99663
344699.9	5057336	3898.25	977.2154	52.31079	18.86966
345009.7	5056753	3900.38	995.2142	51.98016	19.57682
345365.2	5056065	3901.671	1045.677	53.52309	19.61718
345666.5	5055477	3901.772	1085.01	56.38235	19.8877
345044.6	5056204	3901.041	806.3969	41.3236	19.89477
344684.3	5056886	3901.659	864.8834	44.79604	19.57004
344187.9	5057864	3904.44	880.0921	48.69482	17.82362
343876.3	5058444	3897.626	856.6583	46.42672	18.10748
344088.3	5057581	3897.892	1097.626	58.40072	18.80326
344645.3	5056504	3898.16	1132.035	57.94251	18.9243
345009.6	5055825	3893.25	1183.91	61.97255	19.76275
345311	5055236	3896.423	1196.729	60.56708	18.21572
344277.1	5056761	3909.05	779.5303	39.66003	19.58499
344075.6	5057154	3907.605	816.7491	41.97578	19.99983
343763.1	5057738	3905.142	864.7273	44.156	19.43027
343350	5058516	3906.272	908.6599	47.37185	19.296
343700.1	5057405	3899.42	1126.023	58.63845	18.22516
344155.6	5056529	3899.48	1126.655	59.85359	19.0632
344516.9	5055848	3899.214	1143.111	58.34888	18.40632
344724.3	5055460	3898.202	1141.555	62.15761	18.82856
343787.3	5056761	3898.276	687.3659	36.44088	18.51455
343484.2	5057349	3902.5	710.0593	37.00953	19.53361
343282.2	5057741	3900.522	733.8592	38.41329	19.69432
342925.6	5058424	3902.073	781.8588	40.73616	18.67843
343545.3	5056798	3888.457	1073.703	58.23777	18.7787
344304.9	5055336	3895.315	1015.51	57.64833	18.59663
344710.9	5054557	3891.898	1001.87	56.7716	18.9724
343620.1	5056164	3901.083	697.6197	36.56248	19.30916
343421.8	5056556	3902.098	706.7125	39.28754	18.73185

343054	5057232	3895.495	700.9617	37.07038	18.82269
342710.1	5057921	3896.128	718.7299	38.52098	18.67423
343454.6	5056044	3896.857	923.2038	50.44209	18.1967
343602.6	5055748	3899.344	917.0531	52.02982	18.5403
343959.2	5055063	3896.146	950.0998	48.96843	19.17098
344369	5054284	3890.432	967.2537	51.13915	18.89452
343286.1	5055899	3893.268	746.9715	38.78891	18.50213
342979.3	5056484	3890.665	759.5591	39.6875	19.17626
342573.8	5057262	3889.134	751.3113	41.69375	17.856
342217	5057941	3876.946	687.0076	38.67565	17.6604
342988.8	5056045	3899.796	824.9489	43.19932	19.01243
343245.5	5055554	3898.197	851.7944	43.48011	19.44121
343551.5	5054967	3899.833	912.9129	46.73746	20.02573
343967.7	5054190	3888.238	965.0546	49.99146	19.78637
342969.1	5055575	3899.026	789.1387	41.25071	19.31272
342555.1	5056351	3894.489	828.0751	42.84289	19.11557
342353.1	5056742	3890.245	838.1802	44.69788	18.78145
342094.2	5057226	3897.312	834.3635	44.36695	18.76854
343238.6	5054541	3893.18	1143.549	64.09188	17.89826

## Coordinates after 4 iterations

Date	GPS time	Unix time	GPS		
30/09/2020	09:04:18	1601456639	346477.281	5055326.14	3889.054
30/09/2020	09:04:20	1601456642	346430.197	5055423.06	3890.998
30/09/2020	09:04:23	1601456644	346379.468	5055518.332	3891.583
30/09/2020	09:04:26	1601456647	346328.748	5055614.968	3891.895
30/09/2020	09:04:29	1601456650	346275.076	5055709.284	3892.781
30/09/2020	09:04:32	1601456653	346221.53	5055804.677	3892.15
30/09/2020	09:04:35	1601456656	346174.048	5055904.275	3891.47
30/09/2020	09:04:38	1601456659	346127.95	5056003.724	3891.335
30/09/2020	09:04:41	1601456662	346073.831	5056098.328	3890.42
30/09/2020	09:04:44	1601456666	346017.952	5056193.094	3887.367
30/09/2020	09:04:47	1601456669	345966.793	5056290.636	3884.032
30/09/2020	09:04:50	1601456672	345919.625	5056389.682	3883.575
30/09/2020	09:04:54	1601456675	345871.686	5056487.495	3883.011
30/09/2020	09:04:57	1601456678	345820.567	5056584.382	3884.555

30/09/2020	09:05:00	1601456681	345770.218	5056681.62	3886.596
30/09/2020	09:05:03	1601456685	345719.415	5056779.375	3887.832
30/09/2020	09:05:07	1601456688	345669.538	5056877.578	3888.285
30/09/2020	09:05:10	1601456691	345621.538	5056976.39	3891.197
30/09/2020	09:05:14	1601456695	345570.741	5057073.501	3895.712
30/09/2020	09:05:17	1601456698	345520.071	5057170.827	3896.317
30/09/2020	09:05:20	1601456702	345469.187	5057268.481	3894.05
30/09/2020	09:05:24	1601456705	345415.197	5057363.922	3892.631
30/09/2020	09:05:27	1601456708	345362.692	5057461.521	3892.844
30/09/2020	09:05:30	1601456711	345312.955	5057559.974	3894.847
30/09/2020	09:05:33	1601456715	345264.059	5057657.555	3896.827
30/09/2020	09:05:37	1601456718	345212.544	5057754.485	3898.589
30/09/2020	09:05:40	1601456721	345161.47	5057851.072	3898.725
30/09/2020	09:05:43	1601456725	345110.464	5057949.5	3898.069
30/09/2020	09:05:46	1601456728	345057.412	5058046.46	3896.349
30/09/2020	09:05:50	1601456731	345003.682	5058142.535	3896.706
30/09/2020	09:05:53	1601456734	344951.168	5058239.007	3898.425
30/09/2020	09:05:56	1601456737	344899.584	5058336.006	3896.56
30/09/2020	09:05:59	1601456740	344848.165	5058433.845	3894.527
30/09/2020	09:06:02	1601456744	344795.67	5058530.947	3893.521
30/09/2020	09:06:05	1601456747	344743.363	5058627.981	3894.299
30/09/2020	09:06:08	1601456750	344692.594	5058725.409	3894.51
30/09/2020	09:06:11	1601456753	344642.346	5058822.897	3894.696
30/09/2020	09:06:15	1601456756	344591.965	5058921.507	3894.192
30/09/2020	09:06:18	1601456759	344542.13	5059018.987	3893.965
30/09/2020	09:06:21	1601456762	344491.692	5059117.107	3895.143
30/09/2020	09:06:24	1601456765	344443.225	5059215.441	3896.326
30/09/2020	09:06:27	1601456768	344392.858	5059313.097	3895.744
30/09/2020	09:06:30	1601456771	344340.51	5059410.072	3894.792
30/09/2020	09:07:09	1601456810	344326.862	5059204.672	3853.631
30/09/2020	09:07:11	1601456812	344367.13	5059105.882	3851.306
30/09/2020	09:07:13	1601456814	344375.431	5059002.839	3848.812
30/09/2020	09:07:15	1601456816	344337.276	5058906.872	3840.28
30/09/2020	09:07:17	1601456819	344249.784	5058854.206	3826.165
30/09/2020	09:07:20	1601456821	344144.753	5058867.489	3822.221
30/09/2020	09:07:23	1601456824	344064.672	5058940.072	3828.718
30/09/2020	09:07:26	1601456827	344005.538	5059034.097	3837.621
30/09/2020	09:07:29	1601456830	343945.699	5059123.346	3848.85

30/09/2020	09:08:37	1601456898	344213.572	5059171.769	3873.836
30/09/2020	09:08:39	1601456900	344263.221	5059072.924	3878.267
30/09/2020	09:08:41	1601456902	344311.661	5058976.956	3888.314
30/09/2020	09:08:43	1601456905	344363.106	5058882.133	3893.745
30/09/2020	09:08:46	1601456907	344416.045	5058786.107	3892.969
30/09/2020	09:08:48	1601456909	344467.352	5058687.776	3889.596
30/09/2020	09:08:50	1601456912	344516.769	5058590.434	3892.045
30/09/2020	09:08:53	1601456914	344569.875	5058491.84	3895.48
30/09/2020	09:08:55	1601456916	344623.346	5058399.081	3896.656
30/09/2020	09:08:58	1601456919	344677.934	5058302.664	3895.998
30/09/2020	09:09:00	1601456921	344730.402	5058206.663	3895.55
30/09/2020	09:09:02	1601456924	344781.81	5058108.783	3894.806
30/09/2020	09:09:05	1601456926	344831.071	5058009.815	3893.577
30/09/2020	09:09:07	1601456928	344881.51	5057912.57	3892.792
30/09/2020	09:09:09	1601456931	344935.342	5057816.024	3893.062
30/09/2020	09:09:12	1601456933	344988.409	5057720.522	3893.883
30/09/2020	09:09:14	1601456935	345038.885	5057623.419	3895.573
30/09/2020	09:09:16	1601456938	345086.438	5057524.184	3898.454
30/09/2020	09:09:19	1601456940	345132.676	5057423.492	3901.301
30/09/2020	09:09:21	1601456942	345180.086	5057325.341	3901.611
30/09/2020	09:09:24	1601456945	345230.364	5057227.993	3901.617
30/09/2020	09:09:26	1601456947	345282.113	5057130.447	3903.407
30/09/2020	09:09:28	1601456950	345334.506	5057033.371	3904.996
30/09/2020	09:09:31	1601456952	345387.574	5056936.481	3905.481
30/09/2020	09:09:33	1601456954	345440.495	5056840.223	3906.148
30/09/2020	09:09:35	1601456957	345490.899	5056743.169	3907.51
30/09/2020	09:09:38	1601456959	345540.946	5056644.841	3908.778
30/09/2020	09:09:40	1601456961	345591.378	5056546.851	3909.428
30/09/2020	09:09:42	1601456964	345642.382	5056448.683	3907.547
30/09/2020	09:09:45	1601456966	345693.351	5056350.236	3905.783
30/09/2020	09:09:47	1601456968	345743.757	5056251.561	3905.161
30/09/2020	09:09:49	1601456970	345794.73	5056154.261	3904.687
30/09/2020	09:09:51	1601456973	345846.993	5056058.083	3904.53
30/09/2020	09:09:53	1601456975	345902.298	5055961.987	3904.375
30/09/2020	09:09:56	1601456977	345957.857	5055866.609	3903.297
30/09/2020	09:09:58	1601456979	346010.517	5055769.337	3902.924
30/09/2020	09:10:00	1601456981	346060.097	5055671.235	3903.691
30/09/2020	09:10:02	1601456983	346106.786	5055572.249	3905.261

30/09/2020	09:10:04	1601456986	346153.267	5055472.8	3905.873
30/09/2020	09:10:06	1601456988	346201.194	5055372.624	3904.188
30/09/2020	09:10:09	1601456990	346251.145	5055273.762	3902.214
30/09/2020	09:10:11	1601456992	346303.276	5055176.671	3901.64
30/09/2020	09:10:13	1601456994	346359.612	5055081.218	3901.642
30/09/2020	09:11:30	1601457071	346082.834	5055136.509	3904.489
30/09/2020	09:11:32	1601457073	346032.27	5055234.214	3904.113
30/09/2020	09:11:35	1601457076	345980.961	5055332.914	3904.302
30/09/2020	09:11:37	1601457079	345930.718	5055430.339	3904.909
30/09/2020	09:11:40	1601457081	345880.109	5055528.091	3904.581
30/09/2020	09:11:42	1601457084	345829.152	5055626.43	3903.156
30/09/2020	09:11:45	1601457086	345778.29	5055723.673	3903.473
30/09/2020	09:11:47	1601457089	345726.779	5055821.567	3903.336
30/09/2020	09:11:50	1601457091	345676.148	5055918.63	3901.407
30/09/2020	09:11:52	1601457093	345624.597	5056016.113	3898.829
30/09/2020	09:11:55	1601457096	345570.737	5056112.667	3897.291
30/09/2020	09:11:57	1601457098	345516.751	5056208.049	3896.364
30/09/2020	09:12:00	1601457101	345466.117	5056306.686	3896.332
30/09/2020	09:12:02	1601457103	345418.163	5056405.544	3895.165
30/09/2020	09:12:04	1601457106	345370.104	5056504.032	3892.42
30/09/2020	09:12:07	1601457108	345319.879	5056602.148	3889.621
30/09/2020	09:12:09	1601457110	345267.665	5056698.295	3892.893
30/09/2020	09:12:11	1601457113	345215.435	5056794.448	3898.332
30/09/2020	09:12:14	1601457115	345165.242	5056892.452	3901.21
30/09/2020	09:12:16	1601457118	345118.001	5056992.568	3900.45
30/09/2020	09:12:19	1601457120	345071.499	5057091.685	3898.106
30/09/2020	09:12:21	1601457122	345021.486	5057189.031	3899.996
30/09/2020	09:12:26				
30/09/2020	09:12:29	1601457125	344916.966	5057382.129	3901.396
30/09/2020	09:12:31	1601457127	344864.172	5057480.197	3897.472
30/09/2020	09:12:34	1601457130	344811.928	5057576.949	3894.454
30/09/2020	09:12:36	1601457132	344759.279	5057673.255	3893.259
30/09/2020	09:12:39	1601457135	344708.438	5057769.64	3896.884
30/09/2020	09:12:41	1601457137	344659.056	5057865.615	3901.444
30/09/2020	09:12:44	1601457140	344607.754	5057962.62	3900.996
30/09/2020	09:12:46	1601457142	344555.239	5058059.838	3897.398
30/09/2020	09:12:49	1601457145	344503.413	5058157.344	3892.343
30/09/2020	09:12:51	1601457148	344452.817	5058254.731	3888.286

30/09/2020	09:12:54	1601457150	344404.423	5058353.286	3886.502
30/09/2020	09:12:57	1601457153	344353.885	5058451.942	3888.996
30/09/2020	09:12:59	1601457155	344305.468	5058547.894	3890.983
30/09/2020	09:13:02	1601457158	344257.442	5058647.105	3890.009
30/09/2020	09:13:05	1601457160	344210.544	5058746.045	3888.112
30/09/2020	09:13:07	1601457163	344158.485	5058841.37	3889.844
30/09/2020	09:13:10	1601457166	344102.878	5058934.623	3894.719
30/09/2020	09:13:13	1601457169	344051.574	5059031.68	3894.924
30/09/2020	09:13:16	1601457172	344002.707	5059131.227	3891.255
30/09/2020	09:14:17	1601457175	343949.708	5059227.25	3887.095
30/09/2020	09:14:19	1601457177	343849.671	5058996.543	3891.479
30/09/2020	09:14:21	1601457238	343902.909	5058900.527	3887.835
30/09/2020	09:14:23	1601457240	343952.158	5058801.714	3885.959
30/09/2020	09:14:25	1601457242	343999.538	5058703.296	3886.557
30/09/2020	09:14:27	1601457244	344048.736	5058603.728	3891.432
30/09/2020	09:14:29	1601457246	344095.013	5058507.409	3896.067
30/09/2020	09:14:31	1601457248	344140.54	5058408.759	3899.488
30/09/2020	09:14:33	1601457250	344189.932	5058309.406	3898.299
30/09/2020	09:14:35	1601457252	344242.789	5058212.078	3893.579
30/09/2020	09:14:37	1601457257	344295.611	5058115.622	3890.598
30/09/2020	09:14:40	1601457259	344346.874	5058017.97	3890.977
30/09/2020	09:14:42	1601457261	344396.856	5057920.68	3893.743
30/09/2020	09:14:44	1601457263	344446.675	5057824.368	3897.325
30/09/2020	09:14:46	1601457265	344498.687	5057727.22	3900.364
30/09/2020	09:14:48	1601457267	344550.617	5057630.854	3901.61
30/09/2020	09:14:50	1601457269	344602.168	5057532.352	3900.868
30/09/2020	09:14:52	1601457271	344651.556	5057434.064	3899.74
30/09/2020	09:14:54	1601457273	344700.218	5057335.33	3898.751
30/09/2020	09:14:56	1601457276	344749.452	5057237.224	3898.708
30/09/2020	09:14:58	1601457278	344800.239	5057139.256	3898.763
30/09/2020	09:15:00	1601457280	344852.331	5057042.516	3899.384
30/09/2020	09:15:02	1601457282	344905.525	5056946.412	3900.35
30/09/2020	09:15:04	1601457284	344958.822	5056849.552	3901.113
30/09/2020	09:15:07	1601457286	345009.898	5056752.333	3900.749
30/09/2020	09:15:08	1601457288	345060.177	5056652.407	3899.595
30/09/2020	09:15:10	1601457290	345109.765	5056554.442	3899.437
30/09/2020	09:15:12	1601457292	345160.585	5056455.747	3899.721
30/09/2020	09:15:14	1601457294	345211.567	5056357.62	3900.256

30/09/2020	09:15:16	1601457296	345262.268	5056259.7	3901.177
30/09/2020	09:15:18	1601457298	345313.848	5056161.868	3901.338
30/09/2020	09:15:20	1601457299	345365.592	5056064.451	3901.999
30/09/2020	09:15:22	1601457301	345416.93	5055967.749	3903.181
30/09/2020	09:15:24	1601457303	345468.407	5055871.069	3904.018
30/09/2020	09:15:26	1601457305	345519.547	5055773.182	3903.719
30/09/2020	09:15:28	1601457307	345568.902	5055675.129	3902.838
30/09/2020	09:15:30	1601457309	345617.838	5055574.486	3902.428
30/09/2020	09:15:31	1601457311	345667.065	5055476.445	3902.014
30/09/2020	09:15:33	1601457313	345718.861	5055378.759	3901.572
30/09/2020	09:15:35	1601457314	345772.598	5055282.003	3901.004
30/09/2020	09:15:37	1601457316	345826.315	5055185.794	3901.169
30/09/2020	09:15:39	1601457318	345880.85	5055088.743	3903.087
30/09/2020	09:15:40	1601457320	345934.4	5054994.84	3906.308
30/09/2020	09:16:59	1601457322	345988.564	5054899.267	3906.798
30/09/2020	09:17:01	1601457400	345720.941	5054942.655	3897.496
30/09/2020	09:17:04	1601457403	345668.27	5055038.343	3903.823
30/09/2020	09:17:07	1601457405	345614.825	5055132.489	3908.804
30/09/2020	09:17:10	1601457408	345561.857	5055228.405	3913.253
30/09/2020	09:17:12	1601457414	345510.126	5055325.643	3911.434
30/09/2020	09:17:15	1601457416	345456.04	5055424.222	3906.139
30/09/2020	09:17:18	1601457419	345403.875	5055521.534	3906.384
30/09/2020	09:17:20	1601457422	345353.352	5055619.086	3908.284
30/09/2020	09:17:23	1601457424	345302.807	5055716.536	3908.696
30/09/2020	09:17:26	1601457427	345251.578	5055815.081	3908.141
30/09/2020	09:17:28	1601457429	345200.236	5055912.242	3906.85
30/09/2020	09:17:31	1601457432	345148.574	5056009.916	3905.431
30/09/2020	09:17:33	1601457434	345096.636	5056107.555	3903.239
30/09/2020	09:17:35	1601457437	345044.581	5056204.504	3901.391
30/09/2020	09:17:38	1601457439	344991.346	5056301.335	3900.45
30/09/2020	09:17:40	1601457441	344939.145	5056398.537	3901.329
30/09/2020	09:17:43	1601457444	344889.377	5056496.415	3904.284
30/09/2020	09:17:45	1601457446	344841.096	5056594.707	3906.622
30/09/2020	09:17:47	1601457449	344790.845	5056692.86	3906.591
30/09/2020	09:17:50	1601457451	344738.287	5056789.812	3904.979
30/09/2020	09:17:52	1601457453	344684.221	5056886.004	3902.031
30/09/2020	09:17:54	1601457455	344630.677	5056982.585	3898.982
30/09/2020	09:17:56	1601457458	344581.72	5057080.585	3898.348

30/09/2020	09:17:59	1601457460	344533.742	5057179.761	3897.875
30/09/2020	09:18:01	1601457462	344485.904	5057278.045	3904.813
30/09/2020	09:18:04	1601457465	344437.348	5057373.937	3913.355
30/09/2020	09:18:06	1601457467	344384.447	5057471.622	3904.96
30/09/2020	09:18:08	1601457469	344330.019	5057567.172	3897.465
30/09/2020	09:18:10	1601457472	344277.612	5057664.677	3897.733
30/09/2020	09:18:13	1601457474	344232.281	5057763.748	3902.147
30/09/2020	09:18:15	1601457477	344187.931	5057864.238	3904.861
30/09/2020	09:18:18	1601457479	344139.733	5057961.646	3905.699
30/09/2020	09:18:20	1601457481	344083.122	5058054.789	3904.922
30/09/2020	09:18:23	1601457484	344023.822	5058147.693	3903.49
30/09/2020	09:18:25	1601457486	343972.038	5058245.773	3903.114
30/09/2020	09:18:27	1601457489	343925.449	5058345.557	3901.438
30/09/2020	09:18:30	1601457491	343876.306	5058443.999	3898.006
30/09/2020	09:18:32	1601457493	343825.323	5058540.9	3894.503
30/09/2020	09:18:34	1601457496	343773.49	5058638.203	3892.905
30/09/2020	09:18:37	1601457498	343723.753	5058736.075	3894.423
30/09/2020	09:18:39	1601457501	343674.523	5058833.543	3897.147
30/09/2020	09:18:42	1601457503	343622.228	5058930.504	3897.98
30/09/2020	09:20:01	1601457582	343571.049	5059028.205	3895.41
30/09/2020	09:20:03	1601457584	343479.722	5058753.294	3894.497
30/09/2020	09:20:04	1601457586	343532.506	5058656.35	3894.13
30/09/2020	09:20:06	1601457588	343585.332	5058559.083	3894.262
30/09/2020	09:20:08	1601457589	343637.276	5058461.571	3894.974
30/09/2020	09:20:10	1601457591	343687.357	5058364.466	3896.36
30/09/2020	09:20:12	1601457593	343736.088	5058265.681	3898.303
30/09/2020	09:20:14	1601457595	343783.305	5058168.129	3900.332
30/09/2020	09:20:16	1601457597	343832.346	5058068.428	3900.726
30/09/2020	09:20:18	1601457599	343883.109	5057968.191	3899.515
30/09/2020	09:20:21	1601457601	343932.958	5057872.271	3898.09
30/09/2020	09:20:23	1601457603			
30/09/2020	09:20:25	1601457604	344036.715	5057677.261	3897.914
30/09/2020	09:20:27	1601457606	344088.612	5057580.709	3898.402
30/09/2020	09:20:29	1601457608	344140.339	5057484.044	3899.642
30/09/2020	09:20:31	1601457610	344193.181	5057386.619	3901.491
30/09/2020	09:20:33	1601457612	344246.309	5057287.965	3903.289
30/09/2020	09:20:34	1601457614	344295.85	5057193.785	3903.867
30/09/2020	09:20:36	1601457616	344348.365	5057089.823	3903.861

30/09/2020	09:20:38	1601457617	344395.242	5056995.924	3902.982
30/09/2020	09:20:40	1601457621	344444.573	5056897.788	3901.713
30/09/2020	09:20:41	1601457623	344493.176	5056799.243	3900.585
30/09/2020	09:20:43	1601457625	344542.837	5056699.909	3899.653
30/09/2020	09:20:45	1601457626	344593.339	5056602.032	3899.086
30/09/2020	09:20:47	1601457628	344645.502	5056503.673	3898.547
30/09/2020	09:20:48	1601457630	344696.124	5056407.19	3897.93
30/09/2020	09:20:50	1601457631	344747.743	5056306.609	3896.977
30/09/2020	09:20:52	1601457633	344798.276	5056210.07	3895.576
30/09/2020	09:20:54	1601457635	344850.041	5056113.368	3894.091
30/09/2020	09:20:55	1601457637	344903.263	5056016.291	3892.928
30/09/2020	09:20:57	1601457638	344957.137	5055920.028	3892.445
30/09/2020	09:20:59	1601457640	345009.662	5055824.86	3893.55
30/09/2020	09:21:04	1601457642	345060.696	5055728.055	3894.202
30/09/2020	09:21:06	1601457643	345111.316	5055625.961	3894.177
30/09/2020	09:21:07	1601457645	345257.313	5055335.094	3894.97
30/09/2020	09:21:09	1601457647	345311.274	5055235.276	3896.552
30/09/2020	09:21:11	1601457649	345361.715	5055140.925	3897.338
30/09/2020	09:21:13	1601457650	345411.964	5055044.896	3897.788
30/09/2020	09:21:14	1601457652	345463.404	5054947.609	3897.245
30/09/2020	09:21:16	1601457654	345515.212	5054850.305	3896.111
30/09/2020	09:22:48	1601457656	345567.519	5054753.876	3894.278
30/09/2020	09:22:50	1601457658	345620.932	5054656.685	3892.016
30/09/2020	09:22:53	1601457749	345344.908	5054714.11	3893.527
30/09/2020	09:22:56	1601457752	345293.235	5054811.125	3894.921
30/09/2020	09:22:59	1601457755	345243.389	5054911.065	3894.825
30/09/2020	09:23:02	1601457757	345196.656	5055008.799	3897.041
30/09/2020	09:23:05	1601457760	345146.627	5055104.237	3899.545
30/09/2020	09:23:08	1601457763	345095.343	5055202.468	3901.197
30/09/2020	09:23:10	1601457766	345043.9	5055298.633	3902.393
30/09/2020	09:23:13	1601457769	344992.04	5055395.493	3904.275
30/09/2020	09:23:16	1601457772	344941.038	5055492.914	3906.583
30/09/2020	09:23:19	1601457775	344889.148	5055589.115	3907.989
30/09/2020	09:23:22	1601457778	344837.534	5055687.537	3907.237
30/09/2020	09:23:25	1601457780	344787.541	5055785.25	3905.803
30/09/2020	09:23:27	1601457783	344736.538	5055883.079	3904.934

30/09/2020	09:23:30	1601457786	344685.461	5055981.383	3903.7
30/09/2020	09:23:33	1601457789	344634.798	5056078.265	3903.631
30/09/2020	09:23:36	1601457792	344582.47	5056175.61	3904.68
30/09/2020	09:23:38	1601457794	344530.59	5056272.092	3905.231
30/09/2020	09:23:41	1601457800	344478.49	5056369.877	3905.144
30/09/2020	09:23:43	1601457802	344428.197	5056466.714	3905.342
30/09/2020	09:23:46	1601457805	344377.476	5056565.436	3906.065
30/09/2020	09:23:49	1601457807	344327.119	5056663.217	3908.033
30/09/2020	09:23:51	1601457810	344277.046	5056760.91	3909.492
30/09/2020	09:23:54	1601457812	344227.382	5056858.866	3908.303
30/09/2020	09:23:56	1601457815	344176.664	5056958.424	3907.173
30/09/2020	09:23:58	1601457817	344126.012	5057056.855	3907.515
30/09/2020	09:24:01	1601457820	344075.633	5057154.39	3908.08
30/09/2020	09:24:03	1601457827	344024.507	5057252.085	3908.798
30/09/2020	09:24:06	1601457829	343971.804	5057350.666	3909.011
30/09/2020	09:24:08	1601457831	343920.011	5057445.747	3908.108
30/09/2020	09:24:10	1601457834	343866.392	5057543.09	3907.959
30/09/2020	09:24:12	1601457836	343814.37	5057639.728	3906.929
30/09/2020	09:24:15	1601457838	343763.211	5057738.362	3905.702
30/09/2020	09:24:17	1601457841	343713.789	5057836.701	3906.417
30/09/2020	09:24:19	1601457843	343663.862	5057937.071	3908.149
30/09/2020	09:24:22	1601457845	343612.907	5058038.738	3910.073
30/09/2020	09:24:24	1601457847	343561.675	5058137.773	3912.282
30/09/2020	09:24:26	1601457850	343513.215	5058228.764	3912.54
30/09/2020	09:24:28	1601457852	343460.546	5058324.111	3911.684
30/09/2020	09:24:31	1601457854	343405.3	5058419.884	3909.396
30/09/2020	09:24:33	1601457856	343350.222	5058515.992	3906.76
30/09/2020	09:24:35	1601457910	343299.09	5058614.253	3904.649
30/09/2020	09:25:29	1601457912	343251.431	5058712.341	3902.517
30/09/2020	09:25:31	1601457914	343200.94	5058811.01	3899.807
30/09/2020	09:25:32	1601457916	343123.215	5058598.861	3886.275
30/09/2020	09:25:34	1601457917	343169.398	5058496.049	3876.664
30/09/2020	09:25:36	1601457919	343207.872	5058389.729	3869.038
30/09/2020	09:25:38	1601457921	343248.26	5058285.915	3866.303
30/09/2020	09:25:40	1601457923	343296.109	5058186.575	3870.558
30/09/2020	09:25:41	1601457925	343347.448	5058090.042	3880.318
30/09/2020	09:25:43	1601457926	343397.782	5057994.45	3889.088
30/09/2020	09:25:45	1601457928	343447.615	5057898.022	3894.654

30/09/2020	09:25:47	1601457930	343498.049	5057799.019	3895.785
30/09/2020	09:25:49	1601457932	343547.175	5057701.323	3895.93
30/09/2020	09:25:51	1601457934	343596.791	5057602.262	3896.525
30/09/2020	09:25:53	1601457936	343646.638	5057505.103	3897.787
30/09/2020	09:25:54	1601457938	343700.333	5057405.245	3899.992
30/09/2020	09:25:56	1601457939	343751.779	5057310.553	3902.973
30/09/2020	09:25:58	1601457941	343802.951	5057214.888	3904.996
30/09/2020	09:26:00	1601457943	343855.134	5057116.64	3904.765
30/09/2020	09:26:02	1601457945	343906.367	5057019.514	3902.931
30/09/2020	09:26:04	1601457947	343959.756	5056916.459	3901.496
30/09/2020	09:26:05	1601457948	344007.663	5056822.399	3901.053
30/09/2020	09:26:07	1601457950	344056.212	5056726.294	3900.753
30/09/2020	09:26:09	1601457952	344106.063	5056626.947	3900.24
30/09/2020	09:26:11	1601457954	344155.832	5056528.719	3899.883
30/09/2020	09:26:13	1601457956	344206.857	5056431.084	3899.581
30/09/2020	09:26:14	1601457957	344258.723	5056334.15	3899.205
30/09/2020	09:26:16	1601457959	344310.615	5056237.941	3898.995
30/09/2020	09:26:18	1601457961	344363.005	5056140.524	3898.941
30/09/2020	09:26:20	1601457963	344413.962	5056044.783	3898.919
30/09/2020	09:26:22	1601457965	344465.134	5055947.554	3899.01
30/09/2020	09:26:23	1601457966	344517.044	5055847.92	3899.514
30/09/2020	09:26:25	1601457968	344566.929	5055752.718	3899.932
30/09/2020	09:26:27	1601457970	344618.196	5055656.124	3900.001
30/09/2020	09:26:29	1601457972	344670.521	5055559.091	3899.499
30/09/2020	09:26:31	1601457974	344722.283	5055463.157	3898.674
30/09/2020	09:26:33	1601457976	344774.418	5055365.864	3897.066
30/09/2020	09:26:34	1601457978	344826.785	5055265.978	3894.71
30/09/2020	09:26:36	1601457979	344875.428	5055171.023	3891.986
30/09/2020	09:26:38	1601457981	344925.585	5055072.381	3889.027
30/09/2020	09:26:40	1601457983	344975.64	5054974.583	3886.108
30/09/2020	09:26:42	1601457985	345025.799	5054877.28	3883.52
30/09/2020	09:26:44	1601457987	345076.587	5054779.565	3881.465
30/09/2020	09:26:45	1601458087	345127.268	5054681.993	3881.173
30/09/2020	09:28:26	1601458090	345177.083	5054584.973	3883.455
30/09/2020	09:28:28	1601458092	345227.702	5054487.697	3885.792
30/09/2020	09:28:31	1601458095	344960.94	5054524.202	3892.561
30/09/2020	09:28:34	1601458098	344909.218	5054622.085	3889.491
30/09/2020	09:28:37	1601458101	344858.686	5054719.416	3889.669

30/09/2020	09:28:40	1601458104	344809.591	5054817.558	3891.795
30/09/2020	09:28:42	1601458106	344761.591	5054914.777	3893.135
30/09/2020	09:28:45	1601458109	344711.656	5055012.908	3891.812
30/09/2020	09:28:48	1601458112	344660.269	5055110.743	3888.738
30/09/2020	09:28:51	1601458115	344608.681	5055207.54	3886.679
30/09/2020	09:28:54	1601458118	344558.06	5055304.289	3886.687
30/09/2020	09:28:57	1601458121	344507.53	5055401.597	3887.473
30/09/2020	09:29:00	1601458124	344456.98	5055498.496	3888.363
30/09/2020	09:29:03	1601458127	344404.402	5055595.222	3889.098
30/09/2020	09:29:06	1601458130	344350.613	5055691.244	3888.556
30/09/2020	09:29:09	1601458133	344297.715	5055787.632	3886.902
30/09/2020	09:29:12	1601458136	344247.234	5055885.847	3885.548
30/09/2020	09:29:15	1601458139	344198.839	5055984.173	3884.777
30/09/2020	09:29:18	1601458142	344150.521	5056082.504	3886.546
30/09/2020	09:29:21	1601458145	344101.265	5056180.85	3888.318
30/09/2020	09:29:24	1601458148	344049.287	5056277.015	3890.246
30/09/2020	09:29:27	1601458151	343994.907	5056372.864	3892.077
30/09/2020	09:29:30	1601458154	343941.308	5056469.169	3894.095
30/09/2020	09:29:33	1601458157	343889.658	5056566.467	3895.673
30/09/2020	09:29:36	1601458160	343838.711	5056663.33	3897.275
30/09/2020	09:29:38	1601458163	343787.373	5056761.008	3898.701
30/09/2020	09:29:41	1601458166	343735.93	5056858.414	3899.741
30/09/2020	09:29:44	1601458168	343685.274	5056956.304	3900.562
30/09/2020	09:29:47	1601458171	343635.622	5057055.281	3901.331
30/09/2020	09:29:50	1601458174	343586.368	5057153.13	3903.337
30/09/2020	09:29:53	1601458177	343535.927	5057251.609	3903.927
30/09/2020	09:29:56	1601458180	343484.285	5057348.708	3903.028
30/09/2020	09:29:58	1601458182	343431.936	5057446.112	3902.694
30/09/2020	09:30:01	1601458185	343380.882	5057544.447	3901.736
30/09/2020	09:30:04	1601458188	343331.293	5057643.436	3900.914
30/09/2020	09:30:07	1601458190	343282.252	5057741.062	3901.105
30/09/2020	09:30:09	1601458193	343230.377	5057838.906	3900.406
30/09/2020	09:30:12	1601458196	343178.808	5057936.746	3899.484
30/09/2020	09:30:14	1601458198	343127.6	5058034.3	3898.822
30/09/2020	09:30:17	1601458201	343077.231	5058131.294	3898.62
30/09/2020	09:30:20	1601458203	343025.312	5058233.347	3899.469
30/09/2020	09:30:22	1601458206	342977.09	5058327.512	3900.442
30/09/2020	09:30:25	1601458273	342925.784	5058424.304	3902.595

30/09/2020	09:31:32	1601458275	342874.124	5058521.657	3903.112
30/09/2020	09:31:34	1601458277	342824.187	5058620.428	3900.983
30/09/2020	09:31:35	1601458279	342723.092	5058350.317	3885.174
30/09/2020	09:31:37	1601458280	342774.815	5058252.457	3885.262
30/09/2020	09:31:39	1601458282	342827.589	5058157.235	3888.442
30/09/2020	09:31:41	1601458288	342880.658	5058062.209	3891.37
30/09/2020	09:31:43	1601458290	342932.698	5057966.319	3892.267
30/09/2020	09:31:45	1601458292	342984.804	5057868.448	3891.581
30/09/2020	09:31:51	1601458294			
30/09/2020	09:31:53	1601458296			
30/09/2020	09:31:55	1601458298	343036.707	5057771.784	3890.211
30/09/2020	09:31:56	1601458300	343089.248	5057674.809	3889.213
30/09/2020	09:31:58	1601458302	343245.117	5057384.315	3889.129
30/09/2020	09:32:00	1601458303	343300.135	5057282.394	3889.219
30/09/2020	09:32:02	1601458305	343348.952	5057190.313	3889.672
30/09/2020	09:32:04	1601458307	343399.106	5057093.292	3890.052
30/09/2020	09:32:06	1601458311	343448.59	5056995.088	3890.066
30/09/2020	09:32:08	1601458313	343497.566	5056896.386	3889.563
30/09/2020	09:32:10	1601458315	343545.44	5056798.027	3888.915
30/09/2020	09:32:12	1601458317	343593.752	5056698.865	3887.951
30/09/2020	09:32:14	1601458319	343642.463	5056599.89	3886.985
30/09/2020					
30/09/2020	09:32:16	1601458321	343691.551	5056501.562	3888.57
30/09/2020	09:32:18	1601458323	343741.268	5056403.588	3891.577
30/09/2020	09:32:20	1601458325	343791.132	5056306.101	3894.4
30/09/2020	09:32:22	1601458327	343841.852	5056208.638	3895.09
30/09/2020	09:32:24	1601458329	343893.235	5056111.351	3894.289
30/09/2020	09:32:26	1601458331	343944.954	5056013.893	3893.064
30/09/2020	09:32:28	1601458333	343996.62	5055917.867	3893.084
30/09/2020	09:32:30	1601458336	344049.158	5055821.968	3895.079
30/09/2020	09:32:32	1601458338	344102.028	5055726.228	3897.102
30/09/2020	09:32:34	1601458340	344154.702	5055629.785	3897.579
30/09/2020	09:32:36	1601458342	344205.378	5055532.449	3897.363
30/09/2020	09:32:38	1601458344	344255.529	5055434.021	3896.265
30/09/2020	09:32:40	1601458346	344305.038	5055336.167	3895.493
30/09/2020	09:32:42	1601458348	344357.254	5055233.879	3895.453
30/09/2020	09:32:44	1601458350	344404.913	5055140.824	3895.51
30/09/2020	09:32:47	1601458352	344455.152	5055043.691	3895.373

30/09/2020	09:32:49	1601458354	344506.656	5054946.057	3894.887
30/09/2020	09:32:51	1601458436	344558.731	5054848.472	3893.991
30/09/2020	09:32:53	1601458439	344609.977	5054751.829	3892.939
30/09/2020	09:34:15	1601458442	344661.12	5054653.611	3892.198
30/09/2020	09:34:18	1601458445	344711.051	5054556.51	3891.933
30/09/2020	09:34:20	1601458447	344763.829	5054453.78	3891.972
30/09/2020	09:34:23	1601458450	344813.392	5054357.884	3892.379
30/09/2020	09:34:26	1601458453	344596.776	5054319.716	3898.583
30/09/2020	09:34:29	1601458456	344546.6	5054417.401	3895.003
30/09/2020	09:34:32	1601458459	344493.476	5054514.083	3892.052
30/09/2020	09:34:35	1601458462	344441.631	5054610.458	3892.814
30/09/2020	09:34:38	1601458465	344392.049	5054708.05	3895.161
30/09/2020	09:34:41	1601458468	344343.216	5054806.477	3895.051
30/09/2020	09:34:44	1601458471	344292.917	5054904.291	3893.318
30/09/2020	09:34:47	1601458474	344240.577	5055001.571	3892.004
30/09/2020	09:34:50	1601458477	344187.606	5055096.792	3891.514
30/09/2020	09:34:53	1601458480	344133.769	5055193.186	3892.544
30/09/2020	09:34:56	1601458483	344082.005	5055290.333	3894.923
30/09/2020	09:34:59	1601458486	344031.315	5055387.654	3897.126
30/09/2020	09:35:02	1601458489	343979.388	5055484.588	3899.706
30/09/2020	09:35:05	1601458492	343927.794	5055580.645	3901.285
30/09/2020	09:35:08	1601458495	343874.749	5055681.738	3900.288
30/09/2020	09:35:11	1601458498	343825.9	5055776.084	3900.32
30/09/2020	09:35:14	1601458501	343774.381	5055873.024	3900.012
30/09/2020	09:35:16	1601458503	343722.268	5055970.034	3900.212
30/09/2020	09:35:19	1601458507	343670.643	5056067.078	3901.068
30/09/2020	09:35:22	1601458509	343620.19	5056164.278	3901.418
30/09/2020	09:35:25	1601458512	343570.975	5056263.174	3901.216
30/09/2020	09:35:28	1601458515	343522.942	5056362.27	3901.336
30/09/2020	09:35:31	1601458518	343474.054	5056460.236	3901.955
30/09/2020	09:35:34	1601458521	343421.89	5056556.11	3902.487
30/09/2020	09:35:37	1601458524	343367.671	5056655.6	3903.063
30/09/2020	09:35:40	1601458527	343317.431	5056749.436	3903.382
30/09/2020	09:35:43	1601458530	343265.792	5056846.063	3903.205
30/09/2020	09:35:46	1601458533	343212.579	5056942.661	3900.475
30/09/2020	09:35:49	1601458535	343158.502	5057038.754	3898.467
30/09/2020	09:35:51	1601458538	343106.055	5057134.723	3897.27
30/09/2020	09:35:54	1601458541	343054.081	5057231.754	3896.032

30/09/2020	09:35:57	1601458544	343000.94	5057328.398	3894.638
30/09/2020	09:36:00	1601458547	342950.137	5057426.39	3893.391
30/09/2020	09:36:03	1601458550	342901.322	5057529.277	3892.298
30/09/2020	09:36:06	1601458553	342854.695	5057624.126	3892.712
30/09/2020	09:36:09	1601458556	342804.519	5057722.548	3894.138
30/09/2020	09:36:12	1601458559	342756.507	5057820.706	3895.453
30/09/2020	09:36:15	1601458630	342710.253	5057920.424	3896.738
30/09/2020	09:36:17	1601458632	342663.899	5058020.272	3898.437
30/09/2020	09:37:29	1601458634	342614.074	5058118.554	3899.285
30/09/2020	09:37:31	1601458636	342563.648	5058216.365	3899.188
30/09/2020	09:37:35	1601458639	342514.708	5058314.383	3898.888
30/09/2020	09:37:37	1601458641	342464.275	5058411.962	3898.967
30/09/2020	09:37:40	1601458643	342338.567	5058177.331	3881.92
30/09/2020	09:37:42	1601458645	342387.151	5058083.053	3890.801
30/09/2020	09:37:44	1601458648	342484.282	5057894.339	3900.959
30/09/2020	09:37:46	1601458650	342536.904	5057796.298	3895.786
30/09/2020	09:37:49	1601458652	342590.073	5057699.345	3891.763
30/09/2020	09:37:51	1601458654	342641.614	5057601.739	3892.588
30/09/2020	09:37:53	1601458656	342689.989	5057504.832	3895.285
30/09/2020	09:37:55	1601458659	342740.442	5057406.756	3896.999
30/09/2020	09:37:57	1601458661	342794.003	5057310.214	3896.27
30/09/2020	09:37:59	1601458663	342847.918	5057214.162	3894.356
30/09/2020	09:38:02	1601458665	342899.912	5057117.844	3891.418
30/09/2020	09:38:04	1601458667	342950.938	5057019.876	3888.095
30/09/2020	09:38:06	1601458670	343000.686	5056921.479	3886.126
30/09/2020	09:38:08	1601458672	343049.813	5056823.146	3886.36
30/09/2020	09:38:11	1601458674	343098.844	5056725.773	3887.894
30/09/2020	09:38:13	1601458676	343149.615	5056628.275	3890.754
30/09/2020	09:38:15	1601458679	343201.874	5056531.015	3893.434
30/09/2020	09:38:17	1601458681	343253.85	5056435.434	3895.176
30/09/2020	09:38:20	1601458683	343305.753	5056338.108	3896.222
30/09/2020	09:38:22	1601458685	343356.379	5056240.592	3896.642
30/09/2020	09:38:24	1601458688	343405.9	5056142.484	3896.952
30/09/2020	09:38:26	1601458690	343454.644	5056043.83	3897.176
30/09/2020	09:38:28	1601458692	343503.494	5055945.191	3897.694
30/09/2020	09:38:31	1601458694	343552.646	5055846.235	3898.906
30/09/2020	09:38:33	1601458696	343602.633	5055747.628	3899.599
30/09/2020	09:38:35	1601458698	343656.862	5055642.497	3898.283

30/09/2020	09:38:37	1601458700	343704.898	5055551.233	3896.731
30/09/2020	09:38:39	1601458703	343756.422	5055453.205	3896.065
30/09/2020	09:38:41	1601458705	343809.864	5055351.228	3895.169
30/09/2020	09:38:43	1601458707	343858.517	5055257.765	3894.365
30/09/2020	09:38:46	1601458709	343908.719	5055160.472	3894.519
30/09/2020	09:38:48	1601458711	343959.306	5055062.714	3896.28
30/09/2020	09:38:50	1601458713	344010.304	5054966.405	3898.208
30/09/2020	09:38:52	1601458715	344063.096	5054868.99	3899.73
30/09/2020	09:38:54	1601458717	344115.882	5054772.368	3899.753
30/09/2020	09:38:56	1601458720	344168.812	5054674.186	3897.95
30/09/2020	09:38:58	1601458722	344219.208	5054578.905	3896.193
30/09/2020	09:39:00	1601458827	344269.585	5054481.656	3894.147
30/09/2020	09:39:22	1601458830	344319.591	5054382.488	3892.203
30/09/2020	09:39:23	1601458832	344369.13	5054283.999	3890.401
30/09/2020	09:40:46	1601458835	344418.555	5054186.243	3889.294
30/09/2020	09:40:48	1601458838	344468.796	5054088.123	3889.219
30/09/2020	09:40:51	1601458840	345216.522	5053232.889	3904.319

GPA+LA			TA			deltaE	deltaN
346477.371	5055326.13	3888.654	346477.278	5055326	3888.9	-0.093	-0.041
346430.287	5055423.05	3890.598	346430.1172	5055423	3890.891	-0.1698	-0.125
346379.558	5055518.32	3891.183	346379.2934	5055518	3891.429	-0.2646	-0.235
346328.828	5055614.96	3891.495	346328.6482	5055615	3891.68	-0.1798	-0.171
346275.166	5055709.27	3892.381	346274.9543	5055709	3892.553	-0.2117	-0.204
346221.62	5055804.68	3891.75	346221.3784	5055804	3891.913	-0.2416	-0.274
346174.138	5055904.28	3891.07	346173.9109	5055904	3891.211	-0.2271	-0.241
346128.03	5056003.71	3890.935	346127.8547	5056004	3891.069	-0.1753	-0.2
346073.911	5056098.32	3890.02	346073.7108	5056098	3890.171	-0.2002	-0.195
346018.042	5056193.09	3886.967	346017.7571	5056193	3887.074	-0.2849	-0.291
345966.873	5056290.64	3883.632	345966.5645	5056290	3883.67	-0.3085	-0.289
345919.705	5056389.68	3883.175	345919.4769	5056389	3883.223	-0.2281	-0.247
345871.766	5056487.5	3882.611	345871.6006	5056487	3882.688	-0.1654	-0.189
345820.637	5056584.38	3884.145	345820.4388	5056584	3884.185	-0.1982	-0.177
345770.298	5056681.62	3886.186	345770.1878	5056681	3886.202	-0.1102	-0.275
345719.495	5056779.38	3887.432	345719.3574	5056779	3887.406	-0.1376	-0.32
345669.618	5056877.58	3887.885	345669.4693	5056877	3887.854	-0.1487	-0.347
345621.608	5056976.39	3890.787	345621.549	5056976	3890.77	-0.059	-0.267

345570.811	5057073.5	3895.302	345570.6976	5057073	3895.345	-0.0434	-0.275
345520.171	5057170.83	3895.917	345520.0633	5057170	3895.932	-0.0077	-0.353
345469.277	5057268.47	3893.65	345469.2841	5057268	3893.67	0.0971	-0.318
345415.287	5057363.92	3892.231	345415.1562	5057364	3892.243	-0.0408	-0.416
345362.772	5057461.52	3892.444	345362.6263	5057461	3892.464	-0.0657	-0.413
345313.035	5057559.97	3894.447	345312.8855	5057560	3894.472	-0.0695	-0.385
345264.139	5057657.55	3896.427	345264.0637	5057657	3896.467	0.0047	-0.312
345212.624	5057754.49	3898.189	345212.4788	5057754	3898.243	-0.0652	-0.396
345161.56	5057851.07	3898.325	345161.4171	5057851	3898.382	-0.0529	-0.444
345110.554	5057949.5	3897.669	345110.4637	5057949	3897.742	-0.0003	-0.432
345057.502	5058046.46	3895.949	345057.4085	5058046	3896.023	-0.0035	-0.447
345003.762	5058142.54	3896.306	345003.5856	5058142	3896.344	-0.0964	-0.452
344951.258	5058239.01	3898.025	344951.0897	5058239	3898.165	-0.0783	-0.457
344899.684	5058336.01	3896.16	344899.5103	5058336	3896.286	-0.0737	-0.474
344848.255	5058433.85	3894.127	344848.0957	5058433	3894.257	-0.0693	-0.457
344795.75	5058530.95	3893.121	344795.555	5058530	3893.227	-0.115	-0.464
344743.453	5058627.98	3893.899	344743.2198	5058627	3894.073	-0.1432	-0.511
344692.684	5058725.41	3894.11	344692.4286	5058725	3894.295	-0.1654	-0.486
344642.436	5058822.9	3894.296	344642.1892	5058822	3894.539	-0.1568	-0.516
344592.055	5058921.51	3893.792	344591.8029	5058921	3894.028	-0.1621	-0.558
344542.22	5059018.98	3893.565	344541.9701	5059018	3893.772	-0.1599	-0.541
344491.782	5059117.11	3894.743	344491.4708	5059116	3894.985	-0.2212	-0.641
344443.315	5059215.44	3895.926	344443.0789	5059215	3896.223	-0.1461	-0.603
344392.958	5059313.09	3895.344	344392.7084	5059312	3895.658	-0.1496	-0.61
344340.61	5059410.07	3894.392	344340.2787	5059409	3894.648	-0.2313	-0.774
344326.952	5059204.63	3853.231	344327.2038	5059205	3853.671	0.3418	0.399999999
344367.23	5059105.73	3850.936	344368.1811	5059106	3851.231		
344375.491	5059002.6	3848.482	344376.8513	5059003	3848.864		
344337.296	5058906.59	3839.98	344338.0955	5058906	3840.291		
344249.834	5058854.01	3825.805	344250.1729	5058853	3825.726	0.3889	
344144.803	5058867.33	3821.841	344144.4985	5058867	3821.929	-0.2545	-0.775
344064.732	5058940.07	3828.308	344064.3053	5058939	3828.395	-0.3667	-0.734
344005.598	5059034.1	3837.211	344005.4546	5059034	3837.313	-0.0834	-0.472
343945.729	5059123.33	3848.44	343945.7143	5059123	3848.512	0.0153	-0.241
344213.682	5059171.81	3873.446	344213.2875	5059172	3873.328	-0.2845	0.113
344263.381	5059072.96	3877.887	344262.9343	5059073	3877.851	-0.2867	-0.006
344311.811	5058977	3887.934	344311.2567	5058977	3888.098	-0.4043	0.01
344363.236	5058882.17	3893.355	344362.6483	5058882	3893.875	-0.4577	0.071

344416.145	5058786.15	3892.569	344415.9383	5058787	3892.908	-0.1067	0.471
344467.482	5058687.82	3889.206	344467.0031	5058688	3889.291	-0.3489	0.114
344516.909	5058590.47	3891.655	344516.3618	5058590	3891.704	-0.4072	0.06
344570.005	5058491.88	3895.09	344569.4751	5058492	3895.178	-0.3999	0.059
344623.466	5058399.12	3896.266	344623.0427	5058399	3896.328	-0.3033	0.126
344678.054	5058302.7	3895.608	344677.6285	5058303	3895.644	-0.3055	0.149
344730.522	5058206.7	3895.16	344730.0966	5058207	3895.189	-0.3054	0.145
344781.92	5058108.82	3894.416	344781.5741	5058109	3894.45	-0.2359	0.175
344831.181	5058009.87	3893.187	344830.7096	5058010	3893.189	-0.3614	0.158
344881.63	5057912.62	3892.402	344881.1751	5057913	3892.405	-0.3349	0.153
344935.462	5057816.07	3892.672	344935.05	5057816	3892.659	-0.292	0.183999999
344988.529	5057720.57	3893.493	344988.2436	5057721	3893.446	-0.1654	0.219000001
345039.015	5057623.47	3895.183	345038.665	5057624	3895.165	-0.22	0.194
345086.568	5057524.23	3898.064	345086.2396	5057524	3898.079	-0.1984	0.168
345132.796	5057423.54	3900.911	345132.3533	5057424	3900.894	-0.3227	0.19
345180.196	5057325.39	3901.221	345179.7583	5057326	3901.168	-0.3277	0.231
345230.474	5057228.05	3901.227	345230.0643	5057228	3901.173	-0.2997	0.235
345282.223	5057130.51	3903.017	345281.8631	5057131	3903.005	-0.2499	0.177
345334.606	5057033.43	3904.606	345334.238	5057034	3904.634	-0.268	0.225
345387.674	5056936.54	3905.091	345387.3029	5056937	3905.053	-0.2711	0.241
345440.605	5056840.27	3905.758	345440.2858	5056840	3905.735	-0.2092	0.274999999
345491.009	5056743.23	3907.12	345490.6643	5056744	3907.062	-0.2347	0.350000001
345541.056	5056644.89	3908.388	345540.6702	5056645	3908.405	-0.2758	0.352
345591.478	5056546.91	3909.028	345591.0822	5056547	3909.08	-0.2958	0.366
345642.472	5056448.74	3907.147	345642.0591	5056449	3907.189	-0.3229	0.438
345693.451	5056350.29	3905.383	345693.0387	5056351	3905.39	-0.3123	0.418000001
345743.857	5056251.62	3904.761	345743.3391	5056252	3904.834	-0.4179	0.375
345794.83	5056154.32	3904.287	345794.3274	5056155	3904.395	-0.4026	0.345
345847.093	5056058.14	3904.13	345846.5018	5056058	3904.272	-0.4912	0.340000001
345902.388	5055962.05	3903.975	345901.8458	5055962	3904.17	-0.4522	0.426
345957.947	5055866.66	3902.897	345957.5443	5055867	3903.069	-0.3127	0.493
346010.617	5055769.39	3902.524	346010.1601	5055770	3902.664	-0.3569	0.46
346060.197	5055671.29	3903.291	346059.7499	5055672	3903.467	-0.3471	0.415
346106.886	5055572.3	3904.861	346106.3899	5055573	3905.07	-0.3961	0.401000001
346153.367	5055472.85	3905.473	346152.8196	5055473	3905.713	-0.4474	0.452000001
346201.274	5055372.67	3903.788	346200.6465	5055373	3903.957	-0.5475	0.48
346251.235	5055273.81	3901.814	346250.5725	5055274	3902.013	-0.5725	0.496
346303.366	5055176.73	3901.24	346302.6039	5055177	3901.476	-0.6721	0.458

346359.692	5055081.28	3901.242	346358.9703	5055082	3901.503	-0.6417	0.429
346082.884	5055136.44	3904.089	346082.7797	5055136	3904.349	-0.0543	-0.144
346032.32	5055234.14	3903.713	346032.1354	5055234	3903.926	-0.1346	-0.217
345981.011	5055332.84	3903.902	345980.8495	5055333	3904.1	-0.1115	-0.215
345930.768	5055430.27	3904.509	345930.6222	5055430	3904.722	-0.0958	-0.242
345880.159	5055528.02	3904.181	345880.0163	5055528	3904.379	-0.0927	-0.254
345829.202	5055626.36	3902.756	345829.0597	5055626	3902.848	-0.0923	-0.221
345778.34	5055723.6	3903.073	345778.2159	5055723	3903.23	-0.0741	-0.213
345726.829	5055821.5	3902.936	345726.706	5055821	3903.122	-0.073	-0.271
345676.208	5055918.56	3901.007	345676.0844	5055918	3901.153	-0.0636	-0.272
345624.657	5056016.04	3898.429	345624.5782	5056016	3898.51	-0.0188	-0.221
345570.787	5056112.6	3896.891	345570.7314	5056112	3896.972	-0.0056	-0.197
345516.801	5056207.98	3895.964	345516.6581	5056208	3896.027	-0.0929	-0.274
345466.177	5056306.62	3895.932	345465.9962	5056306	3895.983	-0.1208	-0.258
345418.223	5056405.47	3894.765	345418.158	5056405	3894.812	-0.005	-0.249
345370.164	5056503.96	3892.02	345370.1868	5056504	3892.054	0.0828	-0.252
345319.929	5056602.08	3889.221	345319.9674	5056602	3889.083	0.0884	-0.223
345267.695	5056698.23	3892.483	345267.6572	5056698	3892.468	-0.0078	-0.274
345215.475	5056794.38	3897.932	345215.4086	5056794	3897.999	-0.0264	-0.29
345165.292	5056892.38	3900.81	345165.2096	5056892	3900.799	-0.0324	-0.366
345118.071	5056992.5	3900.05	345118.0203	5056992	3900.069	0.0193	-0.378
345071.559	5057091.62	3897.706	345071.5736	5057091	3897.637	0.0746	-0.331
345021.516	5057188.96	3899.596	345021.6505	5057189	3899.351	0.1645	0.028999999
			344969.1566	5057285	3902.801		
344917.016	5057382.06	3900.996	344917.0243	5057382	3901.006	0.0083	-0.365
344864.232	5057480.13	3897.072	344864.1954	5057480	3897.045	-0.0366	-0.322
344811.988	5057576.88	3894.054	344811.9411	5057577	3894.033	-0.0469	-0.322
344759.329	5057673.19	3892.859	344759.2045	5057673	3892.748	-0.1245	-0.306
344708.478	5057769.57	3896.484	344708.3821	5057769	3896.459	-0.0959	-0.345
344659.086	5057865.55	3901.034	344659.0033	5057865	3901.119	-0.0827	-0.311
344607.794	5057962.55	3900.596	344607.7194	5057962	3900.601	-0.0746	-0.364
344555.289	5058059.77	3896.998	344555.1794	5058059	3897.015	-0.1096	-0.417
344503.473	5058157.27	3891.943	344503.3665	5058157	3891.95	-0.1065	-0.401
344452.877	5058254.66	3887.886	344452.683	5058254	3887.879	-0.194	-0.431
344404.473	5058353.22	3886.102	344404.365	5058353	3886.111	-0.108	-0.283
344353.925	5058451.87	3888.596	344353.7016	5058452	3888.64	-0.2234	-0.328
344305.488	5058547.82	3890.573	344305.2849	5058547	3890.735	-0.2031	-0.353
344257.482	5058647.04	3889.609	344257.2605	5058647	3889.693	-0.2215	-0.413

344210.584	5058745.98	3887.712	344210.4543	5058746	3887.779	-0.1297	-0.369
344158.515	5058841.3	3889.434	344158.3529	5058841	3889.419	-0.1621	-0.303
344102.878	5058934.55	3894.309	344102.5747	5058934	3894.499	-0.3033	-0.499
344051.584	5059031.61	3894.514	344051.3515	5059031	3894.654	-0.2325	-0.542
344002.747	5059131.16	3890.855	344002.6718	5059131	3891.008	-0.0752	-0.435
343949.748	5059227.18	3886.695	343949.5586	5059227	3886.884	-0.1894	-0.575
343849.711	5058996.46	3891.079	343849.2363	5058997	3891.153	-0.4747	0.204000001
343902.999	5058900.58	3887.435	343902.7654	5058901	3887.45	-0.2336	0.131
343952.258	5058801.77	3885.559	343951.8295	5058802	3885.609	-0.4285	0.091000001
343999.638	5058703.35	3886.157	343999.1665	5058703	3886.009	-0.4715	-0.001
344048.866	5058603.79	3891.042	344048.417	5058604	3891.063	-0.449	0.049000001
344095.143	5058507.46	3895.677	344094.7509	5058508	3895.677	-0.3921	0.076
344140.66	5058408.81	3899.098					
344190.042	5058309.47	3897.909	344140.1648	5058409	3899.081		
344242.869	5058212.14	3893.179	344189.4569	5058310	3897.947		
344295.701	5058115.67	3890.198	344295.3474	5058116	3890.029	-0.3536	0.137999999
344346.974	5058018.02	3890.577	344346.5938	5058018	3890.488	-0.3802	0.121
344396.966	5057920.73	3893.353	344396.545	5057921	3893.286	-0.421	0.107000001
344446.785	5057824.42	3896.935	344446.3224	5057825	3896.878	-0.4626	0.117000001
344498.797	5057727.27	3899.974	344498.391	5057727	3899.94	-0.406	0.144
344550.727	5057630.9	3901.21	344550.3388	5057631	3901.193	-0.3882	0.155
344602.268	5057532.4	3900.468	344601.8994	5057533	3900.418	-0.3686	0.174000001
344651.646	5057434.11	3899.34	344651.2879	5057434	3899.28	-0.3581	0.212
344700.298	5057335.38	3898.351	344699.9123	5057336	3898.25	-0.3857	0.216
344749.542	5057237.28	3898.308	344749.1037	5057238	3898.269	-0.4383	0.244
344800.319	5057139.32	3898.363	344799.8753	5057140	3898.25	-0.4437	0.251
344852.411	5057042.58	3898.984	344851.9835	5057043	3898.904	-0.4275	0.255000001
344905.605	5056946.47	3899.95	344905.2418	5056947	3899.872	-0.3632	0.260000001
344958.912	5056849.61	3900.713	344958.6352	5056850	3900.705	-0.2768	0.333000001
345009.978	5056752.39	3900.349	345009.6827	5056753	3900.38	-0.2953	0.334000001
345060.247	5056652.48	3899.195	345059.8561	5056653	3899.132	-0.3909	0.299
345109.835	5056554.51	3899.037	345109.4689	5056555	3898.978	-0.3661	0.299
345160.655	5056455.82	3899.321	345160.2258	5056456	3899.346	-0.4292	0.324999999
345211.637	5056357.69	3899.856	345211.2682	5056358	3899.82	-0.3688	0.364999999
345262.338	5056259.77	3900.777	345261.8895	5056260	3900.852	-0.4485	0.318999999
345313.918	5056161.94	3900.938	345313.4807	5056162	3900.984	-0.4373	0.409
345365.662	5056064.52	3901.599	345365.2243	5056065	3901.671	-0.4377	0.405999999
345417	5055967.82	3902.781	345416.5409	5055968	3902.89	-0.4591	0.416

345468.487	5055871.14	3903.618	345467.9969	5055872	3903.74	-0.4901	0.454
345519.617	5055773.24	3903.319	345519.208	5055774	3903.479	-0.409	0.372
345568.972	5055675.2	3902.438	345568.5548	5055676	3902.595	-0.4172	0.481
345617.898	5055574.56	3902.028	345617.3404	5055575	3902.192	-0.5576	0.42
345667.125	5055476.53	3901.614	345666.5359	5055477	3901.772	-0.5891	0.399999999
345718.921	5055378.84	3901.172	345718.3124	5055379	3901.402	-0.6086	0.357000001
345772.658	5055282.08	3900.604	345772.147	5055282	3900.821	-0.511	0.408000001
345826.375	5055185.87	3900.769	345825.8582	5055186	3900.999	-0.5168	0.390000001
345880.92	5055088.82	3902.687	345880.393	5055089	3902.902	-0.527	0.341
345934.48	5054994.92	3905.908	345933.9364	5054995	3906.332	-0.5436	0.379
345988.644	5054899.35	3906.398	345988.1591	5054900	3906.817	-0.4849	0.477
345721.001	5054942.74	3897.096	345720.8119	5054943	3897.333	-0.1891	-0.057
345668.28	5055038.26	3903.423	345668.1244	5055038	3903.724	-0.1556	0.056
345614.835	5055132.41	3908.394					
345561.867	5055228.33	3912.843	345614.6628	5055132	3908.648		
345510.136	5055325.57	3911.024	345561.6958	5055228	3913.128		
345456.07	5055424.14	3905.739	345455.9834	5055424	3905.904	-0.0866	-0.066
345403.895	5055521.45	3905.984	345403.7923	5055521	3906.189	-0.1027	-0.076
345353.362	5055619.01	3907.884	345353.2388	5055619	3908.064	-0.1232	-0.017
345302.827	5055716.46	3908.296	345302.7598	5055716	3908.468	-0.0672	-0.061
345251.608	5055815.01	3907.741	345251.512	5055815	3907.86	-0.096	-0.106
345200.276	5055912.16	3906.45	345200.2136	5055912	3906.533	-0.0624	-0.105
345148.614	5056009.85	3905.031	345148.602	5056010	3905.125	-0.012	-0.098
345096.676	5056107.48	3902.839	345096.6974	5056107	3902.933	0.0214	-0.105
345044.631	5056204.42	3900.991	345044.6309	5056204	3901.041	-0.0001	-0.059
344991.386	5056301.26	3900.05	344991.3656	5056301	3900.067	-0.0204	-0.113
344939.185	5056398.46	3900.929	344939.1301	5056398	3900.914	-0.0549	-0.132
344889.407	5056496.35	3903.884	344889.3631	5056496	3903.892	-0.0439	-0.149
344841.126	5056594.63	3906.222	344841.2248	5056595	3906.273	0.0988	-0.097
344790.875	5056692.78	3906.191	344790.9354	5056693	3906.221	0.0604	-0.132
344738.327	5056789.73	3904.579	344738.405	5056790	3904.653	0.078	-0.119
344684.261	5056885.92	3901.631	344684.3156	5056886	3901.659	0.0546	-0.188
344630.727	5056982.51	3898.582	344630.6367	5056982	3898.546	-0.0903	-0.21
344581.76	5057080.51	3897.948	344581.7438	5057080	3897.921	-0.0162	-0.19
344533.782	5057179.68	3897.475	344533.7104	5057179	3897.149	-0.0716	-0.213
344485.924	5057277.97	3904.413	344485.9525	5057279	3904.62	0.0285	0.66
344437.358	5057373.86	3912.955	344437.4602	5057374	3913.286	0.1022	-0.2
344384.487	5057471.54	3904.56	344384.8342	5057471	3904.252	0.3472	-0.328

344330.079	5057567.09	3897.065	344329.8062	5057567	3896.259	-0.2728	-0.481
344277.642	5057664.6	3897.333	344277.425	5057664	3897.35	-0.217	-0.29
344232.291	5057763.68	3901.737	344232.1582	5057763	3901.765	-0.1328	-0.222
344187.951	5057864.16	3904.461	344187.9134	5057864	3904.44	-0.0376	-0.238
344139.763	5057961.58	3905.289	344139.8451	5057961	3905.256	0.0821	-0.129
344083.142	5058054.71	3904.522	344083.1094	5058054	3904.438	-0.0326	-0.229
344023.842	5058147.61	3903.09	344023.6266	5058147	3902.994	-0.2154	-0.33
343972.068	5058245.69	3902.714	343971.8062	5058245	3902.659	-0.2618	-0.376
343925.489	5058345.49	3901.038	343925.3851	5058345	3901.016	-0.1039	-0.304
343876.346	5058443.92	3897.606	343876.2831	5058444	3897.626	-0.0629	-0.318
343825.363	5058540.82	3894.103	343825.2622	5058541	3894.061	-0.1008	-0.306
343773.52	5058638.12	3892.505	343773.384	5058638	3892.494	-0.136	-0.378
343723.773	5058736	3894.023	343723.6185	5058736	3894.042	-0.1545	-0.338
343674.543	5058833.47	3896.737	343674.496	5058833	3896.764	-0.047	-0.324
343622.248	5058930.42	3897.58	343622.0783	5058930	3897.758	-0.1697	-0.531
343571.079	5059028.13	3895.01	343570.8107	5059027	3894.944	-0.2683	-0.647
343479.762	5058753.21	3894.097	343479.3075	5058753	3894.058	-0.4545	0.189
343532.586	5058656.41	3893.73	343532.1464	5058656	3893.644	-0.4396	0.075000001
343585.422	5058559.13	3893.862	343584.9829	5058559	3893.8	-0.4391	0.141000001
343637.356	5058461.62	3894.574	343636.9412	5058462	3894.478	-0.4148	0.164
343687.447	5058364.52	3895.96	343687.0522	5058365	3895.845	-0.3948	0.185000001
343736.178	5058265.72	3897.903	343735.7376	5058266	3897.804	-0.4404	0.16
343783.395	5058168.17	3899.932	343782.9338	5058168	3899.835	-0.4612	0.191000001
343832.426	5058068.47	3900.326	343831.9362	5058069	3900.269	-0.4898	0.22
343883.189	5057968.23	3899.115	343882.7116	5057968	3899.042	-0.4774	0.242000001
343933.028	5057872.32	3897.69	343932.4908	5057873	3897.538	-0.5372	0.237000001
			343984.5503	5057774	3897.137		
344036.795	5057677.3	3897.514	344036.3954	5057678	3897.455	-0.3196	0.258
344088.692	5057580.76	3898.002	344088.3281	5057581	3897.892	-0.2839	0.277
344140.419	5057484.08	3899.242	344140.0447	5057484	3899.16	-0.2943	0.269
344193.261	5057386.67	3901.091	344192.9243	5057387	3900.995	-0.2567	0.306
344246.389	5057288.01	3902.889	344246.0741	5057288	3902.855	-0.2349	0.306
344295.93	5057193.83	3903.467	344295.6698	5057194	3903.445	-0.1802	0.348999999
344348.445	5057089.86	3903.461	344348.11	5057090	3903.473	-0.255	0.372
344395.312	5056995.96	3902.582	344394.9432	5056996	3902.549	-0.2988	0.339000001
344444.643	5056897.83	3901.313	344444.3047	5056898	3901.276	-0.2683	0.415
344493.236	5056799.28	3900.175	344542.5091	5056700	3899.209	49.3331	-98.957
344542.897	5056699.95	3899.243					

344593.399	5056602.07	3898.676	344593.0082	5056602	3898.684			
344645.562	5056503.71	3898.137	344645.2723	5056504	3898.16	-0.2897	0.380999999	
344696.184	5056407.24	3897.52	344695.8863	5056408	3897.555	-0.2977	-100.098	
344747.803	5056306.65	3896.567	344747.402	5056307	3896.628	-0.401	-96.06	
344798.336	5056210.11	3895.166	344797.9053	5056211	3895.263	-0.4307	-96.223	
344850.101	5056113.41	3893.681	344849.6758	5056114	3893.751	-0.4252	-96.635	
344903.323	5056016.33	3892.518	344902.9165	5056017	3892.624	-0.4065	-95.818	
344957.197	5055920.07	3892.035	344956.9326	5055920	3892.051	-0.2644	0.521	
345009.722	5055824.91	3893.15	345009.6198	5055825	3893.25	-0.1022	195.811	
345060.776	5055728.11	3893.802	345060.3776	5055728	3893.909	-0.3984	197.926	
345111.396	5055626	3893.777	345110.8321	5055626	3893.897	-0.5639	194.565	
			345157.5801	5055531	3893.38			
			345206.0414	5055433	3893.159			
345257.383	5055335.13	3894.57	345256.9368	5055335	3894.799	-0.4462	0.356000001	
345311.344	5055235.32	3896.152	345310.9522	5055236	3896.423	-0.3918	0.333000001	
345361.785	5055140.97	3896.938	345361.4141	5055141	3897.186	-0.3709	0.372	
345412.044	5055044.94	3897.388	345411.5409	5055045	3897.67	-0.5031	0.391	
345463.484	5054947.66	3896.845	345462.9803	5054948	3897.117	-0.5037	0.446	
345515.292	5054850.35	3895.711	345514.7593	5054851	3896.021	-0.5327	0.435000001	
345567.599	5054753.92	3893.878	345567.0688	5054754	3894.216	-0.5302	0.412	
345621.002	5054656.73	3891.616	345620.5055	5054657	3891.967	-0.4965	0.41	
345344.978	5054714.15	3893.127	345344.7638	5054714	3893.361	-0.2142	0.083	
345293.305	5054811.17	3894.521	345293.0484	5054811	3894.852	-0.2566	-0.009	
345243.459	5054911.11	3894.425	345243.2186	5054911	3894.643	-0.2404	-0.023	
345196.726	5055008.84	3896.641	345196.5436	5055009	3896.874	-0.1824	0.008	
345146.697	5055104.2	3899.145	345146.4546	5055104	3899.386	-0.2424	0.02	
345095.423	5055202.43	3900.797	345095.213	5055202	3901.016	-0.21	0.067	
345043.98	5055298.59	3901.993	345043.7187	5055299	3902.215	-0.2613	0.131999999	
344992.11	5055395.45	3903.875	344991.8905	5055396	3904.054	-0.2195	0.104	
344941.108	5055492.86	3906.183	344940.7901	5055493	3906.305	-0.3179	-0.021	
344889.228	5055589.08	3907.589	344888.9937	5055589	3908.059	-0.2343	0.265	
344837.614	5055687.5	3906.837	344837.5995	5055687	3906.904	-0.0145	-0.012	
344787.621	5055785.21	3905.403	344787.637	5055785	3905.486	0.016	0.033	
344736.618	5055883.04	3904.534	344736.547	5055883	3904.613	-0.071	0.029	
344685.551	5055981.34	3903.3	344685.4853	5055981	3903.34	-0.0657	0.026	
344634.898	5056078.24	3903.231	344634.8331	5056078	3903.254	-0.0649	0.056000001	
344582.57	5056175.57	3904.28	344582.4588	5056176	3904.347	-0.1112	0.064999999	
344530.69	5056272.05	3904.831	344530.5957	5056272	3904.86			

344478.59	5056369.85	3904.744						
344428.297	5056466.68	3904.942	344428.2371	5056467	3904.912	-0.0599	-0.007	
344377.576	5056565.41	3905.665	344377.485	5056565	3905.609	50.682	-98.531	
344327.229	5056663.19	3907.633	344327.1353	5056663	3907.617	50.3991	-97.639	
344277.156	5056760.88	3909.092	344277.0606	5056761	3909.05	51.1336	-97.809	
344227.492	5056858.84	3907.903	344227.479	5056859	3907.798	52.7208	-98.692	
344176.764	5056958.39	3906.773	344176.694	5056958	3906.712	-53.6703	97.188	
344126.112	5057056.83	3907.115	344126.0321	5057057	3907.014	-52.0669	96.478	
344075.743	5057154.36	3907.68	344075.6406	5057154	3907.605	-51.2497	98.466	
344024.627	5057252.06	3908.408	344024.5248	5057252	3908.319	-49.5008	98.16	
343971.914	5057350.64	3908.611	343866.3407	5057543	3907.426	-49.999	100.197	
343920.121	5057445.72	3907.708						
343866.502	5057543.06	3907.559						
343814.48	5057639.7	3906.529	343814.3251	5057640	3906.439	-0.1549	-0.13	
343763.331	5057738.33	3905.312	343763.1203	5057738	3905.142	-52.6955	95.124	
343713.909	5057836.67	3906.027	343713.7102	5057837	3905.865	-55.3366	95.516	
343663.982	5057937.04	3907.759	343663.79	5057937	3907.617	-55.3068	95.708	
343613.027	5058038.71	3909.683	343612.8407	5058039	3909.499	-51.3834	97.868	
343561.795	5058137.74	3911.892	343561.6383	5058138	3911.826	-47.7183	97.8	
343513.325	5058228.73	3912.14	343513.1995	5058229	3912.047	-50.5878	98.375	
343460.656	5058324.08	3911.284	343460.5195	5058324	3911.21	-77.49	-211.687	
343405.41	5058419.85	3908.996	343405.2094	5058420	3908.909	46.251	-102.362	
343350.332	5058515.96	3906.36	343349.9932	5058516	3906.272	37.98	-106.106	
343299.21	5058614.22	3904.259	343298.8386	5058614	3904.158	39.7134	-103.792	
343251.551	5058712.3	3902.127	343251.3717	5058712	3902.019	47.5666	-99.202	
343201.06	5058810.97	3899.417	343200.8432	5058811	3899.313	51.1605	-96.386	
343123.335	5058598.83	3885.885	343123.45	5058599	3885.607	50.1496	-95.417	
343169.528	5058496.02	3876.274	343169.466	5058496	3875.947	49.6047	-96.192	
343208.002	5058389.7	3868.648	343207.378	5058390	3868.332	50.1785	-98.757	
343248.38	5058285.88	3865.913	343247.5854	5058286	3865.584	48.8794	-97.408	
343296.139	5058186.46	3870.168	343295.8266	5058187	3869.937	49.3596	-98.815	
343347.498	5058089.97	3879.918	343347.2695	5058090	3879.68	49.5496	-96.903	
343397.812	5057994.38	3888.688	343397.5976	5057995	3888.594	53.4671	-99.649	
343447.625	5057897.94	3894.244	343447.3867	5057898	3894.273	51.269	-94.429	
343498.099	5057798.95	3895.385	343497.7935	5057799	3895.234	50.9637	-95.399	
343547.215	5057701.24	3895.53	343546.9284	5057702	3895.353	51.9627	-97.925	
343596.821	5057602.19	3896.125	343596.5346	5057603	3895.969	51.0406	-96.817	
343646.648	5057505.03	3897.377	343646.3406	5057505	3897.211	53.2308	-102.789	

343700.333	5057405.18	3899.582	343700.1051	5057405	3899.42	47.7498	-93.775
343751.779	5057310.48	3902.563	343751.602	5057311	3902.505	48.3766	-95.794
343802.961	5057214.82	3904.586	343802.7427	5057215	3904.565	49.6463	-99.018
343855.144	5057116.57	3904.355	343854.9137	5057117	3904.292	49.5457	-97.933
343906.387	5057019.44	3902.531	343906.1746	5057020	3902.44	50.8323	-97.318
343959.776	5056916.39	3901.086	343959.5978	5056917	3901.023	51.674	-96.623
344007.673	5056822.33	3900.643	344007.5058	5056823	3900.582	51.712	-95.882
344056.222	5056726.22	3900.343	344056.0396	5056727	3900.319	52.2409	-97.096
344106.073	5056626.88	3899.83	344105.8583	5056627	3899.79	50.8151	-95.425
344155.832	5056528.65	3899.473	344155.6087	5056529	3899.48	51.0526	-96.927
344206.857	5056431.01	3899.171	344206.6643	5056431	3899.187	51.7646	-99.355
344258.723	5056334.08	3898.795	344258.531	5056334	3898.82	49.6174	-94.858
344310.615	5056237.87	3898.585	344310.435	5056238	3898.617	51.0327	-96.152
344363.015	5056140.45	3898.531	344362.8559	5056141	3898.582	52.268	-96.807
344413.972	5056044.71	3898.509	344413.8201	5056045	3898.585	53.7924	-99.362
344465.144	5055947.48	3898.6	344465.0146	5055948	3898.707	54.1351	-97.475
344517.064	5055847.85	3899.104	344516.8986	5055848	3899.214	52.0788	-99.442
344566.949	5055752.65	3899.522	344566.6614	5055753	3899.672	48.4551	-94.58
344618.216	5055656.05	3899.591	344617.9617	5055657	3899.814	49.895	-98.317
344670.541	5055559.02	3899.089	344670.464	5055559	3899.265	49.7746	-97.436
344722.303	5055463.09	3898.264	344724.3134	5055460	3898.202	49.8903	-96.971
344774.438	5055365.79	3896.656	344776.4181	5055366	3897.253	50.5267	-97.39
344826.805	5055265.91	3894.3	344826.4968	5055266	3894.533	50.4828	-97.272
344875.448	5055170.95	3891.576	344875.2401	5055171	3891.793	49.5405	-96.746
344925.595	5055072.31	3888.617	344925.323	5055073	3888.87	50.2769	-97.001
344975.65	5054974.51	3885.698	344975.3596	5054975	3885.963	-266.878	36.643
345025.799	5054877.21	3883.11	345025.5303	5054878	3883.4	-51.8535	98.013
345076.587	5054779.5	3881.055	345076.3257	5054780	3881.356	-50.67	97.47
345127.268	5054681.92	3880.763	345127.0698	5054682	3880.941	-49.2153	98.263
345177.083	5054584.9	3883.045	345176.8085	5054585	3883.399	-48.0865	97.363
345227.702	5054487.63	3885.382	345227.3599	5054488	3885.745	-50.0106	98.235
344960.94	5054524.13	3892.151	344960.824	5054524	3892.514	-51.4566	97.91
344909.238	5054622.01	3889.091	344909.0865	5054622	3889.345	-51.7146	96.72
344858.706	5054719.35	3889.259	344858.548	5054720	3889.587	-50.7105	96.872
344809.611	5054817.49	3891.385	344809.4707	5054818	3891.705	-50.5984	97.409
344761.671	5054914.87	3892.745	344761.5045	5054915	3893.082	-50.5894	97.112
344711.726	5055013	3891.412	344711.5804	5055013	3891.71	-52.6134	96.893
344660.329	5055110.83	3888.338	344660.1994	5055111	3888.556	-53.8278	96.131

344608.741	5055207.63	3886.279	344608.5544	5055207	3886.549	-52.9733	96.492
344558.13	5055304.39	3886.287	344557.9705	5055304	3886.5	-50.5269	98.325
344507.6	5055401.7	3887.083	344507.4616	5055402	3887.27	-48.4343	98.456
344457.04	5055498.61	3887.973	344456.9406	5055499	3888.16	-48.3743	98.477
344404.452	5055595.33	3888.708	344404.3666	5055595	3888.863	-49.2544	98.514
344350.653	5055691.35	3888.166	344350.5742	5055691	3888.298	-52.0228	96.297
344297.765	5055787.74	3886.512	344297.6397	5055788	3886.625	-54.4561	95.938
344247.274	5055885.96	3885.158	344247.1881	5055886	3885.256	-53.6975	96.386
344198.889	5055984.28	3884.387	344198.7997	5055984	3884.407	-51.7134	97.395
344150.571	5056082.61	3886.156	344150.4647	5056083	3886.213	-51.0245	96.968
344101.325	5056180.96	3887.928	344101.2666	5056181	3887.983	-51.3797	97.753
344049.347	5056277.13	3889.856	344049.2422	5056277	3889.9	-51.5282	97.464
343994.957	5056372.96	3891.677	343994.8309	5056373	3891.675	-50.7369	97.912
343941.368	5056469.27	3893.705	343941.2095	5056469	3893.71	-49.7413	99.058
343889.718	5056566.57	3895.283	343889.5946	5056567	3895.262	-49.3338	97.901
343838.771	5056663.43	3896.885	343838.6335	5056663	3896.852	-50.5114	98.54
343787.433	5056761.11	3898.311	343787.3313	5056761	3898.276	-51.735	97.146
343735.99	5056858.52	3899.351	343735.8448	5056858	3899.276	-52.4656	97.417
343685.334	5056956.41	3900.172	343685.1931	5056956	3900.107	-51.1751	98.329
343635.682	5057055.39	3900.941	343635.5327	5057055	3900.817	-49.6759	98.994
343586.428	5057153.24	3902.947	343586.2882	5057153	3902.851	-49.0935	97.659
343535.977	5057251.72	3903.537	343535.8566	5057252	3903.424	-51.9724	97.79
343484.335	5057348.82	3902.638	343484.192	5057349	3902.5	-51.6666	97.814
343431.986	5057446.22	3902.304	343431.8194	5057446	3902.14	-51.3209	97.502
343380.932	5057544.56	3901.346	343380.7609	5057544	3901.131	-50.511	96.918
343331.353	5057643.55	3900.524	343331.2061	5057643	3900.338	-52.0492	101.977
343282.312	5057741.17	3900.715	343282.1995	5057741	3900.522	-48.3394	94.066
343230.437	5057839.02	3900.016	343230.2796	5057839	3899.838	-51.4488	96.682
343178.858	5057936.86	3899.094	343178.7104	5057937	3898.92	-51.8206	97.163
343127.65	5058034.41	3898.432	343127.4871	5058034	3898.255	-50.0879	98.583
343077.291	5058131.4	3898.23	343077.089	5058131	3898.004	-101.325	-269.937
343025.372	5058233.46	3899.079	343025.1818	5058233	3898.862	51.3874	-97.808
342977.15	5058327.62	3900.052	342976.9726	5058327	3899.842	52.575	-95.091
342925.844	5058424.41	3902.205	342925.6412	5058424	3902.073	52.9024	-94.83
342874.184	5058521.78	3902.722	342873.9634	5058521	3902.531	51.8576	-95.724
342824.247	5058620.54	3900.593	342824.0361	5058620	3900.353	51.8728	-97.694
342723.142	5058350.43	3884.784	342722.8617	5058350	3884.342	156.7757	-290.582
342774.875	5058252.57	3884.872	342774.4794	5058253	3884.43	156.7628	-291.175

342827.649	5058157.35	3888.052	342827.39	5058157	3887.75	155.6548	-290.299
342880.718	5058062.33	3890.98	342880.4914	5058062	3890.766	54.8975	-101.732
342932.708	5057966.25	3891.857				48.7008	-91.842
342984.814	5057868.37	3891.171				-52.2984	98.117
		3889.811	342932.5156	5057966	3891.656	-52.1462	96.921
		3888.813	342984.5708	5057869	3890.951	-52.1462	96.921
343036.717	5057771.7	3888.719	343141.5797	5057578	3888.467	104.8627	-193.838
343089.248	5057674.73	3888.819	343193.4698	5057481	3888.498	48.1621	-98.901
343245.127	5057384.24	3889.272	343244.9028	5057385	3888.541	48.5901	-98.751
343300.145	5057282.31	3889.652	343300.0145	5057283	3888.629	98.7264	-196.058
343348.962	5057190.23	3889.656	343348.8358	5057191	3889.133	99.487	-195.245
343399.116	5057093.21	3889.153	343399.0101	5057094	3889.527	100.4731	-194.706
343448.6	5056995.01	3888.505	343448.4878	5056995	3889.559	102.0125	-194.517
343497.576	5056896.31	3887.541	343497.4747	5056897	3889.059	102.9867	-194.484
343545.45	5056797.95	3886.575	343545.3154	5056798	3888.457	103.2893	-193.263
343593.762	5056698.79	3888.17	343593.6021	5056699	3887.483	104.1176	-191.699
343642.473	5056599.81	3891.167	343642.3421	5056600	3886.486	105.322	-191.404
		3894	343741.1894	5056404	3891.178	105.4727	-191.898
343691.561	5056501.48	3894.69	343791.038	5056306	3894.012	103.2578	-193.486
343741.278	5056403.51	3893.889	343841.7411	5056209	3894.725	100.7406	-195.528
343791.152	5056306.02	3892.664	343893.1445	5056112	3893.928	99.557	-196.09
343841.872	5056208.56	3892.684	343944.8387	5056014	3892.739	101.6259	-199.922
343893.255	5056111.27	3894.679	343996.5243	5055918	3892.755	99.7186	-195.084
343944.964	5056013.81	3896.692	344049.0716	5055822	3894.771	97.7174	-189.929
343996.62	5055917.79	3897.179	344101.942	5055726	3896.831	101.5616	-194.491
344049.158	5055821.89	3896.963	344154.6307	5055630	3897.334	103.4281	-194.943
344102.028	5055726.15	3895.855	344205.2858	5055533	3897.129	103.2006	-193.97
344154.712	5055629.71	3895.083	344255.4426	5055434	3896.049	102.2538	-194.6
344205.388	5055532.37	3895.043	344304.935	5055336	3895.315	100.904	-195.035
344255.539	5055433.94	3895.11	344357.1549	5055234	3895.274	102.5289	-199.547
344305.038	5055336.09	3894.963	344404.7566	5055141	3895.357	102.145	-198.317
344357.254	5055233.8	3894.487	344454.9714	5055044	3895.226	-167.151	-133.821
344404.913	5055140.74	3893.591	344506.4746	5054946	3894.777	-266.831	59.799
344455.162	5055043.61	3892.539	344558.5801	5054849	3893.896	-103.439	194.582
344506.676	5054945.98	3891.798	344609.8566	5054752	3892.856	-105.151	193.286
344558.751	5054848.39	3891.533	344660.9848	5054654	3892.131	-101.545	194.177
344609.997	5054751.75	3891.572	344710.881	5054557	3891.898	-98.4873	196.256
344661.14	5054653.53	3891.979	344763.6489	5054454	3891.947	-99.1804	196.457

344711.071	5054556.43	3898.183	344813.196	5054358	3892.37	-102.713	195.313
344763.849	5054453.7	3894.603	344596.6785	5054320	3898.643	-105.382	192.694
344813.412	5054357.8	3891.652	344546.5609	5054418	3894.984	-106.895	191.802
344596.796	5054319.65	3892.404	344493.3372	5054514	3891.937	-105.68	193.744
344546.62	5054417.32	3894.751	344441.449	5054611	3892.757	-102.499	194.678
344493.496	5054514.01	3894.641	344391.9313	5054708	3895.101	-102.672	194.466
344441.651	5054610.39	3892.928	344343.1437	5054807	3894.97	-103.579	193.192
344392.069	5054707.98	3891.614	344292.8686	5054905	3893.216	-104.693	197.339
344343.236	5054806.41	3891.124	344240.5029	5055002	3891.868	-101.921	195.658
344292.947	5054904.4	3892.144	344187.5355	5055097	3891.368	-100.391	191.483
344240.617	5055001.68	3894.523	344133.6815	5055193	3892.369	-103.667	194.139
344187.636	5055096.9	3896.736	344081.9265	5055291	3894.737	-103.802	194.244
344133.789	5055193.3	3899.316	344031.2699	5055388	3896.934	-102.165	194.423
344082.035	5055290.44	3900.895	343979.3331	5055485	3899.506	-99.7603	196.266
344031.345	5055387.77	3899.898	343927.7358	5055581	3901.078	-97.2415	198.261
343979.428	5055484.71	3899.92	343874.6952	5055682	3900.054	-96.8349	197.41
343927.834	5055580.76	3899.622	343825.8728	5055776	3900.06	-101.134	194.031
343874.789	5055681.85	3899.822	343774.3578	5055873	3899.713	-106.473	195.532
343825.93	5055776.19	3900.678	343722.2329	5055970	3899.901	-104.553	193.501
343774.411	5055873.14	3901.028	343670.5785	5056067	3900.754	-101.94	190.633
343722.298	5055970.15	3900.826	343620.103	5056164	3901.083	-104.921	193.394
343670.673	5056067.2	3900.946	343570.8827	5056263	3900.842	-107.415	192.84
343620.23	5056164.4	3901.565	343522.9485	5056363	3900.896	-106.634	192.182
343571.015	5056263.29	3902.097	343474.1401	5056461	3901.562	-104.496	193.148
343522.972	5056362.39	3902.673	343421.8082	5056556	3902.098	-105.261	193.775
343474.084	5056460.36	3902.992	343367.5809	5056656	3902.632	-104.16	194.696
343421.92	5056556.23	3902.815	343317.3367	5056750	3902.939	-99.7271	201.016
343367.701	5056655.72	3900.085	343265.7307	5056846	3902.749	-95.5625	197.887
343317.461	5056749.56	3898.067	343212.5101	5056943	3899.984	-96.9684	193.378
343265.822	5056846.18	3896.88	343158.3772	5057039	3897.969	-98.357	196.669
343212.609	5056942.77	3895.642	343105.945	5057135	3896.752	-94.4322	197.953
343158.542	5057038.86	3894.248	343054.0064	5057232	3895.495	-92.7447	199.662
343106.095	5057134.83	3893.001	343000.7936	5057328	3894.085	-96.3463	198.184
343054.121	5057231.86	3891.908	342949.9206	5057426	3892.819	-100.429	196.057
343000.98	5057328.51	3892.322	342901.2129	5057529	3891.71	-99.4832	195.866
342950.187	5057426.5	3893.748	342854.5745	5057624	3892.12	-99.5514	195.569
342901.372	5057529.39	3895.063	342804.3536	5057723	3893.559	-176.228	-137.065
342854.735	5057624.24	3896.348	342756.338	5057821	3894.861	-77.1538	-329.037

342804.559	5057722.67	3898.047	342710.0868	5057921	3896.128	95.3995	-185.673
342756.547	5057820.83	3898.895	342663.7623	5058020	3897.804	96.9307	-188.616
342710.293	5057920.54	3898.798	342613.9067	5058119	3898.689	52.4195	-97.887
342663.929	5058020.39	3898.498	342563.4696	5058216	3898.578	53.0874	-96.829
342614.114	5058118.67	3898.577	342514.5908	5058314	3898.229	51.4849	-97.477
342563.678	5058216.49	3881.53	342464.0966	5058412	3898.309	48.2658	-96.821
342514.738	5058314.5	3890.411	342338.4802	5058177	3880.928	50.2424	-97.981
342464.305	5058412.08	3900.559	342387.1212	5058083	3890.095	53.4435	-96.384
342338.597	5058177.45	3895.396					
342387.181	5058083.17	3891.373	342433.9665	5057992	3898.702	51.9124	-96.121
342484.322	5057894.45	3892.198	342484.0817	5057894	3900.411	50.9582	-97.772
342536.944	5057796.42	3894.885	342536.7015	5057796	3895.097	49.6492	-98.201
342590.113	5057699.47	3896.599	342589.9914	5057699	3890.991	49.0345	-98.164
342641.644	5057601.86	3895.86	342641.5579	5057602	3891.937	48.9457	-97.282
342690.009	5057504.76	3893.956	342689.8798	5057505	3894.685	50.6873	-97.37
342740.472	5057406.69	3891.018	342740.2314	5057407	3896.46	52.1863	-97.1
342794.013	5057310.14	3887.685	342793.8855	5057310	3895.714	51.9483	-95.392
342847.948	5057214.09	3885.716	342847.8564	5057214	3893.835	51.8734	-97.138
342899.942	5057117.77	3885.95	342899.8304	5057118	3890.869	50.6087	-97.329
342950.948	5057019.81	3887.484	342950.8702	5057020	3887.541	49.4954	-97.899
343000.686	5056921.41	3890.344	343000.5872	5056922	3885.578	48.6905	-98.464
343049.813	5056823.08	3893.034	343049.7205	5056823	3885.838	48.8137	-98.421
343098.854	5056725.7	3894.776	343098.7587	5056726	3887.371	49.0819	-98.755
343149.645	5056628.21	3895.822	343149.5313	5056628	3890.315	49.9419	-98.387
343201.914	5056530.95	3896.232	343201.8013	5056531	3893.02	54.1311	-104.918
343253.89	5056435.36	3896.542	343253.8223	5056436	3894.779	48.005	-91.036
343305.783	5056338.04	3896.766	343305.7234	5056338	3895.861	51.4886	-97.82
343356.389	5056240.52	3897.284	343356.3617	5056241	3896.271	53.4217	-101.791
343405.9	5056142.41	3898.496	343405.8744	5056143	3896.601	48.6199	-93.255
343454.654	5056043.75	3899.189	343454.5905	5056044	3896.857	50.1616	-97.116
343503.504	5055945.11	3897.873	343503.4577	5055945	3897.378	50.5262	-97.594
343552.646	5055846.16	3896.321	343552.5759	5055846	3898.638	50.9064	-96.113
343602.633	5055747.55	3895.655	343602.5879	5055748	3899.344	52.7135	-97.214
343656.872	5055642.43	3894.759	343656.7641	5055643	3898.066	52.7313	-96.38
343704.908	5055551.15	3893.955	343704.867	5055551	3896.486	52.8566	-97.906
343756.432	5055453.13	3894.109	343756.3866	5055453	3895.871	50.3146	-95.018
343809.874	5055351.16	3895.87	343809.8437	5055351	3894.995	50.2903	-97.003
343858.527	5055257.69	3897.808	343858.4839	5055258	3894.213	49.8977	-98.931

343908.729	5055160.4	3899.32	343908.6786	5055161	3894.388	49.4329	-98.26
343959.326	5055062.63	3899.353	343959.2452	5055063	3896.146	49.3055	-97.498
344010.334	5054966.34	3897.55	344010.2124	5054967	3898.113	50.1127	-97.887
344063.116	5054868.92	3895.783	344063.0175	5054869	3899.679	-275.47	53.57
344115.912	5054772.3	3893.737	344115.8273	5054773	3899.736	-1073.41	1004.771
344168.842	5054674.12	3891.793	344168.7386	5054674	3897.882	-1166.93	1135.652
344219.238	5054578.84	3889.991	344219.1266	5054579	3896.176	-154.052	290.957
344269.595	5054481.59	3888.884	344269.4983	5054482	3894.139	-155.266	293.076
344319.601	5054382.42	3888.809	344319.4827	5054383	3892.21	-155.432	292.065
344369.14	5054283.93	3903.909	344369.0239	5054284	3890.432	-154.978	290.95
344418.575	5054186.17	3904.757	344418.4355	5054187	3889.33	-252.071	486.915
344468.826	5054088.05	3894.081	344468.6677	5054088	3889.221	-250.397	489.009
345216.552	5053232.82	3895.034	344193.3257	5054142	3894.613	-247.754	490.667

<b>xi+1-xi</b>	<b>Velocità</b>	<b>Distanza tra le due camere</b>	<b>Offset</b>	<b>Planar distance</b>
107.7691	39.6064145	0.266548	0.00673	0.101637
107.9376	38.49415286	0.36106	0.00938	0.210848
109.1381	38.01397833	0.430803	0.011333	0.35389
108.5218	37.03815187	0.309209	0.008348	0.248131
109.3956	36.45304609	0.340799	0.009349	0.293995
110.3393	36.56041041	0.400125	0.010944	0.365303
109.6136	36.4164878	0.360053	0.009887	0.331143
108.9937	35.19330519	0.297825	0.008463	0.265951
110.0563	34.84998431	0.317434	0.009109	0.279473
110.1944	35.33004431	0.421033	0.011917	0.407246
109.7048	35.33165259	0.42445	0.012013	0.422721
108.9305	34.7576525	0.339598	0.00977	0.336212
109.5565	33.98154264	0.262581	0.007727	0.251154
109.519	33.18758283	0.268661	0.008095	0.26573
110.1749	32.79991633	0.296669	0.009045	0.296258
110.1442	32.82987212	0.34929	0.010639	0.34833
109.8922	32.97095146	0.378755	0.011488	0.377519
109.6871	32.26092004	0.273969	0.008492	0.273441
109.7277	31.9347179	0.300555	0.009412	0.297464
110.1391	32.88716479	0.369367	0.011231	0.369064

109.6627	33.41338974	0.308719	0.009239	0.308082
110.8259	33.94362002	0.436252	0.012852	0.436079
110.3212	34.07079542	0.438395	0.012867	0.437947
109.1641	33.8388258	0.413735	0.012227	0.413008
109.7831	33.43986621	0.313856	0.009386	0.311246
109.2594	33.31079863	0.425193	0.012764	0.421781
110.8608	33.72704185	0.469927	0.013933	0.466429
110.5383	34.14837676	0.44731	0.013099	0.441337
110.0793	34.43205205	0.462563	0.013434	0.456674
109.8523	34.29668152	0.48668	0.01419	0.485202
109.8781	34.64000192	0.506628	0.014626	0.487005
110.5464	35.34093496	0.520404	0.014725	0.504824
110.3881	35.68965897	0.501207	0.014043	0.483968
110.2371	35.68699574	0.514312	0.014412	0.50331
109.8624	35.7741502	0.588033	0.016437	0.561697
109.6759	35.87697658	0.579231	0.016145	0.549022
110.7359	36.08206662	0.621564	0.017226	0.571984
109.4803	36.34802964	0.656081	0.01805	0.612306
110.3309	36.32892042	0.622331	0.01713	0.586865
109.6359	36.41178286	0.696193	0.01912	0.712549
109.8812	36.52963693	0.628953	0.017218	0.647574
110.206	36.93231758	0.633879	0.017163	0.649846
209.9277	5.377936187	0.820525	0.152572	0.841924
106.707	54.66546851	0.527697	0.009653	0.506955
105.941	39.19387634	1.47272	0.037575	
108.275	38.58694645	0.691829	0.017929	0.686255
111.4307	38.30548742	0.85346	0.02228	0.849016
108.0379	36.14515593	0.569669	0.015761	0.493303
273.3588	4.028750749	0.415065	0.103026	0.221488
110.7023	50.4108642	0.593326	0.01177	0.401197
107.9687	48.41644173	0.50564	0.010444	0.449062
108.0161	46.9023599	0.458548	0.009777	0.555111
109.6546	46.70127917	0.480997	0.010299	0.588517
110.9629	47.23836826	0.486831	0.010306	0.478002
109.1948	47.10732858	0.477046	0.010127	0.484584

112.0394	46.43157435	0.534485	0.011511	0.547565
107.0736	46.07298947	0.50479	0.010956	0.530241
110.7995	46.05131581	0.46419	0.01008	0.431948
109.4042	46.18160559	0.490502	0.010621	0.439239
110.5614	46.27937862	0.494719	0.01069	0.438167
110.5569	46.60913163	0.461774	0.009907	0.371311
109.5504	47.17934982	0.553582	0.011734	0.483613
110.54	47.50321168	0.534046	0.011242	0.466415
109.2585	47.33902677	0.530219	0.0112	0.433244
109.4517	46.89447206	0.515631	0.010996	0.331684
110.078	46.13496902	0.50211	0.010883	0.378465
110.8374	45.51845026	0.456688	0.010033	0.348956
109.0019	45.64570345	0.553276	0.012121	0.464309
109.5651	46.34733671	0.597409	0.01289	0.473648
110.4372	46.65705146	0.584602	0.01253	0.44551
110.3236	46.68794921	0.505017	0.010817	0.37844
110.4723	46.90966362	0.503702	0.010738	0.403298
109.8484	47.0846302	0.560697	0.011908	0.412888
109.3705	46.96026561	0.538136	0.011459	0.39053
110.339	47.01280048	0.615284	0.013088	0.450464
110.2082	47.17817215	0.582568	0.012348	0.489945
110.6431	47.77337287	0.585528	0.012256	0.500294
110.8727	48.47955129	0.651153	0.013431	0.559795
110.8057	48.94245667	0.653224	0.013347	0.552644
109.8443	49.30172876	0.650012	0.013184	0.606173
109.4607	49.70969318	0.605339	0.012177	0.577782
110.8743	50.19207099	0.650816	0.012967	0.654154
110.3854	50.58907553	0.65426	0.012933	0.654169
110.6122	50.83280543	0.626883	0.012332	0.598679
109.9216	50.91322129	0.637482	0.012521	0.613887
109.4557	50.76796406	0.5856	0.011535	0.577168
109.7769	50.86972745	0.595271	0.011702	0.607714
111.0633	51.51360951	0.655788	0.01273	0.679154
110.7822	52.47853579	0.763776	0.014554	0.760695
110.2027	53.31528536	0.783807	0.014701	0.798638
110.8378	54.1464649	0.829708	0.015323	0.859768
282.261	3.666774679	0.784252	0.213881	0.810563
110.0142	42.84042332	0.208364	0.004864	0.127885

111.24	43.0662058	0.316615	0.007352	0.235979
109.6192	43.34485901	0.315452	0.007278	0.217042
110.0765	43.61191975	0.320195	0.007342	0.225481
110.7664	44.02481869	0.337551	0.007667	0.23285
109.7417	44.28640449	0.390098	0.008809	0.207486
110.6193	44.35418452	0.331763	0.00748	0.18934
109.4918	44.67228053	0.352947	0.007901	0.235648
110.3045	45.13278192	0.377314	0.00836	0.236814
110.571	45.39038522	0.388286	0.008554	0.170325
109.6042	45.38474452	0.374989	0.008262	0.138638
110.8741	45.58967091	0.44381	0.009735	0.249071
109.8811	45.84108408	0.450626	0.00983	0.260831
109.6225	46.13740983	0.432093	0.009365	0.190436
110.2594	46.46413851	0.452334	0.009735	0.183423
109.4589	46.1268037	0.588873	0.012766	0.157745
109.558	45.1041593	0.505482	0.011207	0.207473
110.1472	44.57595915	0.4426	0.009929	0.229802
110.7046	44.80152458	0.551367	0.012307	0.307255
109.5085	45.43921157	0.537049	0.011819	0.312145
109.4583	45.23069453	0.578614	0.012793	0.261408
219.5751				0.167007
111.4448	44.90119903	0.365244	0.008134	0.365094
218.7371	87.88150437	0.325157	0.0037	0.324073
217.0576	88.99452109	0.326058	0.003664	0.325398
217.705	89.29653752	0.348534	0.003903	0.330358
220.2656	89.53884951	0.358969	0.004009	0.358081
221.0868	88.04728989	0.332925	0.003781	0.321808
220.3556	84.94818005	0.371595	0.004374	0.371566
219.6051	84.30138554	0.431493	0.005118	0.431163
220.636	85.81716971	0.414959	0.004835	0.414901
218.3677	86.41380588	0.472704	0.00547	0.472649
217.6945	86.31817877	0.303029	0.003511	0.302908
219.7331	84.70820871	0.399247	0.004713	0.396852
218.017	84.20895523	0.438403	0.005206	0.407257
217.2494	80.97254846	0.476181	0.005881	0.468648
218.343	81.71519566	0.396784	0.004856	0.391131
220.6793	81.1619381	0.34397	0.004238	0.343636

220.6481	77.47476565	0.613982	0.007925	0.583945
203.8623	69.55384676	0.606083	0.008714	0.589763
330.0585	113.1499896	0.467181	0.004129	0.441452
220.2099	76.78168959	0.634297	0.008261	0.60539
219.6335	3.630905557	0.521996	0.143765	0.516678
220.3536	109.4109392	0.268243	0.002452	0.267824
218.123	107.5026964	0.44086	0.004101	0.438056
215.652	107.1296559	0.494082	0.004612	0.471501
219.59	105.3189629	0.452169	0.004293	0.451666
221.6747	107.6090969	0.399398	0.003712	0.399398
109.413	52.62768509	0.415337	0.007892	0.379575
108.4932	52.21037156	0.408846	0.007831	0.39899
110.2371	52.97314029	0.439597	0.008298	0.434385
109.4746	51.34830217	0.480531	0.009358	0.477166
111.1787	52.2456225	0.432124	0.008271	0.430781
110.0044	51.06984333	0.418351	0.008192	0.418
110.0789	51.9976032	0.410609	0.007897	0.407605
109.7669	52.26996236	0.420473	0.008044	0.416149
110.3497	53.20620614	0.453534	0.008524	0.442064
109.8753	53.13121162	0.503129	0.00947	0.50164
109.8477	53.71524674	0.522134	0.00972	0.509775
110.5577	54.35483568	0.504124	0.009275	0.497776
109.82	53.83331611	0.453489	0.008424	0.44667
111.8683	55.49022393	0.43309	0.007805	0.433021
109.8004	54.06224984	0.446899	0.008266	0.445823
111.0111	56.35079252	0.496105	0.008804	0.492142
111.0111	56.35079252	0.659203	0.011698	0.472684
110.2713	56.34712735	0.652457	0.011579	0.538366
110.5967	56.92056697	0.684566	0.012027	0.518882
110.3084	57.03641775	0.632684	0.011093	0.550376
109.4909	57.23520097	0.70001	0.01223	0.598759
109.5336	57.89301234	0.685253	0.011837	0.597007
110.4412	58.40358328	0.687029	0.011763	0.619539
109.7774	57.89948117	0.721033	0.012453	0.668067
111.9103	59.68548952	0.59919	0.010039	0.55287

109.7065	57.92316117	0.695243	0.012003	0.636724
110.5693	60.22294489	0.737187	0.012241	0.698081
110.6784	60.44697356	0.754226	0.012477	0.712067
110.1895	60.57693795	0.721591	0.011912	0.70558
111.3402	61.75274986	0.68932	0.011163	0.6539
108.1469	59.29105657	0.677148	0.011421	0.647443
109.8553	61.5780612	0.648293	0.010528	0.627702
271.2768	148.6448318	0.652845	0.004392	0.662678
109.4096	1.398348595	0.688869	0.49263	0.680189
108.3727	40.19759712	0.20923	0.005205	0.197504
109.6598	40.13903748	0.177602	0.004425	0.16537
219.6494	41.45893017	0.197611	0.004766	0.108883
220.8439	41.93768552	0.241502	0.005759	0.127763
220.9639	42.04832166	0.218696	0.005201	0.124367
220.4038	42.49157929	0.194126	0.004569	0.090757
221.118	43.45018562	0.186282	0.004287	0.14301
220.6702	44.01959721	0.147681	0.003355	0.122142
220.5549	44.89209566	0.136579	0.003042	0.098732
220.8293	45.59761637	0.142708	0.00313	0.107159
220.1558	45.78948045	0.077168	0.001685	0.059
219.3725	45.95150531	0.116042	0.002525	0.114827
219.7829	46.23114715	0.143731	0.003109	0.142962
220.541	46.32242076	0.155555	0.003358	0.155333
220.6673	46.44650497	0.147387	0.003173	0.138457
220.8558	46.93069356	0.14833	0.003161	0.145163
219.9586	47.28258831	0.160399	0.003392	0.142285
219.718	48.01529504	0.197808	0.00412	0.195768
219.5745	48.41774621	0.231396	0.004779	0.228592
217.3379	47.51593403	0.192542	0.004052	0.190689
218.5534	47.1528425	0.396345	0.008406	0.224712
221.6118	46.61585213	0.6924	0.014853	0.660615
220.7627	46.4079723	0.3999	0.008617	0.224599
219.5832	47.10063183	0.568068	0.012061	0.477631
218.902	47.17715276	0.977806	0.020726	0.552975
218.498	46.74753513	0.362598	0.007757	0.3622

217.4732	45.95799963	0.260201	0.005662	0.258689
219.2116	45.76442636	0.241899	0.005286	0.240952
220.9475	45.31327644	0.156395	0.003451	0.15291
220.9788	45.09771111	0.246042	0.005456	0.231309
220.1914	45.4846934	0.405556	0.008916	0.394078
219.6183	45.92603454	0.461484	0.010048	0.458165
219.8007	46.37145366	0.322041	0.006945	0.321265
220.0222	46.62474203	0.324771	0.006966	0.324161
219.021	46.29485396	0.324846	0.007017	0.322175
219.3687	46.17315819	0.401874	0.008704	0.401721
220.4613	45.69145848	0.372102	0.008144	0.371637
227.428	46.60409064	0.32848	0.007048	0.327391
373.8494	4.593759773	0.585177	0.127385	0.557458
221.0689	2.734849907	0.703537	0.257249	0.700424
221.1704	58.43338066	0.493788	0.00845	0.492231
219.7482	58.05765181	0.454181	0.007823	0.445952
219.426	58.26501196	0.465287	0.007986	0.461183
218.5635	57.94367214	0.45617	0.007873	0.446044
219.4999	58.22279354	0.450804	0.007743	0.435995
223.4652	58.97736332	0.478889	0.00812	0.468564
220.4706	57.41422371	0.508544	0.008857	0.499186
328.9949	87.54520185	0.539965	0.006168	0.53694
330.5097	89.08617286	0.5402	0.006064	0.535233
219.2572	58.95596341	0.606536	0.010288	0.587157
109.6167	59.54194238	0.459006	0.007709	0.455197
218.4754	118.736661	0.646251	0.005443	0.428897
222.8811	119.635604	0.625776	0.005231	0.438795
221.4239	117.2795891	0.636493	0.005427	0.422969
214.7977	119.7311427	0.580934	0.004852	0.412211
219.7276	112.2204456	0.576631	0.005138	0.403962
220.9438	126.1094593	0.59521	0.00472	0.471645
221.1946	121.6023098	0.625507	0.005144	0.474778
221.4721	61.43470278	0.659433	0.010734	0.505046
				0.511493
113.0574	63.33745423	0.467679	0.007384	0.47863

108.974	63.80209028	0.600599	0.009413	0.466376
109.6955	64.22451911	0.622665	0.009695	0.597537
110.7153	64.59469162	0.61521	0.009524	0.614999
110.3141	64.73833684	0.58146	0.008982	0.61116
108.7062	64.51407733	0.483926	0.007501	0.571705
109.4354	64.07223831	0.460678	0.00719	0.483666
113.9542	63.80416783	0.563646	0.008834	0.449765
325.4526	194.8817875	0.750805	0.003853	0.553334
113.4809	66.28559488	219.746	3.31514	0.741178
113.4809	62.87032851	0.614954	0.009781	0.570816
110.2426	63.35779589	0.581341	0.009176	0.514195
109.7175	61.98730006	0.580993	0.009373	0.52531
110.9241	62.59824726	0.696646	0.011129	0.637174
281.9382	160.1012138	0.72568	0.004533	0.672778
109.927	61.86101319	0.75435	0.012194	0.687746
111.681	1.221999286	0.751826	0.615242	0.671458
108.3551	38.60173192	0.733296	0.018996	0.643904
107.7849	37.77949305	0.327849	0.008678	0.229719
110.8247	40.0378119	0.418732	0.010458	0.256758
109.0666	38.82754862	0.325158	0.008374	0.241498
109.8857	37.77438157	0.295709	0.007828	0.182575
109.9881	38.28336036	0.342375	0.008943	0.243224
109.3123	37.61607529	0.311032	0.008269	0.220429
111.1371	38.08674633	0.367119	0.009639	0.292749
109.7688	37.72123181	0.30193	0.008004	0.242891
110.3294	37.60374572	0.341139	0.009072	0.318593
110.7884	38.99625445	0.588265	0.015085	0.353725
109.3292	38.76920498	0.070063	0.001807	0.018822
110.5232	39.58566181	0.09068	0.002291	0.036674
109.5473	40.23037586	0.110022	0.002735	0.076694
110.7986	40.43743529	0.08102	0.002004	0.070658
109.1184	40.45918394	0.088761	0.002194	0.085721
110.9918	20.90240754	0.145365	0.006954	0.128804
110.9918	43.02007213	0.433064	0.010067	0.060308

110.0037	42.98700536	0.459454	0.010688	0.094112
109.7878	43.61850617	0.422788	0.009693	0.104382
109.8331	43.63650282	0.445196	0.010202	0.098621
111.738	45.42196351	0.541374	0.011919	0.140602
110.6996	45.72474623	0.47265	0.010337	0.098995
109.779	45.41954662	0.511626	0.011264	0.108904
110.2665	15.38530514	0.48811	0.031726	0.132445
111.7849	47.8736205	0.491632	0.010269	0.130406
108.2762	46.45051729	219.2998	4.721148	
111.1189	47.28464946	0.221409	0.004682	0.202223
110.0618	47.68709526	0.304137	0.006378	0.25187
112.1153	52.56226553	0.296644	0.005644	0.24844
113.7378	50.70790139	0.278437	0.005491	0.239401
111.5237	49.34675637	0.309691	0.006276	0.248863
103.0912	46.02286718	0.23077	0.005014	0.221113
108.9303	49.33436885	0.251565	0.005099	0.233579
110.5885	51.55642475	0.247705	0.004805	0.236392
110.8029	51.10834827	0.315226	0.006168	0.302935
110.7888	2.059309959	0.509312	0.247322	0.501683
109.0742	56.36909809	0.528993	0.009384	0.519333
110.8705	58.84843236	0.324538	0.005515	0.306027
110.8705	61.35609024	0.349878	0.005702	0.333943
113.1174	63.76403496	0.576678	0.009044	0.505261
113.3241	63.30954286	0.583944	0.009224	0.483988
111.4272	61.66418869	0.74086	0.012014	0.670009
110.3452	60.03548192	0.862299	0.014363	0.797015
109.7705	58.26461385	0.466278	0.008003	0.405164
108.3894	58.81137873	0.395197	0.00672	0.315121
108.6861	58.52778097	0.33881	0.005789	0.325565
111.1146	60.95152779	0.39681	0.00651	0.395781
109.3522	57.79712214	0.46482	0.008042	0.43953
110.7934	61.31346464	0.498877	0.008136	0.466437
109.2071	59.77398807	0.454119	0.007597	0.426475
113.4003	60.60948314	0.477862	0.007884	0.448075
107.8061	58.78194074	0.395109	0.006722	0.360249
108.5102	56.39821975	0.381532	0.006765	0.377118

111.2465	63.86138306	0.401264	0.006283	0.400688
109.8255	61.94332474	0.459807	0.007423	0.455508
116.0723	63.56641895	0.443944	0.006984	0.434459
105.5583	58.54593956	0.385461	0.006584	0.38033
107.672	59.81779701	0.397169	0.00664	0.392404
111.154	61.99330806	0.423081	0.006825	0.422411
110.1173	61.79422037	0.454902	0.007362	0.453097
110.1646	61.03301504	0.42795	0.007012	0.427888
109.9383	62.00692163	0.432627	0.006977	0.432322
109.3115	60.66118643	0.427394	0.007046	0.426644
110.611	59.78970943	0.437082	0.00731	0.4359
108.4572	60.9652452	0.425161	0.006974	0.42213
109.8729	60.4694105	0.421668	0.006973	0.414813
112.3469	61.12456804	0.408021	0.006675	0.393863
107.4807	58.9905242	0.401635	0.006808	0.38621
109.3559	59.17526408	0.525895	0.008887	0.504093
110.2432	58.36061014	0.613745	0.010516	0.571675
109.0106	61.10460825	0.352654	0.005771	0.305851
110.3928	59.83349856	3.914295	0.06542	
112.8054	61.77734812	2.071268	0.033528	
106.724	58.80110388	0.642865	0.010933	0.599319
110.7011	60.69137408	0.536863	0.008846	0.491169
109.9021	60.15441134	0.542059	0.009011	0.479593
109.5011	59.73874313	0.584182	0.009779	0.520534
110.1447	59.09053423	0.563858	0.009542	0.483533
109.9497	1.096875815	0.561231	0.511663	0.473606
109.0854	39.66741427	0.455821	0.011491	0.419742
109.683	40.20638678	0.564776	0.014047	0.440098
269.3332	97.12702807	0.60651	0.006245	0.485857
110.7505	39.72399194	0.433907	0.010923	0.23816
109.6669	38.42570011	0.362502	0.009434	0.258944
109.7574	38.3767182	0.41951	0.010931	0.262002
108.4312	38.30138683	0.397938	0.01039	0.236992
110.1133	38.85438815	0.37989	0.009777	0.175038
110.5521	38.34619329	0.332359	0.008667	0.146272
109.7052	37.68641421	0.254154	0.006744	0.130465
109.1918	36.70313278	0.368272	0.010034	0.250417
109.6483	36.53724885	0.267379	0.007318	0.16115

109.2955	36.5903987	0.232997	0.006368	0.138404
110.095	37.0565416	0.235594	0.006358	0.143141
110.0626	37.61537605	0.186273	0.004952	0.102675
109.9617	37.38922958	0.154	0.004119	0.078806
110.4371	37.09677202	0.168993	0.004555	0.125444
109.5932	36.72694908	0.130175	0.003544	0.0859
109.5753	36.23521559	0.093608	0.002583	0.091512
110.0056	36.36548226	0.125982	0.003464	0.112231
109.3304	36.39494151	0.098979	0.00272	0.082308
110.216	37.14728842	0.115895	0.00312	0.107084
110.2342	37.04105988	0.126592	0.003418	0.126579
110.1686	37.30733678	0.159721	0.004281	0.159635
109.4559	37.34423255	0.125211	0.003353	0.123436
110.3568	37.85823864	0.141516	0.003738	0.137591
110.1608	38.30346354	0.110409	0.002882	0.104728
110.2232	38.06050261	0.171401	0.004503	0.15423
110.7355	38.90918085	0.178414	0.004585	0.166123
109.5646	38.68807405	0.196398	0.005076	0.15209
110.647	39.48857813	0.179325	0.004541	0.151354
109.9815	39.81949688	0.172202	0.004325	0.129989
110.5806	40.91031995	0.20876	0.005103	0.156263
110.8025	40.64656565	0.252838	0.00622	0.192781
110.7184	41.15926004	0.298557	0.007254	0.206715
109.2515	41.24254854	0.259103	0.006282	0.180567
110.7472	42.54600051	0.23592	0.005545	0.136328
110.6023	40.8579012	0.28891	0.007071	0.227312
110.1793	44.19547091	0.265822	0.006015	0.200703
109.2928	42.31234534	0.290112	0.006856	0.22974
114.5038	44.17584519	0.355429	0.008046	0.274591
105.7987	41.24703777	0.343442	0.008326	0.26603
109.5702	1.637404795	0.345301	0.210883	0.274138
110.2117	58.1592346	0.326842	0.00562	0.299212
110.6975	59.03869207	0.425736	0.007211	0.380479
288.8426	152.5040342	0.437018	0.002866	0.365079
110.6881	58.01263266	0.527692	0.009096	0.287514
108.9148	56.25764882	0.596088	0.010596	0.399829
108.8799	19.0150023	0.398555	0.02096	0.25985
109.1048	57.12293159	0.32064	0.005613	0.239005

110.2982	60.67010825	220.3887	3.632574	
329.6694	172.3310957	#REF!	#REF!	
115.8226	59.9806409	219.5794	3.660839	
104.222	53.80585955	109.3459	2.03223	
109.2183	56.82535332	116.1734	2.044394	0.354811
109.9668	56.77169595	104.5248	1.841142	0.298984
110.1861	57.00266573	109.5602	1.92202	0.343056
109.393	28.1143712	110.2857	3.92275	0.320973
110.309	55.82440311	110.4925	1.979287	0.303501
110.3166	55.26882051	0.381024	0.006894	0.372056
109.9115	54.92829176	0.342691	0.006239	0.343472
109.9078	54.84421824	109.579	1.998004	0.376628
109.5359	55.26531096	109.2256	1.976387	0.330985
109.8728	54.85411527	109.5252	1.996663	
110.0255	54.38730505	109.6969	2.016958	0.317194
110.3377	53.87585439	109.9723	2.041217	0.349444
109.043	53.13984624	108.7279	2.04607	0.331933
109.3656	52.98721751	109.0575	2.058186	0.363292
109.3868	53.4898932	109.072	2.039115	0.315847
109.891	51.25512544	109.5374	2.137101	0.317964
109.7379	56.10320392	109.3597	1.949259	0.326529
110.4735	53.94215429	110.1466	2.041938	0.373945
109.6683	53.08244423	109.3732	2.060441	0.386748
114.8449	55.56113926	114.5328	2.061383	0.330377
104.5496	51.17454227	104.177	2.03572	0.290849
109.3563	52.88021599	108.9722	2.060736	0.315944
110.387	54.08477319	109.9819	2.03351	0.373339
110.6139	51.18645326	110.2173	2.153252	0.388908
109.3944	54.07531987	109.0274	2.016214	0.409021
110.7381	1.352873646	110.3623	81.57618	0.394896
109.1869	37.96484491	108.776	2.865178	0.366
115.4945	40.15802122	115.08	2.865679	0.374657
107.9477	37.59932705	107.5051	2.85923	0.410604
220.0404	75.3047243	220.1137	2.922974	0.415375
109.8763	37.09531372	110.2046	2.970849	0.444946
110.3552	37.25700017	110.6829	2.970795	0.334328

109.4378	36.90987259	109.7997	2.974806	0.366793
109.4901	37.483772	109.8101	2.929536	0.326255
109.8751	37.09491691	110.1914	2.970524	0.360839
110.0026	37.037911	110.2838	2.977592	0.312028
110.4744	37.12178776	110.617	2.979841	0.320575
108.9642	36.18871975	109.0897	3.014466	0.131843
110.4142	36.75571298	110.5409	3.007448	0.157797
110.1032	35.34612611	110.2364	3.118768	0.130343
109.7529	38.33494112	109.8807	2.866332	0.132232
109.9967	37.37569801	110.1216	2.946342	0.142903
109.0476	37.15421209	109.1682	2.938247	0.117218
114.169	39.03213757	114.2813	2.927877	0.13148
106.2421	36.52187693	106.37	2.9125	0.133881
109.7801	37.62168609	109.8816	2.920699	0.122635
110.1215	38.0253812	110.2133	2.898413	0.123097
109.9246	38.02302653	110.0314	2.893809	0.093591
109.5147	37.59515542	109.6212	2.915832	0.094863
110.4653	36.26568277	110.569	3.04886	0.117602
110.1236	38.33051644	110.2722	2.876878	0.140036
109.4886	36.92702138	109.6677	2.969849	0.141433
109.1476	36.81199127	109.2634	2.968146	0.150842
113.3062	38.59202699	113.4056	2.938577	0.2348
106.4394	36.79206179	106.5465	2.89591	0.13244
109.56	37.91003822	109.6473	2.892302	0.129337
110.3189	38.21227997	110.412	2.889438	0.135925
110.2824	38.38581725	110.3944	2.875917	0.104095
109.3717	37.21391593	109.4538	2.941207	0.115162
110.0811	40.33751792	110.1705	2.731216	0.169352
110.2995	38.27184788	110.3828	2.884178	0.150333
110.3854	38.50204917	110.4615	2.868977	0.120736
113.8852	39.37938417	113.9799	2.894406	0.186668
105.691	36.30744431	105.8025	2.914071	0.271052
110.4833	37.65619516	110.5718	2.93635	0.161375
109.2789	37.33477334	109.3408	2.928659	0.165654
109.9307	38.07783758	109.9763	2.888197	0.205811
110.0963	38.16164144	110.1456	2.886291	0.211287
110.1935	1.544191032	110.2226	71.37887	0.210636
110.0445	53.08464054	110.0066	2.072287	0.168419

109.557	52.31949408	109.5497	2.09386	0.217553
109.8415	48.49514604	109.8061	2.264271	0.26032
266.7298	117.8655938	266.941	2.264792	0.168988
106.4313	48.33391395	106.598	2.205449	0.255606
212.4867	96.54097417	103.1146	1.068091	0.177006
111.3906	50.86330013	0.282692	0.005558	0.255108
110.3815	49.21156858	0.401346	0.008156	0.240599
108.3438	48.71574224	0.275001	0.005645	0.244872
110.3057	50.32193992	0.284577	0.005655	0.121666
110.4068	50.46016456	0.323073	0.006403	0.086569
110.1657	50.79099755	0.299481	0.005896	0.202555
109.495	50.55173184	0.344331	0.006811	0.291742
110.5098	51.13828603	0.325512	0.006365	0.261228
110.2756	50.07975226	0.312157	0.006233	0.322291
109.9222	49.16020708	0.315357	0.006415	0.289385
109.0316	49.09122826	0.279641	0.005696	0.277144
109.9624	48.61291644	0.218609	0.004497	0.283756
110.4432	48.97701677	0.230208	0.0047	0.256276
108.813	48.29693234	0.256519	0.005311	0.187091
110.3058	49.04658942	0.267714	0.005458	0.228324
109.8751	49.00762676	0.26758	0.00546	0.256127
109.8982	48.90883817	0.261393	0.005344	0.267702
110.0393	49.05896639	0.286294	0.005836	0.264795
110.0738	46.30787313	0.29183	0.006302	0.258446
110.4974	54.05939512	0.315762	0.005841	0.280172
110.5555	50.85350561	0.322421	0.00634	0.277367
118.3006	52.74215202	0.340867	0.006463	0.301575
103.1454	50.61111108	0.359307	0.007099	0.289612
110.7459	52.48621232	0.351599	0.006699	0.303371
115.1354	54.10497736	0.362976	0.006709	0.302872
105.3712	49.75033741	0.349493	0.007025	0.310717
109.4815	50.59217592	0.388766	0.007684	0.291556
110.0853	51.10737842	0.37601	0.007357	0.257787
108.9951	50.15882619	0.377384	0.007524	0.291207
110.8106	53.09564692	0.422593	0.007959	0.25209
110.1007	52.1557262	0.460183	0.008823	0.25703
111.5551	52.39788865	0.501514	0.009571	0.292477

107.8022	51.30994843	0.490533	0.00956	0.288346
109.5418	52.68963729	0.527187	0.010006	0.323293
111.0796	53.1990274	0.520201	0.009778	0.36112
110.2608	1.047419417	0.531368	0.507311	0.35114
109.5458	40.81439712	0.545375	0.013362	0.330465
110.2347	40.20231101	0.571182	0.014208	0.329004
1136.111	416.4628542	0.535066	0.001285	0.320749
53.62915	19.81860853	1368.624	69.0575	0.356433
1421.804	526.3989733	1523.859	2.894875	0.341859
108.3449	39.78878611	218.975	5.503435	0.341859
110.284	13.46733941	221.0138	16.4111	1368.592

# Bibliography

- Anon., s.d. *I Ghiacciai della Valle d'Aosta The Glaciers of Aosta Valley*, s.l.: s.n.
- Anon., s.d. *I Ghiacciai della Valle d'Aosta*. [Online] Available at: <https://sites.unimi.it/glaciol/wpcontent/uploads/2019/02/4-valle-daosta.pdf>.
- Aschwanden, A. et al., 2019. *C L I M A T O L O G Y Contribution of the Greenland Ice Sheet to sea level over the next millennium*, s.l.: s.n.
- Banff, G., 2022. *PCI Geomatica Banff*. [Online] Available at: <https://support.pcigeomatics.com/hc/en-us/articles/360035645811>
- Baroni, C. B. A. C. L. & C. M., 2020. Annual glaciological survey of Italian Glaciers 2019. In: s.l.:Geografia Fisica e Dinamica Quaternaria, p. 45–142.
- Bendle, J., s.d. *Types of glaciers*, s.l.: s.n.
- Bertolo, D., s.d. *I dati dei ghiacciai valdostani*, s.l.: s.n.
- Boccardo, P., s.d. *Remote sense basics*, Turin: s.n.
- Bonetto, F. B. G., 2015. *La Thuile, Paesaggi storici e geologici*. s.l.:Maggioli Editore.
- Catalyst, 2022. *Catalyst DEM Extraction*. [Online] Available at: <https://catalyst.earth/2021/08/18/dem-extraction-satellite-new/>
- center, N. S. a. i. d., 2015. *What is a glacier?* | National Snow and Ice Data Center. [Online] Available at: <https://nsidc.org/cryosphere/glaciers/questions/what.html>
- Cina, A., 2014. *Dal GPS al GNSS*. s.l.:Celid.
- Comitato Glaciologico Italiano, s.d. *Il Nuovo Catasto dei Ghiacciai Italiani*. [Online] Available at: <http://catastoghiacciai.partout.it/>
- ComitatoGLaciologicoItaliano, s.d. *CAMPAGNE GLACIOLOGICHE*. [Online] Available at: <https://web.archive.org/web/20070622143502/http://www.disat.unimib.it/comiglacio/campagne.htm> [Consultato il giorno January 2022].
- ConveRgo, s.d. *CPSG – Comitato Permanente Sistemi Geografici*. [Online] Available at: [https://www.cisis.it/?page\\_id=3214](https://www.cisis.it/?page_id=3214) [Consultato il giorno March 2022].

Core Writing Team, R. P. a. L. M. (, 2014. *IPCC, 2014: Climate Change 2014: Synthesis Report. Contribution of Working Groups I, II and III to the Fifth Assessment Report of the Intergovernmental Panel on Climate Change*, Geneva, Switzerlan: s.n.

D'Aosta, A. V., s.d. *Arpa Valle D'Aosta*. [Online]  
Available at: <https://www.arpa.vda.it/it/>

Digisky, S., 2021. *Digisky*. [Online]  
Available at: <https://www.digisky.it/about-us/>

Diolaiuti, G. A. et al., 2012. The 1975-2005 glacier changes in Aosta Valley (Italy) and the relations with climate evolution. *Progress in Physical Geography*. In: s.l.:s.n., pp. 764-785.

DJI, s.d. <https://www.dji.com/it/phantom-4>. [Online]  
Available at: <https://www.dji.com/it/phantom-4>

ESA, 2021. *eoPortal Directory*. [Online]  
Available at: <https://earth.esa.int/web/eoportal/satellite-missions/p/pleiades>  
[Consultato il giorno 12 Dicembre 2021].

ESA, s.d. *Time reference in GNSS*. [Online]  
Available at: [https://gssc.esa.int/navipedia/index.php/Time\\_References\\_in\\_GNSS](https://gssc.esa.int/navipedia/index.php/Time_References_in_GNSS)  
[Consultato il giorno February 2022].

F.Bonetto, G., 2014. *Ambienti Glaciali di alta montagna*. s.l.:Archivio Comune La Thuile.

Freppaz, M. W. M. W. G. J. G. R. M. I. A.-J. J. E. M. & C. L., 2021. Characterization of organic-rich mineral debris revealed by rapid glacier retreat, Indren Glacier, European Alps.. *Journal of Mountain Science*, p. 1521–1536.

Fronteddu, M., 2020. *Tesi di laurea 'Tecniche Geometriche di Monitoraggio dei Ghiacciai'*. s.l.:s.n.

Geoportale, s.d. *SPIN GNSS*. [Online]  
Available at: <https://www.springnss.it/stazione/?id=RUMI>  
[Consultato il giorno February 2022].

Giovanni Kappenberger, M. L.-M., 2006. Che cos'è un ghiacciaio.

Giulio Tonolo, F., Cina, A., Manzino, A. & Fronteddu, M., 2020. *3D GLACIER MAPPING by MEANS of SATELLITE STEREO IMAGES: The BELVEDERE GLACIER CASE STUDY in the ITALIAN ALPS*. [Online].

GNSSCALENDAR, s.d. *GNSS CALENDAR*. [Online]  
Available at: <https://www.gnsscalendar.com/index.html?year=2020>  
[Consultato il giorno February 2022].

Gomarasca, M. A., 2009. *Basics of geomatics*.. s.l.:pringer Science & Business Media.

Haeberli, W., Cihlar, J. & Barry, R. G., 2021. *Glacier monitoring within the Global Climate Observing System* \*, s.l.: s.n.

Haeberli, W., Global Environmental Monitoring System, International Hydrological Programme & World Glacier Monitoring Service, s.d. *World Glacier Inventory : Status 1988 : a Contribution to the Global Environment Monitoring system (GEMS) and the International Hydrological Programme*. s.l.:s.n.

Haeberli, W., Hoelzle, M., Paul, F. & Zemp, M., 2021. *Integrated monitoring of mountain glaciers as key indicators of global climate change: the European Alps*, s.l.: s.n.

Hambrey, M. &. A. J., 2004. Earth, the icy planet. In: *In Glaciers*. Cambridge: Cambridge University Press, pp. 1-10.

Hock, R. G. R. C. A. B. C. S. G. Y. H. M. J. A. K. S. K. S. K. A. M. U. M. S. M. B. O. a. H. S., 2019. *High Mountain Areas*. Geneve, Switzerland, s.n., p. High Mountain Areas. In:.

Italiana, I. d., 2011. *Vocabolario Treccani*. [Online]  
Available at: <http://www.treccani.it>

ItalianPositioningService, s.d. *Italian Positioning Service*. [Online]  
Available at: <https://hxgnsmartnet.com/it-it>  
[Consultato il giorno MArch 2022].

M. Benoit Boissin, A. G. C. T., 2012. *THE PLÉIADES SYSTEM AND DATA DISTRIBUTION*. Munich, Germany, IEEE International Symposium on Geoscience and Remote Sensing IGARSS, pp. 7098-7101.

M. Kasser, Y. E., 2002. *Digital Photogrammetry*. s.l.:Taylor & Francis.

Marshall, S. J., 2011. *The cryosphere*. Vol. 2. s.l.:Princeton University Press,.

Organization, W. -. W. M., s.d. *Major Cryosphere Elements*. [Online]  
Available at: <https://public.wmo.int/en/our-mandate/focus-areas/cryosphere/elements>

Organization, W. -. W. M., s.d. *Major Cryosphere Elements*. [Online]  
Available at: <https://public.wmo.int/en/our-mandate/focus-areas/cryosphere/elements>

Pfirman, S. et al., 2021. *POTENTIAL CONSEQUENCES OF "DIRTY" ARCTIC SEA ICE (Abstract)*, s.l.: s.n.

PhaseOne, 2021. *Phaseone cameras*. [Online]  
Available at: <https://geospatial.phaseone.com/cameras/ixm-rs150f/>

Rasul, G., Pasakhala, B., Mishra, A. & Pant, S., 2020. Adaptation to mountain cryosphere change: issues and challenges. In: s.l.: Taylor and Francis Ltd., pp. 297-309.

Science World, s.d. *Modified Julian Date*. [Online]  
Available at:  
<https://scienceworld.wolfram.com/astronomy/ModifiedJulianDate.html#:~:text=A%20modified%20version%20of%20the,0%20of%20the%20Julian%20calendar.>  
[Consultato il giorno February 2022].

Service, W. G. M., s.d. *World Glacier Monitoring Service*. [Online]  
Available at: <http://www.wgms.ch>.

Spehn, E. M., Körner, C. & Maselli, D., 2010. *Mountain Biodiversity and Global Change Plant ecology View project Micro-climatology and habitat demands of alpine tussock graminoids View project*, s.l.: s.n.

Taylor, L. S. et al., 2021. Remote sensing of the mountain cryosphere: Current capabilities and future opportunities for research. 45(6), pp. 931-964.

Tognetto, F. P. L. V. C. C. N. & G. M., 2021. Geomorphology and geosystem services of the Indren-Cimalegna area (Monte Rosa massif–Western Italian Alps). *Journal of Maps*, p. 161–172.

University, C., 2021. *Cambridge Dictionary online*. [Online]  
Available at: <https://dictionary.cambridge.org/dictionary/>

UnixTime, s.d. [Online]  
Available at: <https://www.unixtimestamp.com/>  
[Consultato il giorno February 2022].

Valle D'Aosta Region, s.d. *Geoportale Valle D'aosta*. [Online]  
Available at: <https://geoportale.regione.vda.it/>  
[Consultato il giorno February 2022].

Vaughan, D. G. et al., 2013. *Observations: Cryosphere*. In: *Climate Change 2013: The Physical Science Basis. Contribution of Working Group I to the Fifth Assessment Report of the Intergovernmental Panel on Climate Change Coordinating Lead Authors: Lead Authors*, s.l.: s.n.

Vaughan, D. J. C. I. A. J. C. G. K. R. K. P. M. T. M. F. P. J. R. E. R. O. S. K. S. a. T. Z., 2013. *Observations: Cryosphere.*.. ambridge, United Kingdom and New York, NY, USA, ambridge University Press.

Villa, F., De, M. & Maggi, V., 2007. *EPICA-European Project for Ice Coring in Antarctica View project nextdata project*, s.l.: s.n.

Villa, F., Tamburini, A., Sironi, S. & Maggi, V., 2008. *Volume decrease of Rutor Glacier (Western Italian Alps) since Little Ice Age: a quantitative approach combining GPR, GPS and cartography EPICA-European Project for Ice Coring in Antarctica* , s.l.: s.n.

WMO, I. (I. U. e. U., s.d. *world glacier monitoring service*. [Online] Available at: <https://wgms.ch/> [Consultato il giorno February 2022].